Non-equilibrium dynamics of strongly coupled gauge theory and gauge/string duality.

Przemysław Witaszczyk

A dissertation
Presented to the Faculty
of Jagiellonian University
in Candidacy for the Degree
of Doctor of Philosophy

Adviser: Prof. Romuald A. Janik

Contents

Chapter 1

Introduction

To see a World in a Grain of Sand
And a Heaven in a Wild Flower
Hold Infinity in the palm of your hand
And Eternity in an hour

William Blake

1.1 New horizons in quantum field theory

For decades quantum field theory has served as a foundation of our repeated successful attempts at understanding Nature and explained phenomena of ever increasing complexity. From simple double-slit quantum interference to spectacular high energy multiparticle collisions and beyond it proved itself as the most successful endeavour in physics of microcosm. Except for gravity. Perplexing problems arise with attempts to merge fourth force with quantum realm and no real physically attractive solution has yet been proposed to complete our picture of known interactions.

Embedded in this clash a new set of ideas emerged within superstring theory known as the gauge/string or gauge/gravity duality and started to reshape our perspective on gravity quantisation, and even on what Quantum Field Theory might itself be. The fusion of gravity and field theory methods constituting the duality is contemporarily recognised as a new way to understand strong coupling dynamics of a wide class of field theories.

In parallel to these developments exciting events took place in high energy physics with the advent of new powerful particle colliders. This allowed to explore the hypothesis of a new state of matter formation, based on strong interactions. For years a new substance called quark-gluon plasma was theorized to exist at energies high enough to melt strong forces confinement. In this model quarks and gluons released for a fraction of a second would roam almost freely and evolve as constituents of this new state of matter. The collision energies necessary for this to happen would have to exceed critical temperature of roughly $T_c = 170$ MeV. Based on this it was expected, that due to the asymptotic freedom the resulting state would be within the reach of perturbative QCD description. The experiments indeed led to phenomena, which could be understood as the quark-gluon plasma formation.

However two surprising features were observed. The first concerned the way the system evolved in post collision period. It was discovered, that to explain the spectra of particles recorded by the detector it is necessary to assume, that the deconfined matter followed

collective fluid evolution almost immediately after the collision. This observation was surprising, because it was difficult to imagine thermodynamic equilibrium formation at the time-scale of 10^{-23} seconds. The mechanism of equilibration at such a short period was mysterious.

The second revelation was that apparently the colourful matter was still *strongly* coupled. Contrary to the perturbative expectations one can not use asymptotic freedom and describe it as the foreseen gas of free quarks and gluons. The chief argument behind this observation is based on perturbative calculations of the so-called normalized shear viscosity η, which expressed in units of entropy density s would in perturbation theory behave as $\eta/s \propto 1/\alpha_s^2 \log(1/\alpha_s)$ for small gauge coupling α_s. Should the fluid consist of weakly coupled partons, mean free path would be large and viscosity would be correspondingly significant [Wiedemann 2013]. What was found instead, is that to reconstruct collision data one has to assume this ratio to be small, and hence incompatible with weak coupling. The perspective for understanding the system from first principles became challenging.

In these circumstances string/gauge duality entered the stage. In 2001, soon after its discovery in 1997, it was realised, that the newly founded correspondence between gravity and a version of gauge theory called $\mathcal{N} = 4$ super-Yang-Mills may provide insight into this theory's thermal state properties at strong coupling. The primary result leading to this speculation was the computation of the viscosity to entropy density ratio,

$$\frac{\eta}{s} = \frac{1}{4\pi}. \tag{1.1}$$

It was found, that this is parametrically close to the small value observed at RHIC and mentioned above. This in turn led to the hope, that maybe gauge theory present in the duality is phenomenologically close enough to QCD, to qualitatively describe some of its quark-gluon plasma properties. In this way fluid/gravity research began to grow and emerged as the primary field of theoretical speculation on the possible mechanisms at work in strongly coupled fluids.

This sparked the idea of research programme summarized in this Thesis, concerned with non-equilibrium dynamics of strongly coupled gauge theory in AdS/CFT correspondence. The motivation to focus on this set of topics was two-fold.

On the one hand the signalled above confusing findings of RHIC on quark-gluon plasma properties raised interesting questions, answering which seemed formidable in pure QCD. The newly formed AdS/CFT correspondence offered a viable possibility to deliver these answers using an alternative theory as a proxy to ideas, which could be common to all gauge theories. Using holographic duality would allow to investigate rapid thermalization mechanism and other properties of states analogous to the real world quark-gluon plasma.

On the other hand the study of string theory inspired non-trivial strongly coupled field theory posed a very attractive research opportunity on its own, even if analogies to QCD would turn out to be remote. Regardless of phenomenological motivation it was therefore a valuable theoretical system, which is much more interesting than just a mere toy model for QCD.

As we shall see the research justified by the above arguments led to new insights into both phenomenology and gravity duals used in the correspondence. We will soon give a roadmap to questions asked and answers reported in this Thesis. Before that however let us cover in a more detailed way some facts concerning quark-gluon plasma, which sourced the initial research questions of this Thesis.

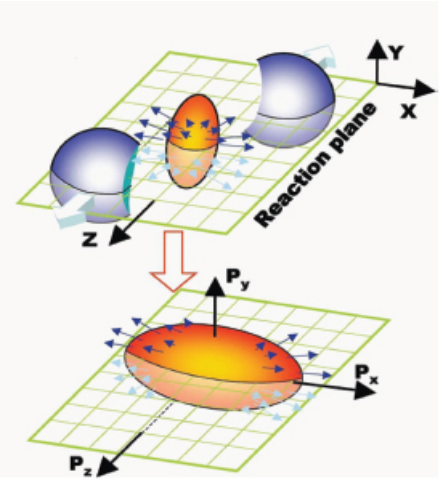

Figure 1.1: Spatial geometry of a two-ion off-center collision and the resulting final state momentum anisotropy. Picture courtesy Brookheaven National Laboratory.

1.2 The most perfect fluid known is colourful

Let us first briefly describe a schematic picture of heavy-ion collision event covering main expected stages of the subsequent evolution. Experiments leading to quark-gluon plasma formation use heavy ions smashed at each other at near-luminal velocities. Originally gold and lead were used, however recent discoveries showed the possibility of thermalization also for very high energy proton-proton collisions (the latter fact is non-trivial due to the very small size of the p-p system).

Apart from the overall energy each collision event is parametrized by the impact parameter b, which reflects centrality of the scattering. Most of the time $b \neq 0$ and the resulting state is asymmetric in the plane transverse to the beam axis. This asymmetry arises because when $b \neq 0$ the two nuclei at the moment of collision overlap only partially. In addition due to Lorentz contraction along beam axis the nuclei are Lorentz contracted. All this leads to a subsequent formation of almond-like shape, highly compressed in the beam direction with spatial elliptic anisotropy in the transverse plane. A standard cartoon of this process is depicted in Fig. 1.1, where we can see the distorted spatial geometry. The initial anisotropy of the system is transferred through the evolution into the final state momentum anisotropy, as was also depicted in the figure. We will describe below how important role this asymmetry plays in establishing the hydrodynamic behaviour of the plasma.

In Figure 1.2 we can see a causal center of mass picture of such a highly energetic two-body collision. The primordial particles travel along the light-cone after going through each other, and in between a very complicated glue-dominated state of matter is created. The subsequent evolution can be divided into four major stages: the early non-equilibrium phases, the locally equilibrated fluid phase called quark-gluon plasma, the mixed hadronization phase and the late freeze-out phase, where no collective phenomena occur any more, and where final particle states travel to detectors.

The properties of this system are probed by recording these particles and counting the so-called charged particles multiplicities, defining final hadron spectra. The most basic and direct observable is the differential particles multiplicity per unit rapidity and transverse momentum,

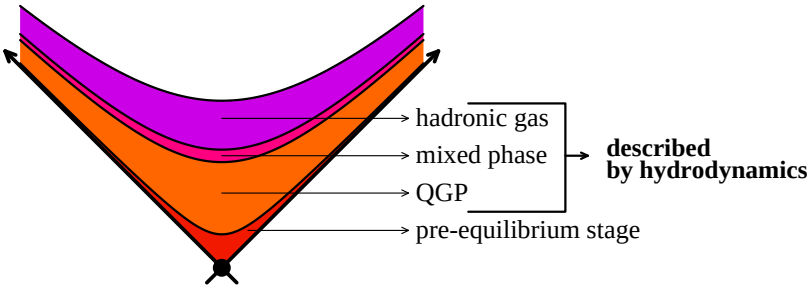

Figure 1.2: Spacetime evolution of highly energetic nuclear matter collision remnants. The collision takes place at the apex and leads to subsequent four stages of the evolution, up to the late hardonization and final state detection. Hydrodynamic codes aim at describing the system from some finite moment of thermalization, whereas more fundamental approach of AdS/CFT offers access to model also the initial stage of the evolution (Picture reproduced following [Beuf 2009].

$$\frac{\mathrm{d}N}{p_\perp \mathrm{d}y \mathrm{d}p_\perp} \tag{1.2}$$

from which other observables are formed. The goal of describing recorded data largely amounts to reconstructing this spectrum and descendant observables from some theoretical model. If this succeeds one confirms the assumptions on which the model is based. This led in the case of RHIC to the conclusion, that already at some early stage the system must be described by thermalized strongly coupled fluid of very low viscosity, that is, nearly perfect fluid. The key ingredient of that observation was the so-called collective flow. Let us briefly describe its meaning and origin.

Collectivity means, that there is a large correlation among the recorded particles evolution in spacetime. This correlation emerges in the system, because upon thermalization temperature and pressure appear, and pressure represents common push of the fluid medium constituents on the vacuum surrounding the collision. Therefore by observing specifically correlated particles spectra in (1.2) one can identify the underlying hydrodynamic behaviour.

The quantities used for this purpose are called flow coefficients and are introduced by recalling the aforementioned high initial spatial anisotropy of the off-center collisions. This imbalance is transferred by the subsequent evolution into the final particles momentum anisotropy, and this process is particularly sensitive to the details of the dynamics. By analysing the resulting flow coefficients we can tell, if indeed collective behaviour is necessary to explain the observed values.

This granular information on the collision shape is stored in Fourier modes of the multiplicity (1.2) decomposed in the transverse plane of $p_\perp$, parametrized by an angle ϕ_p, [Heinz 2013]

$$\frac{\mathrm{d}N}{\mathrm{d}\phi_p} = \frac{N}{2\pi}\left(1 - 2\sum_{n=1}^{\infty} \nu_n(p_\perp, y; b)\cos(n\phi_p)\right). \tag{1.3}$$

The discussed flow coefficients are defined with the above as the angular harmonic modes $\nu_n(p_\perp, y; b)$, encoding final particles spectrum departures from rotational symmetry in $p_\perp$ plane.

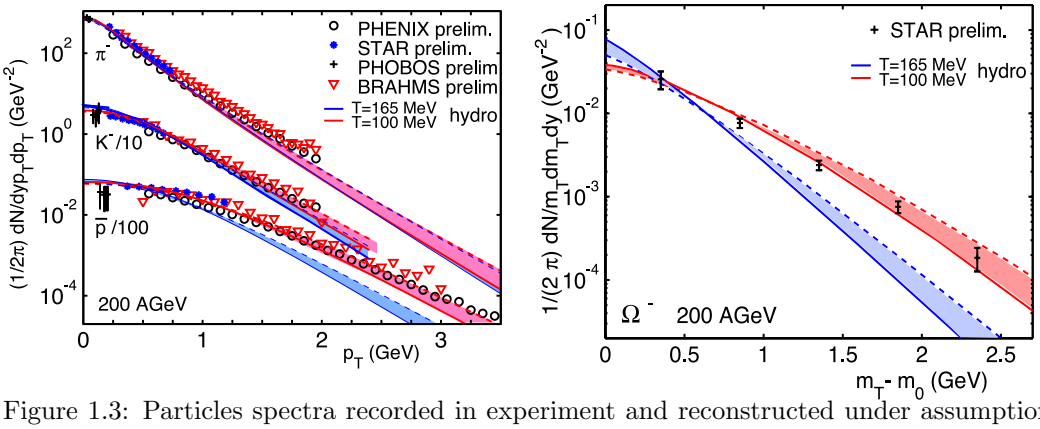

Figure 1.3: Particles spectra recorded in experiment and reconstructed under assumption of early thermalization followed by hydrodynamic expansion.

First two coefficients $\nu_1(p_\perp, y; b)$ and $\nu_2(p_\perp, y; b)$ are called radial and elliptic flow. They are functions of transverse momentum $p_\perp$, rapidity y and impact parameter b. The first one represents an overall expansion of the collision zone, whereas the latter one is related to the leading spatial anisotropy, which we discussed above. Radial flow coefficient represents generically expected uniform expansion in all directions, and is not particularly sensitive to any specific time period of the evolution. However ν_2 due to its relation to anisotropy is sensitive to very early times after the collision, because this asymmetry is washed promptly after the collision and therefore it mostly probes (along with all higher even subtler coefficients) the earliest stage of the expansion. It captures some of its geometry and additionally the early time equation of state $E = E(P)$, which can reveal, apart from the fact of thermalization, some details of the coupling strength. For these reasons elliptic flow ν_2 is used as the *signature* of the quark-gluon plasma formation [Heinz 2013]. Hence its significance.

With its aid it was indeed shown, that to explain the data one must summon the notion of nearly-perfect hydrodynamics. To show this let us present four plots exemplifying this statement from [Kolb 2003, Heinz 2005].

Figure 1.3 shows differential charged particles multiplicities (1.2) as functions of $p_\perp$ recorded in RHIC experiments. The series represent four different final hadron species produced in central Au+Au collisions at $\sqrt{s} = 200A$ GeV. The data points are interposed with hydrodynamics predictions chosen with two different decoupling temperatures, the more correct one occurring at $T_{\mathrm{dec}} = 100$ MeV. The width of the band represents sensitivity of the spectra to the initial radial flow (the detailed discussion can be found in [Heinz 2005]). What is significant here is that these spectra are very well reproduced by hydrodynamics, confirming the assumption of early thermalisation.

The second set of plots tackles more directly with collectivity by depicting the elliptic flow reconstruction. Figure 1.4 shows total ν_2 as a function of centrality on the left (related to the b argument in (1.3)) and per-species ν_2 as a function of $p_\perp$ on the right. One can see, that reconstruction based on hydrodynamics works very well for highly central collisions and lower momenta (the discrepancies are understood [Heinz 2005], and correspond to insufficient time given by the corresponding QGP event to fully transfer the spatial anisotropy into momentum before the freeze-out).

The significance of this (already classic) analysis lies in its high sensitivity to the adjustment of parameters used when employing hydrodynamics. If one would assume different equilibration time, viscosity, lack of collective flow, weak coupling with higher viscosity, the predictions would swiftly miss the data. It follows, that high energy heavy ion collision

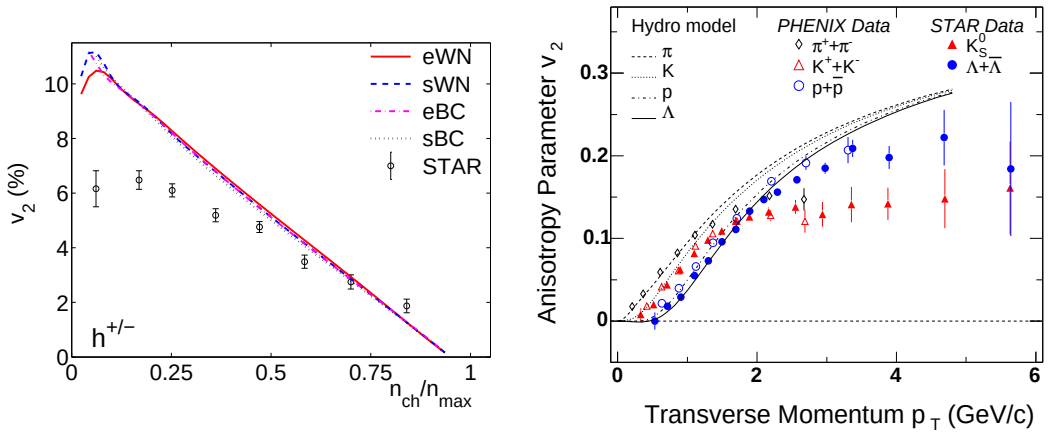

Figure 1.4: Elliptic flow spectrum determined for different particles species as a function of transverse momentum.

produces colourful (deconfined) fluid of extremely low viscosity, which is even more perfect than liquid helium at near absolute zero. We must conclude, that hydrodynamics is an inevitable ingredient of the complete process description.

1.3 Problem statement and overview of the Thesis

The consequence of the last paragraph is that we have found the correct phenomenological model describing the data, and we are now facing the task of explaining its applicability from firs principles. Since QCD is too challenging for such a fundamental approach we shall use the closely related large N $d = 4$ $\mathcal{N} = 4$ super-Yang-Mills of the AdS/CFT correspondence as the theoretical model, according to what we mentioned above.

The Thesis is based on a series of five papers, which have been published in established scientific journals, and their findings were disseminated during many scientific events. We list the papers below together with the corresponding chapters based on them.

- 'Towards the description of anisotropic plasma at strong coupling',
  Romuald A. Janik, Przemyslaw Witaszczyk
  JHEP, vol. 09, page 026, 2008, [Janik 2008] - Chapter 5

- 'A numerical relativity approach to the initial value problem in asymptotically Anti-de Sitter spacetime for plasma thermalization - an ADM formulation',
  Michal P. Heller, Romuald A. Janik, Przemyslaw Witaszczyk
  Phys. Rev. D 85, 126002 (2012), [Heller 2012a] - Chapter 6

- 'The characteristics of thermalization of boost-invariant plasma from holography',
  Michal P. Heller, Romuald A. Janik, Przemyslaw Witaszczyk
  Phys. Rev. Lett., vol. 108, page 201602, 2012, [Heller 2012b] - Chapter 6

- 'Hydrodynamic gradient expansion in gauge theory plasmas',
  Michal P. Heller, Romuald A. Janik, Przemyslaw Witaszczyk
  Phys. Rev. Lett., vol. 110, page 211602, 2013, [Heller 2013a] - Chapter 7

- 'Coupling hydrodynamics to nonequilibrium degrees of freedom in strongly interacting quark-gluon plasma',
  Michal P. Heller, Romuald A. Janik, Michal Spalinski, Przemyslaw Witaszczyk
  Phys. Rev. Lett., vol. 113, page 261601, 2014, [Heller 2014] - Chapter 8

Let us give now an outline of the Thesis, along with the set of considered problems addressed in the above publications. The list below is intended as a brief opening guide to the Thesis, summarizing the main research topics and contents of the remaining chapters. The corresponding conclusions and summary will be presented in the final Chapter 9.

- Chapter 2 introduces the notion of hydrodynamics. We begin with a few general arguments for its existence, describe its appearance in quantum field theory and narrow down to the cases relevant for the subsequent holographic analysis. We emphasize the role of coupling in the hydrodynamic approximation by exemplifying two constructions, using strongly coupled holography and weakly coupled Boltzmann equation.

- Chapter 3 lays down a theoretical background for the whole holographic analysis by introducing super-Yang-Mills theory and the core superstring theory concepts, on which gauge/string duality is founded. We subsequently introduce it and focus on the area of thermal holography relevant for the bulk of the following research. Based on it we introduce the fluid/gravity duality, which is the core conceptual and technical tool used in the Thesis.

- Chapter 4 covers the technical tools from General Relativity necessary for numerical simulations used in Chapter 6.

- Chapter 5 begins the genuine research discussion. We focus in it on the central issue of rapid anisotropic plasma thermalization. We study a static holographic model, in which we seek an instability mechanism similar to the one known from weakly coupled QED. This research serves also as a preliminary for the time dependent system study.

- Chapter 6 deals with the fully dynamical holographic model of boost-invariant expanding plasma studied with the aid of numerical integration. The key research topics addressed here are the rapid plasma thermalization in a dynamical fluid, properties of the early non-equilibrium stage, its subsequent transition to hydrodynamics and ultimately properties of an array of final thermal state parameters.

- Chapter 7 asks and studies the question, if all-order dissipative hydrodynamics as defined in Chapter 2 actually at all exists. This amounts to checking, if the so-called hydrodynamical gradient expansion is convergent. Apart from its fundamental significance we are motivated to address this issue to understand better the thermalizaton process studied in Chapter 6.

- Chapter 8 builds upon the peculiar findings of Chapters 6 and 7, and aims at generalizing conventional hydrodynamics to include genuinely non-equilibrium (non-hydrodynamical) degrees of freedom. The core motivation here came from the question, if one can construct a purely four-dimensional fluid theory enriched with holographical information, which however could be used without any reference to string and gravity theory at all.

- Chapter 9 summarizes the whole Thesis by recapitulating all the findings and presenting the closing discussion of conclusions, open questions and future development directions.

- Appendices contain auxiliary technical details for completeness.

Let us therefore begin our endeavour of studying quantum field theory with the aid of gravity.

Chapter 2

Relativistic hydrodynamics

2.1 Introduction to hydrodynamics and its selected properties

Hydrodynamics is most likely the oldest effective field theory in physics. Its study somewhat unexpectedly become relevant in the context of string theory in a way, which will be described in Chapter 3.

In this chapter we will introduce basic notions of conventional hydrodynamics with an aim to present its features relevant for later chapters. Overall, hydrodynamics is of course a vast subject and we shall not attempt to give any deeper or complete description of it.

We will also not be solving hydrodynamics equations directly, so we will not need to describe their properties in so much detail. The motivation is to outline how this theory is justified and constructed. Later we will see how it is embedded in higher dimensional gravity, and how some of its properties can be formally (and in certain regime rigorously) derived from spacetime geometry.

2.1.1 In search for the hydrodynamic degrees of freedom

We begin by stating, that hydrodynamics is an approximation to quantum field theory's low energy dynamics, which in principle applies to states with finite charge or energy densities. Such highly occupied states have a chance to equilibrate after certain time, called thermalisation time, which is determined by the details of the microscopic dynamics, like e.g. mean free path of the microscopic (quasi-) particles. Formally hydrodynamics is obtained as a low frequency and long wavelength limit of the theory:

$$\omega \to 0,\ k \to 0, \tag{2.1}$$

followed by spatial averaging of thermal expectation values over the system's macroscopic characteristic length and time scales. More precisely hydrodynamics can be considered for quantum field theories admitting power-like tails in conserved charges late time correlators [Kovtun 2003], like e.g. :

$$\int d^3x \langle \left[T^{ij}(t,\mathbf{x}), T^{kl}(0)\right]\rangle \sim t^{-3/2} \text{ for } t \to \infty. \tag{2.2}$$

Power-like fall-off indicate long relaxation times of perturbations inducing stress-energy tensor fluctuations. This implies an existence of long-lived excitations, which could be understood as the field theory's low frequency degrees of freedom.

Our task now will be to discover these low energy variables adequate for hydrodynamics construction, and we shall see that they are delivered by the global continuous symmetries of the theory. We will see later in Chapter 3 how this process is mimicked in the gravity setting, where also fundamental symmetries will provide us with appropriate low energy degrees of freedom.

The global symmetries mentioned above imply in an invariant theory the existence of conservation laws, which are valid at all energy scales, starting at the fully dynamical UV sector, down to the IR or equilibrium states (we exclude anomalous cases), including supersymmetric theories. In this way any potential effective low energy description inherits certain exact features from the fundamental microscopic theory. We should stress here, that by IR in the following we mean long wavelength of (2.1), and not necessarily RG-flow IR. That is, we may speak of hydrodynamics of quark-gluon plasma as well as cold neutrons, and not just cold hadrons, which are the IR limit of QCD. Each of these systems may have its own hydrodynamical regime.

For standard Poincaré invariant theories, possibly with additional global continuous symmetries (like e.g. $U(1)$), we have mandatory charges of the momentum density current $T^{\mu 0}$ induced by the four-parametric Poincaré symmetry, and charges resulting from potential additional global (super-) symmetries J^0_a, where a labels some appropriate charge representation. The global charges are then:

$$P^\mu = \int d^3x T^{\mu 0}(x),\ N_a = \int d^3x J^0_a(x), \tag{2.3}$$

and their conservation laws are:

$$\nabla_\mu T^{\mu\nu} = 0,\ \nabla_\mu j^\mu_a = 0. \tag{2.4}$$

The above properties are fundamental and not limited to equilibrium states. The conserved charges are protected by global symmetries, which are insensitive to energy scale and dynamics details (spontaneous symmetry breaking can also be handled). Therefore we expect that any low energy configuration of the field, in particular after equilibration, should be characterized by their values, because such charges are macroscopically observable by our IR probes. For example P^μ describes the total energy or momentum of the medium (the fluid), that is, a rigid motion of the system as a whole. And indeed, this expectation is embodied in the fact that an equilibrium state described in quantum theory by the density operator is parametrized by global charges:

$$\hat{\rho} = Z^{-1} e^{\beta(u_\alpha P^\alpha + \mu_a N_a)}. \tag{2.5}$$

The charges P^μ and N_a are the only parameters that are left in the thermodynamic limit to uniquely describe the macroscopically distinguishable thermalized states. They parametrize the manifold of globally equilibrated states, just like the customary space and time independent pressure, temperature and volume in thermodynamics. The values of these charges are conjugate in the above grand canonical ensemble to the standard (constant) thermodynamic parameters:

$$\beta,\ u^\alpha,\ \text{and}\ \mu_a. \tag{2.6}$$

These are the inverse temperature, $\beta = 1/T$, velocity field[1] (with $u^2 = -1$) and chemical potential of the charges N_a. Variations of these thermodynamic parameters lead to changes of conserved charges values, which amounts to traversing the equilibrium manifold. This process is a hint for us, how to look for the proper hydrodynamic variables.

[1] We can use Poincaré symmetry to pass to the global rest frame and eliminate the spatial momentum P^α, but one can not dismiss energy P^0 like that.

Recall that we seek for the low energy effective QFT degrees of freedom that would persist in the IR limit, but simultaneously allow us to capture some of the theory's dynamics. To this end one can notice, that thermodynamic variations of equilibrium parameters (2.6):

$$\beta \to \beta + \delta\beta,\ u^\alpha \to u^\alpha + \delta u^\alpha,\ \mu_a \to \mu_a + \delta\mu_a. \tag{2.7}$$

induce global changes in values of the charges (2.3). But from a dynamical field theory perspective since they are conserved, the effects of these variations do not relax, that is, have infinite relaxation times[2]. This implies, that such variations within the *dynamic* Minkowski field theory should be retained in the IR as relevant perturbations, and one may hope that they will serve as prototypes for dynamic hydrodynamic variables.

2.1.2 Overview of gradient expansion construction

Based on the above, we see what should be done to define *hydrodynamic* fields: we must depart from the equilibrium manifold in a controlled way. If we heuristically assume, that we can consider the thermodynamic parameters (2.6) to be *slowly varying* functions of spacetime, with respect to certain scales, we can hope to stay approximately close to the equilibrium state (the equilibrium hypersurface of thermal states), but allow for local spacetime dynamics of the conserved charge densities. We thus introduce *local equilibrium* parameters, or hydrodynamic fields:

$$\beta \to \beta(x),\ u^\alpha \to u^\alpha(x),\ \mu_a \to \mu_a(x). \tag{2.8}$$

The interpretation of these fields is such that an infinitesimal piece of matter located at x^α is in thermodynamic equilibrium parametrized by the values of the local temperature $T(x)$, local chemical potential $\mu_a(x)$ and local velocity field $u^\mu(x)$. This last concept is particularly important as it introduces the idea of a co-moving or Lagrangian frame. It is defined as a frame in which the momentum density $T^{i0}(x)$ vanishes, and where the velocity vector is unit, $u^\alpha = \delta^{\alpha 0}$. Physically it is a parameter of the boost, that would have to be applied at the given spacetime point x^α to put the fluid cell into rest there[3]. Moreover, it is a timelike eigenvector of the stress-energy tensor, $T^\alpha_{\ \beta} u^\beta = -T_{00} u^\alpha$.

Since now we are out of equilibrium, the values of the fields (2.8) should be specified by the hydrodynamic equations of motion, which we are looking for. At this point however these are arbitrary functions not determined in any way by the density operator (2.5). We need to formulate further hypothesis to construct equations for them.

To this end the only equations touching upon dynamics, which at the moment we have at our disposal are the microscopically exact charge conservation laws. Thus we now have to promote them to be the actual *equations* for the new fields (2.8) (before they were just constant charges parametrizing the field theory state). To do this we need to express the charge densities $T^{\mu\nu}$ and J^μ_a through the fields 2.8:

$$T^{\mu\nu}(x) = T^{\mu\nu}(T(x), u^\alpha(x), \mu_n(x)),\ J^\mu_a = J^\mu(T(x), u^\alpha(x), \mu_n(x)). \tag{2.9}$$

This is the central step in the derivation of hydrodynamics and is referred to as postulating the *constitutive relations*. It is an analogue of thermodynamic limit. These relations contain the essence of the assumption of the QFT's hydrodynamic behaviour and represents

[2] Equilibrium thermodynamics is Euclidean so there can be no dynamics at all. Any variation there is necessarily constant in the real time.

[3] We will see in Chapter 3 how such a construction emerges in the black brane setting of fluid/gravity.

the gigantic reduction in the number of the QFT's degrees of freedom from the microscopic scale to just the few classical variables of (2.8). A guiding principle that allows us to perform consistently such an *ad hoc* operation on the QFT is the set of global symmetries, which suggested the inception of (2.8) as the low energy degrees of freedom.

Of course the relations (2.9) can not be accurate and needs to be corrected to match better the exact microscopic stress tensor. The idea behind this procedure is called *gradient expansion* and is the second crucial step in the hydrodynamics construction. In this approach the equations 2.9 are systematically corrected as a derivative expansion of the basic spacetime dependent hydrodynamic fields $T(x)$, $u^\alpha(x)$ and $\mu_a(x)$. The primary rule in finding this expansion is to write down all possible tensorial structures with a given fixed number of derivatives ∇_μ, acting on the variables (2.8) in a way consistent with symmetries of the system. Schematically it can be represented as:

$$\begin{aligned} T^{\mu\nu}(x) &\sim T^{\mu\nu}_{(0)}(T(x), u^\alpha(x), \mu_n(x)) + T^{\mu\nu}_{(1)}(\nabla_\rho T(x), \nabla_\rho u^\alpha(x), \nabla_\rho \mu_n(x)) + \dots, \\ J^{\mu}(x) &\sim J^{\mu}_{(0)}(T(x), u^\alpha(x), \mu_n(x)) + J^{\mu}_{(1)}(\nabla_\rho T(x), \nabla_\rho u^\alpha(x), \nabla_\rho \mu_n(x)) + \dots. \end{aligned} \tag{2.10}$$

One then obtains an *a priori* infinite series of terms. Such a procedure is very cumbersome due to proliferation of allowed tensors, among other problems, and poses considerable challenge. Due to this fact only low order explicit hydrodynamic expansions are know to date. Constructing it and analysing its structure at very high order is one of the subjects our Thesis. We will cover the details of the gradient expansion procedure shortly.

In the case of $d = 4$ $\mathcal{N} = 4$ SYM, which is described by AdS/CFT correspondence, the hydrodynamics is subject to an additional conformal symmetry. Such a symmetry is also approximately exhibited by the QCD plasma equation of state for $T \gg T_c$, were we are trying to mimic it with our simpler holographic theory.

A crucial consequence of conformal symmetry is tracelessness of the energy-momentum tensor:

$$T^\mu_{\ \mu}(x) = 0. \tag{2.11}$$

Apart from reducing the number of allowed tensorial structures at each expansion order, this relation provides conformal hydrodynamics with an equation of state, which otherwise would have to be inferred from e.g. experiment or lattice simulations.

Third important fact about hydrodynamics is that every contribution to the series (2.10) is endowed with a set of scalar functions called transport coefficients, which are left entirely undetermined by the described gradient expansion procedure. These functions are of fundamental interest when one wishes to apply hydrodynamics to a concrete physical system, because they encode the microscopical properties of a given fluid. The success of AdS/CFT in hydrodynamics partially stems from the fact, that it actually allows one to compute these coefficients for gauge theory possessing a holographic gravitational dual, as we shall see in the upcoming chapters.

We said above that gradient expansion can be in principle carried *ad infinitum*, leading to a series of terms representing higher and higher momenta in the evolving fluid. A crucial question, which must be asked at some point, is if the resulting series is actually convergent. We will address this point in Chapter 8.

We shall now move to more concrete example of hydrodynamic stress-energy tensor and its evolution equations.

2.1.3 Hydrodynamic gradient expansion of viscous conformal fluid

The starting point of gradient construction is the zero-derivative term, representing perfect fluid stress-energy tensor of charged fields:

$$T^{\mu\nu}(x) = \varepsilon(x)u^{\mu}(x)u^{\nu}(x) + P(x)\Delta^{\mu\nu}(x), \tag{2.12}$$
$$J^{\mu}_{a}(x) = n_a(x)u^{\mu}(x), \tag{2.13}$$

where

$$\Delta^{\mu\nu}(x) = g^{\mu\nu}(x) + u^{\mu}(x)u^{\nu}(x) \tag{2.14}$$

is the projector onto the directions transverse to the flow, $\Delta^{\mu\nu}u_{\mu} = 0$.

The above expression is identical to the stress tensor of a non-interacting ideal gas with constant energy density ε, constant isotropic pressure P and constant charge density n_a, modulo the insertion of spacetime dependence. We have indicated this explicitly in (2.12) to show the general idea: any departure from equilibrium case is *locally* undetectable from the globally static case *at this order* of the expansion. Such a procedure resembles the method of varying parameters describing some state or solution to unravel their collective dynamics[4]. In this way the global equilibrium state forms the basis for local hydrodynamic expansion.

At the present perfect fluid order we can already obtain an important formula characterising the specific type of the fluid we study: the speed of sound. In the absence of dissipation the fluid is described by just few parameters present above, which are related through an equation of state following from the conformal symmetry of the system:

$$T^{\mu}_{\ \mu}(x) = \varepsilon - (d-1)P = 0, \text{ so } P(\varepsilon) = \frac{\varepsilon}{3}. \tag{2.15}$$

The speed of sound of any conformal inviscid fluid is then obtained as follows,

$$c_s^2 \equiv \frac{\partial P}{\partial \varepsilon} = \frac{1}{d-1}, \text{ so } c_s = \frac{1}{\sqrt{d-1}}. \tag{2.16}$$

This relation is based purely on conformal symmetry, which expresses pressure $P(\varepsilon)$ as a function of energy density $\varepsilon(x)$. Since the basic fluid degrees of freedom induced by conserved charges are energy density ε and flow velocity u^{α}, we can think of pressure as a sort of zeroth order transport coefficient. We will see soon, that up to numerical coefficients conformal symmetry in fact specifies dependence of *all* transport coefficients on energy density (or effective temperature), similarly to what happened above in (2.15).

Having defined the starting point for the gradient expansion we can from this moment on[5] start constructing derivative terms to represent departures from the isotropic and equilibrium fluid. An important rule that allows one to reduce the number of possible tensors entering higher order terms is to impose strict transversality condition on anything appearing at higher expansion order. This step is quite natural, since it avoids introducing redundant terms in the expansion. Any term proportional to u^{μ} could be removed by an appropriate local boost and redefinition of $u^{\mu}(x)$. Such a condition is called Landau frame,

[4] We shall later see, that this analogy is made manifest by the fluid/gravity construction.

[5] Later we will be focused mostly on the case of uncharged fluids dynamics, so we now set $J^{\mu}_{a} = 0$ for the rest of the discussion. The procedure for this current construction is identical to the one for $T^{\mu\nu}$, just technically more involved.

and allows one to fix certain ambiguity in hydrodynamic expansion[6] [Landau 1987]. We can schematically collect all possible higher terms in the so-called viscous tensor $\Pi^{\mu\nu}(x)$ and write the full energy-momentum tensor as follows:

$$T^{\mu\nu} = \varepsilon u^\mu u^\nu + P(\varepsilon)\Delta^{\mu\nu} + \Pi^{\mu\nu}, \tag{2.17}$$

$$\Pi^{\mu\nu} u_\mu = 0. \tag{2.18}$$

Then $\Pi^{\mu\nu}$ has the following form:

$$\Pi^{\mu\nu}(x) = \sum_{n=1}^{\infty} l_{\text{mfp}}^n \Pi_{(n)}^{\mu\nu}(x). \tag{2.19}$$

The tensors $\Pi_{(n)}^{\mu\nu}(x)$ contain exactly n derivatives and are gauged by powers of the formal small parameter[7] l_{mfp}, which characterizes microscopic scale of the fluid quasiparticles scattering. Effectively each term of the above expansion is of the order of $(l_{\text{mfp}}/L)^n$, where L denotes the macroscopic fluid variations scale, $L \gg l_{\text{mfp}}$.

The explicit form of viscous tensor at first order contains only first derivatives of thermodynamic fields:

$$\Pi^{\mu\nu} = -\eta(\varepsilon)\sigma^{\mu\nu} - \zeta(\varepsilon)\Delta^{\mu\nu}(\nabla_\alpha u^\alpha). \tag{2.20}$$

The tensor $\sigma^{\mu\nu}$ is called shear tensor and is a function of the permitted velocity gradients:

$$\sigma^{\mu\nu} = 2^{\langle}\nabla^\mu u^{\nu\rangle}. \tag{2.21}$$

The operation used above is a projection onto the symmetric transverse traceless part, and is defined for arbitrary rank-2 tensor as follows:

$$^{\langle} A^{\mu\nu\rangle} \equiv A^{\langle\mu\nu\rangle} \equiv \frac{1}{2}\Delta^{\mu\alpha}\Delta^{\nu\beta}(A_{\alpha\beta} + A_{\beta\alpha}) - \frac{1}{d-1}\Delta^{\mu\nu}\Delta^{\alpha\beta}A_{\alpha\beta} \tag{2.22}$$

The scalars $\eta(\varepsilon)$ and $\zeta(\varepsilon)$ are the aforementioned first order viscous transport coefficients. The lack of temperature gradients in the expression above follows from its elimination at the given order from lower order equations of motion and from the transversality condition imposed on the viscous tensor, (2.18). For conformal fluids, in which we are interested, the so called bulk viscosity $\zeta(\varepsilon)$ has to vanish by the tracelessness condition. The dependence of η on the energy density is specified as

$$\eta(\varepsilon) = \tilde{\eta}_0 \varepsilon^{\frac{d-1}{d}}, \text{ with } \tilde{\eta}_0 \text{ constant.} \tag{2.23}$$

As we mentioned before such a dependence is determined from dimensionality by conformal symmetry, because the energy density ε is the only dimensionful quantity in absence of mass, or any other dimensionful coupling. The value of the proportionality constant $\tilde{\eta}_0$ (and analogous quantities for higher transport coefficients) depends on the microscopic

[6] Another well know choice is the Eckart frame, more well suited to processes with particle number conservation. Landau frame insists on the lack of energy dissipation. Since we are considering uncharged fluids we have $n_a = 0$, and we use Landau frame.

[7] This parameter will not show up explicitly in the series, its presence is embedded in the effective ratio of the transport coefficients and derivatives entering the expansion. The (assumed) smallness of the subsequent gradient terms could be better seen in the Fourier space, where each derivative contributes a factor of momentum, $k^\alpha \ll 1$.

dynamics of the specific QFT which has been determined at strong coupling *exactly* from the AdS/CFT correspondence, and this has been one of the many successes of the duality. The above shear viscosity coefficient is the only one present in first order conformal viscous hydrodynamics.

At second order of derivative expansion we have at our disposal many more allowed tensorial structures. A full (but looking concise due to appropriate notation) viscous tensor is [Baier 2008]

$$\begin{aligned}\Pi^{\mu\nu} &= -\eta\sigma^{\mu\nu} \\ &+ \eta\tau_\Pi\left[{}^{\langle}D\sigma^{\mu\nu\rangle} + \frac{1}{d-1}\sigma^{\mu\nu}\nabla_\alpha u^\alpha\right] + \kappa\left[R^{\langle\mu\nu\rangle} - (d-2)u_\alpha R^{\alpha\langle\mu\nu\rangle\beta}u_\beta\right] \\ &+ \lambda_1\sigma^{\langle\mu}{}_\lambda\sigma^{\nu\rangle\lambda} + \lambda_2\sigma^{\langle\mu}{}_\lambda\Omega^{\nu\rangle\lambda} + \lambda_3\Omega^{\langle\mu}{}_\lambda\Omega^{\nu\rangle\lambda}.\end{aligned} \tag{2.24}$$

The parameters τ_Π, κ, λ_1, λ_2, and λ_3 are newly introduced second order transport coefficients. Their scaling with energy density will be demonstrated below.

The above expression is valid in a general curved spacetime, with Riemann and Ricci tensors explicitly present. They are allowed now, because as we know a non-trivial curvature is made of second order metric derivatives. The transport coefficient κ is called thermal conductivity and vanishes in flat spacetime. Determining it without curved background would be more involved. We have also introduced a directional derivative D along the streamline:

$$D \equiv u^\mu\nabla_\mu. \tag{2.25}$$

Finally, the tensor $\Omega^{\mu\nu}$ is called vorticity and is an antisymmetric counterpart of the shear tensor:

$$\Omega^{\mu\nu} = \frac{1}{2}\Delta^{\mu\alpha}\Delta^{\nu\beta}(\nabla_\alpha u_\beta - \nabla_\beta u_\alpha). \tag{2.26}$$

Let us now notice, that even at second order of (more restrictive) conformal hydrodynamics there are already 1+5=6 transport coefficients. We can expect that their number will grow significantly with the growing order of the expansion, on the par with the growth of the allowed tensorial structures. The question of the nature (or strength) of this growth is of course a vital one for the theoretical definition of hydrodynamics as a closed theory and will be addressed in Chapter 7.

Expression (2.24) is the highest order of a generic hydrodynamic viscous tensor known in the case of $\mathcal{N} = 4$ super Yang-Mills theory in four dimensions, without assuming any further symmetries. In principle it is very hard to obtain such an explicit form of hydrodynamic stress-energy tensor for field theory. The are two sources of difficulty in this task. First, classifying all permitted tensorial structures is very tedious and worsened by redundancies appearing in definitions of new structures entering at each order. Second, much harder is the problem of computing exact values of transport coefficients. This in principle requires one to compute n-point correlation functions, which may have to be done at strong coupling, like in our case. In the traditional approach to strongly coupled QFT this would be almost hopeless situation, because these correlation functions have to evaluated in Minkowski signature because they contain dynamical information, and usually has been out of reach of lattice methods. In fact there has been recently certain progress in extracting dynamical data from euclidean lattice simulations through spectral decomposition and

analytic continuation of numerical correlators [Meyer 2007, Philipsen 2014]. Nevertheless, these methods are always burdened with numerical errors and systematic uncertainties. With the gauge/gravity duality, the enumeration of the allowed tensors is systematized by the conformal symmetry and Einstein equations. This simplifies hydrodynamic expansion construction, because the rules of fluid/gravity duality render this process semi-automatic as compared to the pure field theory based derivation. The exact numerical values of *a priori* all transport coefficients *at strong coupling* are then provided by solutions of Einstein equations, and it is quite a miraculous situation compared to field theories without known holographic dual.

Let us now make an interesting remark, that at second order of hydrodynamic gradient expansion we can incidentally obtain certain independent equation for the whole viscous tensor $\Pi^{\mu\nu}$ directly from its definition [Baier 2008]. The point is that by construction the equation (2.24) is valid only up to terms of the order $O(\partial^3)$. Thus we can insert into it a lower order relation, originating from the perfect fluid equations of motion and the first order viscous fluid tensor, which can easily be solved for $\sigma^{\mu\nu}$ at this order:

$$D\eta = -\eta\nabla_\mu u^\mu + O(\partial^2),\ \ \sigma^{\mu\nu} = -\frac{1}{\eta}\Pi^{\mu\nu} + O(\partial^2). \tag{2.27}$$

Upon inserting these into at least one derivative terms in (2.24) the error will be of the accepted order $O(\partial^3)$. In this way we obtain an *independent* equation for the viscous part as a whole, as if it was an independent set of degrees of freedom, not expressed through the velocity and temperature fields. The two sets of variables, perfect fluid ones, u^μ, T and viscous ones $\Pi^{\mu\nu}$ are then coupled by the fundamental hydrodynamic equation of motion, $\nabla_\mu T^{\mu\nu} = 0$. The resulting additional equation takes the form:

$$\begin{aligned}\Pi^{\mu\nu} &= -\eta\sigma^{\mu\nu} \\ &- \tau_\Pi\left[\langle D\Pi^{\mu\nu\rangle} + \frac{d}{d-1}\Pi^{\mu\nu}\nabla_\alpha u^\alpha\right] + \kappa\left[R^{\langle\mu\nu\rangle} - (d-2)u_\alpha R^{\alpha\langle\mu\nu\rangle\beta}u_\beta\right] \\ &+ \frac{\lambda_1}{\eta^2}\Pi^{\langle\mu}{}_\lambda\Pi^{\nu\rangle\lambda} - \frac{\lambda_2}{\eta}\Pi^{\langle\mu}{}_\lambda\Omega^{\nu\rangle\lambda} + \lambda_3\Omega^{\langle\mu}{}_\lambda\Omega^{\nu\rangle\lambda}.\end{aligned} \tag{2.28}$$

The reasons for presenting this derivation are that it will be useful later for computing dispersion relations of hydrodynamic perturbations and because it represents an approach to viscous tensor as an independent entity. This in turn is close to results that we will describe in Chapter 8 on generalized hydrodynamics.

2.1.4 Small perturbations of hydrodynamics

Having constructed a generic hydrodynamic tensor at second order let us now move to the last important ingredient of a hydrodynamic description of low energy QFT: linearised perturbations. Hydrodynamics is of course a nonlinear theory, but one can also analyse how small perturbations propagate in the fluid. This knowledge is crucial for understanding what are its basic effective degrees of freedom. In particular analysing perturbations unravels the causal structure of hydrodynamics by revealing the characteristic speed of information propagation in the medium. This in turn is crucial for the study of shock waves in e.g. explosions, ultrarelativistic nuclear collisions and jet Mach cone REF [Casalderrey-Solana 2006]. Moreover, dispersion relations of the linear perturbations are intrinsically related to the linear response theory and field theory's low frequency Green's functions, which are linked to transport coefficients through the Kubo's formulas [Kapusta 2006], as we shall see later.

Additionally linear perturbations allow for a (linear) stability analysis, which in the related case of weakly coupled QED plasma led to the discovery of rapid isotropisation through instability [Mrowczynski 1993]. Lastly, investigating linear perturbations played a crucial role in matching AdS/CFT to hydrodynamics.

There are three channels of linear perturbations, which lead to a specific dispersion relations for the corresponding modes. These are: scalar, shear and sound modes [Kovtun 2005]. Their names follow from their physics and corresponding equations of motion.

To investigate fluctuations we need some fixed equilibrium state in which we can induce various perturbations. In all cases below we will assume that our thermal system resides in flat Minkowski background metric, has constant temperature $T = \text{const.}$, translational invariance and remains at rest, which implies that $u^\mu = (1, 0, 0, 0)$.

2.1.4.1 Scalar channel

Scalar perturbation is obtained using linear response theory from a generic background metric perturbation, playing the role of auxiliary source, like in e.g. magnetization computations. To find it we insert the following metric perturbations into our generally covariant expressions (2.20), (2.24) (in dimension $d = 4$):

$$h_{xy} = h_{xy}(t, z). \tag{2.29}$$

Such a background metric perturbation exerts certain force on the fluid, which however remains globally at rest and its temperature is constant. The resulting hydrodynamic stress tensor of the field theory is then give by:

$$T^{xy} = -Ph_{xy} - \eta\dot{h}_{xy} + \eta\tau_\Pi\ddot{h}_{xy} - \frac{\kappa}{2}[(d-3)\ddot{h}_{xy} + h''_{xy}]. \tag{2.30}$$

Since the flat background metric and the considered thermal system are translationally invariant, the metric perturbation can be Fourier-transformed and characterized by a wave vector $k^\alpha = (\omega, 0, 0, k)$: $h_{xy}(t, z) \sim h_0 e^{-i\omega t + ikz}$. Subsequently, linear response theory [Kapusta 2006, Baier 2008] in the presence of a source $h_{xy}(t, z)$ gives us the following retarded Green's function of the stress tensor, $i\langle[\hat{T}_{xy}(0)\hat{T}_{xy}(\omega, k)]\rangle_T$ in equilibrium thermal state and momentum space:

$$G_R^{xy,xy}(\omega, k) = P - i\eta\omega + \eta\tau_\Pi\omega^2 - \frac{\kappa}{2}[(d-3)\omega^2 + k^2]. \tag{2.31}$$

This expression contains several hydrodynamic coefficients: pressure P, shear viscosity η, relaxation time τ_Π and thermal conductivity κ. At this stage they are unconstrained, but if some other way of computing $G_R^{xy,xy}$ was known, they could be identified by a simple comparison. This is exactly how the gauge/string duality is used to compute correlation functions in holographic field theory, by matching gravitational computation to expressions like the one above. We will demonstrate this procedure in the next chapter.

It should be noted here that the resulting expression for the Green's function $G_R^{xy,xy}(\omega, k)$ is regular in the low momentum limit $k \to 0$. The lack of hydrodynamic pole implies that there are no quasiparticles in the low energy limit. Accordingly, there is no hydrodynamic scalar degree of freedom in this system.

2.1.4.2 Shear channel

Second type of perturbations is called shear mode, or shear channel. It is related to the physical motion of the fluid, in which its layers flow in one direction, but momentum is transferred in the direction transverse to this motion, hence the name shear. Such a phenomenon represents genuinely viscous effects and requires at least first gradient correction to the perfect fluid stress tensor. Physically it represents gradient of velocity in the direction transverse to the flow, like in the case of shearing layers of a viscous fluid near some fixed boundary, e.g. pipe, where the flow velocity vanishes. The only non-constant hydrodynamic fields are in this case:

$$u^y(t,x),\ \Pi^{xy}(t,x). \tag{2.32}$$

In this approach we treat the whole viscous tensor perturbation as one independent set of degrees of freedom, as discussed in the last section. The stress tensor fluctuations assume now the form:

$$\delta T^{0y} = (\varepsilon + P)u^y(t,x),\ \delta T^{xy} = \Pi^{xy}(t,x). \tag{2.33}$$

First equation for this perturbation is obtained by inserting the above functions into the stress-energy tensor, (2.17) with $\Pi_{\mu\nu}$ being second order in gradients, (2.24):

$$\partial_\mu(T^{\mu\nu}_{(0\text{th})} + \delta T^{\mu\nu}) \equiv \partial_\mu(\delta T^{\mu\nu}_{(2\text{nd})}(t,x)) = 0. \tag{2.34}$$

The y-component of this equation evaluates to:

$$(\varepsilon + P)\partial_t u^y + \partial_x \Pi^{xy} = 0. \tag{2.35}$$

To close the system we use the iterated equation for the cumulated second order viscous tensor, (2.28), which upon linearisation yields

$$\tau_\Pi \partial_t \Pi^{xy}(t,x) + \Pi^{xy}(t,x) = -\eta \partial_x u^y(t,x). \tag{2.36}$$

By appropriate eliminations and Fourier transforms we arrive at dispersion relation for the shear mode:

$$\omega = -i\frac{\eta}{\varepsilon + P}k^2 + O(k^4) \tag{2.37}$$

This is an important formula, because it reveals the existence of an overdamped mode[8] in the presence of viscosity. The related fluctuation vanishes faster with time for more energetic fluctuations, $u^y \sim e^{-Dk^2 t}$, where $D = \eta/(\varepsilon + P)$ is the shear diffusion coefficient. This reflects the dissipative character of this mode.

There is also a second solution, $\omega = -i\tau_\Pi^{-1}$, but as was argued in e.g. [Baier 2008] it is not compatible with hydrodynamics, because it remains finite in the long wave-length

[8] Overdamping is a phenomenon known from a damped oscillator system, where it refers to a uniformly decaying mode without oscillations, which however takes longer to decay than e.g. critically dumped solution. In our case quadratic dependence on the momentum, k^2, means, that in the hydrodynamic limit $k \to 0$ such a mode will live longer before it decays.

limit, $k \to 0$. Only gap-less modes can be accepted in the near-equilibrium hydrodynamics, as we discussed at the beginning of this chapter.

The analysis of this paragraph will be important in Chapter 5, where we will be looking for a similar dispersion law in hope for finding instabilities in quark-gluon plasma. Here however we have just learned, that dissipation induces fast decay of certain perturbations, providing thus stabilising mechanism for the fluid.

2.1.4.3 Sound modes

The last type of fluctuation is sound channel related to the natural signal propagation mode of the fluid. It is a collective excitation of energy density, stress and longitudinal mechanical wave propagation, i.e. the sound.

Stationary equilibrium background for this mode is as before constant energy density at rest, $T_{(0)} = \text{const.}$, $u^\alpha_{(0)} = (1, 0, 0, 0)$. The excited tensor channels are

$$\delta T^{00} = \delta\varepsilon,\ \delta T^{0i} = (\varepsilon + P)u^i,\ \delta T^{ij} = c_s^2 \delta\varepsilon \delta^{ij} + \Pi^{ij}. \tag{2.38}$$

The only non-zero perturbations corresponding to the longitudinal momentum flow in one-dimensional motion are

$$\delta\varepsilon = \delta\varepsilon(t, x),\ u^x = u^x(t, x),\ \Pi^{xx} = \Pi^{xx}(t, x). \tag{2.39}$$

Energy-momentum conservation (2.24) and auxiliary equation (2.28) evaluate on these perturbation to the following coupled set of equations:

$$\begin{aligned} \partial_t \delta\varepsilon + (\varepsilon + P)\partial_x u^x &= 0, \\ (\varepsilon + P)\partial_t u^x + c_s^2 \partial_x \delta\varepsilon + \partial_x \Pi^{xx} &= 0, \\ \tau_\Pi \partial_t \Pi^{xx} + \Pi^{xx} + \frac{2(d-2)}{d-1}\eta \partial_x u^x &= 0. \end{aligned} \tag{2.40}$$

Due to the background's translational symmetry we can look as before for a common plane wave solution with wave vector $k^\alpha = (\omega, k, 0, 0)$ (since the equations are linear and separable, each wave normalization is irrelevant). We obtain in this way three solutions, which can be trusted only in the small momentum limit, up to the order to which our hydrodynamic equations are defined. We thus have two characteristic lines reflecting propagation in the left and right direction, which define the Mach cone of the fluid, i.e. the speed of sound,

$$\omega_\pm = \pm c_s k - i\Gamma k^2 \pm \frac{\Gamma}{c_s}(c_s^2 \tau_\Pi - \frac{\Gamma}{2})k^3 + O(k^4),\ \Gamma = \frac{d-2}{d-1}\frac{\eta}{\varepsilon + P}. \tag{2.41}$$

The above expression exhibits the desired hydrodynamic property of vanishing dispersion relation in the limit $k \to 0$. In the leading linear order we obtain just free plane waves propagating with the characteristic speed of sound defined before as $c_s = \partial P(\varepsilon)/\partial\varepsilon$. As we already know in conformal hydrodynamics the value of c_s follows from the equation of state $T^\mu_{\ \mu} = 0$ and is equal to $1/\sqrt{d-1}$. It can be seen from the above expression, that there is a qualitative difference between perfect and viscous fluids, because at the leading gradient-free level small perturbations propagate freely and indefinitely, whilst in a dissipative medium decaying imaginary part appears, with decay rate proportional to the shear

viscosity constant. It may be thus intuitively clear, that the question of weather quark-gluon plasma is described by a perfect or viscous fluid tensor is relevant for the proper description of RHIC collisions.

The third frequency solution has different nature,

$$\omega_3 = -i\tau_\Pi^{-1}. \tag{2.42}$$

This mode has been encountered before. It remains finite as we move towards longer wavelengths, and thus should not be considered as hydrodynamical. In fact this mode is likely not even physical, as it originates from the implicit resummation of the whole gradient expansion performed by the heuristic Israel-Stewart hydrodynamics construction. If we were analysing perturbations of the pure gradient expansion based hydrodynamics alone, even of a very high order, such a mode would not appear in the resulting spectrum. This imaginary frequency is linked to exponentially suppressed excitation, which can not be seen is a direct gradient expansion solution to IS hydrodynamics, and is found by an explicit exponential Ansatz for a solution.

Having obtained a complete description of the uncharged conformal hydrodynamics laws we will now discuss its specific realisation, which is of particular importance for the quark-gluon plasma research, as well as for a significant part of the Thesis. It is called boost-invariant hydrodynamics.

2.1.5 Boost-invariant hydrodynamics

General laws of Lorentz-covariant fluid mechanics constructed above are correct in a wide range of kinematical regimes. A particular limit which in fact allows one to solve analytically equations of ideal hydrodynamics was introduced by J.D. Bjorken in his 1983 paper on ultrarelativistic heavy ion collisions [Bjorken 1983]. Bjorken's nuclear collision model expanded upon previous nucleus matter model by Landau [Landau 1953] and since its inception gained a lot of attention. It has also been the basis of successful RHIC data analysis.

The key assumption of this model is that due to extremely high collision energy the evolution of some small cell of matter inside the nuclear fireball should not depend on the spacetime rapidity. Also the tiny bit of matter inside the collision is for some time causally disconnected with the fireball boundary, so that it can be thought of as being translationally invariant. In other words, the interior of the colliding system observed from different longitudinally boosted Lorentz frames should look the same, as at such a high (nearly "infinite") energies such boost has little effect.

It should be stressed, that general equations as exactly the same as for other kinematic regimes, and in particular transport coefficients are the same as for the finite energy collision of the same field theory. The situation is identical to the case when we assume spherical symmetry or irrotational fluid. Then in equations of motion some terms and hence transport coefficients might be absent, like in the case of vanishing vorticity tensor $\omega^{\mu\nu}$ above, but otherwise equations and microscopic degrees of freedom are the same. This simplification however allows one to carry the gradient construction of hydrodynamics *one order higher*, to third order in derivatives. This is the highest *analytic* order of hydrodynamic expansion, and was obtained using AdS/CFT correspondence [Heller 2009, Booth 2009] (for recent development see also [Grozdanov 2016a]).

It is also worth mentioning that numerous generalizations of this model were proposed, with early semi-numerical attempt by [Baym 1983] to describe less symmetric plasma configurations, which led to quantitative differences in nuclear evolution features, like smaller thermalization time.

To discuss Bjorken model it is best to adopt natural coordinates suitable for describing relativistic system: spatial rapidity-proper time coordinates. As is well known Lorentz transformations can be described as hyperbolic rotations with analogues of invariant non-negative radius and rotation angle. These are respectively given by:

$$\tau = \pm\sqrt{t^2 - z^2},\ y = \operatorname{arctanh}(z/t), \tag{2.43}$$

where the future light-cone is foliated by $\{+\tau,\ y\}$. In these coordinates boosts act naturally as translations in rapidity, $y \to y + y'$, which also represents fluid cell velocity. The boost-invariance is thus implemented in these variables as simple translation invariance in y. Any quantity depending solely on τ is hence boost-invariant. The flat Minkowski space written in hyperbolic coordinates assumes the following form,

$$ds^2 = -d\tau^2 + \tau^2 dy^2 + dx_1^2 + \ldots + dx_{d-2}^2. \tag{2.44}$$

Important feature to note about this metric is that for initial proper time $\tau = 0$ the metric has zero eigenvalue, which means that volume form vanishes and there are non-zero vectors of vanishing norm, namely the null vectors. Hypersurface $\tau = 0$ is therefore a null light-cone. It should also be stressed here for completeness, that these coordinates are curvilinear, but still flat. The connection is evaluated as $\nabla_\mu u_\nu \to \nabla_y u_y = \tau$ and this is one of the reasons for which we have been presenting hydrodynamics derivation in a manifestly covariant manner.

Bjorken model in general imposes several restriction on plasma dynamics. The complete list of enforced symmetries is the following: translational symmetry in every spatial transverse direction x_i, boost invariance along the beam direction, rotation symmetry in the transverse space and rapidity reflection symmetry $y \to -y$.

Let us first discuss implications of these symmetry assumptions on the dynamics of the energy-momentum tensor without assuming anything about the validity of hydrodynamics. In four dimensions under these assumptions the only non-vanishing components of the stress tensor are $T_{\tau\tau}$, T_{yy} and $T_{xx} \equiv T_{x_1x_1} = T_{x_2x_2}$, all of which are functions of just the proper time τ. On the top of that we demand conformal invariance, which means $T^\mu_{\ \mu} = 0$. All these constraints allow one to completely fix the flow velocity vector to be constant $u^\mu = (1, 0, 0, 0)$. This highly simplifies equations analysis because velocity is no longer a degree of freedom, but instead serves as a unique temporal vector singled out symmetries. This fact will be of use in Chapter 6.

In four dimensions, the conservation laws $\nabla_\mu T^{\mu\nu} = 0$ lead to the following relations between the remaining components of the stress tensor:

$$-T_{\tau\tau} + \frac{1}{\tau^2} T_{yy} + 2T_{xx} = 0 \tag{2.45}$$

$$\tau \frac{d}{d\tau} T_{\tau\tau} + T_{\tau\tau} + \frac{1}{\tau^2} T_{yy} = 0. \tag{2.46}$$

The equations reduce the number of independent components by two and the stress tensor is specified by just one unknown function of proper time, which can be chosen to be the energy density $\varepsilon(\tau)$:

$$T_{\mu\nu} = \begin{pmatrix} \varepsilon(\tau) & 0 & 0 & 0 \\ 0 & -\tau^3 \frac{d}{d\tau}\varepsilon(\tau) - \tau^2 \varepsilon(\tau) & 0 & 0 \\ 0 & 0 & \varepsilon(\tau) + \frac{1}{2}\tau \frac{d}{d\tau}\varepsilon(\tau) & 0 \\ 0 & 0 & 0 & \varepsilon(\tau) + \frac{1}{2}\tau \frac{d}{d\tau}\varepsilon(\tau) \end{pmatrix}. \tag{2.47}$$

One further physical requirement imposed is the non-negativity of energy density, or more generally the time-like energetic condition: for any timelike vector t^{mu} we demand

$$T_{\mu\nu}t^{\mu}t^{\nu} \geq 0 \tag{2.48}$$

This translates to the constraint on energy density rate of change:

$$-\frac{4\varepsilon(\tau)}{\tau} \leq \varepsilon'(\tau) \leq 0. \tag{2.49}$$

Later we will find this condition to be moderately violated during highly non-equilibrium initial stage of plasma expansion. Nevertheless we expect it to hold in the late time hydrodynamic regime.

Is should be stressed, that the reduced form (6.92) does not assume any sort of equilibrium and is completely general, within the symmetries bounds. In particular the function $\varepsilon(\tau)$ may not be related to hydrodynamics at all. We additionally note, that due to velocity vector fixed constant there is no vorticity and also background metric is flat, so λ_2, λ_3 and κ coefficients must be absent in this model.

Let us now write down the hydrodynamic equations of Bjorken flow in general dimension:

$$D\varepsilon + (\varepsilon + P)\nabla_{\mu}u^{\mu} + \Pi^{\mu\nu}\nabla_{\mu}u_{\nu} = 0. \tag{2.50}$$

This time $\Pi^{\mu\nu}$ is treated in a standard non-iterated way, using its conventional gradient definition (2.24). Using the fact, that for conformal fluid $P = \varepsilon/(d-1)$ we have simply that

$$\partial_{\tau}\varepsilon + \frac{d}{d-1}\frac{\varepsilon}{\tau} = \tau\Pi^{yy}(\varepsilon). \tag{2.51}$$

This equation can be solved perturbatively in $1/\tau$, in the late time expansion $\tau \to \infty$ starting from perfect fluid equation with viscous tensor absent. This is exactly what should be done according to hydrodynamic approach. The leading solution takes the asymptotic form:

$$\varepsilon(\tau) = C\tau^{-2+\nu} + o(\tau^{-2+\nu}),\ \nu \equiv \frac{d-2}{d-1}. \tag{2.52}$$

and C is integration constant, whose meaning will be clarified later in Chapter 6. Even if we found an exact solution to the non-linear ODE above, we would be allowed to trust it only up to the asymptotic expansion of the same order as the equation used to find it. Having found the leading initial solution we can compute the form of the non-vanishing component of the viscous tensor Π^{yy} using (2.24):

$$\Pi^{yy} = -2\nu\eta\tau^{-3} - 2\nu^2(\eta\tau_{\Pi} - 2\lambda_1\frac{d-3}{d-2})\tau^{-4} + O(\tau^{-5}). \tag{2.53}$$

As we know, the various transport coefficients present in the above formula are in fact functions of energy density of the form dictated by the conformal symmetry:

$$\eta = C\eta_0 \left(\frac{\varepsilon}{C}\right)^{(d-1)/d}, \ \tau_\Pi = C\tau_\Pi^0 \left(\frac{\varepsilon}{C}\right)^{-1/d}, \ \lambda_1 = C\lambda_1^0 \left(\frac{\varepsilon}{C}\right)^{(d-2)/d}. \tag{2.54}$$

In the above we have conveniently introduced reduced dimensionless constant transport coefficients, and defined them to include C in a way removing energy density's leading normalization.

Using our leading order solution and the above relations we can obtain the explicit form of the viscous tensor Π^{yy} and insert it back into (2.51), to compute the first subleading viscous correction. Since Π^{yy} is of second order in derivatives, the total error will be of the order ∂^3, which is acceptable[9].

The resulting asymptotic solution of the equation (2.50) is finally obtained as

$$\frac{\varepsilon(\tau)}{C} = \tau^{-2+\nu} - 2\eta_0\tau^{-2} + \left[\frac{2(d-1)}{d}\eta_0^2 - \frac{d-2}{d-1}\left(\eta_0\tau_\Pi^0 - 2\lambda_1^0\frac{d-3}{d-2}\right)\right]\tau^{-2-\nu} + ... \tag{2.55}$$

The numerical constants present in the above solution must be provided by some microscopic theory, as was mentioned before. We shall do this later using gauge/string duality in the form of fluid/gravity correspondence. Also, there exists a one order higher expression for the energy density (2.55), but we shall not present its (analogous) derivation here. It can be found in e.g. [Heller 2009, Kinoshita 2009, Booth 2009]. This third order solution will be used in later chapters.

2.1.6 Hydrodynamics from Boltzmann equation

To close this general introduction to hydrodynamics we will now very briefly describe one last method of its construction for a given system from kinetic theory. We shall only glance through the main conceptual points in this involved derivation, whose details can be found in e.g. [Stewart 1971, Brandt 1995]. We are only interested in exemplifying how tensorial structure of hydrodynamics *along with* transport coefficients are accessible at weak coupling.

The discussion given above is valid for arbitrary coupling strength, like for the nuclear plasma matter in RHIC. Such regimes in direct approach have no known stable quasiparticles that could be used to describe the system perturbatively. However in a weakly coupled regime one can construct hydrodynamic approximation to finite temperature field theory state from first principles using Boltzmann equation, where one has access to exact microscopic degrees of freedom. The advantage of such an approach is that one can approximately compute various transport coefficients. Moreover, in kinetic theory one is not limited to equilibrium states and can in addition access non-equilibrium configurations. On the downside of this approach, due to the complexity of full Boltzmann hierarchy there is a central problem of specifying what simplified model of particle interactions and distribution functions should one adopt for computations. This introduces certain ambiguity which ultimately again has to be fixed by comparison to e.g. experimental data.

To begin with, as we already know the hydrodynamic approximation amounts to stating that field theory energy-momentum tensor assumes a certain specific form resembling the

[9] We remind here, that the formal hydrodynamic expansion parameter is $(\nabla)/T \sim \tau^{-2/3}$, for the leading solution behaving like $T \sim \tau^{-1/3}$. Also, to check the scaling of Π^{yy} with proper time, one has to remember about the coordinates transformation between $\{t, z\}$ and $\{\tau, y\}$ variables. It gives an extra factor of $\tau^{-2} \sim (\partial y/\partial z)^2$ for a second rank tensor $\Pi^{\mu\nu}$.

thermodynamic limit. Equilibrium states corresponding to this are characterized by one-particle distribution function in phase space $f(p,x)$ obeying classical Boltzmann equation, which in curved spacetime take the following form:

$$\left[p^\mu \frac{\partial}{\partial x^\mu} - \Gamma^\lambda_{\mu\nu} p^\mu p^\nu\right] f(p,x) = -\mathcal{C}[f]. \tag{2.56}$$

The whole merit of using this approach to describe field theory state lies in the structure of the term $\mathcal{C}[f]$ called the collision integral and the structure of the form factor $f(p,x)$. The collision integral encodes information on the type of interactions and couplings of the field theory under consideration. Knowing it exactly is part of the problem signalled above and one usually adopts some justified Ansatz for it. The statement of being close to equilibrium requires further assumption on the split of distribution function $f(p,x)$ into its equilibrium $f_{\text{eq}}(p,x)$ and non-equilibrium $\delta f(p,x)$ parts, and suitable parametrization of the equilibrium part, which introduces hydrodynamic temperature and velocity fields:

$$f(p,x) = f_{\text{eq}}(-u(x)\cdot p/T(x))(1+\delta f(p,x)). \tag{2.57}$$

In principle for a generic form factor $f(p,x)$ a whole sequence of hydrodynamic equations can be obtained by taking moments[10] of the Boltzmann equation (2.56) with respect to the particle momentum p^μ. The zero-th moment

$$\int d\chi \equiv \int d^4\delta(-p^2)\theta(p^0), \tag{2.58}$$

of the equation (2.56) upon integrating by parts leads to:

$$\nabla_\mu \int d\chi p^\mu \sqrt{-g} f(p,x) = -\int d\chi \sqrt{-g}\mathcal{C}[f]. \tag{2.59}$$

For a theory with conserved charges or only elastic collisions the integral of the collision term on the right hand side vanishes [Baier 2008], and one arrives at the familiar conservation of the particles current, $\nabla_\mu j^\mu = 0$. Next, taking first moment $\int d\chi p^\mu$ of the Boltzmann equation yields the relation defining stress-energy tensor conservation:

$$\nabla_\mu \int d\chi p^\mu p^\nu \sqrt{-g} f(p,x) \equiv \nabla_\mu T^{\mu\nu} = 0. \tag{2.60}$$

One can carry this procedure further, which leads to infinite Boltzmann hierarchy of chained moments equations. If one could solve them order by order, one could recover the full distribution function $f(p,x)$. In practise we must use approximations (2.57) mentioned above for the near-equilibrium particle distribution functions. Under certain assumptions one can introduce a tensor field $\Pi^{\mu\nu}(x)$ in the non-equilibrium part $\delta f(p,x)$, which encapsulates dissipative effects:

$$\delta f(p,x) \sim T^{-6} p^\mu p^\nu \Pi_{\mu\nu}. \tag{2.61}$$

[10] We are only interested in conformal hydrodynamics, which requires massless particles, so the projector is onto positive energy null momenta.

By taking moments of such a particle number distribution one can derive an expression for $\Pi^{\mu\nu}$ similar to the one encountered before in the hydrodynamic gradient expansion:

$$\Pi^{\mu\nu} = -\eta\sigma^{\mu\nu} - \tau_\Pi \left[D\Pi^{<\mu\nu>} + \frac{4}{3}\Pi^{\mu\nu}(\lambda \cdot u) \right] + 2\tau_\Pi \Pi^{\alpha(\mu}\Omega^{\nu)}_{\ \alpha} + \frac{\lambda_1}{\eta^2}\Pi^{\alpha<\mu}\Pi^{\nu>}_{\ \alpha}. \qquad (2.62)$$

This formula is one of the reasons for which we describe the Boltzmann approach to hydrodynamics. It contains transport coefficients like the ones we have seen before, but of *different* values. In particular we can notice, that here $\lambda_2 = -2\tau_\Pi\eta$, $\lambda_3 = 0$ and $\kappa = 0$. In other words, weakly coupled hydrodynamics has similar tensorial structure as the strongly coupled one, but mechanical properties of such a fluid are different. One thus concludes, that indeed another approach is necessary to construct hydrodynamics for strongly coupled field theory.

Another virtue of Boltzmann equation is the access to strongly non-equilibrium states of field theory, which is difficult from purely thermodynamic point of view. An example of such an application is the derivation of tensorial structures of the stress tensor in such a non-equilibrium regime given in e.g. [Florkowski 2011, Florkowski 2013]. By an appropriate parametrization of the particles density $\delta f(p, x)$ one derives their stress-energy tensor not originating from near-equilibrium gradient expansion. This result is particularly interesting in view of the results of [Heller 2014], which we will describe in Chapter 8 on effective non-equilibrium causal hydrodynamics generalization.

2.2 Closing remarks

In this chapter we have made an attempt at concisely introducing ideas, notion and important details of the hydrodynamic approximation to evolving near-equilibrium state in quantum field theory at arbitrary coupling. The main systematic approach leading to arbitrary high order gradient expansion has been described to prepare background for upcoming chapters, where effectively *infinite order* hydrodynamics will be analysed along with evolution of strictly non-equilibrium (non-hydrodynamical) degrees of freedom.

An important lesson is that while we are able to construct tensorial structures and even solutions to simplified non-linear equations of motion, at strong coupling we are forced to rely on some external source of information, which must supplement our effective theory derivation with microscopic information cumulated in transport coefficients. This data will be provided by the AdS/CFT correspondence, which we shall introduce in the next chapter.

Chapter 3

AdS/CFT Correspondence

3.1 Introduction

In this chapter we will survey the fundamental ingredients of the gauge/string duality. The first part of the review will be necessarily brief and synthetic as the topic is vast, well established in theoretical physics by now and the relevant detailed literature is abundant. The second part will concentrate on the thermal field theory region of the correspondence, which will conclude with more detailed discussion of the fluid/gravity duality mechanisms. The general aim is to first give a broader perspective on what AdS/CFT duality is and then to introduce only the technical tools of the correspondence that we would need in the present Thesis.

As a brief historical background let us describe how AdS/CFT emerged. String theory originated as a model aiming to describe strong (nuclear) interactions in the confusing era of 1960's discoveries, when myriads of new strongly interacting particles and states were being discovered [Witten 2012]. These phenomena had features seemingly incompatible with quantum field theory, like certain dualities in scattering amplitudes and Regge trajectories, stating, that spectrum of states m should roughly form families parametrized by angular momentum J of particles:

$$m^2 \sim J\alpha'. \tag{3.1}$$

with α' being the famous Regge slope. The suggestion was to use an extended object, a string vibrating at the length scale of nuclear physics and reproducing spectrum of states. Unfortunately among other problems this model failed at reproducing all the required scattering amplitudes properties and was rejected in favour of QCD.

However a surprise came when it was realised, that the theory developed on this basis was able to manufacture a massless spin-2 state coupled naturally to other states in the theory. By reducing typical lengths to the Planck scale it appeared, that one might be able to derive a unified theory of gravity. However further problems arose, with the unphysical negative mass squared state of Tachyon, and more gruesome Lorentz symmetry anomaly, which hampered progress for some time. The solution came with an advent of superstring theory and anomaly cancellation calculation, which spurred the so-called superstring revolution of the 1980's. The solution is to some taste very elegant and determines what should be the physical spacetime dimension (as the only theory in physics). It was found, that ten is the only spacetime dimension, in which supersymmetric string theory is fully consistent and free of Tachyon instability. One such a theory called type IIB chiral superstring is our master framework, within which everything we are going to discuss takes place. Second crucial progress came with the unexpected discovery of large non-perturbative objects hidden in the light of the string theory, the D-branes. Termed unseen elephants roaming in the room these new elements of the superstring theory discovered in early 1990's brought non-abelian gauge theories into the string theory picture.

In our context their main feature was that, put simplistically (by an account of a witness from that time), D-branes were monopoles of the theory and 'people did, what one does with

a monopole - they started scattering stuff on D-branes'. By computing scattering cross-section of a closed string in 10-dimensional D-brane background a surprising behaviour was found, that the string absorption cross-section behaves as

$$\sigma(\omega) \sim \omega^3, \tag{3.2}$$

where ω is the energy of the string. This means, that probability of graviton-D-brane interaction vanishes with decreasing energy. In other words, closed strings decouple from D-branes at low energies. As a result two subsystems being initially parts of the same theory, the D-brane and its surrounding spacetime with closed strings seem to become disconnected. However it appears that a non-trivial link between the two subsystems survives the decoupling. This point is the heart of the AdS/CFT discovery, which we will describe in more detail in Section 3.5.

3.2 $\mathcal{N} = 4$ super-Yang-Mills theory in four dimensions

Let us begin by reviewing the key features of the particular field theory playing the major role in the correspondence and our applications. As we mentioned in the introduction with the discovery of D-branes it was found, that one can construct a non-Abelian supersymmetric gauge theories using certain string theory states. The most important example of such a theory is the maximally supersymmetric $SU(N)$ $\mathcal{N} = 4$ super-Yang-Mills theory in four dimensions [Sohnius 1978]. It is called maximally supersymmetric because in $d \geq 4$ SUSY algebra higher than $\mathcal{N} = 4$ it would force inclusion of massless field of spin higher than one, which would lead to a gravitational theory. Its Lagrangian is given by

$$\begin{aligned}\mathcal{L} \;=\; \mathrm{tr}\Big\{ & -\frac{1}{2g^2} F_{\mu\nu}F^{\mu\nu} + \frac{\theta_I}{8\pi^2} F_{\mu\nu}\tilde{F}^{\mu\nu} - \sum_a i\bar{\lambda}^a \bar{\sigma}^\mu D_\mu \lambda_a - \sum_i D_\mu X^i D^\mu X^i \\ & + \sum_{a,b,i} g C_i^{ab} \lambda_a [X^i, \lambda_b] + \sum_{a,b,i} g \bar{C}_{iab} \bar{\lambda}^a [X^i, \bar{\lambda}^b] + \frac{g^2}{2} \sum_{i,j} [X^i, X^j]^2 \Big\}. \end{aligned} \tag{3.3}$$

The Yang-Mills coupling is g and is dimensionless. θ_I is the instanton angle. The field content of this theory is $\mathcal{N} = 4$ gauge supermultiplet and in $d = 4$ is uniquely specified by supersymmetry:

$$\begin{aligned} A_\mu^a(x) \;&:\; SU(N) \text{ adjoint gage field, } SU(4)_R \text{ singlet} \\ \lambda_a,\ \bar{\lambda}^a \;&:\; \mathbf{4} \text{ and } \bar{\mathbf{4}}\ SU(4)_R \text{ left Weyl fermions in the adjoint of } SU(N),\ a = 1..4, \\ X^i \;&:\; \text{six real } SO(6) \text{ scalars in the adjoint of } SU(N),\ i = 1..6. \end{aligned} \tag{3.4}$$

Full global continuous symmetry of the theory is the superconformal group $SU(2,2|4)$, containing:

$$\text{Conformal group} \;:\; SO(2,4), \tag{3.5}$$

$$\text{R-symmetry} \;:\; SO(6)_R \sim SU(4)_R, \tag{3.6}$$

$$\text{Poincaré supersymmetry} \;:\; \mathcal{N} = 4, \tag{3.7}$$

$$\text{Conformal supersymmetry.} \tag{3.8}$$

The indices $i = 1..6$ and $a = 1..4$ in $\mathcal{L}$ are related to the listed above internal supersymmetry automorphism group $SO(6)_R$ called R-symmetry. It is a global continuous symmetry rotating supercharges (SUSY generators) into each other, and for extended supersymmetry

like $\mathcal{N} = 4$ it is usually non-abelian. R-symmetry induces a conserved current and one can consider its $U(1)$ subgroup. We shall be interested in this particular case in Chapter 5.

Depending on the values of scalar fields X^a the theory can have two phases, the superconformal point

$$\langle X^i \rangle = 0 \ \rightarrow \ -g^2 \sum_{ij} \int \mathrm{tr}[X^i, X^j]^2 = 0, \tag{3.9}$$

and the Higgs phase (called also Coulomb branch),

$$\langle X^i \rangle \neq 0. \tag{3.10}$$

In the former case the gauge group $SU(N)$ as well as the full symmetry group $SU(2,2|4)$ remain intact, while in the latter one we observe spontaneous symmetry breaking of $SU(N)$, while the scale of $\langle X^i \rangle$ VEV breaks also the superconformal group.

We will work exclusively with the above field theory above the superconformal vacuum. Many other theories can be constructed using AdS/CFT correspondence, like the $\mathcal{N} = 2^\star$ or ABJM superconformal Chern-Simons gauge theories. But QCD near-conformal heavy-ion plasma system we wish to model can be most simply approximated with the aid of $\mathcal{N} = 4$ super-Yang-Mills. It has also several distinctive properties making it very interesting object of study of its own. The most crucial one is that it remains conformal both classically and quantum mechanically once we are in the conformal phase (in which we will only be interested in). It is so by the remarkable property of supersymmetry-led protection, which renders the β function one-loop exact. It is found to be vanishing exactly to all orders:

$$\beta = 0. \tag{3.11}$$

Owing to this there is no dynamical scale generation nor running coupling, the interaction strength can be set at will through the dimensionless coupling constant.

Being non-abelian gauge theory in four dimensions makes super-Yang-Mills quite a good approximation to real world QCD. There are however important differences, which we must keep in mind using any results we are going to derive later from holography. The most important differences include

- Supersymmetry,
- No asymptotic freedom,
- Conformality,
- No matter in fundamental representation,
- No chiral symmetry breaking,
- No confinment, no phase transition,
- Large N in AdS/CFT context.

Some of these differences become less relevant in the particular physical system we are going to analyse. In the presence of finite temperature supersymmetry is broken by different boundary conditions imposed on fermions and bosons at the thermal circle. Temperature introduces an explicit scale, which becomes the only relevant one, due to the strict conformality of the theory. Quark-gluon plasma in QCD is in the deconfined phase and is dominated by glue, which further narrows the gap with large N non-confining SYM. Lastly, QCD in the physical temperature range beyond the confinment, $T \geq 1.5T_c$ exhibits nearly conformal stress-energy tensor (the so-called conformal window), alleviating the strict SYM conformality problem. There are more subtle differences regarding e.g. detailed perturbative scattering processes [Huot 2007, Caron-Huot 2008]. However as a tool to understand qualitatively properties of non-perturbative thermal non-abelian gauge theory in real time, as long as we stay above and away from T_c, super-Yang-Mills provides us with an excellent theoretical laboratory with explicit simple computational framework of AdS/CFT, and we shall use it to see what one might at all expect of gauge theory fluid at strong coupling.

3.3 String theory preliminaries

Let us now come back to the topic of D-branes mentioned in the introduction to explain how AdS/CFT, or gauge/string correspondence is introduced. First we need a few general mandatory remarks on the string theory construction to lay out standard terminology used in the field.

Formally superstring theory is a theory of extended objects going beyond the notion of a point as its basic constituent. Classically it considers one dimensional[1] finite line segments, i.e. strings propagating in spacetime,

$$X^\mu : \{\tau, \sigma\} \to \mathbb{R}^D, \ \sigma \in [0, \pi], \ \tau \in \mathbb{R} \tag{3.12}$$

embedded in a classical background of arbitrary dimension

$$G^{MN} = \eta^{MN}, \ M, N = 0..D-1. \tag{3.13}$$

The so-called world-sheet coordinates $\{\tau, \sigma\}$ parametrize the surface of the string, which is seen in the embedding space as a set of spatial intervals merged into a timelike stripe, which for a free string can have either two edges or cylindrical topology. The corresponding theories are called open and closed strings. The simplest action describing the system is the famous Nambu-Goto proper area functional

$$S = \frac{1}{2\pi\alpha'} \int \mathrm{d}\tau \mathrm{d}\sigma \sqrt{X'^2 \dot{X}^2 - (\dot{X} \cdot X')^2}, \ \dot{X} = \partial_\tau X, \ X' = \partial_\sigma X, \tag{3.14}$$

with $2\pi\alpha' = T$ called the string tension and α' called the Regge slope, reminiscent of the primal application to strong physics. It is related to the **only** dimensionful parameter in the whole string theory, the Planck length: $\alpha' = \ell_P^2$. It is worth stressing, that contrary to our customary field theories like the Standard Model, all other properties and parameters describing physics are in string theory generated, and not put in by hand, apart from the overall scale ℓ_P.

The Nambu-Goto action is highly non-linear. There is however a way to recast it in a much more tractable form of the non-linear sigma model, called in this context the Polyakov

[1] One can, and one does, in principle consider higher dimensional objects, but upon quantisation it appears, that two dimensional objects quantisation is free of pathologies plaguing other possibilities of the so-called membranes, [Becker 2006].

action [Witten 2012]

$$S = -\frac{T}{2}\int \mathrm{d}\tau\mathrm{d}\sigma h^{ab} G_{MN}(X)\partial_a X^M \partial_b X^N,\ a,b = 0,1, \tag{3.15}$$

with h^{ab} being newly introduced non-dynamical world-sheet metric, necessary to rewrite Nambu-Goto action in the above form. The crucial feature of this theory is that it enjoys many symmetries, including conformal, Weyl and diffeomorphisms invariance. These are the sources of computational power of string theory as it largely reduces to two dimensional conformal field theory, where conformal group is extremely powerful. The full formulation of the theory requires also inception of fermionic supersymmetry world-sheet fields, ghosts and many other details, which we will not cover here and which can be found in many excellent positions of the literature on string theory, e.g. [Witten 2012, Blumenhagen 2012, Polchinski 1998].

Classical equations of motion following from the Polyakov action require boundary conditions on the fields $X^M(\tau,\sigma)$. As we mentioned these can be periodic, for the closed string, or can be imposed at the two distinct ends of the string. This point is essential. For some time the only accepted choice for the open string was the freely moving Neumann condition, because of the requirement of Poincaré invariance. The other possibility of fixed-end Dirichlet condition seemed to violate i.a. translational invariance of empty embedding space, and as such was discarded as unphysical. However in 1995 it was realized by Polchinsky, that there are good reasons to violate this symmetry by inclusion of new physical objects into the theory, namely the D-branes, on which the open string can (and must) end. The role of a D-brane is similar to that of a monopole (e.g. electron) in standard field theory. D-branes are $(p+1)$ dimensional hypersurfaces in the embedding space $\mathbb{R}^D$, where strings terminate, and along which they can freely propagate. They have also additional properties, which we will cover in the next section. As a technical remark, let us note, that to indicate the dimensionality of the D-brane sometimes they are called Dp-branes, which corresponds to the mentioned $(p+1)$ worldvolume of the brane. This means, that the Dp-brane has p spatial dimensions, but also propagates through time, hence the +1 (in this language the ordinary string would be called a D1-brane).

Before moving on let us say, that strings can propagate not just in a flat Minkowski space, but in more general so-called background fields. The simplest of these is curved spacetime $G^{MN} = G^{MN}(X)$, as opposed to Minkowski space $G^{MN} = \eta^{MN}$. Such a substitution in (3.15) results in a non-trivial X^M field dynamics, which makes the theory generically difficult to solve. There are nonetheless examples, when this can be done exactly, and these include $AdS_5 x S^5$ spacetime as well as the so-called PP-wave background.

We can however generalize (3.15) even further. We can consider other classical fields in the embedding space and think how would they interact with the string subject to their influence. This question is in exact analogy to to considerations of how to couple a classical point particle to e.g. external magnetic or electric fields. The way to think of it is to analyse what tensor structures one can build out of the world-sheet fields $X^M(\tau,\sigma)$, the metric $h^{ab}(\tau,\sigma)$ and their gradients, and how to couple them to the external tensors. It appears, that string can interact with a variety of background fields, with many more possibilities that just gauge potential as for an ordinary point particle. We can consider the so-called dilaton field, which is spacetime scalar $\Phi(X)$. We can have the so-called B-field, which is rank 2 antisymmetric tensor $B_{\mu\nu}(X)$. Importantly we can also have the so-called Ramond gauge p-form fields, which are generalizations of the $U(1)$ gage potential A_μ to higher rank forms: $A_{\mu_1..\mu_p}(X)$ (with totally antisymmetric indices). These are subject to abelian gauge transformations,

$$A'_p \sim A_p + d\phi_{p-1}. \tag{3.16}$$

Each A_p Ramond field gives raise to its field strength form

$$F_p = dA_{p-1} \tag{3.17}$$

and the resulting theory is to some extent similar to ordinary electrodynamics. In particular Ramond potentials sport standard conserved charges defined by flux integrals over appropriate spacetime hypersurfaces:

$$Q_p^{RR} = \int_{\Sigma_p} F_p. \tag{3.18}$$

We shall soon see how prominent role these bizarre objects play in the correspondence.

These various possible coupling can be summarized by writing the superstring Polyakov action in a more general form including some of the background fields. The bosonic part including the dilaton, and B-field is

$$S_x = \frac{1}{4\pi\alpha'} \int_\Sigma \sqrt{h} \Big[\{ h^{ab} G_{MN}(X) + \varepsilon^{ab} B_{MN}(X) \} \partial_a X^M \partial_b X^N + \alpha' R_h^{(2)} \Phi(X) \Big] \tag{3.19}$$

Here $R^{(2)}$ is the two dimensional Ricci scalar of the metric h_{ab}, whose determinant we denote by h. The fermionic part is considerably more involved and we shall not give it here explicitly (see e.g. [D'Hoker 2002, Di Vecchia 2000, Di Vecchia 2003]).

Before moving to D-branes we shall make few last important words of comment concerning superstrings *per se*. Firstly, we have seen that string theory in flat spacetime seems to define a non-interacting two dimensional field theory. One may ask, how then all those famous interacting low energy effective supergravity theories come from? How do we impose interactions upon strings? Secondly, we have argued that one can insert into (3.15) some background tensor fields taken out of the blue sky and expect to still have a well defined theory. Is that assertion correct? The answer to these objections is delivered by one of the more amusing and unexpected mechanisms one can experience in physics. Firstly, we need to ask how do we actually quantize the string theory? It is done via path integrals using the Polyakov action. The formula for quantum amplitudes is schematically given by

$$\langle \text{Amplitude} \rangle = \sum_{\text{top}} \int \mathcal{D}h_{ab} \mathcal{D}\chi_c \int \mathcal{D}X^M \mathcal{D}\psi e^{-S_x + S_\psi}, \tag{3.20}$$

where just for completeness we have included in the measure the other superstring world-sheet fields: the gravitino χ_c, the fermions ψ, and also standard bosonic string coordinate field X^M and the metric h_{ab} (there could also be ghost fields for the BRST quantisation). The crucial point is that since we are integrating over all possible string world-sheet metrics we should in fact include all possible two-dimensional topologies. This amounts to saying, that instead of a simple infinite strip or cylinder one can have multiple splits and joining of the string world-sheet, in direct analogy to the field theory Feynman graphs. The structure of the path integral is understood better if we assume the dilaton field Φ to be non-zero and constant, e.g. $\Phi_0 = \varphi$. Then the two dimensional integral of Ricci curvature in S_x gives just the Euler characteristics of the string world-sheet (for the closed string):

$$\frac{\Phi_0}{2\pi} \int_\Sigma \sqrt{h} R_h^{(2)} = \Phi_0 \chi(\Sigma) = \varphi(2 - 2\mathrm{h}), \tag{3.21}$$

where h is the number of handles in the surface. The crucial point is now that each term of h is accompanied by φ and one can effectively expand the amplitude path integral in $e^{(2-2h)\varphi}$. In this way we see, that the dilaton field plays the role of string interaction

coupling constant, $g_s = e^{\varphi}$, and the given string surface genus plays the role of the loop order. In this way we discover genuine interactions among strings induced and organized by the dilaton background field. We can say therefore, that string theory generates its own coupling constant dynamically as a background field [2].

Having observed that the dilaton serves as a coupling we can also notice, that the other classical background fields can be though of as effective coupling generating functions. We could e.g. expand the classical background metric field $G^{MN}(X)$ in powers of X^M and observe, that it introduces infinitely many factors of X^n_M with some coefficients, akin to higher coupling in the string action. The reason for which we give this lengthy discussion will soon be revealed: we can try to compute quantum β functions for the background fields regarding them as running couplings of the quantum string theory. Of course since the string theory is conformally invariant on the world-sheet we should demand, that all these β functions vanish. Let us see what condition follows from this procedure for the background metric field G^{MN}, [D'Hoker 2002]. By defining

$$\beta^G_{MN}(X) = \frac{\partial G_{MN}}{\partial \ln \Lambda} \tag{3.22}$$

we get

$$\beta^G_{MN} = \frac{1}{2} R_{MN} - \frac{1}{8} H_{MAB} H_N{}^{AB} + \partial_M \Phi \partial_N \Phi + O(\alpha'), \tag{3.23}$$

and for conformal anomaly free quantum string theory we should impose $\beta^G_{MN} = 0$.

This expression truncated at the order α' is nothing but a piece of type IIA supergravity (i.e. Einstein) equations with source fields. H is the strength tensor for the B-field, $H = \mathrm{d}B$. We arrive at the advertised answer, that string theory based on the conformality constraint puts self-consistency conditions on all the possible background fields, on which the string can at all propagate. This is the origin of the supergravity approximation to the low energy string effective action, which we shall use in the next section to discover AdS/CFT. The mechanism described above shows, that from seemingly free theory one obtains a unique set of classical interacting physics equations, which happen to be exactly the laws of general relativity, i.e. we have derived Einstein's theory from string theory as the vanishing of its quantum beta function. What is even more exciting however, is that at the same time we see how string theory can produce consistent classical corrections to General Relativity: by computing higher α' terms of β^G_{MN} we would obtain gradient corrections to Einstein equations in the form of higher curvature terms.

3.4 Gauge theories emergence from superstrings

Let us now describe in a little more detail, how the $\mathcal{N} = 4$ super-Yang-Mills and supergravity theories emerge from certain limits of the type II B superstring theory in ten dimensions. We have already signalled in Section 3.2, that d-dimensional non-Abelian gauge theory can be derived form Dp-branes. As we mentioned above Dp-branes are dynamical objects in string theory, on which open strings worldsheets can terminate. The tension of such a string is related to its mass. The more stretched the string, the more massive state it represents. Open strings attached to a D-brane can also interact with closed strings propagating in the space surrounding the Dp-brain. In particular D-brane can emit or absorb a closed string, for instance in a process when two open strings scatter on the D-brane, and upon joining depart from it. We have referred to this process in the Introduction,3.1.

[2] To be honest here we have just inserted the Φ field by hand, but it actually originates from the string spectrum in the first place. We shall not describe this process here due to the lack of space.

The spectrum of open superstring states very roughly behaves as

$$m^2 \sim \frac{n}{\alpha'}, \; n = 0, 1, 2, \ldots, \tag{3.24}$$

where the natural number n is related to the string excitation level (recall that for the IIB superstring the negative mass squared tachyon is absent), and this pattern is remotely similar to the harmonic oscillator spectrum. As we know from string theory [Witten 2012] these excitations correspond to various tensor fields constructed as products of creation operators entering the solutions $X^M(\tau, \sigma)$ to the Polyakov action Euler-Lagrange equations of motion. These tensor fields have dispersion relations implied by the symmetries and GSO projections used to construct the physical Hilbert space of quantum states.

The mass formula contains the familiar parameter α'. It is interesting to observe what happens, if we consider the limiting case, when $\alpha' \to 0$. It is readily seen, that all non-zero masses become infinitely heavy and effectively decouple from the theory. However the massless modes remain. This sector of the theory corresponds inter alia to gauge fields. Intuitively, they are localized on the D-brane, because their zero masses correspond to the minimal stretching (with endpoints of the strings attached to the Dp-brane). We can consider also a more complex geometric setup, involving N Dp-branes, which can then be connected by open string with endpoints attached to *different* D-branes. Still, we can consider in such a situation the limit $\alpha' \to 0$, which leaves us with the massless sector. The crucial point is now that if we consider the case, when the N Dp-branes approach each other and eventually meet at one spatial point, all the endpoints of open strings again propagate over the same manifold. *But*, a trace of the original setup remains, in the so-called Chan-Patton factors matrices. Very roughly these represent the initial pattern of open strings connections, with index (i, j) of the matrix stating, that the string connects Dp-brane i to Dp-brane j. This is exactly where the non-Abelian gauge theory comes from, as it turns out that such a construction for the massless spectrum sector leads to a local gauge symmetry $SU(N)$. Additionally if we consider $p = 3$ case of D3-brane, in the limit of coalescing D3-branes the string theory configuration turns out to possess $\mathcal{N} = 4$ superconformal symmetry (in the case of type IIB superstring). Now the final crucial point is the following. All we said concerned the full string theory configuration with a Dp-brane, although in a specific limit $\alpha' \to 0$. Having realised, that we are left with the purely massless sector we could wish to formulate an effective theory of the low energy massless excitations of the Dp-brane. It indeed happens to be possible, [Tseytlin 1997, Di Vecchia 2000], and the D3-brane case of a resulting theory is exactly the aforementioned four-dimensional $\mathcal{N} = 4$ $SU(N)$ super-Yang-Mills theory. We will return to the described construction and limiting procedure in the section below, as it is one of the founding stones of the AdS/CFT correspondence.

The other fundamental ingredient comes from realizing, what is the influence of the stack of D3-branes on the surrounding embedding space. This part concerns the mentioned above closed strings interacting with it. Without going into much detail, one can also formulate a consistent low energy effective theory describing the massless sector of these closed strings. It turns out to be precisely the ten-dimensional supergravity theory, whose equations of motion were discovered with the aid of superstring theory β function above, (3.23). If one confines attention to the supergravity approximation, one finds, that Dp-branes possess masses and certain charges, which regarded as classical sources lead to appearance of specific classical Einstein equations solutions, which by analogy are also called p-branes. These supergravity solutions are understood as being the background fields over which superstrings can propagate. These are exactly the fields, which we were considering from the string world-sheet perspective above, (3.19).

3.5 The AdS/CFT correspondence

As we justified above, we have arrived at the equations defining what background fields are allowed for superstrings. These happen to be solutions to classical supergravity equations. For the type IIB superstring theory in which we are interested the corresponding background fields should follow 10-dimensional type IIB supergravity equations. The solutions to these are known as p-branes, and in particular they are solutions to Einstein equations in the presence of dilaton field and precisely the Ramond-Ramond p-forms we have mentioned before. Exactly these fields are sourced by the Dp-branes, as we mentioned above and as we will see in a more detail below.

Let us focus on the case relevant to us, which is the D3-brane, because as we said it leads to a four-dimensional gauge theory. The geometry of the system is such that flat $1+3$ dimensional D3 brane worldvolume is aligned along X^0, X^1, X^2, X^3 directions, which we now call x^μ, and there are six directions orthogonal to the brane hypersurface in the overall ten dimensional string embedding space $\mathbb{R}^{10}$. These transverse directions are called now y^m, $m = 4, 5, 6, 7, 8, 9$. From their point of view, brane is a pointlike object and one can introduce spherical coordinates around it, with radial distance y and five sphere Ω_5 parametrized by angles ϑ_i, $i = 1..5$. Subject to these symmetry constraints the type IIB SUGRA has a solution of the form:

$$\begin{cases} g_s = e^{\varphi},\ C \text{ constant} \\ B_{\mu\nu} = A_{2\mu\nu} = 0 \\ ds^2 = H(y)^{-1/2} dx^\mu dx_\mu + H(y)^{1/2}(dy^2 + y^2 d\Omega_5^2) \\ F^+_{5\mu\nu\rho\sigma\tau} = \varepsilon_{\mu\nu\rho\sigma\tau\upsilon}\partial^\upsilon H(y) \end{cases} \tag{3.25}$$

Here C is the so-called axion field, g_s is the familiar dilaton and both these are constant. A_2 and B are our 2-form Ramond and Kalb-Ramond B-fields, F^+ is the field strength tensor for the only non-zero Ramond-Ramond field, the self-dual (as indicated by $+$ sign) 4-form field $A^+_{4\mu\nu\rho\sigma}$ and metric is the ten dimensional D3-brane itself, depending on just one scalar function

$$H(y) = 1 + \frac{4\pi g_s N(\alpha')^2}{y^4}. \tag{3.26}$$

The parameter N in the solution is equal to the Ramond-Ramond five form F_5^+ flux through the five-sphere around the D3-brane,

$$N = \int_{\Omega_5} F_5^+. \tag{3.27}$$

This is a very crucial point, as that is how the future gauge group parameter N enters the correspondence. It is equal to the Ramond-Ramond 5-charge of the D3-brane. Its physical meaning is twofold. On the one hand it is the mentioned charge, but it can also be thought of as the number of individual D3-branes, each carrying a unit of Ramond-Ramond 5-charge, which are brought together and stacked on the top of each other, as we discussed in Section 3.4.

The second crucial feature of the D3-brane metric is the presence of both constant dilaton g_s and string slope α' in $H(y)$. We shall see now what is the significance of this combination.

AdS/CFT correspondence [Maldacena 1999, Witten 1998, Gubser 1998] is discovered by performing the Maldacena limit of superstring theory in the background fields (3.25).

To perform the limit we recast the flux N D3-brane metric in the form more suitable for what we intend to do with it,

$$ds^2 = \left(1+\frac{L^4}{y^4}\right)^{-\frac{1}{2}} \eta_{\mu\nu}\mathrm{d}x^\mu \mathrm{d}x^\nu + \left(1+\frac{L^4}{y^4}\right)^{\frac{1}{2}} (\mathrm{d}y^2 + y^2 \mathrm{d}\Omega_5^2), \tag{3.28}$$

with $L^4 \equiv 4\pi g_s N(\alpha')^2$. The above geometry can be inserted verbatim into the string theory action (3.15). Let us now take the limit $\alpha' \to 0$, i.e. the same as we considered in Section (3.4). Upon such a substitution we can ask the following question: what are the properties of the string propagating in various regions of the above D3-brane background?

We can address this question with two limits: $y \gg L$ and $y < L$. In the first case we recover the flat ten dimensional spacetime far away from the brane, where string propagates freely as if there was no brane. In the former case we seem to have a singular geometry near $y \sim 0$. This is however only a superficial divergence. We can analyse this region of the solution called the throat by introducing a new radial variable:

$$z = \frac{L^2}{y} \equiv \frac{\sqrt{4\pi g_s N}\alpha'}{y}. \tag{3.29}$$

Now in the large z limit the metric (3.28) reaches the following form,

$$ds^2 = L^2\left[\frac{1}{z^2}\eta_{\mu\nu}\mathrm{d}x^\mu \mathrm{d}x^\nu + \frac{\mathrm{d}z^2}{z^2} + \mathrm{d}\Omega_5^2\right] = L^2 G_{MN}^{AdS_5\times S^5} dX^M dX^N. \tag{3.30}$$

This is now a product geometry consisting of two parts, one being the five sphere S^5 with metric $L^2\mathrm{d}\Omega_5^2$ and radius L^2. The second part is five dimensional hyperbolic anti-de Sitter space AdS_5 with the same radius as the five-sphere L^2 and constant negative curvature. The most important feature of this new space is that AdS geometry has conformal isometry group, which means that it is invariant under the full conformal group in five dimensions. Many forthcoming results rely on this emergent enhanced symmetry property of the near horizon geometry.

However, again, since we are considering the limit $\alpha' \to 0$, which implies $L \to 0$, the geometry with vanishing metric (3.30) seems to be singular. We could be anxious therefore, if this is a sensible construction. To answer this question we will take a closer look at the string action in the background geometry of (3.30). This point brings us to the celebrated Maldacena limit.

Maldacena considered keeping N, g_s fixed in (3.28) background and letting

$$\alpha' \to 0. \tag{3.31}$$

This corresponds in string action to precisely the limit where (3.29) is finite and y is small, because L^2 contains the factor of α'. It is sometimes called the near horizon limit of the D3-brane.

Let us now check what does this mean for the string theory action, which being multiplied by $1/\alpha'$ should naively be singular. If we adopt the background geometry to be (3.30), then the non-linear sigma model of (3.15) becomes

$$S_G = \frac{L^2}{4\pi\alpha'}\int_\Sigma \sqrt{h}h^{ab} G_{MN}^{AdS_5\times S^5}(x)\partial_a X^M \partial_b X^N. \tag{3.32}$$

As a result we can observe how background metric field parameters blend with the string world-sheet action to produce new effective string coupling:

$$\frac{L^2}{4\pi\alpha'} = \sqrt{\frac{\lambda}{4\pi}},\ \lambda \equiv g_s N. \tag{3.33}$$

When we allow $\alpha' \to 0$ keeping λ fixed we in fact put $L \to 0$. Contrary to our concerns however, the string action turns out to possess a smooth limit in this process, given by

$$S_G = \sqrt{\frac{\lambda}{4\pi}} \int_\Sigma \sqrt{h} h^{ab} G_{MN}^{AdS_5 \times S^5}(x) \partial_a X^M \partial_b X^N, \tag{3.34}$$

with $G_{MN}^{AdS_5 \times S^5}$ being just the pure $AdS_5 \times S^5$ metric

$$ds^2 = \frac{1}{z^2} \eta_{\mu\nu} \mathrm{d}x^\mu \mathrm{d}x^\nu + \frac{\mathrm{d}z^2}{z^2} + \mathrm{d}\Omega_5^2, \tag{3.35}$$

We can see, that now $1/\sqrt{\lambda}$ plays the role of the string coupling and the geometry scale factor L cancelled completely. This means, that we have recovered finite conformally invariant theory, owing to the conformal symmetry of the empty AdS spacetime.

Let us now ask the following question: how does the Maldacena limit affect the quantum string theory spectrum? Repeating what we have been discussing in Section 3.4 we know, that in this limit only massless string states remain.

The point is that in the $\alpha' \to 0$ limit all massive states, the so called excitations tower (3.24), becomes infinitely massive and decouples from the string dynamics, leaving only the few massless states with $n = 0$. Complementarily, we can also ask how the string spectrum behaves if we vary the effective coupling λ. The case of $\lambda \to 0$ leads the full perturbative string spectrum. In $\lambda \to \infty$ case however, we reach again the massless supergravity sector. In any case therefore we can construct a low energy effective action for the massless superstring states in the presence of D3-branes. This theory consists of open string excitations localised on the brane worldvolume and closed string states in the spacetime surrounding it. The effective theory localised on the D3-brane is in our case precisely the large N super-Yang-Mills theory described in Section 3.2, with effective coupling constant being exactly $\lambda = g_{\mathrm{YM}}^2 N = g_s N$. The theory of closed massless string states is in turn the type IIB supergravity, which provided us with the classical D3-brane background.

The essential point of AdS/CFT correspondence is that these two theories being parts of the same physical system are dual to each other and we are going to formally verbalize this relation now.

The AdS/CFT correspondence states, that the full quantum $d = 4$ $SU(N)$ $\mathcal{N} = 4$ super-Yang-Mills theory is completely equivalent to the full quantum IIB superstring theory in the product background space $AdS_5 \times S^5$. The equivalence postulates isomorphism of Hilbert spaces and duality between all the correlation functions for all $g_s \equiv g_{\mathrm{YM}}^2$ and N, and is summarized as equality of generating functionals:

$$Z_{\mathrm{IIB}}[\phi(x)] = Z_{\mathrm{CFT}}[\phi(x)], \tag{3.36}$$

where $\phi(x)$ is the source for the field theory operator on the one hand, and classical field boundary condition imposed in the string theory path integral at the AdS_5 space conformal boundary $z \to 0$, on the other hand.

The above statement formally allows to compute correlation functions in conformal field theory using string theory generating functional. Of course we do not know it explicitly. However, very importantly upon Maldacena limit we can additionally perform the strong 't Hooft limit of $\lambda \to \infty$. In this case the type IIB string theory reduces to the aforementioned classical type IIB supergravity. Because of this AdS/CFT correspondence is often termed weak-strong duality, because in the CFT side it corresponds to large coupling $\lambda \to \infty$, while on the string theory side it leads to the weak gravity approximation of small

curvature $1/L \to 0$. We obtain in this regime a very important practical approximation

$$Z_{\mathrm{IIB}}[\phi(x)] \sim Z_{\mathrm{SUGRA}}[\phi(x)] = \int_{\Phi(x,z=0)\sim\phi(x)} \mathcal{D}\Phi e^{-S_{\mathrm{SUGRA}}[\Phi(x,z)]}, \tag{3.37}$$

and $S_{\mathrm{SUGRA}}[\Phi(x,z)]$ is the IIB supergravity action with boundary conditions on SUGRA fields collectively denoted by $\phi(x)$ imposed at $z \to 0$. The specific operator, whose correlation function would be computed by (3.37) is specified by the concrete dual field $\Phi(x,z)$ allowed in the SUGRA action. Scalar $\Phi(x,z)$ would induce scalar CFT operator coupling, e.g. $\phi(x)\mathrm{Tr}\hat{F}^2(x)$, vector source would induce another vector, e.g. $\hat{O}^\mu(x)J_\mu(x)$, and so on. In this sense one often claims, that the dual field theory resides at the boundary $z = 0$ of the AdS space. Interior of the AdS space with $z > 0$ where the gravity lives is commonly called the *bulk*.

The logarithm of $Z_{\mathrm{IIB}}[\phi(x)]$ serves therefore as an effective connected correlation functions generator at strong 't Hooft coupling $\lambda \to \infty$. This is precisely the regime, in which we will perform all the subsequent calculations.

An important remark should be made here concerning the actual space used in the duality (3.36), (3.37). We have seen how the $AdS_5 \times S^5$ string background descented from the general D3-brane solution in the near horizon limit $y \to 0$. This canonical AdS_5 spacetime is relevant for vacuum calculations in SYM CFT. However we have mentioned various boundary conditions to be imposed in (3.37) on the way to finding solutions. It may happen, that these conditions will influence bulk geometry so much, that it will no longer be pure anti-de Sitter, but some other space. Such a situation is generic, expected, and allowed provided one universal condition is satisfied: all the possible solutions must be *asymptotically* AdS, meaning, that its local near-boundary expansion around $z \sim 0$ *is* equivalent to AdS space. As it turns out many physical systems described by AdS/CFT duality fall into this category. In our case it will be the so-called AdS-black brane solution, which will be described shortly in subsequent sections. It should be understood from now on, that by AdS spaces we most of the time mean AAdS, asymptotically-AdS spaces. All such spaces can be cast in the following form generalizing pure AdS space (3.35), called Fefferman-Graham chart of AAdS:

$$ds^2 = \frac{1}{z^2} g_{\mu\nu}(x,z)\mathrm{d}x^\mu \mathrm{d}x^\nu + \frac{\mathrm{d}z^2}{z^2} + \mathrm{d}\Omega_5^2. \tag{3.38}$$

We remind, that the above $x \in \mathbb{R}^4$ are coordinates transverse to the bulk dimension z. They are called boundary or field theory directions, because they are parallel to the AAdS boundary. The generic four-dimensional metric $g_{\mu\nu}(x,z)$ represents all the allowed departures from pure AdS space, and defines the induced boundary metric as

$$g^0_{\mu\nu}(x) = \lim_{z\to 0} z^2 g_{\mu\nu}(x,z). \tag{3.39}$$

This entity is what we will understand as the boundary metric or boundary condition for the full five dimensional metric $G_{MN}(x,z)$. In our case it will be flat Minkowksi $\eta_{\mu\nu}$, but *a priori* it could be any metric supporting super-conformal field theory, also of non-trivial topology.

As a closing remark let us say, that the correspondence statement above was phrased in its strongest form, and as such is still conjectural. In practice most of the calculations were and are performed in the classical supergravity approximation corresponding to the strongly coupled super-Yang-Mills theory with $\lambda \to \infty$. Powerful and complicated computations in $1/\sqrt{\lambda}$ were performed in the vast field of integrability leading to $1/\alpha'$ corrections and gave perfect agreement with perturbative SYM computations. Corrections in $1/N$ on the other hand remain a challenge and mystery, and are in fact related to strongly quantum regime of superstring theory, where its understanding is still scarce.

3.6 Holographic renormalization

The core technique we are going to use in all the subsequent considerations is called holographic renormalization, basics of which we shall recall following [de Haro 2001, Skenderis 2002]. It is a systematic procedure of computing correlation functions from gravity by employing formulas (3.36) with approximation (3.37).

Unfortunately amid this simplification the SUGRA partition function (3.37) for finite λ is still beyond reach of exact computations. However the quark-gluon plasma system we are interested in is strongly coupled. Therefore we can confine our attention to the large effective gauge coupling λ limit, in which case the path integral (3.37) can be evaluated by the saddle point approximation with prescribed boundary conditions at $z = 0$. This leads to an operational formula for the connected correlation functions generating functional:

$$W_{\mathrm{CFT}}[\phi(x)] \equiv \ln\langle e^{-\int_{\partial AdS}\phi(x)\hat{O}(x)}\rangle_{\mathrm{CFT}} = -S^{\text{on-shell}}_{\mathrm{SUGRA}}[\Phi(x,0)]. \tag{3.40}$$

The action is on-shell, meaning we evaluate the integral on the classical gravity solutions and integrate over the whole AdS spacetime. Of course the proper volume of the entire involved AdS space is formally infinite, and therefore we need to suitably regularize and renormalize the action before using it in computations. This fact is the source of the term holographic renormalization. The divergence of the gravity action closely mimics the corresponding UV divergences in the dual CFT.

Regularization and renormalization routines also bear resemblance to field theory in that one isolates and removes divergence with covariant counterterms. A regulator is introduced as a cut-off on the radial direction $\mathrm{d}z$ integral by shifting away from the spatial infinity, which gives $S^{\mathrm{reg}}_{\varepsilon}$. Then counterterms are obtained as induced on-shell action at $z = \varepsilon$

$$S = \int_{AdS_5} \mathrm{d}\vec{x}\mathrm{d}z\sqrt{G(x,z)}\mathcal{L}_{\mathrm{EH}} \to S^{\text{c-t}}_{\varepsilon} = \langle\text{singularities of}\rangle \int_{AdS_5|z=\varepsilon} \mathrm{d}\vec{x}\sqrt{G(x,\varepsilon)}\mathcal{L}_{\mathrm{EH}}. \tag{3.41}$$

$\mathcal{L}_{\mathrm{EH}}$ is the SUGRA Einstein-Hilbert action (sometimes conventionally metric determinant $\sqrt{G(x,z)}$ is included in it).

Holographic renormalization is carried out by subtracting counterterms from regulated on-shell gravity action and taking the limit $\varepsilon \to 0$:

$$S^{\text{on-shell}}_{\mathrm{ren}} = \lim_{\varepsilon\to 0}[S^{\mathrm{reg}}_{\varepsilon} - S^{\text{c-t}}_{\varepsilon}]. \tag{3.42}$$

Once the renormalized on-shell action is found with appropriate bulk fields dual to our operators of interest we can use the holographic formula to compute their correlation functions. Our forthcoming cases of interest will include only stress-energy operator and R-charge current operator of super-Yang-Mills theory dual to $AdS_5 \times S^5$ supergravity with flat Minkowski boundary metric $\eta_{\mu\nu}$ at $z = 0$. According to the holographic dictionary, the supergravity field dual to the stress tensor is the five dimensional metric G_{MN} itself and R-charge current at the boundary is dual to the bulk $U(1)$ Maxwell gauge field A_M.

For these cases we shall use two holographic relations:

$$\langle\hat{T}^{\mu\nu}(x)\rangle_{\mathrm{CFT}} = \frac{2}{\sqrt{g^0}}\frac{\delta S^{\text{on-shell}}_{\mathrm{ren}}[G_{MN}]}{\delta g^0_{\mu\nu}(x)}\bigg|_{g^0_{\mu\nu}=\eta_{\mu\nu}} \tag{3.43}$$

$$\langle\hat{J}^{\mu}_{R}(x)\rangle_{\mathrm{CFT}} = \frac{2}{\sqrt{\eta}}\frac{\delta S^{\text{on-shell}}_{\mathrm{ren}}[G_{MN};A_M]}{\delta A^0_{\mu}(x)}\bigg|_{A^0_{\mu}=0} \tag{3.44}$$

where $\mu,\nu = 0..3$ are bulk tensor indices M, N restricted to boundary dimensions of the dual field theory. In the above we have indicated two arbitrary boundary conditions serving as

auxiliary sources used for the purpose of functional differentiation (in complete analogy to e.g. magnetisation computations on statistical physics). The metric boundary components are $G_{\mu\nu}(x, z = 0) \equiv g^0_{\mu\nu}(x)$ and the gauge potential boundary part is $A_\mu(x, z = 0) = A^0_\mu(x)$. The boundary metric determinant absolute value is denoted η or g^0 and after the functional derivative is evaluated we put these auxiliary sources to the physical boundary values.

We should now ask how do we actually use (3.43)? We need to solve classical gravity equations following from $S_{\mathrm{SUGRA}}[G, A, \Phi, ...]$ including equations for the additional fields and evaluate the action on the solutions. This means we need to solve

$$R_{MN} - \frac{1}{2}RG_{MN} = \Lambda G_{MN} + T^{\mathrm{matter}}_{MN} \tag{3.45}$$

and additional equations for the matter fields. Here Λ in the negative cosmological constant necessary to obtain AAdS spacetime as a solution. In our applications based on AdS_5 it will always be fixed as $\Lambda = -6$. The second order system above requires two boundary conditions for each field, and possibly initial conditions if we are looking for dynamic solutions (as will be the case in our applications). Most of the time solving Einstein equations is a formidable effort. There is however a very efficient strategy of solving them perturbatively as a power series near $z = 0$. This approach allows one to iteratively obtain the solution starting with the boundary value and proceeding inward the bulk. This approach will be utilized by us on several occasions later on, so let us give a very brief account on it.

If we adopt metric Ansatz of the form (3.38) and introduce expansion

$$g_{\mu\nu}(x, z) = g^0_{\mu\nu}(x) + \sum_{n=1}^{\infty} g^n_{\mu\nu}(x)z^n, \tag{3.46}$$

it can be shown upon insertion to (3.45) by an explicit calculation, that coefficients of all odd powers z^n vanish, $g^0_{\mu\nu}(x)$ and $g^4_{\mu\nu}(x)$ are undetermined by the equations and all other series coefficients are algebraically determined in terms of these two functions. The two mentioned components are unspecified by the equations because they are precisely the boundary conditions we must impose in order to find a unique local solution. Once they are given, one can produce as many terms of the expansion as one likes. This procedure however does not in general lead to an analytical, because one would have to sum the corresponding series, which is generically not doable. The utility of the described procedure is however very significant, as will be demonstrated by the following argument (it will also play a significant role in developments of chapters 6 and 7).

The key use of the formula (3.46) is that one can use it to evaluate (3.43), to express the expectation value of the gauge theory energy-momentum tensor in terms of the gravity solution:

$$\langle \hat{T}^{\mu\nu}(x) \rangle = g^4_{\mu\nu}(x). \tag{3.47}$$

That is simply all. Just fourth order term (for this dual operator), which is exactly the boundary condition needed to find the solution in the bulk. How to understand this mutual dependence? One can use the prescription (3.43) in a twofold way depending on the application. If we want to find geometry dual to the specific known boundary operator expectation value, e.g. $\langle \hat{T}^{\mu\nu}(x) \rangle$ we use it along with the boundary metric as boundary conditions for the classical Einstein equations and solve them. That ends one application. The second possibility is that we have somehow obtained an exact gravity solution and want so see the corresponding expectation value of the dual operator. In this case we simply use holographic prescription in the form of (3.47) and obtain the desired expectation value. In our applications we will follow this path to extract gauge theory stress tensor from gravity.

Finally let us state, that the described procedures translate verbatim to other fields, in particular to the bulk gauge potential $A_M(x,z)$, with just different equation of motion for it. We will see this in action in Chapter 5.

This concludes our introduction to string theory and basics of holography. We shall now pass to themes specific to our applications with an aim of showing how fluid/gravity duality emerges from string theory by breathing life into the cold and static D3-brane solutions.

3.7 Strongly coupled thermodynamics

For future reference we begin with a description of some important results derived from a static black brane gravity dual in five AdS dimensions. The main outcome of these considerations will be basic thermodynamics of strongly coupled $\mathcal{N}=4$ super-Yang-Mills field theory at equilibrium.

The AdS dual to equilibrium state also lays down a convenient minimalistic foundation for describing important properties of the correspondence and possible generalisations, the most important one for us being the derivation of the fluid/gravity duality. Considerations of equilibrium dual geometry properties played an important role in the inception of AdS/CFT as being relevant in the context of quark-gluon fluid model research. This part of the correspondence is of course the main subject of the present Thesis. The literature covering thermal systems duality is already vast. In what follows we shall rely on the concise discussion of [Janik 2011] and later on the main paper introducing fluid dynamics is AdS/CFT, [Bhattacharyya 2008b].

In contrast to the vacuum field theory configuration of Section 3.5, our goal will now be to construct a gravity dual to static uniform thermal state in four dimensional $\mathcal{N}=4$ SYM gauge theory. Such a state is specified in field theory by the set of symmetries respected by the corresponding matter and energy distribution: full translational and rotational symmetry, parity and the equation of state following from conformal invariance.

As we have already discussed in Chapter 2, such a state can be represented by field theory stress-energy tensor thermal expectation value. The listed constraints reduce it to the following form:

$$T_{\mu\nu} = \begin{pmatrix} E & 0 & 0 & 0 \\ 0 & p & 0 & 0 \\ 0 & 0 & p & 0 \\ 0 & 0 & 0 & p \end{pmatrix}. \tag{3.48}$$

The above tensor parametrizes system of homogeneous energy density E and pressure p, filling the whole infinite space. Conformal symmetry provides us with an equation of state coming from the tracelessness condition: $E=3p$.

According to the AdS/CFT correspondence and holographic renormalization described above, to find the gravity dual to this thermal system,

$$G_{MN}(z)dx^M dx^N \quad = \quad \frac{g_{\mu\nu}(z)dx^\mu dx^\nu + dz^2}{z^2} \tag{3.49}$$

we have to solve static vacuum Einstein equations $E_{MN}=0$ with appropriate boundary conditions:

$$g_{\mu\nu}(z) \quad = \quad \eta_{\mu\nu} + z^4 \frac{2\pi^2}{N^2} T_{\mu\nu} + \mathcal{O}(z^6). \tag{3.50}$$

The numerical constant in front of the z^4 term is specific to the particular theory we are building dual geometry to, and reflects among other things qualitative number of adjoint gauge degrees of freedom at large N.

Given the above an exact solution can be found, since the stress tensor $T_{\mu\nu}$ is time independent and Einstein equations reduce to one dimensional ordinary differential equation in the bulk variable z, which can be solved analytically (metric dependence on the directions x_i is removed by symmetries).

The solution reads:

$$ds^2 = -\frac{(1-z^4/z_0^4)^2}{(1+z^4/z_0^4)z^2}dt^2 + (1+z^4/z_0^4)\frac{dx_i^2}{z^2} + \frac{dz^2}{z^2}. \tag{3.51}$$

This geometry is standard planar AdS-Schwarzschild black brane in Fefferman-Graham coordinates. Its other form can be revealed by the following coordinates transformation:

$$z_S = \frac{z}{\sqrt{1+z^4/z_0^4}}. \tag{3.52}$$

This transformation brings the solution to the Schwarzschild-like form, modulo the scaling factor $1/z_S^2$, with variable z_S playing the role of the standard Schwarzschild spatial radius:

$$ds^2 = -\frac{1-z_S^4/z_{S0}^4}{z_S^2}dt^2 + \frac{dx_i^2}{z_S^2} + \frac{1}{1-z_S^4/z_{S0}^4}\frac{dz_S^2}{z_S^2}. \tag{3.53}$$

The solution parameters in the two coordinate systems are related as $z_{S0} = z_0/\sqrt{2}$. With the above metric representation one can identify z_{S0} and accordingly z_0 with the black brane horizon position. It shows, that static thermal field theory state is represented by the simplest spacetime black object, the planar static black brane.

Let us make a remark on one feature of solution (3.51). The SYM theory we are building holographic dual to is exactly conformally invariant and as such has conformally invariant vacuum. This fact is reflected on the gravity side by the conformal isometry of the corresponding state's gravity dual, which is empty AdS. Among other symmetries it is invariant under scalings:

$$ds^2 = \frac{-dt^2 + dx_1^2 + dx_2^2 + dx_3^2 + dz^2}{z^2} \text{ is invariant under } z \to \lambda z,\ x^\mu \to \lambda x^\mu. \tag{3.54}$$

However thermal state (3.48) breaks conformal invariance by the introduced fixed energy scale E. Conformal symmetry now manifests itself by relating different thermal black brane solutions to each other with rescaled horizon locus parameter,

$$x^\mu \to \lambda x^\mu,\ z \to \lambda z \Rightarrow z_0 \to \tilde{z}_0 = z_0/\lambda. \tag{3.55}$$

In this sense symmetry breaking solution becomes a representation of the underlying symmetry, like in particle physics.

The connection between field theory variables and the gravity solution parameters is established with the aid of holographic formula for the stress-energy tensor expectation value. It yields a relation between the only scales present on both sides, the energy density E and the metric parameter z_0. By expanding the temporal metric component (often called warp-factor) near the boundary $z = 0$

$$-\frac{(1+z^4/z_0^4)^2}{(1+z^4/z_0^4)z^2} = -\frac{1}{z^2} + \frac{3}{z_0^4}z^2 + \mathcal{O}(z^6), \tag{3.56}$$

and subsequently keeping (along the lines of the holographic dictionary) only the $z^2 \equiv z^4/z^2$ coefficient, we obtain:

$$E = \frac{3N^2}{2\pi^2 z_0^4}. \tag{3.57}$$

This important formula states that the static energy density is inversely proportional to the fourth power of the horizon locus, z_0, with the coefficient scaling as the number of $SU(N)$ gauge degrees of freedom. This is consistent with the deconfined phase of field theory, which amid strong coupling exhibits scaling with N^2. This relation is one of the building blocks in the construction of the fluid/gravity duality, which will be introduced further below. The thermodynamic relation to pressure is given by the vanishing trace[3], $E = 3p$.

The compact result (3.51) is an efficient laboratory with which one can derive exact microscopic formulas for certain class of strongly coupled non-Abelian gauge field theories. We will demonstrate this inter alia by identifying temperature of the equilibrium system, which we shall accomplish by using Wick rotation approach working both in field theory and in General Relativity. In the realm of QCD the prevailing approach to derive such quantities is still based on complicated lattice simulations. The existence of AdS/CFT is a promising development towards completely different dynamical framework of non-perturbative gauge theory analysis, which however is yet to be completed.

In order to find the temperature on the gravity side we pass to the Euclidean section $t = i\tau$ on the complex time plane of the complex-continued metric (3.51), and compactify the temporal direction to a circle S^1 with the condition

$$\tau \sim \tau + 1/T. \tag{3.58}$$

The spacetime is now $R_+ \times R^3 \times S^1$, with the boundary at $z = 0$ being $R^3 \times S^1$. The periodicity (equivalently the inverse of the Hawking temperature) will be found from the requirement, that the Euclidean geometry is nonsingular. The next step is to focus on the near-horizon region of the geometry (3.51), $z \sim z_0$ which amounts to adopting a new bulk coordinate suggested by the vanishing of the metric at the horizon:

$$\rho = \frac{z}{z_0},\ \zeta = 1 - \rho,\ \zeta \in [0, 1]. \tag{3.59}$$

Then the (τ, ζ) part of the metric $ds^2_\perp$ can be approximated as:

$$ds^2_\perp = \frac{(1-\rho)^2(1+\rho)^2(1+\rho^2)^2 d\tau^2}{(1+\rho^4)\rho^2 z_0^2} + \frac{d\rho^2}{\rho^2} \sim \frac{8\zeta^2}{z_0^2} d\tau^2 + d\zeta^2 + \mathcal{O}(\zeta)^3. \tag{3.60}$$

The obtained expression resembles the standard polar coordinates metric, however with angular coordinate τ having wrong periodicity (3.58). To assure that there is no conical singularity we must thus demand that:

$$\phi \equiv \frac{8^{1/2}}{z_0}\tau \in [0, 2\pi], \tag{3.61}$$

[3]It can be independently confirmed by the direct expansion of all components in (3.51), and taking the trace.

so using (3.58) we obtain the condition:

$$T = \frac{\sqrt{2}}{\pi z_0}. \tag{3.62}$$

From the field theory point of view, which lives at the conformal boundary $z \to 0$, $R^3 \times S^1$, we also have the same compactified Euclidean time direction, τ. By standard statistical field theory path integral arguments and canonical ensemble we obtain, that T should be interpreted as the temperature. Owing to the previous arguments we see, that its value is strictly related to the black hole horizon locus.

The second quantity crucial for building thermodynamics is entropy. This entity is also present in the gravitational system, as is known from the work of Bekenstein and Hawking [Bekenstein 1973, Hawking 1975]. It is derived from geometrical properties of the event horizon, most important of which is the area growth theorem. We shall rely on this concept later in the Chapter 6, where its generalisation to dynamical case will be explored. In general the black hole entropy reads:

$$S = \frac{A}{4G_N}, \tag{3.63}$$

where A is the spatial horizon area and G_N is the gravity coupling parameter, the Newton constant.

The original derivation of the Bekenstein-Hawking entropy was carried out for compact horizons (whose spatial sections are homotopic to sphere), while presently we are considering planar black brane horizons of infinite spatial volume. The quantity of interest to us is thus the densitized entropy per unit spatial 3-volume element (since we are considering D3-branes):

$$s = \frac{1}{4G_N} \frac{d(\text{Area})}{d(\text{3-Volume})}. \tag{3.64}$$

The Newton constant in our case is $G_N = \pi/(2N^2)$. The area is computed as the volume element induced at the horizon locus $z = z_0$ *and* constant time $t_\star$:

$$d(\text{Area}) = \sqrt{\gamma}\Big|_{z_0, t_\star} dx_1 dx_2 dx_3. \tag{3.65}$$

The spatial unit 3-volume of the D3-brane is in turn

$$d(\text{3-Volume}) = dx_1 dx_2 dx_3. \tag{3.66}$$

Upon division we obtain, after using the spatial longitudinal (along the horizon) part of (3.51) the final expression for the entropy density:

$$s = \frac{N^2}{2\pi} \left(\frac{\sqrt{2}}{z_0} \right)^3. \tag{3.67}$$

As we see the gravitational entropy is parametrized by the horizon locus z_0, and scales as N^2. This quantity is identified with the entropy of the dual field theory by virtue of the

holographic principle: the entropy of gravitating system (loosely counting the dominant gravitational degrees of freedom) is equal to the boundary field theory entropy in one dimension lower. With the aid of the temperature T obtained above, it can be expressed exclusively through the field theory variables:

$$s = \frac{1}{2} N^2 \pi^2 T^3. \tag{3.68}$$

It is worth noting, that field theory entropy which roughly counts degrees of freedom scales with the number of colors like in free theory, N^2, being again an indication of a deconfined phase.

The last field theory formula that can be assembled here is the relation between energy density and temperature:

$$E = \frac{3}{8} N^2 \pi^2 T^4. \tag{3.69}$$

We can make an observation, that both the entropy density and the energy density have numerical coefficients different from the corresponding free gas expressions, that could be obtained by weakly coupled perturbative methods. We have thus obtained a *prediction* from AdS/CFT for the strongly coupled SYM theory. The entropy is smaller by a factor of 3/4 from the free gas answer, reflecting the heuristic argument, that strong coupling binds degrees of freedom together decreasing their total count (however maintaining N^2 scaling). It is worth noting, that high temperature thermodynamics of QCD plasma obtained from lattice QCD has a similar deviation from the free Yang-Mills expression. For instance, based on lattice simulations, above but close to the T_c the entropy density of QCD plasma is reduced to 30 % of the ideal gas value, whereas for higher temperatures $T \sim (2-3)T_c$ it approaches the perturbative answer [Karsch 1990] (it is argued there, that the difference can be attributed mostly to the non-perturbative pressure behaviour).

With the temperature, entropy and equation of state we have completed basic construction of the strongly coupled plasma thermodynamics. The variables s and T are constants, as required by global thermal equilibrium, and this fact corresponds to the static spacetime geometry. Non-equilibrium generalizations of thermodynamics are usually difficult to obtain, but as we shall see, AdS/CFT provides us with means to achieve this, starting with hydrodynamics, but going significantly beyond that.

To close this paragraph let us mention one last important point concerning the metric (3.51). As we have seen, it was described in two coordinate systems, each making explicit different aspects of the geometry (E.g. Schwarzschild form allows to enter the black hole, in contrast to Fefferman-Graham [Kinoshita 2009], which in turn makes simpler the holographic relations). For future purposes it will be useful to present the same solution in one more form, namely the ingoing Eddington-Finkelstein coordinates:

$$t_{EF} = t - \frac{1}{4} z_{S0} (2 \arctan \frac{z_S}{z_{S0}} + \log \frac{z_{S0} + z_S}{z_{S0} - z_S}). \tag{3.70}$$

This chart is constructed by changing only the time coordinate, while maintaining the radial Schwarzschild variable z_S. These famous coordinates allow one to safely observe the black brane geometry through the horizon up to the central curvature singularity at $z \to \infty$. The two previously used coordinates systems are singular at the horizon (z_0 or z_{S0}), which although unphysical, makes computations cumbersome. The Eddington-Finkelstein chart in turn makes the metric manifestly regular there:

$$ds^2 = -\frac{1 - z_S^4/z_{S0}^4}{z_S^2} dt_{EF}^2 + 2\frac{dt_{EF} dz_S}{z_S^2} + \frac{dx_i^2}{z_S^2}, \tag{3.71}$$

which is also often used in the inverse radial variable $r = 1/z_{\mathrm{S}}$, known from the D3-brane considerations:

$$ds^2 = -r^2(1 - \frac{r_0^4}{r^4})dt_{EF}^2 - 2dt_{EF}dr + r^2 dx_i^2, \text{ with } r_0 = 1/z_{S0}. \tag{3.72}$$

The introduction of these coordinates helped to solve certain puzzling problems [Heller 2009], which appeared during early days of fluid/gravity duality construction. They will be used in the next paragraph as a starting point for the general understanding how hydrodynamics emerges from the dual gravitational picture.

3.8 Hydrodynamics from string theory

So far we have been working in the realm of vacuum or static equilibrium systems. The natural question is then, can we make the system evolve? Can we introduce dynamics to the equilibrium, so that it is no longer balanced and study the various near- and far-from-equilibrium processes? It is very interesting to ask these questions, because they involve systems where entropy should be produced, or may even not be defined, as well as thermodynamics may not be applicable due to the lack of global equilibrium.

The first step on the way to considering such situations is the construction of the aforementioned fluid/gravity duality. The first hints, that hydrodynamical behaviour may be embedded somehow in the gauge/string duality were given in the papers by Starinets and others at the dawn of AdS/CFT correspondence [Policastro 2001], who considered linear response theory in the AdS-black brane backgrounds. Their findings based on the so-called quasinormal modes revealed unexpected universal formula on the viscosity-to-entropy ratio of the holographic plasma, as well as hydrodynamic dispersion relations in static gravity (and hence fluid) backgrounds. Below we introduce the fully developed dynamical scheme of fluid/gravity duality, which is the cornerstone for most of the developments to be discussed later on.

The technical summary of the whole construction is contained in Subsection 3.10.2.

3.8.1 Hydrodynamic expansion from gravity

As we have seen in the Chapter 2, hydrodynamics is essentially an effective theory, obtained heuristically under certain assumptions as an approximation to some obfuscated theory governing the microscopic evolution of the given system. The basic method of obtaining it is through an expansion at consecutively finer scales, realized as a derivative expansion with respect to time and space.

This mechanism, introduced to some extent *ad hoc* by an employment of Newton mechanics to extended bodies [Huang 1987] can be made formally exact in AdS/CFT correspondence. By this we mean the following. In the traditional construction of hydrodynamics (or some other effective theories) one must supplement the expansion with certain missing information, most often numbers or operators encapsulating microscopic information lacking from the expansion. These quantities must then be determined from experiment and are external to the effective theory. In our case AdS/CFT allows one to both justify the specific expansion structure microscopically, and *compute* the effective parameters exactly (for the class of theories possessing holographical dual). In the case of hydrodynamics these

parameters are commonly known as transport coefficients. For some generic theory these must be inserted by hand into the equations of motion, whilst AdS/CFT delivers their precise values.

We begin the construction with a remark of why one should at all expect hydrodynamics emerging as an expansion of Einstein equations. Firstly, we have seen that the static black brane in AdS_5 leads holographically to a perfect gas stress-energy tensor, and its thermodynamics. Secondly, the first dynamic realisation of a *perfect fluid* hydrodynamics was put forward in [Janik 2006a]. There Einstein equations for boost-invariant system in Fefferman-Graham coordinates were subject to large proper time expansion, which led to the discovery of the scaling variable organizing the expansion of the equations in its inverse powers.

It is thus intuitive, that one should seek a model based on a dynamic spacetime in asymptotically-AdS space. Unfortunately finding explicit solutions to time dependent Einstein equations in generic settings is often impossible. We are thus led to exploiting the discovered expansion schemes.

The derivation we are about to describe employs such a scaling variable inspired approach, but using Eddington-Finkelstein coordinates for more general, non-boost-invariant case. The use of non-singular geodesic coordinates is crucial for avoiding problems encountered in the Fefferman-Graham coordinates based approach, and leads to a healthy series expansion.

The starting point are Einstein equations in $d = 1 + 4$ with negative cosmological constant, $\Lambda = -6$:

$$G_{MN} \equiv R_{MN} - \frac{1}{2} g_{MN} R - 6 g_{MN} = 0. \tag{3.73}$$

Apart from the empty AdS_5 metric (3.54) this equation admits a static black brane solutions, like the one discussed previously, (3.72) (with $r_0 = 1$). It can be recast in the form

$$ds^2 = -r^2 f(r) dv^2 - 2 dv dr + r^2 d\mathbf{x}^2, \qquad f(r) = 1 - \frac{1}{r^4}. \tag{3.74}$$

The r variable ranges from AdS interior at $r = 0$ to the conformal boundary at $r \to \infty$, and v (customarily relabelling t_{EF}) is the null-geodesic time. Such a choice resembles an infinite ball, centred at the former D3-branes locus $r = 0$ and extending indefinitely. The warp-factor $f(r)$ is the horizon function vanishing at the normalized fixed horizon position $r = r_0 = 1$.

The key ingredient if one wishes to speak of non-equilibrium physics is to have some explicit dynamics in the system. We should therefore find a way to induce some dynamics in the static solution (3.74). The most trivial way to introduce simple time dependence in a Poincaré-covariant theory is to push something with a boost, and watch it moving from some selected rest frame. We should thus try crafting a solution by boosting the black brane with some 3-velocity parameter 3-vector β^i, along the horizon direction:

$$ds^2 = -2 u_\mu dx^\mu dr - r^2 f(br) u_\mu u_\nu dx^\mu dx^\nu + r^2 P_{\mu\nu} dx^\mu dx^\nu, \tag{3.75}$$

$$\text{with } u^v = \frac{1}{\sqrt{1-\beta^2}}, \; u^i = \frac{\beta^i}{\sqrt{1-\beta^2}}, \text{ and } P^{\mu\nu} = u^\mu u^\nu + \eta^{\mu\nu}. \tag{3.76}$$

Apart from the constant boost parameter β^i we have also introduced a constant b, representing arbitrary possible position of the event horizon at $r = 1/b$, which corresponds

to rescaling the initial solution. Let us emphasize, that this is still an exact solution to Einstein equations. The reason, for which this is not a trivial step is the following.

These parameters can also be understood from an equivalent but in a sense deeper perspective. One can notice, that the presence of the black brane horizon breaks the full conformal isometry group $SO(4,2)$ of the empty AdS_5 space, which represents symmetric vacuum of the conformal field theory. The remaining residual symmetries of the thermal state consists of boosts and translations along the horizon $r = r_h$, $SO(3)$ rotations acting on the boundary directions x^i and scalings. The rotations and translations annihilate the black brane solution (in the sense of Killing vector generators defining the solution isometries, acting analogously to symmetry charges), but the remaining symmetry subalgebra acts non-trivially and transforms one solution into another. This gives a total of $(1+3) = 4$ parameters of the active transformations, $\{b, \beta^i\}$, with which one can write the most general form of a 4-parametric static black brane solution family (3.75), which as we mentioned are still trivially exact solutions.

The reason to adopt the above point of view, is that now we can make the most important and interesting observation: the four-parameter family of metrics (3.75) in fact forms a sort of moduli space for the Einstein equations (3.73) five dimensional asmymptotically AdS solution space, with moduli parameters represented by β^i and b. These are remnants of the symmetry algebra broken by the introduction of the black brane horizon into the empty AdS spacetime. We can thus try to understand the low energy dynamics of this moduli space, as is often done by gauging the moduli parameters β^i and b, and promoting them to be dynamical fields, which turns them into a sort of Goldstone modes. One could also call them a collective coordinates fields, since u^μ represents the motion of the brane as a whole. Therefore by allowing parameters to vary we no longer have an exact metric solution, but instead Einstein equations result in some constraints for their form. The theory of these parameters low energy dynamics turns out to be exactly the advertised hydrodynamics obtained from AdS/CFT, known as the fluid/gravity duality.

A concrete way of realizing this idea is to introduce new fields[4],

$$b = b(x^\alpha), \;\; \beta^i = \beta^i(x^\alpha), \tag{3.77}$$

and rewrite the metric solution as follows:

$$ds^2 = -2u_\mu(x^\alpha)dx^\mu dr - r^2 f(b(x^\alpha)r)u_\mu(x^\alpha)u_\nu(x^\alpha)dx^\mu dx^\nu + r^2 P_{\mu\nu}(x^\alpha)dx^\mu dx^\nu. \tag{3.78}$$

The new fields (3.77) in (3.78) represent a sort of ripples on the geometry, understood as local distortions of the brane from its static form. Physically $u^\mu(x^\alpha)$ and $b(x^\alpha)$ are the boost and scaling that would have to be applied at the point x^α, to turn the metric locally *at that point* into the static form (3.74).

The meaning of these new fields in the dual boundary field theory can be understood, if we holographically read-off the stress-energy tensor dual to the above metric. The stress tensor for arbitrary bulk geometry is defined conveniently in the following more general form not restricted to the Fefferman-Graham coordinates:

$$T_{\alpha\beta} = \left(\frac{N^2}{4\pi^2}\right) \lim_{r\to\infty} r^2 \left[K_{\alpha\beta} - (K-3)\gamma_{\alpha\beta} + \frac{1}{2}G^{(4)}_{\alpha\beta}\right]. \tag{3.79}$$

[4]Notice the lack of r dependence. We are interested only in the directions 'along the moduli', parallel to the unperturbed horizon, which corresponds to light (gap-less) excitations. Explicit perturbation dependence on r would be like a motion in the Higgs potential direction, corresponding to massive excitations. These will be generated as a back-reaction to this low-energy perturbation, as shall will see.

Here $K_{\mu\nu}$ and K are the constant r hypersurface second fundamental form (extrinsic curvature) and its trace, $\gamma_{\mu\nu}$ is the induced metric and $G^{(4)}_{\mu\nu}$ is its Einstein tensor. If we evaluate this formula on the gauged metric (3.78) and drop all the derivative terms we obtain a familiar looking tensor:

$$T_{\alpha\beta} = \frac{1}{b^4}\left(\eta_{\alpha\beta} + 4u_\alpha u_\beta\right). \tag{3.80}$$

Formally this resembles the stress-energy tensor of a perfect fluid. At this stage the fields b and $u^\alpha(\beta^i)$ are completely undetermined, but the obtained structure hints, that they could be fluid dynamics variables: local temperature and fluid flow velocity. To confirm this we must obtain and analyse their equations of motion. This is the goal of the subsequent discussion and the central point of the fluid/gravity duality.

The expression (3.78) is now our candidate for a dynamical solution. Of course as we mentioned for arbitrary new fields (3.77) it will not satisfy Einstein equations. But one may hope that if the dynamics of b and β^i would be *sufficiently* slow, then one could improve the the perturbative metric and approximate the real fully dynamic solution. By slow evolution we mean variations of our new fields small enough, so they are close to constant fields, which of course correspond to an exact solution discussed above. We could instead consider corrections to b and β to be just small in the amplitude. However as we just said the rapidity of the perturbation is more relevant, because for arbitrarily small but constant b and β metric (3.78) is again exact solution. We will see below what overall conditions on the β^i and b form are provided by Einstein equations.

We have used a phrase 'sufficiently slow' in the description above. This implies an existence of a certain scale, with respect to which we shall tell, if something is slow. This is exactly where the gradient expansion of hydrodynamics appears in the present context. The expansion scale in our case is provided by the only dimensionful parameter available to us in our system: the horizon locus. In the static case it is specified by a single constant, serving as the only global scale and directly translating to the temperature via $T = 1/(\pi b)$. In the present dynamic spacetime we shall call $T(x^\alpha)$ a dynamic or local temperature. This will be justified in subsequent chapters. We will use the local temperature T to form a proper expansion parameter for Einstein equations.

We henceforth treat the metric (3.78) as a slowly-varying perturbation of the exact black brane geometry (3.75), and try to improve it by adding and refining corrections. Einstein equations will guide us in this task. Upon inserting the Ansatz (3.78) into the equations terms of first and second orders in spacetime derivatives of b and β^i appear:

$$G_{MN} = G_{MN}[g^{(0)}_{\mu\nu}, \partial^n_\mu b, \partial^n_\mu \beta^i] = 0, \text{ with } n = 1, 2. \tag{3.81}$$

Here $g^{(0)}_{\mu\nu}$ is the exact background solution with suitably inserted local parameters. We will now employ the scale represented by $b(x^\alpha)$. By rescaling the bulk variable r with it, so that the putative horizon defined by $f(r) = 0$ lies at $r = 1$ (which sets the unit scale as $b = 1$), we unravel certain hierarchical structure. The nature of (3.81) is such, that all appearances of derivatives along x^α which were not scaled by b, of $\log b$ (terms like $\partial b/b$) or β^i, are accompanied by a multiplicative factor of $b(x^\alpha)$ after this step. Let us assume, that L^n represents a common b and β^i fields space-time variation scale, originating in the n-th ∂_α derivative, and T related to b is the temperature. It follows therefore from the structure of (3.81), that each boundary coordinate n-derivative contribution to Einstein equations is associated with a factor of $(b/L)^n \sim 1/(TL)^n$.

We thus see, that Einstein equations with the help of the scale b dictate a natural expansion parameter for the solutions. It is defined as a combination of the local temperature $T(x^\alpha)$ and the *number of* boundary (or transverse to r) directions derivatives ∂_α, which correspond to L. The small parameter we are looking for is thus $1/(TL)$, and we shall seek a metric solution as a power series when $TL \gg 1$. This translates to the number of derivatives at each order of the metric expansion ($TL \to \infty$ amounts to no derivatives at all, hence constant and exact equilibrium solution (3.75)). Such an expansion scheme performed for a linear problem would be manifest in the Fourier space, where we could directly define a small parameter as k/T, enforcing small momenta perturbations.

This description may seem a little convoluted, but in fact such an expansion parameter is quite easy to implement. To effectively keep track of the number of differentiations it suffices to introduce an auxiliary parameter through boundary coordinates rescaling:

$$x^\alpha \to \varepsilon x^\alpha. \tag{3.82}$$

After this operation each partial boundary differential applied to b or β^i will yield a power of ε. We should thus think of ε as a small number, use it to expand Einstein equations and set it to unity afterwards. Of course in principle one would also have to show, that the resulting expansion in powers of ε is convergent at $\varepsilon = 1$. We will be dealing with this issue in Chapter 7. The perturbative metric takes now the following shape:

$$\begin{aligned} g_{\mu\nu}(x^\alpha, r) &= g^{(0)}_{\mu\nu}(b(\varepsilon x^\alpha), \beta^i(\varepsilon x^\alpha), r) + \varepsilon g^{(1)}_{\mu\nu}(b(\varepsilon x^\alpha), \beta^i(\varepsilon x^\alpha), r) \\ &+ \varepsilon^2 g^{(2)}_{\mu\nu}(b(\varepsilon x^\alpha), \beta^i(\varepsilon x^\alpha), r) + o(\varepsilon^2) \end{aligned} \tag{3.83}$$

The corrections take the form of additional r-dependent terms in the expansion, because after introducing perturbations in b and β^i it is likely that the metric will no longer strictly maintain its initial structure (3.75). It would not suffice to focus just on the x^α dependent gauged parameters.

Such an Ansatz is inserted into Einstein equations and results in an infinite chain of coupled equations for $g^{(i)}_{\mu\nu}$. The complete scheme of the derivative counting combines the ε parameter in the functions arguments with the ε coefficient in front of the functions, to collectively indicate, what is the order of the given term in the full equations chain obtained from (3.81), upon inserting into them (3.83). Such a hierarchy of equations must be supplemented with appropriate boundary conditions at the horizon, conformal boundary, and subsequently solved order by order.

We again should clarify here, that this procedure aims at slow transverse evolution, not equations linearisation. We admit arbitrarily large amplitude variations, necessary for nonlinear horizon evolution, but small in momenta involved.

We shall not cover now the technical details and main steps of the whole construction, but instead refer the reader to the Appendix 3.10 located at the end of the present chapter. Here for brevity we proceed directly to the outcome of the above procedure, which at first order (after further complicated operations described in the appendix) summarizes in the following formulae:

$$\begin{aligned} ds^2_{(1)} &= -2u_\mu dx^\mu dr - r^2 f(br) u_\mu u_\nu dx^\mu dx^\nu + r^2 P_{\mu\nu} dx^\mu dx^\nu \\ &+ 2r^2 b F(br) \sigma_{\mu\nu} dx^\mu dx^\nu + \frac{2}{3} r u_\mu u_\nu \partial_\lambda u^\lambda dx^\mu dx^\nu - r u^\lambda \partial_\lambda (u_\mu u_\nu) dx^\mu dx^\nu. \end{aligned} \tag{3.84}$$

The stress-energy tensor holographically extracted from this metric using (3.79) and $b = 1/(\pi T)$ is:

$$T^{(1)}_{\mu\nu} = (\pi T)^4 \left(\eta_{\mu\nu} + 4u_\mu u_\nu\right) - 2(\pi T)^3 \sigma_{\mu\nu}. \tag{3.85}$$

With $\sigma_{\mu\nu}$ we denote the first order shear tensor:

$$\sigma^{\mu\nu} = P^{\mu\alpha} P^{\nu\beta} \partial_{(\alpha} u_{\beta)} - \frac{1}{3} P^{\mu\nu} \partial_\alpha u^\alpha. \tag{3.86}$$

The above expression has the precise form of a first order viscous hydrodynamics stress-energy tensor, like the one encountered in Chapter 2. The general hydrodynamics equations

$$\nabla_\mu T^{\mu\nu} = 0 \tag{3.87}$$

are found in the Appendix 3.10 and are discovered as a direct consequence of imposing Einstein equations on (3.84). In the case at hand we would have above $T_{\mu\nu} = T^{(1)}_{\mu\nu}$ of (3.85). Again, following the appendix it can be noted, that the coefficient of the shear tensor in (3.85) is not free, but is completely fixed through solving Einstein equations with appropriate boundary conditions and non-singularity of the solution at the horizon. The value $-2(\pi T)^2 \sigma_{\mu\nu} \equiv -2\eta(T)\sigma_{\mu\nu}$ seen above corresponds precisely to the shear viscosity to entropy ratio, which we mentioned already in the opening introductory chapter, and which was originally found from Kubo formula for stress tensor correlation function [Policastro 2001]. For our gauge theory at strong coupling we have equilibrium entropy density[5] $s = 4\pi^4 T^3$, so with the above shear viscosity $\eta = \pi^3 T^3$ we find in agreement with the classical result, that

$$\frac{\eta}{s} = \frac{1}{4\pi}. \tag{3.88}$$

This proves the statement made at the beginning of our considerations, that AdS/CFT can justify the structure of hydrodynamic gradient expansion and give exact numerical values of the dual theory transport coefficients.

3.9 Closing remarks

We close this chapter with a few noteworthy remarks. There are several important or even remarkable facts following from the whole fluid/gravity duality programme:

- The obtained tensor, as well as all higher derivable corrections, is unique and specified by the microscopic theory.
- The systematic derivation gives us well justified constitutive relations[6] for the hydrodynamic stress-energy tensor. These would otherwise have to be postulated at the level of heuristic hydrodynamics construction.

[5] We have found previously s in (3.67) with different normalization conventions. However, by noticing that the leading part of (3.85) is the perfect fluid expression, we retrieve its pressure as $(\pi T)^4$. Then from thermodynamics and free energy density to pressure relation $P = -f$, we have with $f = u + Ts$, where u and s are energy and entropy densities, that $(\pi T)^4 = P = -u + Ts$, and since for our conformal fluid $u = 3P$ we obtain $s = 4\pi^4 T^3$.

[6] As we introduced in Chapter 2, these are parametrisations of the stress tensor by the fluid variables of temperature and velocity.

- Transport coefficients are computed exactly, and in principle we can obtain as many of these, as we need, although it becomes more cumbersome with their order.
- There were no assumptions on the form of the stress-energy tensor. It all followed uniquely from the structure of Einstein equations solution in AdS space.
- We have constructed a map from the space of hydrodynamics solutions into the space of Einstein equations solutions. The latter one is generally much richer that the former, but in the regime of gradient expansion they coincide.
- The fact that a *precise* hydrodynamic equation was found in gravity has many potentially profound consequences. To name just one, we may have found another way to attack the long standing challenges of hydrodynamics, like the turbulence. There has already been some development in this direction [Eling 2010].
- Lastly, it is fascinating that we have gained a way to investigate near-equilibrium physics from gravity. Black holes have long been known to have thermodynamic properties, but with the AdS/CFT duality we can have alternative access to microscopically justified non-equilibrium physics.

We the above we have completed the introduction to the dynamic fluid/gravity duality. As a final remark let us note, that the above procedure carried with aim at generality is necessarily excessively complicated and not simple to algorithmize on a computer. However in the case of more specialized boost-invariant system, in which we shall be mostly interested in later on, there is an equivalent but operationally more efficient way to compute the metric in a gradient expansion. It is based on the use of the mentioned before scaling variable. We shall rely on this approach in Chapter 7, where we will describe very high order gradient expansion computations.

3.10 Appendix A: The technical details of fluid/gravity duality

In this technical appendix we resume the detailed explanation of how fluid/gravity works.

3.10.1 Iterative fluid/gravity duality expansion scheme

The functions $g^{(i)}_{\mu\nu}$ introduced in (3.83) are geometry corrections that must be determined from the set of equations (3.81). We must however refine a little bit the picture of the perturbative structure based on these corrections. Namely, the functions b and β^i, as a part of the metric $g_{\mu\nu}$, satisfy certain equations of motion derived together with equations for $g^{(i)}_{\mu\nu}$ from the Einstein tensor (3.81). But these equations for b and β^i will also themselves be corrected with each order in the ε expansion, so their solutions are in fact also of the form:

$$b(x^\alpha) = b^{(0)}(\varepsilon x^\alpha) + \varepsilon b^{(1)}(\varepsilon x^\alpha) + \mathcal{O}(\varepsilon^2), \tag{3.89}$$

$$\beta(x^\alpha) = \beta^{(0)}(\varepsilon x^\alpha) + \varepsilon \beta^{(1)}(\varepsilon x^\alpha) + \mathcal{O}(\varepsilon^2). \tag{3.90}$$

To dismantle a possible confusion with the ultimate appearance of the ε parameters in (3.83) we should state more explicitly, how higher order corrections are constructed. The

term $g^{(1)}$ in the final solution of Einstein equations is assembled from two main pieces. Assuming the knowledge of the zero-th order terms[7], $b^{(0)}$ and $\beta^{(0)}$, first we insert $\beta = \beta^{(0)}(\varepsilon x^\alpha)+\varepsilon\beta^{(1)}(\varepsilon x^\alpha)$ and $b = b^{(0)}(\varepsilon x^\alpha)+\varepsilon b^{(1)}(\varepsilon x^\alpha)$ into the zero-th order term $g^{(0)}(b,\beta^i)$, expand it to the first order in ε, and then we write the Ansatz for $g^{(1)}$ in the form:

$$\begin{aligned} g^{(1)}_{\mu\nu}(x^\alpha, r) &= \left[\partial_\varepsilon g^{(0)}_{\mu\nu}\left(b^{(0)}(\varepsilon x^\alpha)+\varepsilon b^{(1)}(\varepsilon x^\alpha), \beta^{(0)}(\varepsilon x^\alpha)+\varepsilon\beta^{(1)}(\varepsilon x^\alpha)\right)\right]\Big|_{\varepsilon=0} \\ &+ \tilde{g}^{(1)}_{\mu\nu}(r). \end{aligned} \tag{3.91}$$

In the first part coming from the lower order only the $b^{(0)}(x^\alpha)$ and $\beta^{(0)}(x^\alpha)$ will survive (in fact their derivatives ∂_α), and the second one, $\tilde{g}^{(1)}_{\mu\nu}(r)$, is the generic first order r-dependent metric correction. So this is the complete term contains all the information related to the one-derivative contribution to the solution $g_{\mu\nu}$.

Let us now finally turn to the structure of the perturbative system of equations, obtained from (3.81). In an inductive manner let us assume, that for some n we already know the solutions for $g^{(i)}$ up to the order $(n-1)$, and for $b^{(i)}$ and $\beta^{(i)}$ to the order $(n-2)$[8]. By inserting them to the Ansatz (3.83) and expanding Einstein equations (3.81) in ε, we get the following chain of equations:

$$H\left[g^{(0)}(\beta^{(0)}, b^{(0)})\right] g^{(n)}_{\mu\nu}(x^\alpha, r) = s^{(n)}_{\mu\nu}(x^\alpha),\ \ n = 0, 1, ... \tag{3.92}$$

Each such an object is a coefficient of the Einstein tensor expansion parameter ε^n, and thus represents an n-th order contribution to Einstein equations. This expression represents a system of ordinary differential equations second order in variable r, coupled through the sources $s^{(n)}$. These equations possesses certain important features.

First of all the left hand side is arranged so that it does not depend on any boundary derivatives ∂_α or lower order metric contributions $g^{(i<n)}$. This is because each such a term would carry appropriate factors of ε, which would increase the overall expression order beyond ε^n, since the term $g^{(n)}$ is already of this order. Only the unscaled r-derivatives remain. In this way we effectively linearise[9] *and* separate the system of equations for $g^{(i)}_{\mu\nu}$. All the dependence on the transverse directions x^α is encoded algebraically in the zero-th order functions $b^{(0)}$ and $\beta^{(0)}$, but not in their derivatives. We have thus obtained an operator H, that is a local function of the boundary variables x^α, whose values at any such point is specified only by the values of $b^{(0)}$ and $\beta^{(0)}$ there. In other words it means, that to evaluate this differential operator at some point one only needs to know the values of the b and β^i fields at that point, and not their derivatives. This property is called ultralocality and plays an important role in the construction, as will be noted below.

Second feature of the equations (3.92) is that they can be further divided into disjoint tensorial channels for different metric components, according to the scalar, vector and tensor representations of the spatial rotation group $SO(3)$, acting on the boundary directions x^i. In this way we utilize the part of the unbroken symmetry algebra annihilating the exact stationary brane solution. The decomposition guarantees a decoupling of these distinct channels, just like in the linear metric perturbations analysis [Kovtun 2005]. In fact what we do here is a sort of linear analysis on the top of every lower order metric. The net nonlinear

[7] Of course $g^{(0)}_{\mu\nu}$ is known exactly from the boosted black brain solution, discussed above.

[8] For $n \leq 1$ we assume these terms to be unconstrained or absent. Terms with $i < 0$ will not appear in the equations and terms $b^{(0)}$ and $\beta^{(0)}$ are unconstrained at the zero-th order $n = 0$, since they are at this order equivalent to constant boost and scaling. They can to this order be removed by a change of coordinates.

[9] For the leading order expression $g^{(n)}$ only, the combined evolution is still nonlinear.

evolution is achieved through the sources. Each such a channel possesses its own differential operator, H_R, the same at every order ε for each $SO(3)$ irreducible representation R. Also, these operators do not depend on the order n.

The third point involves sources $s^{(n)}_{\mu\nu}(x^\alpha)$. These on the other hand depend on all lower order contributions $b^{(i)}$, $\beta^{(i)}$, $g^{(i)}_{\mu\nu}$ for $i < n$, and their combinations with boundary ∂_α derivatives, that give in total expressions of the order ε^n. For example $s^{(n)}$ contains terms like $\partial^k_\alpha b^{(l)}$, with $(k+l) = n$. These expressions are in principle very complicated, with their complexity degree growing rapidly with n. They carry all the burden of communicating various components of the metric between different perturbation orders and couple them together.

Lastly, we should mention that $b^{(n)}(x^\alpha)$ and $\beta^{(n)}(x^\alpha)$ are absent from the equations at the order ε^n altogether. They can not appear at this order, since with derivatives they would exceed the considered perturbation order n, and without derivatives they would be simply equivalent to some strictly constant b and β^i terms. But such terms solve Einstein equations exactly, since they are equivalent to global boost and rescaling of the exact static black brane solution that we have started with, and thus are a symmetry of the exact solution. The purely algebraic occurrence of the functions $b^{(0)}$ and $\beta^{(0)}$ on the left in H stems from the fact, that they are of zero-th order in ε and thus do not contribute to the power counting.

Also we could note, that we are in fact considering a (possibly huge) perturbation of an *existing* horizon, put in by hand into the AdS bulk. In such case no matter what we do we should always reach the equilibrium black brane configuration. From this perspective we are always in a local neighbourhood of the equilibrium state, sourced by the near-equilibrium metric $g^{(0)}_{\mu\nu}$ in H.

To proceed further with the construction we shall now observe that Einstein equations in general consist of dynamical equations, and constraints. The same holds for the expanded version, (3.92). By counting, as for a symmetric tensor in five dimensions they form a total of $5 \times 6/2 = 15$ equations. Upon closer analysis it can be discovered, that four of these equations do not contain genuine metric corrections, $g^{(i)_{\mu\nu}}$, but only the boundary fields b and β^i. These equations do not depend on the second order bulk r derivatives. Consequently they are regarded as *constraint* equations[10].

To extract these qualitatively different equations from the complete system (3.92) we utilize the projection of Einstein tensor (3.81) onto the bulk direction dr. By contracting this tensor with the vector ξ^M dual to the 1-form dr[11]

$$\xi^M = (0, 0, 0, 0, \frac{1}{\sqrt{-g_{vv}}}), \tag{3.93}$$

we obtain the following vector:

$$G_{MN}\xi^M = E_N, \;\; N = t, x, y, z, r. \tag{3.94}$$

The components $N = t, x, y, z$ form a subset of constraints, a vector confined to the hypersurfaces $r =$ const. parallel to the boundary. If one evaluates this expression on a

[10] Usually constraints are understood as relations up to first order in derivatives, imposed at a constant time hypersurface, which are carried further in time by the dynamic equations. In the context of AdS/CFT we often encounter a so-called radial evolution, which means solving Einstein equations in the bulk variable r. Thus relations stated at constant r hypersurface are termed constraints. They appear to be conserved by the radial Einstein equations 'evolution', and thus are correct also at the boundary.

[11] Since we will be considering equation at the order n, the vector ξ^M may be computed with respect to the static initial metric (3.74), because all the metric corrections would exceed the order n.

metric expanded up to the order n, $E_\alpha^{(n)} = 0$, its Taylor expansion near the boundary $r \to \infty$ will reveal its important content:

$$\partial_\alpha T^{\alpha\beta}_{(n-1)}(x^\sigma) = 0. \tag{3.95}$$

In this expression $T^{\alpha\beta}_{(n-1)}$ is precisely the stress-energy tensor (3.79) holographically obtained from the lower order solution, $g^{(n-1)}_{\mu\nu}$. As such $T^{\alpha\beta}_{(n-1)}$ satisfies the boundary conformal symmetry (essentially is traceless) and is a local function of $b(x^\alpha)$ and $\beta^i(x^\alpha)$, interpreted before as the potential boundary temperature and velocity fields. This equation confirms this expectation and the tensor itself is now interpreted as the stress-energy tensor of the *fluid* dual to the gravity solution under construction. The equation (3.95) is the long-pursued hydrodynamics equation and this result is the very core of fluid/gravity duality. Part of Einstein equations have the functional form of fluid equations.

It should be noted, that this tensor at the order $(n-1)$ is a function of all the lower order hydrodynamic fields $b^{(i)}$ and $\beta^{(i)}$, up to the order $(n-1)$. Since we are considering Einstein equations at the order n, we discover that to find a solution at this order, we first need to know the form of the one order lower *fluid* stress-energy tensor, solving (3.95).

3.10.2 Solving one step of the fluid/gravity expansion scheme

We have at this point completed the construction of the iterative scheme. To conceptually clarify this somewhat involved procedure let us now point out the major steps taken to arrive at a solution of the order n. The detailed procedure is transparent but highly technical. The in-depth discussion is contained in the original work of [Bhattacharyya 2008b] (see also [Hubeny 2012]).

The steps are as follows.

- We start with the zero-th order Ansatz (3.75) for $ds^2_{(0)} = g^{(0)}_{\mu\nu}(b, \beta^i)dx^\mu dx^\nu$, with the fields $b = b^{(0)}(x^\alpha)$ and $\beta = \beta^{(0)}(x^\alpha)$ completely unconstrained.
- We holographically extract the zero-th order stress tensor $T^{\alpha\beta}_{(0)}$, (3.80).
- We evaluate Einstein equations on the above initial metric $ds^2_{(0)}$ to obtain constraint equations (3.94) for the fields $b^{(0)}$ and $\beta^{(0)}$:

$$\nabla_\alpha T^{\alpha\beta}_{(0)}(x^\alpha) = 0. \tag{3.96}$$

- Due to the ultralocal nature of equations (3.92) we only need a local solution at a given point (e.g. $x^\mu = 0$), instead of a general nonlinear hydrodynamics solution of (3.96), which is hard to obtain. The constraint equations impose relations of first order in derivatives between the stress tensor components, but does not completely determine the hydrodynamic fields. However at a single point x^α used for the ultralocal analysis we can impose $b = 1$ and $u^\mu = (1, 0, 0, 0)$ by an appropriate coordinate transformation. Then only the gradients of these fields will remain in the expanded Einstein equations[12], and they are bound by the hydrodynamic constraint equation. To the first order in derivatives (and for the hydrodynamic fields of the order ε^0) the constraint (3.96) evaluates to:

$$\partial_v b^{(0)} = \frac{\partial^i \beta^{(0)}_i}{3},\ \partial_i b^{(0)} = \partial_v \beta^{(0)}_i,\ b(0) = 1,\ u^\mu(0) = (1, 0, 0, 0). \tag{3.97}$$

[12] We can now appreciate the boundary ∂_α derivatives absence in the operator H of (3.92).

No further restrictions can be imposed on these fields at this order.

- Next we construct the first order metric (3.91) by expanding the zero-th order metric $g^{(0)}_{\mu\nu}(b^{(0)}, \beta^{(0)})$ to the first order in gradients of $b^{(0)}$ and $\beta^{(0)}$, and add the genuine metric correction $g^{(1)}_{\mu\nu}(r)$.

- We then plug this corrected metric into Einstein equations, use the hydrodynamic constraints of (3.97) and obtain the equations for three different $SO(3)$ channels: scalar, vector tensor, with appropriate source terms $s^{(1)}_{\mu\nu}$ built from the lower order metric components, $g^{(0)}_{\mu\nu}$ and their gradients ∂_α.

- The resulting second order equations are integrated in the bulk, from $r' = \infty$ to some given $r' = r$. Since we are using manifestly regular Eddington-Finkelstein-like coordinates the r-integration boundary condition in the bulk must ensure that the metric will be non-singular up to the AdS curvature blow-up at $r \to 0$. For example, for a tensorial metric correction the solution reads:

$$\alpha^{(1)} = -\int_r^\infty \frac{dx}{f(x)x^5} \int_1^x s(y)dy, \text{ with } f(x) = 1 - \frac{1}{x}, \tag{3.98}$$

  and the regularity at the initial equilibrium horizon locus $r = 1$ is achieved by the internal integral's lower limit. When its upper limit reaches $x = 1$, the singularity in $f(x)$ is cancelled. This mechanism persists to all orders in the gradient expansion, since as we said the evolution operator H of (3.92) is the same at every order n. The second condition at the conformal boundary $r \to \infty$ is that the metric there remains unchanged as a Minkowski metric. This imposes vanishing Dirichlet condition on all the metric corrections at $r = \infty$. This is implemented in the above integral similarly as before, by the upper limit of the external integral. The whole metric correction vanishes when lower limit tends to the boundary, $r \to \infty$.

- In the above bulk variable integration the transport coefficients emerge. This is exactly where we extract the information from the so-called near boundary UV sector of the theory and coin it into the specific numerical constants, creating the effective IR hydrodynamical description of the theory. This is one of the most important points, as transport coefficients are of major phenomenological interest. The various numbers emerging during integrations like (3.98) and forming these coefficients appear to be of the precise value necessary to assure metric regularity. Should these be different we would obtain a naked singularity in the bulk, contradicting physicality. This mechanism is Eddington-Finkelstein incarnation of the original Fefferman-Graham non-singularity condition [Janik 2011] determining transport coefficient from Riemann tensor squared (i.e. coordinate invariant) regularity. Here we do not need to use such additional structures because coordinates themselves are regular and can determine transport coefficients.

- After obtaining the solution $g^{(1)}_{\mu\nu}$ in all the channels we need to covariantize it to revert the fixing of b and u^μ fields. This is done by a general boost and rescaling, or considering what four dimensional structures could be formed from three dimensional velocity and scaling.

- Subsequently we insert this complete solution $g^{(1)}_{\mu\nu}$ to the metric Ansatz and repeat the procedure to construct $g^{(2)_{\mu\nu}}$.

Chapter 4

Geometric tools from General Relativity

The essential part of fluid/gravity duality introduced in the previous chapter relies on obtaining solutions to non-linear time dependent Einstein equations. This is a challenging task which we will face in chapters 6 and 7, and requiring knowledge beyond pure differential equations theory. This includes certain tools from differential geometry, which is the very fabric of General Relativity.

In this chapter we gather and summarize several gravitational physics mathematical techniques, which will be instrumental in our developments of chapter 6.

To solve the nonlinear set of Einstein equations one often has to resort to numerical methods. The field of numerical General Relativity is vast and among others, deals with problems of colliding black holes, gravitating hydrodynamics and gravitational radiation. It turned out to be instrumental in the recently successful search for gravitational waves by preparing templates of possible signal waveforms. However the possibility of solving numerically dynamical gravity comes at a price. The problem must be well posed for simulations on the computer which has finite memory and requires proper handling of singularities. Several approaches to numerical GR have been developed over the years to tackle specific problems. One of the most widely known utilizes the famous Arnowitt, Deser, Misner [Arnowitt 1959] Hamiltonian formulation of General Relativity or the so called BSSN 3+1 formulation. As will be discussed later, specific variation of the ADM method allowed us to obtain for the first time a full numerical dynamical geometry dual to gauge theory fluid with canonical Minkowski boundary conditions at the AdS space boundary. The only previous successful attempt of [Chesler 2009] dealt with distorted non-Minkowski boundary condition, which however is not exactly the physical plasma system we are modelling with holography. The approach we developed is the first implementation of ADM formulation in the realm of AdS/CFT, dealing with non-asymptotically flat spacetime. The introduction of this method led us to a novel (to our knowledge) technique of handling singularities in the numerical integration domain. We will elaborate more on this in Chapter 6. Here we shall collect some relevant facts on General Relativity and describe the details of the ADM formulation, following mostly the discussion of [Poisson 2004] and [Baumgarte 2003].

4.1 ADM formulation of General Relativity

The unity of space and time is the founding stone of relativity. Equal footing on which those dimensions are treated is expressed as diffeomorphisms invariance (or redundancy) of General Relativity. Under general (nonlinear) coordinates transformation temporal and spatial directions can be mixed to form a new coordinate system. The role of coordinates is just to cover (or map) the manifold and we are free to do this in any way convenient. This freedom is the gauge redundancy of the theory. Often to perform specific computations it is necessary to specify an explicit form of the metric. This breaks the diffeomorphisms invariance. In the case we will be interested in a particular distinction between temporal

and spatial dimensions will turns out to be useful. We shall describe a way to introduce such a scheme leading to the ADM formulation.

Let us assume that on the manifold of interest $(M, g_{\mu\nu})$, $\mu = 0, ..., d$, covered by some reference coordinates $\{x^\mu\}$ one can define a single valued real scalar function $\lambda(x)$. The only additional condition on the function is that its gradient 1-form

$$\Omega_\mu = \nabla_\mu \lambda(x), \tag{4.1}$$

gives a future directed time-like vector field

$$n^\mu = -\alpha g^{\mu\nu} \nabla_\nu \lambda(x), \ \alpha = \frac{1}{\sqrt{-g^{\mu\nu} \nabla_\mu \lambda(x) \nabla_\nu \lambda(x)}}. \tag{4.2}$$

This condition implies that the spatial hypersurfaces defined by $\lambda(x) = const.$ will not intersect, since the vector n^μ normal to the hypersurface is not allowed to turn around (which would change the norm from time-like). Thus the function $\lambda(x)$ specifies an ordered collection of hypersurfaces called foliation of the manifold and is in a sense monotonic. Apart from that the foliation is arbitrary, we can slice the space as desired and this freedom is one of the most advantageous features of the ADM formulation. Spatial slices of the foliation can be thought of as constant time hypersurfaces with consecutive values of $\lambda(x)$. The quantity α being the norm of the normal 1-form is called lapse and is central to our present and future discussion. It will be described in more detail later in what follows.

In general a hypersurface can be specified in two complementary ways. By the constraint equation,

$$\Phi(x) \equiv \lambda(x) - C = 0, \tag{4.3}$$

and by parametric equation in a given coordinates system,

$$\{x^\mu = f^\mu(\lambda = C, y^a)\}. \tag{4.4}$$

The parameters y^a play the role of induced coordinates on the hypersurface.

Apart from the foliation one can also cover the whole spacetime with time-like parametric curves (e.g. geodesics, but not necessarily) intersecting each hypersurface once, like straight lines would densely cover the Euclidean plane. Such a collection of lines is called a congruence. Each member curve would pierce the foliation leaf $\lambda(x)$ at some point $\{y^a\}$ and can be parametrized with the value of λ along the flow through the foliation leaves:

$$\gamma_y(\lambda) = \{x^\mu(\lambda, y^a)\}. \tag{4.5}$$

By demanding that each curve γ_y crosses the hypersurfaces at the same values of parameters $\{y^a\}$ we can fix their values between the hypersurfaces and align them. In this way a new coordinate system covering spacetime can be introduced, by choosing $\lambda(x)$ as the new time and $\{y^a\}$ as the new spatial coordinates. As seen in the above expression for $\gamma_y(\lambda)$, one such curve can be obtained from the hypersurface's parametric equation by fixing the spatial parameters $\{y^a\}$ and letting λ vary freely.

The congruence need not to be orthogonal to the foliation, the covering of spacetime with it is again to some extent arbitrary. By taking the derivative of $\gamma_y(\lambda)$ with respect to the level function, we obtain a vector field tangent to the congruence:

$$t^\mu = \frac{d}{d\lambda} x^\mu(\lambda, y^a). \tag{4.6}$$

Similarly the hypersurface tangent basis can be found as:

$$e^\mu_a = \frac{\partial}{\partial y^a} x^\mu(\lambda, y^c),\ e^\mu_a n_\mu \propto e^\mu_a \partial_\mu \lambda(x) = 0. \tag{4.7}$$

The vector t^μ is time-like but not necessarily parallel to the normal vector n^μ. In fact, it can be decomposed into the normal and tangent parts, as seen from the definitions of the unit normal and tangent vectors (4.2),(4.6):

$$t^\mu = \alpha n^\mu + \beta^a e^\mu_a. \tag{4.8}$$

The spatial projection $\beta^\mu(x)$ is called the shift vector and is tangent to the spatial hypersurfaces. It reflects the freedom of the congruence orientation relative to the foliation. It also can be seen as sliding of the subsequent spatial coordinates on the successive slices. An important property of the vector t^μ is that it is dual to the level 1-form Ω for any shift β^μ:

$$t^\mu \Omega_\mu = 1, \tag{4.9}$$

as opposed to the unit normal vector n^μ. This means that t^μ connects hypersurfaces separated by the same amount of proper time parameter along the curves γ. In other words γ is an integral curve of the vector field t^μ and Lie derivative along $t^\mu \partial_\mu$ is a derivative with respect to λ in orthogonal $\{\lambda, y^a\}$ coordinates.

Thus far we have discussed the issues of coordinates and spacetime mapping. To gain access to more detailed information about the space, foliation embedding in the ambient space, its curvature and evolution we have to turn to more complicated quantities. An important object related to hypersurfaces is the first fundamental form, or induced metric:

$$\gamma_{\mu\nu} = g_{\mu\nu} + n_\mu n_\nu. \tag{4.10}$$

It is a purely transverse (spatial) tensor: $\gamma_{\mu\nu} n^\nu = 0$ and also a projection operator:

$$\gamma_\mu{}^\alpha \gamma_{\alpha\nu} = \gamma_{\mu\nu}. \tag{4.11}$$

The tensor $\gamma_{\mu\nu}(x)$ is confined to the hypersurface and contains information on its intrinsic properties. With it one can project various tensors onto the foliation leaves. There is a covariant derivative compatible with it,

$$D_\mu T^\beta_\alpha = \gamma_\mu{}^\sigma \gamma_\iota{}^\beta \gamma_\alpha{}^\kappa \nabla_\sigma T^\iota{}_\kappa,\ D_\mu \gamma_{\alpha\beta} = 0. \tag{4.12}$$

Further objects like the Christoffel symbols, induced Riemann tensor $\mathcal{R}^\mu{}_{\nu\alpha\beta}$ and others can also be introduced.

Next important tensor is the second fundamental form or extrinsic curvature, defined as:

$$K_{\mu\nu} = -\frac{1}{2} \mathcal{L}_n \gamma_{\mu\nu}. \tag{4.13}$$

The Lie derivative is taken along the unit normal vector n^μ. This tensor contains information about the embedding of the hypersurface in the ambient space. It describes

how it bends with the foliation function $\lambda(x)$ but also how the induced metric changes with advancing λ.

With the projection operator at hand we can now decompose Einstein equations,

$$R_{\mu\nu} - \frac{1}{2}Rg_{\mu\nu} = 8\pi G_N T_{\mu\nu}, \tag{4.14}$$

into the transverse and longitudinal parts. Although in the later discussion we will be interested in vacuum equations, we leave the present considerations at a general level and keep the stress tensor $T_{\mu\nu}$ non-zero. It is useful in view of future AdS/CFT applications, as precisely this term contains the cosmological constant Λ. The projection results in separation of constraints from dynamical equations and also casts (4.14) in the form of a first order differential system. For later convenience let us define the projected densities:

$$\rho = T_{\mu\nu}n^\mu n^\nu,\ j_\alpha = -T_{\mu\nu}n^\mu \gamma^\nu{}_\alpha,\ S_{\mu\nu} = T_{\alpha\beta}\gamma^\alpha{}_\mu \gamma^\beta{}_\nu. \tag{4.15}$$

Using appropriate projections of the Riemann tensor we arrive at the so called Hamiltonian and momentum constraints, following from the Gauss and Codazzi equations respectively:

$$\mathcal{R} + K^2 - K_{\mu\nu}K^{\mu\nu} = 16\pi G_N \rho, \tag{4.16}$$

$$D_\alpha K^\alpha{}_\mu - D_\mu K = 8\pi G_N j_\mu. \tag{4.17}$$

Those relations represent the inner stress of the given hypersurface and relates it to the projected energy and momentum current densities. They also reflect the decomposition of the spacetime, since there are no components in the direction orthogonal to the surface.

The dynamics of spacetime in encoded in the definition of extrinsic curvature and Ricci equation. Recall from (4.13) that given the extrinsic curvature $K_{\mu\nu}$ one can evolve the induced metric along the normal vector. In the view of (4.9) we adopt the vector t^μ as the time flow direction and rewrite (4.13) as an evolution equation for $\gamma_{\mu\nu}$:

$$\mathcal{L}_t \gamma_{\mu\nu} = -2\alpha K_{\mu\nu} + D_\mu \beta_\nu + D_\nu \beta_\mu. \tag{4.18}$$

Accordingly, after brief calculations using Einsten and Ricci equations, one obtains the evolution equation for the extrinsic curvature [Baumgarte 2003]

$$\begin{aligned} \mathcal{L}_t K_{\mu\nu} &= -D_\mu D_\nu \alpha + \alpha(\mathcal{R}_{\mu\nu} - 2K_{\mu\sigma}K^\sigma{}_\nu + K_{\mu\nu}K) \\ &+ \beta^\sigma D_\sigma K_{\mu\nu} + K_{\sigma\mu}D_\nu \beta^\sigma + K_{\sigma\nu}D_\mu \beta^\sigma \\ &- 8\pi G_N \alpha[S_{\mu\nu} + \frac{\rho - S}{d-1}\gamma_{\mu\nu}]. \end{aligned} \tag{4.19}$$

In the last equation d is the dimension of the spatial slice and $S = S^\mu{}_\mu$ is the trace of the projected stress-energy tensor. These last two equations for $\gamma_{\mu\nu}$ and $K_{\mu\nu}$ complete the list of physical equations governing the shape and evolution of the spacetime M. Upon the $d+1$ decomposition Einstein equations naturally separate into purely spatial constraint equations, (4.16), (4.17) and evolution equations, (4.18), (4.19). This set is first order

in time and forms a Hamiltonian system, suitable for numerical implementation. The equations should be supplemented with appropriate initial and boundary conditions.

The last missing piece of information are the lapse and shift fields. Those quantities are almost completely arbitrary and as stated above represent the residual gauge redundancy of Einstein equations. But their role is not to be underestimated, a wrong choice of e.g. lapse function may jeopardize the efforts to solve equations numerically while a good choice may allow for a long and accurate simulation. The utility of the ADM formulation and its derivatives stem in part from the singularity avoidance properties of a properly chosen lapse [Alcubierre 2003], which on its own is a small piece of a sophisticated numerical kitchen in General Relativity.

The reformulation of equations was thus far performed in a manifestly covariant way without explicitly adopting any coordinates system. The reference coordinates $\{x^\mu\}$ used at the beginning of this section were just dummy variables. As one may expect, further simplifications may be achieved by adopting coordinates suitable for the problem. By choosing $\lambda(x)$ as the new time variable and passing to the transverse coordinates $\{\lambda, y^a\}$, the metric can be cast in the following form:

$$ds^2 = -\alpha^2 d\lambda^2 + \gamma_{ij}(dy^i + \beta^i d\lambda)(dy^j + \beta^j d\lambda). \tag{4.20}$$

As an immediate consequence we have that $t^\mu = (1, 0, ..., 0)$ and the Lie derivative reduces to an ordinary partial differential, ∂_λ. Furthermore, the $d+1$ dimensional indices of purely spatial tensors may be confined to just spatial values, since temporal coordinates are simply zero, $X^{0\mu} = 0$.

4.2 Geodesic expansion scalars

We will now briefly discuss important element of General Relativity called geodesic expansions. These objects are key element in the definition of dynamic apparent horizon, which in turn serves to define holographically the notion of entropy. We will also heavily rely on them later when dealing with the definition of a numerical cut-off (to localize event horizon). We start by briefly covering the general congruence evolution and then we confine our attention to the so called expansion scalars. Based on this we finish by defining the apparent horizon. General informations on expansions can be found e.g. in the book by Poisson, [Poisson 2004].

The starting point is the question how does a congruence of geodesics behave while traversing the spacetime manifold? If we consider a continuous collection of nearby geodesics we can think of them as a certain flow through space. We can also think of such a congruence as a non-local probe of the spacetime and introduce an effective description of its dynamics. One such an effective parameter, which intuitively and accurately reflects the behaviour of the congruence, is its orthogonal cross-sectional area. We can think of shrinking and stretching of the congruence by the spacetime curvature and this relative motion of aligned geodesics would then be seen as respective change in the area of the congruence cross-section, and its shape. This is basically the focusing and defocusing of the family of geodesics. If we consider specifically null geodesics, we can investigate causal structure of the whole spacetime, in particular in the case of a black hole (or brane).

With the prospect on our future applications let us think about trajectories of light rays consistent with the assumption of boost-invariance in AdS_5 spacetime with transverse spatial homogeneity. We have then only two families of null geodesics, travelling towards the AdS boundary and inwards the infinite AdS throat. These are called outgoing and ingoing

geodesics respectively. With these two geodesics one can associate two tangent null vector fields, denoted as n^μ and l^μ. In the case of boost-invariant metric in five AdS dimensions these vectors are simplified by the symmetry constraints. We additionally impose on them the null and cross-normalization conditions:

$$l^\mu l_\mu = 0,\ n^\mu n_\mu = 0,\ l^\mu n_\mu = -1. \tag{4.21}$$

The above relations ensure that both vectors will point in the same time direction (future or past), but leave an irrelevant (in our case) ambiguity of an overall multiplicative normalization of l and n.

The aforementioned geodesic expansion scalars for each of the two vector fields l^μ, n^μ (4.21) are formed using the general Raychandhuri equation [Poisson 2004]. Let us briefly introduce it here for completeness.

For a timelike unit vector field X^μ and metric $g_{\mu\nu}$ it can be written as

$$\dot{\theta} = -\frac{\theta^2}{3} - 2\sigma^2 + 2\omega^2. \tag{4.22}$$

The dot represents affine parameter derivative and quantities involved are defined as follows:

$$\theta_{\mu\nu} = h^\alpha{}_\mu h^\beta{}_\nu \nabla_{(\alpha} X_{\beta)} \tag{4.23}$$

is the expansion tensor, defined as the the projected vector field symmetrized gradient. The projector operator onto the congruence transverse direction is defined as

$$h_{\mu\nu} = g_{\mu\nu} + X_\mu X_\nu. \tag{4.24}$$

Further,

$$\sigma^2 = \frac{1}{2}\sigma^{\mu\nu}\sigma_{\mu\nu},\ \omega^2 = \frac{1}{2}\omega^{\mu\nu}\omega_{\mu\nu} \tag{4.25}$$

are squares of respectively the shear and vorticity tensors defined as

$$\sigma_{\mu\nu} = \theta_{\mu\nu} - \frac{1}{3}\theta h_{\mu\nu},\ \omega_{\mu\nu} = h^\alpha{}_\mu h^\beta{}_\nu X_{[\alpha;\beta]}. \tag{4.26}$$

The square brackets on the right indicate antisymmetrized covariant derivative. Ultimately, the expansion scalar itself is defined as the trace of the expansion tensor

$$\theta = \theta^\mu{}_\mu. \tag{4.27}$$

The Raychandhuri equation describes a worldlines congruence evolution through spacetime. It contains information about divergence, rotation and shearing of nearby geodesics (and can be also given for more general trajectories). In the most symmetric and simplified case, like the one we analyse the shear and vorticity tensor can be put to zero, and one is left with a simple equation for the expansion flow along the geodesics affine parameter:

$$\dot{\theta} = -\frac{\theta^2}{3}. \tag{4.28}$$

This equation encodes the focusing and defocusing properties of spacetime mentioned above, and is instrumental in defining the apparent horizon properties, discussed further below.

When X^μ is a null vector field, like for our expressions (4.21), the corresponding expansions follow a similar equation, but with slightly different projection operators. In this case we define two expansions for our tangent null vector fields

$$\theta_l = (g^{\mu\nu} + l^\mu n^\nu + l^\nu n^\mu)\nabla_\mu l_\nu, \tag{4.29}$$
$$\theta_n = (g^{\mu\nu} + l^\mu n^\nu + l^\nu n^\mu)\nabla_\mu n_\nu. \tag{4.30}$$

The geometric intuition behind these definitions has been given above. They measure how nearby null geodesic lines behave for the same affine parameter value while progressing along the flow. Changes due to the gravitation force of the geodesic deviation vector connecting neighbouring rays is then reflected in contraction or expansion of the congruence. The above scalars measure this change. This in turn is the crucial ingredient of the apparent horizon definition. Let us introduce it here for later convenience.

4.3 Apparent horizons

Let us first remark, that the notion of a *horizon* is one of the most fundamental concepts in the theory of General Relativity, and we have already seen in Chapter 3 what physical phenomena can be associated with it. The prime example of this is the notion of black brane entropy introduced there. The definition of event horizon is to some extent simple in the static case, where we can analyse the causal structure of spacetime and define unambiguously interior and exterior of the black brane (or black hole). We are however interested in studying dynamical spacetimes. In such a case it appears, that there is actually a multitude of horizons types, each one corresponding to different physical properties associated to it. One can speak of e.g. event, trapping, focusing, null, Cauchy, Killing horizons to name just few. All these correspond to the same entity in the case of a simple Schwarzschild spherical black hole. Once we start complicating the geometry, by adding charge, angular momentum or time dependence, the single event horizon begins to sort of fibrate into specific hypersurfaces, which no longer have to coincide. The horizon specimen, which will be of chief interest to us is called the apparent horizon, which more precisely is known as the future outer trapping horizon [Booth 2005, Booth 2009].

This type of a horizon has the property that it grows instantaneously whenever infalling radiation crosses it, thus enlarging its surface causally with the evolving perturbation. This is the source of the main virtue of an apparent horizon, as opposed to the event horizon, in the dynamical spacetime case. Owing to this causality it can be localized in space at any given instance of time. The event horizon in contrast can only be found once all time dependence has already passed away and static configuration has been reached, which usually corresponds to the impractical future infinite time limit. Once this static stage is reached one can again simply find the event horizon position, and using null geodesic equation propagate it backward in time, to read its locus *a posteriori*. This property of being computable only from the global future infinity data is referred to as the teleological nature of event horizons. We will return to this property in Chapter 6, Section 6.7.2, where we will be interested in implementing the backtracking procedure in our numerical study of dynamical geometry.

Going back to the the apparent horizon we note, that it is always covered by the genuine event horizon and the two approach each other when the evolution arrives at the final equilibrium state. An important property of apparent horizon is also that, again in contrast to the event horizon, it is focusing. That is, when radiation falls behind it, it may only travel inwards the black object and not stay at constant radius from its centre[1]. Geometrically it

[1] In the zone between event and apparent horizons matter can in principle travel parallel to the event horizon. If the gap between the horizons would eventually close the matter would be swallowed by the focusing horizon.

means, that as time increases the transverse cross section of the focusing congruence patch contracts and shrinks in space.

The condition for localizing apparent horizon follows from the above physical intuition on its influence on the radiation. As we discussed in the section above in spacetime there are *a priori* two families of geodesics: rays ingoing and outgoing relative to the black hole horizon. The focusing property of the apparent horizon means that the outgoing rays in its interior must in fact be *focused*, exactly as the ingoing rays, which are always focused. It means that it is a boundary of a whole trapped region, because outside of it the outgoing rays can be expanding, not contacting (even inside the event horizon). Hence the name 'trapping horizon' mentioned before. The change of the outgoing congruence's expansion behaviour at this boundary is the key to localizing apparent horizon. Mathematically this is expressed by the following condition on the expansions corresponding to the two families of null geodesics:

$$\theta_l = 0,\ \theta_n < 0. \tag{4.31}$$

Here n corresponds to the infalling geodesics, which is always focusing on its way towards the black brane interior. l in turn is tangent to the outgoing geodesics congruence, for which normally we would have $\theta_l > 0$. At the apparent horizon however, this expansion changes sign to be negative in its interior, and has zero at the horizon locus. Owing to the Raychandhuri flow equation (4.28) we are assured, that the sign of the expansion will be preserved along the congruence evolution, since once it becomes negative it remains so due to the negative derivative sign. That is therefore how we can determine the apparent horizon position is space, by computing two opposite null geodesics types and evaluating the expansions on them. Once the condition (4.31) is met we have found the apparent horizon. This prescription will be used in 6.6.2 to define dynamic entropy density.

4.4 Closing remarks

The above elements of General Relativity will be of great use in Chapter 6, where fully dynamical non-linear system of Einstein equations will be solved. In particular expansions will play a major role in this process, both physically and as a technical tool for the numerics. As a first step towards these considerations we will however analyse static Einstein equations in the following Chapter 5, to gain some intuition on the anisotropic brane solutions.

Chapter 5

Static approach to anisotropic strongly coupled SYM plasma

5.1 Introduction

In this chapter we are going to touch upon the AdS/CFT approach to plasma anisotropy for the first time, by reporting research in our first paper[Janik 2008]. The motivation for the work described below came from two main directions: the problem of rapid Quark-Gluon Plasma isotropisation introduced in the opening Chapter 1 and the mechanism of instabilities proposed to address this puzzling issue at weak coupling in [Mrowczynski 1993]. This mechanism is based on the observation, that in a certain kinematic regime a rapid transverse collective flow of nuclear matter might emerge as a consequence of instability in highly saturated flow with strong momentum anisotropy. Such a phenomena known as filamentation instability is present also in QED plasma and can even be observed in Nature outside the lab as splitting of lightnings, or laser beams broadening and refocusing in refracting media. Equilibrating effect in this case comes from the direction of flow generated by the instability, which is transverse to the dominating momentum flow, i.e. the beam. Perturbative approach valid in QED however turned out to be inapplicable in the quark-gluon plasma setting of RHIC and LHC, due to the apparent strong coupling of the gauge theory fluid. Thus with the advent of holography and dual descriptions of static as well as dynamic thermal systems we have initiated the study of strongly anisotropic plasma systems in AdS/CFT correspondence. The main theme of this investigation was to analyse the spectrum of light excitations in the thermal anisotropic gauge matter and try to see, if weak-coupling instabilities make appearance also at strong coupling. This could give a hint on the possible mechanism introducing the very short time-scale of the plasma isotropisation, which according to the established views is necessary for thermal equilibrium[1].

5.1.1 Introducing anisotropy

In a hot nuclear matter system anisotropy is generated during the collision process. Initial longitudinal momentum of the particles ascending along the ion beam axis is transformed into the momentum distribution function $f(x,p)$ of the thermal medium formed during the collision. At weak coupling this process can be tracked in the framework of kinetic theory, which we described in the Chapter 2 on the hydrodynamics development. As was pointed out, in the realm of finite density field theory we use thermal expectation value of the stress-energy tensor to describe the system. Due to the complexity of the problem most of the research focused on infinitely extent homogeneous *non-expanding* plasmas, in which case the energy density is constant and only equilibration of the momenta is expected. The basic degrees of freedom in this approach are the energy density ε and *two* pressures,

[1] We shall shake this view a little bit in the forthcoming chapters, here however we seek genuinely isotropic configuration.

transverse p_T and longitudinal p_L ones. The study of anisotropy focuses then on finding time evolution of these quantities, embedded in the stress-energy tensor:

$$T_{\mu\nu} = \begin{pmatrix} \varepsilon & 0 & 0 & 0 \\ 0 & p_L(t) & 0 & 0 \\ 0 & 0 & p_T(t) & 0 \\ 0 & 0 & 0 & p_T(t) \end{pmatrix}. \tag{5.1}$$

Naturally the main way of research here is through numerical simulations. However in the wake of instabilities known from QED plasmas, one can also attack the problem analytically through the analysis of the thermal gluon propagator, $G_T^{ab}(\omega, k)$. The poles of this quantity reflect perturbative degrees of freedom in the thermal medium, and if unstable excitation is to exist, then an imaginary dispersion relation should be found with a *wrong* sign, signalling exponential growth of the mode. Such a mechanism would require an existence of a numerical constant present in the exponent,

$$A_\mu^{ab}(x) \sim e^{+t\omega/\tau_{\Pi}}, \tag{5.2}$$

which we would interpret as the time-scale over which isotropizing instability develops to the regime, where non-linear effects would enter and tranquillize the system.

The thermal state in which such a correlation function would be computed is characterized by the momentum distribution function of the form similar to the one encountered in the Chapter 2:

$$f(\mathbf{p}) = \sqrt{1+\xi} f_{\text{iso}}(\mathbf{p}^2 + \xi \mathbf{p}_L^2). \tag{5.3}$$

The function f_{iso} is spherically symmetric and represents isotropic momentum distribution distorted by the anisotropy parameter ξ, expressing the ratio of the pressures in (5.5)

$$\xi = \frac{p_T}{p_L} - 1. \tag{5.4}$$

It follows that at weak coupling a pattern of instabilities is found, which crucially depends on the relative sign of the instability and the orientation of the mode momentum $\mathbf{k}$ with respect to the beam (represented by the longitudinal momentum $\mathbf{k}_L$).

If ξ is positive, $p_T > p_L$ and the modes with transverse momentum $\mathbf{k}_T$ remain stable, while those with $\mathbf{k}_L$ develop instability forcing the fluid to equilibrate. In the reverted situation ξ is negative, p_L is greater that p_T and modes k_L along the dominating pressure are stable, whilst those with transverse momentum k_T are unstable. We thus see, that both these instabilities combined together allow for equilibration even in the situation when there are oscillations in the pressures ratio, e.g. after plasma backreaction.

5.1.2 Introducing anisotropy to holography

The analysis of anisotropy evolution in strongly coupled QCD is of course hampered by the lack of analytic tools to attack the problem. Thus as was pointed out on numerous occasions in the preceding chapters, a tractable model for this system is provided by the $\mathcal{N} = 4$ super-Yang-Mills theory, which as we already know from the Chapter 3 bears justifying resemblance to QCD. Nevertheless, even though we have such a powerful framework at our disposal, the full analytic analysis of the dynamic time-dependent plasma stress tensor evolution is not possible due to the complexity of Einstein equations. In the present work we

have proposed a simplifying approach based on static anisotropic plasma configuration, and paralleling the reasoning of the previous paragraph, we have been searching for instabilities of such a system.

The basis of the present holographic dual construction is thus the anisotropic static stress-energy tensor:

$$T_{\mu\nu} = \begin{pmatrix} \varepsilon & 0 & 0 & 0 \\ 0 & p_L & 0 & 0 \\ 0 & 0 & p_T & 0 \\ 0 & 0 & 0 & p_T \end{pmatrix}. \tag{5.5}$$

The thermal medium we model with it is somewhat artificial as it persists in a non-equilibrium state. We perceive it as a frozen initial stage of some fully dynamic situation, analysed on timescales much shorter than macroscopic relaxation time. The conclusions drawn from such a reasoning would point at the possible direction of the anisotropic plasma evolution, should the time be released in the system.

Since we are considering conformal plasma, the three parameters of the stress tensor are bound together through the vanishing trace condition $\langle T^{\mu}_{\ \mu} \rangle = 0$, which yields $\varepsilon = p_L + 2p_T$. On the top of that this stress tensor enjoys several other symmetries reflecting the physical state configuration. These are independent spacetime translational symmetry in longitudinal and transverse directions, transverse rotational symmetry and reflection symmetry (which excludes off-diagonal terms in $T_{\mu\nu}$).

5.1.3 Holographic dual to anisotropic gauge theory state

The highly constrained state described by the tensor (5.5) allows one to construct an exact analytic solution to Einstein equations, representing the full quantum state in 5D gravitational field $G_{AB}(x^C)$. Along the lines of Chapter 3 introducing holography, the problem one has to solve is the following:

$$E_{AB}(x^{\mu}, z) = R_{AB} + 4G_{AB} = 0, \tag{5.6}$$

$$G_{AB}(t, x_1, x_2, x_3, z \sim 0) = \frac{1}{z^2}(\eta_{\mu\nu} dx^{\mu} dx^{\nu} + dz^2) + O(z^2), \tag{5.7}$$

$$\partial_z^4 z^2 G_{\mu\nu}(t, x_1, x_2, x_3, z)|_{z=0} = \frac{2\pi}{N_c^2} \langle T_{\mu\nu} \rangle. \tag{5.8}$$

In the above, capital Latin indices represent 5-dimensional spacetime, $A, B = t, x_1, x_2, x_3, z$, and Greek letters indicate our flat boundary Minkowski spacetime $\eta_{\mu\nu}$, where the physical ions collision takes place: $\mu, \nu = t, x_1, x_2, x_3$. Directions transverse to the collision axis are denoted x_1, x_2 and the longitudinal direction is x_3. Bulk coordinate in Fefferman-Graham chart is parametrized by z.

Problem stated above is a typical Robin-type boundary condition imposed at the conformal boundary of the integration domain $z \in [0, \infty)$. Finding a general solution to the non-linear Einstein equation is of course difficult, but a suitable Ansatz respecting all the symmetries can be used to find the desired solution. It is closely related to the static isotropic plasma dual geometry, which in Fefferman-Graham coordinates take the following form:

$$ds^2 = \frac{1}{z^2}(-a(z)dt^2 + b(z)dx_L^2 + c(z)d\mathbf{x}_L^2 + dz^2). \tag{5.9}$$

Einstein equations evaluated on the above metric yield a coupled system of ordinary non-linear differential equations for the three unknown functions. The solution can be found and assumes the form

$$a(z) = (1+A^2z^4)^{\frac{1}{2}-\frac{1}{4}\sqrt{36-2B^2}}(1-A^2z^4)^{\frac{1}{2}+\frac{1}{4}\sqrt{36-2B^2}}, \tag{5.10}$$

$$b(z) = (1+A^2z^4)^{\frac{1}{2}-\frac{B}{3}+\frac{1}{12}\sqrt{36-2B^2}}(1-A^2z^4)^{\frac{1}{2}+\frac{B}{3}-\frac{1}{12}\sqrt{36-2B^2}}, \tag{5.11}$$

$$c(z) = (1+A^2z^4)^{\frac{1}{2}+\frac{B}{6}+\frac{1}{12}\sqrt{36-2B^2}}(1-A^2z^4)^{\frac{1}{2}-\frac{B}{6}-\frac{1}{12}\sqrt{36-2B^2}}. \tag{5.12}$$

The integration constants A and B are related to the boundary stress-energy tensor parameters, encoding the energy density and pressures of the plasma. The precise expressions follow from the holographic relations and are given by

$$\varepsilon = \frac{1}{2}A^2\sqrt{36-B^2}, \tag{5.13}$$

$$p_L = \frac{1}{6}A^2\sqrt{36-B^2}-\frac{2}{3}A^2B, \tag{5.14}$$

$$p_T = \frac{1}{6}A^2\sqrt{36-B^2}+\frac{1}{3}A^2B. \tag{5.15}$$

With these expressions we can relate the geometry anisotropy parameter B to the momentum distribution anisotropy ξ,

$$B = \frac{6\xi}{\sqrt{18\xi^2+48\xi+36}}. \tag{5.16}$$

The geometry (5.10) has smooth isotropic limit as B tends to zero, resulting in the well known AdS-Schwarzschild black brane solution describing static plasma at rest with a constant temperature, which we have seen in Chapter 3. It turns out however, that our present geometry is pathological because it contains a naked singularity. By computing the Kretschmann scalar (a Riemann tensor squared, $\mathcal{R}^2 = R^{\mu\nu\alpha\beta}R_{\mu\nu\alpha\beta}$) for small values of B, we can observe the emergence of an essential (non-coordinate) singularity with the appearance of the anisotropy:

$$\begin{aligned}\mathcal{R}^2 &= \frac{8\left(5A^8z^{16}+20A^6z^{12}+174A^4z^8+20A^2z^4+5\right)}{\left(A^2z^4+1\right)^4} \\ &+ \frac{256A^6B^2z^{12}\left(9A^4z^8-2A^2z^4+9\right)}{3\left(A^4z^8-1\right)^4}\end{aligned} \tag{5.17}$$

The first term represents $\mathcal{R}^2$ for the AdS-Schwarzschild black brane and is regular up to the interior AdS singularity at $z\to\infty$. Nevertheless the second term has a pole at $z=1/\sqrt{A}$, which indicates the curvature singularity not cloaked by any horizon. This term vanishes as we put $B\to 0$. One can also notice, that the metric determinant is insensitive to the anisotropy B, but vanishes as well and is thus singular at $z=1/\sqrt{A}$:

$$\det(G_{AB}) = -\frac{\left(A^4z^8-1\right)^2}{z^{10}} \tag{5.18}$$

The nature of this singularity however varies and depends on the presence of B.

Since our spacetime is not shielded from the singularity by any horizon, our solution is clearly not a standard geometry one expects to encounter in the theory of relativity. We should nonetheless keep in mind, that in our setting the spacetime is not an effect of a matter collapse, but instead gravity here represents certain state in the quantum field

theory Hilbert space, and therefore is not bound by the standard cosmological postulates. Thus pathology which is not welcome may properly indicate that the corresponding state in the quantum theory is not a regular configuration.

On the other hand, however worrisome may the solution seem, its issue may only be superficial due another interpretation. One could contemplate the dynamics of AdS spacetime which for a significant amount of (boundary) time seems to be static and anisotropic. In this scenario one considers *initial* instead of boundary problem with initial geometry profile given on a constant time hypersurface $t = 0$. The initial geometry would then coincide with (5.9) for a wide range of z's and would be modified for $z > z_{\max}$ by some perturbation, which would cloak the singularity of (5.9). If now one considers temporal evolution of such a metric, the pulse of geometry distortion from the interior region $z \gg 0$ has to travel towards the boundary for a significant amount of time. Only after this period the boundary expectation value of the almost-static stress tensor $\langle T_{\mu\nu} \rangle$ is be subject to change. And only now the existence of a potential event horizon in the spacetime interior is revealed to the boundary observer, an event which can be called thermalization, an emergence of temperature. We shall soon see how such an interpretation of the initial snapshot geometry (5.10) rationalizes *a posteriori* the fact, that we are able to ascribe the bulk fields a plausible boundary conditions *at the singularity*.

5.1.4 Boundary conditions at the singularity

In physics (and maybe broader) singularity frequently represents a lack of knowledge. Singularity is where the natural information on the values of the given function is unavailable and often one has to supplement it by assigning the function some arbitrarily justified values. It is especially sound problem in our gravity setting, where in the presence of the event horizon one has naturally the physical ingoing boundary condition, but in the case of naked singularity one faces the problem of interpretation, how to treat it. It seems natural to try to morph it into a spacetime behaving *as if* it was still attracting-only entity and try to impose purely ingoing boundary condition at anything propagation in such a background. This is exactly what we considered in the present case.

Let us consider the spacetime (5.10) with the singularity locus set to one, $A = 1$. To test if we can make sense of our geometry we shall solve massless real scalar wave equation in such a geometry and try to consistently impose ingoing wave condition at the singularity. Since propagating scalar is a prototype for any dynamics, also non-linear (e.g. characteristics dynamics) and probes causal structure of the light-cones, its satisfactory performance will assure us of the geometry sanity.

We thus have d'Alembert equation and owing to the metric symmetries, Fourier plane wave expansion:

$$\Box\Phi(x^A) = 0, \;\; \Phi(x^A) = \phi(z) e^{-i\omega t + ik_1 x^1 + k_2 x^2 + ik_3 x^3}. \tag{5.19}$$

A standard step in analysing such an equation is to pass to a Schrödinger-like equation, which unveils the effective gravity potential, in which the scalar wave propagates. It is performed by the transformation

$$x = \frac{1}{4}\mathrm{ath}(z^4), \tag{5.20}$$

which puts the $z = 1$ singularity at $x = \infty$. The resulting equation assumes the form

$$\begin{aligned} \frac{d^2\phi}{dz^2} \;&+\; \frac{8}{(e^{16x}-1)^{\frac{3}{2}}} \Big(\omega^2 e^{2(6+\sqrt{36-2B^2})x} - k_L^2 e^{2(6+\frac{4B}{3}-\frac{1}{3}\sqrt{36-2B^2})x} \\ &-\; k_T^2 e^{2(6-\frac{2B}{3}-\frac{1}{3}\sqrt{36-2B^2})x} \Big) \phi = 0. \end{aligned} \tag{5.21}$$

This reformulation has the advantage, that one can easily analyse the structure of asymptotic boundary condition, exactly like in the related case of wave function equation. Next we elicit the dominant part of the above potential near $x \to \infty$, which is proportional to the frequency squared ω^2:

$$\frac{d^2\phi}{dx^2} + 8\omega^2 e^{-2(6-\sqrt{36-2B^2})x}\phi = 0. \tag{5.22}$$

This asymptotic expression unravels the boundary conditions structure at the singularity[2]. In the isotropic limit $B \to 0$ we recover two linearly independent solutions:

$$\phi_+(t,x) = e^{-i\omega t + i\sqrt{8}\omega x},\ \phi_-(t,x) = e^{-i\omega t - i\sqrt{8}\omega x}. \tag{5.23}$$

These can of course form a basis of the ordinary ingoing and outgoing solutions. If we now allow for small anisotropy $B \sim 0$, we obtain a combination of two Airy functions (with certain function of frequency $K(\omega)$),

$$\phi(x) \sim \mathrm{AiryAi}(K(\omega)x) + \mathrm{AiryBi}(K(\omega)x), \tag{5.24}$$

which look almost like flat waves and only close to the singularity this behaviour is modified. So with anisotropy we also have a sort of separation onto ingoing and outgoing modes. Finally with the aid of independent variable transformation

$$x = -\frac{1}{C}\ln z, \tag{5.25}$$

mimicking the Eddington tortoise coordinate, we can recast the equation (5.22) in the form of a cylindrical Hankel-Bessel differential equation, which subsequently yields the solutions for arbitrary anisotropy B

$$\phi(x) \sim A_1 H_0^1(\frac{\sqrt{8}}{C}\omega e^{-C}x) + A_2 H_0^2(\frac{\sqrt{8}}{C}\omega e^{-C}x), \tag{5.26}$$

with $C = 6 - \sqrt{36 - 2B^2}$. This result finally assures us, that the singular geometry (5.10) admits a plausible set of boundary conditions for the fields propagating over it. The Hankel functions asymptote at $x \to \infty$ (which is close to the singularity) to damped plane waves, thus allowing for a purely ingoing condition at the singularity. Hence although we have no horizon, we can suppress the radiation from the singularity and effectively act as in the standard black brane geometry.

A word of comment is in order here, since it may be rather special that such a physical choice exists. Earlier investigation of different naked singularity solution, a *negative* mass-parameter M AdS-Schwarzschild solution revealed it to be much less forgiving and does not allow for such a boundary conditions in the case of non-vanishing wave vector k^i. In such a case the hierarchy of terms in (5.21) is inverted, the momentum terms dominates the asymptotics $x \to \infty$ and no familiar boundary conditions pattern emerges (i.e. we would have elliptic-like instead of the hyperbolic-like differential operator and purely decaying solutions would be expected).

The existence of the almost-horizon-like conditions may have its origins in the discussed above connection to the highly distorted *dynamic* geometry, which only initially looks as if it was static. Since deep in the near-singularity region we should in fact be touching the horizon if the geometry was dynamical, then one may speculate that this marginally allows for an outgoing boundary conditions.

[2]Perhaps intriguing is the fact, that no momentum dependence survives in this expression, as if purely long-wavelength $k \to 0$ information contributed here.

5.1.5 Dynamic probe of the static anisotropy

Having found the physically acceptable boundary conditions at the singularity, we are allowed to think about probing the anisotropic plasma for instabilities with the aid of linear perturbations. The objective of this analysis is to understand the dispersion relation of small fluctuations propagating throughout the static anisotropic plasma, and check if their spectrum is purely decaying. In analogy to the weakly coupled instabilities described above we only need to look for the gapless perturbations of the form

$$\omega(k) \sim k^s + O(k^s), \text{ with } s > 0. \tag{5.27}$$

Only such modes lead to sufficiently long lived perturbation when k tends to zero, allowing unstable collective motion to build up before dissipation kills it. All other low energy gapped modes are extinguished in finite time from the perturbation onset.

The techniques of obtaining fluctuations spectrum of a thermal system in AdS/CFT relies on solving linearised evolution equation for a field $\Phi(z,x)$ dual to the operator $\hat{O}(x)$ we are interested in. This usually reduces to a wave-like equation in black brane background with vanishing Dirichlet condition on the AdS boundary $\Phi(0,x) = 0$, and purely ingoing-wave condition at the horizon. For example if we were interested in computing poles of a two-point scalar operator function

$$G_{\mathrm{F2}}(x-y) = \langle \mathrm{T}[\mathrm{Tr}F^2(x)\mathrm{Tr}F^2(y)]\rangle \tag{5.28}$$

we would have to solve scalar wave equation

$$\Box\Phi(x,z) = 0. \tag{5.29}$$

The resulting solution contains generically a dispersion relation $\omega(k)$ which determines our fluctuations spectrum:

$$\tilde{G}_{\mathrm{F2}}(\omega,k) \sim \frac{\text{const.}}{\omega - \omega(k)}. \tag{5.30}$$

This is the reason for which we were so interested in finding ingoing boundary conditions at the singularity, as they lead to determination of poles in the correlation function.

Application of this technique led in the past to discovery of gapless modes in the $\mathcal{N} = 4$ SYM theory, [Son 2007], matching exactly to the spectrum of hydrodynamics fluctuations introduced in Chapter 2. In particular, holographic calculations allowed to analyse the real time thermal 2-point correlation functions of the super-Yang-Mills stress-energy tensor, $\langle \hat{T}_{\mu\nu}\hat{T}_{\alpha\beta}\rangle_T$. Stress tensor in the holographic dual theory corresponds to the bulk metric and hence fluctuations of the stress-energy tensor operator can be computed from the corresponding modes of the linearised gravity perturbations. In this way the so called graviton shear and sound channels on the static black brane background were obtained[3], giving respectively the following relations:

$$\omega = -i\frac{\eta}{\varepsilon+p}k^2 + \ldots, \qquad \omega = \pm\frac{1}{\sqrt{3}}k - i\frac{2}{3}\frac{\eta}{\varepsilon+p}k^2 + \ldots, \tag{5.31}$$

where $\varepsilon(T)$, $p(T)$ and $\eta(T)$ are the introduced before temperature-dependent energy density, pressure and shear viscosity of the plasma. These relations are of the type we have encountered in the Chapter 2 and agree with solutions to the linearised hydrodynamics.

[3] These quantities correspond to the poles of a specific tensors in the 2-point correlation function $G^{TT}_{R\,\mu\nu\alpha\beta}$ tensorial decomposition, see [Kovtun 2005].

Apart from stress tensor itself we can also excite another current of super-Yang-Mills theory, the R-charge current introduced in Chapter 3. It corresponds to the global R-symmetry responsible for rotating supersymmetry charges of the theory. Due to its simplicity it will be our main probe of the anisotropic plasma system.

Dispersion relation of the R-current 2-point correlation function obtained from holography in the isotropic background exhibits diffusive behaviour of the R-charge:

$$\omega = -iD_R k^2 + \dots \tag{5.32}$$

The lack of propagation term (k) above is not strange due to the fact, that R-charge current is just a conserved quantity. The R-charge diffusion constant D_R is a function of the isotropic event horizon temperature: $D_R = 1/2\pi T$. If we fix its locus to unity, $z = 1$, which corresponds to setting $A = 1$ in the isotropic geometry with $B = 0$ in (5.10), the diffusive dispersion relation will be

$$\omega = -i\frac{k^2}{2\sqrt{2}} + \dots \tag{5.33}$$

All these small momentum frequency expansions represent moderately damped decaying modes, yielding in correlators behaviour like $e^{-k^s t}$, with $s > 0$. In addition to these gapless modes there are infinitely many gapped modes, which retain damping even in the limit $k \to 0$. These are not compatible with hydrodynamics and will not be present in our analysis.

Our main point of interest is to check how the above stable spectrum (5.33) of dynamics probes is modified, if we replace the isotropic background by our anisotropic solution (5.10).

5.2 Dynamics of the U(1) gauge field on the anisotropic background

In the weakly coupled case [Mrowczynski 1993] plasma instabilities were probed with electric field. The essential piece of the observable was the dispersion relation of small fluctuations in thermal anisotropic medium. The dependence of the oscillation frequency $\omega(k)$ on the perturbation momentum k was obtained by computing 2-point correlation function, or the propagator of a gauge particle in the thermal plasma state. Subsequently the dispersion relation was extracted from the poles of the resulting expression as in (5.30). We shall take a similar approach in the strongly coupled case of the $\mathcal{N} = 4$ SYM with the aid of the introduced above R-symmetry current. Let us remark, that such an observable may seem rather abstract from the QCD point of view, but it serves as a simple probe of the anisotropic dynamics. One should stress however, that in this theory it is as physical as any other current. Our goal is therefore to obtain the spectrum of R-charge fluctuations in the thermal anisotropic state (5.10) and inspect the analogues of relations (5.31) for the presence of growing modes.

According to the correspondence the bulk field dual to the boundary vector current operator $\hat{J}^\mu_R(x)$ is the five dimensional $U(1)$ Maxwell field $A^M(x,z)$. One can see for example, that both of these are subject to the vanishing divergence condition, being current conservation on the one hand, $\partial_\mu j^\mu_R(x) = 0$, and Lorentz gauge condition $\nabla_M A^M(x,z) = 0$ on the other. These two entities are related by the holographic formula:

$$\left\langle e^{i\int_{\partial\mathcal{M}} A^{(0)}_\mu(x)\hat{J}^\mu_R(x)} \right\rangle = e^{iS_{\rm cl}[A_M(x,z)]}, \tag{5.34}$$

where $\hat{J}^{\mu}_{R}(x)$ is the current operator and $S_{\rm cl}$ is the classical on-shell action of the gauge field in the bulk. Fields in the on-shell action are subject to a boundary condition imposed by the value of the bulk Maxwell field $A^{(0)}_{\mu}(x, z=0)$ at $\partial\mathcal{M}$.

The main holographic relation on which we will rely is that the dispersion relation of the boundary quantum current operator is obtained as the dispersion relation of its dual classical field $A^{M}(x,z)$ in the bulk. To obtain the later we need to solve the bulk equation of motion following from the semiclassical formula (5.34). The classical action on the right hand side is the Maxwell action in curved five-dimensional spacetime, evaluated in the fixed background (5.10):

$$S[A] = -\frac{N^2}{64\pi^2 R}\int \sqrt{-g}F_{MN}F^{MN}d^5x,\ F_{MN} = \nabla_M A_N - \nabla_N A_M. \tag{5.35}$$

The vacuum Maxwell equations following from this are

$$\partial_M(\sqrt{-g})F^{MN}(x^{\alpha}, z) = 0. \tag{5.36}$$

We must remember, that we are dealing with a gauge system and hence we need to fix the bulk gauge freedom before looking for the solution. We impose the condition standard to holography, $A_5 = 0$, stating, that the vector current is parallel to the boundary.

We can now start analysing the above equations. The best approach to solve them in curved spacetime is to employ the Fourier analysis, which is applicable due to the translational symmetry of our anisotropic geometry along the boundary directions x^{α}. We thus pass to the momentum space with the following transform:

$$A_{\mu}(x) = \int \frac{d\omega d^3k}{(2\pi)^4}e^{-i\omega t + i\mathbf{k}\cdot\mathbf{x}}A_{\mu}(\omega, \mathbf{k}, z),\ \mu = 0, ..., 3. \tag{5.37}$$

The spatial anisotropy of our solution (5.10) singles out the direction x_L, which influences the momentum space by splitting it into two families of longitudinal and transverse modes:

$$k^{\alpha}_{L} = (\omega, k, 0, 0) \text{ and } k^{\alpha}_{T} = (\omega, 0, 0, k). \tag{5.38}$$

Therefore we will be considering two families of solutions, based on the relative orientation of the momentum vectors k, anisotropy B and fields polarisation i.

As a consequence of the gauge symmetry, apart from fixing it as above we should pass to the manifestly gauge invariant field variables. In electromagnetism these are e.g. electric fields E_i. By taking into account the split of the momentum vectors into two families we are led to introduce corresponding gauge sectors.

The first family contains perturbations with momentum k_L parallel to the geometry anisotropy x_L:

$$E_y(k_L, z) = \omega A_y(k_L, z) + k_L A_t(k_L, z) \qquad \text{with } E_y \parallel k_L, \tag{5.39}$$

$$E_1(k_L, z) = \omega A_1(k_L, z),\ E_2(k_L, z) = \omega A_2(k_L, z) \text{ with } E_{1,2} \perp k_L. \tag{5.40}$$

Among these modes E_y is longitudinal with respect to the momentum and the remaining ones, $E_1,\ E_2$ are transverse.

The second family consists of perturbations with momentum p_T transverse to the geometry anisotropy and the configuration of the polarizations reflecting this:

$$E_1(k_T, z) = \omega A_1(k_T, z) + k_T A_t(k_T, z) \qquad \text{with } E_1 \parallel k_T, \tag{5.41}$$

$$E_y(k_T, z) = \omega A_y(k_T, z),\ E_2(k_T, z) = \omega A_2(k_T, z) \text{ with } E_{y,2} \perp k_T. \tag{5.42}$$

These expressions are of course the standard definitions of vector potentials in terms of the physical electric fields, but taken in momentum space. An important consequence of introducing them is the decoupling of equations of motion (5.36) into independent sets, making it easier to solve them.

Even with all the steps taken above the equations remain still too difficult for analytical treatment. However, we are only interested in generic character of the evolution in the presence of the anisotropy, so we will linearise the equations for $E_i(k^\alpha, z)$ and consider only the small anisotropy limit, $|B| \ll 1$. This will allow for a perturbative treatment of the electric fields evolution equations, which as we shall see will yield qualitatively satisfactory results. The question of the behaviour at high anisotropy $B \geq O(1)$ would have to be attacked numerically, but it seems unlikely that larger anisotropy would heal any potential instability. Ultimately we are left with two sets of decoupled ordinary differential equations in the bulk variable z, and the outgoing boundary condition elucidated in the previous paragraphs.

The longitudinal equations linearised in B assume the form given below, with all the field components being functions of k^α and z: $E_i(\omega, k; z)$. For the longitudinal case we have:

$$\begin{aligned}
E_1'' &- \frac{3+4\sqrt{A}(3+B)z^4+9Az^8}{3z(1-Az^8)}E_1' \\
&+ \left(\frac{\omega^2(1+\sqrt{A}z^4)}{(1-\sqrt{A}z^4)^2} - k_L^2(1-\sqrt{A}z^4)^{-\frac{B}{3}}(1+\sqrt{A}z^4)^{-1+\frac{B}{3}}\right)E_1 = 0, \\
E_y'' &- \left(\frac{3k_L^2(1-\sqrt{A}z^4)^2(1+\sqrt{A}z^4)^{\frac{B}{3}}(1-3\sqrt{A}z^4(4-\sqrt{A}z^4))}{3z(1-Az^8)(k_L^2(1-\sqrt{A}z^4)^2(1+\sqrt{A}z^4)^{\frac{B}{3}} - \omega^2(1-\sqrt{A}z^4)^{\frac{B}{3}}(1+\sqrt{A}z^4)^2)}\right. \\
&+ \left.\frac{\omega^2(1-\sqrt{A}z^4)^{\frac{B}{3}}(1+\sqrt{A}z^4)^2(3+\sqrt{A}z^4(12-8B+9\sqrt{A}z^4))}{3z(1-Az^8)(k_L^2(1-\sqrt{A}z^4)^2(1+\sqrt{A}z^4)^{\frac{B}{3}} - \omega^2(1-\sqrt{A}z^4)^{\frac{B}{3}}(1+\sqrt{A}z^4)^2)}\right)E_y' \\
&+ \left(\frac{\omega^2(1+\sqrt{A}z^4)}{(1-\sqrt{A}z^4)^2} - k_L^2(1-\sqrt{A}z^4)^{-\frac{B}{3}}(1+\sqrt{A}z^4)^{-1+\frac{B}{3}}\right)E_y = 0.
\end{aligned} \tag{5.43}$$

The equation for the E_1 component is exactly the same as for the E_2 in this case. In the transverse case we have in turn three distinct equations:

$$\begin{aligned}
E_2'' &- \frac{3+4\sqrt{A}(3+B)z^4+9Az^8}{3z(1-Az^8)}E_2' \\
&+ \left(\frac{\omega^2(1+\sqrt{A}z^4)}{(1-\sqrt{A}z^4)^2} - k_T^2(1-\sqrt{A}z^4)^{-\frac{B}{6}}(1+\sqrt{A}z^4)^{-1-\frac{B}{6}}\right)E_2 = 0, \\
E_y'' &- \frac{3+\sqrt{A}z^4(12-8B+9\sqrt{A}z^4)}{3z(1-Az^8)}E_y' \\
&+ \left(\frac{\omega^2(1+\sqrt{A}z^4)}{(1-\sqrt{A}z^4)^2} - k_T^2(1-\sqrt{A}z^4)^{-\frac{B}{6}}(1+\sqrt{A}z^4)^{-1-\frac{B}{6}}\right)E_y = 0, \\
E_1'' &+ \left(\frac{-3k_T^2(1-\sqrt{A}z^4)^{2+\frac{B}{6}}(1-3\sqrt{A}z^4(4-\sqrt{A}z^4))}{3z(1-Az^8)(k_T^2(1-\sqrt{A}z^4)^{2+\frac{B}{6}} - \omega^2(1-\sqrt{A}z^4)^{2+\frac{B}{6}})}\right. \\
&+ \left.\frac{\omega^2(1+\sqrt{A}z^4)^{2+\frac{B}{6}}(3+4\sqrt{A}(3+B)z^4+9Az^8)}{3z(1-Az^8)(k_T^2(1-\sqrt{A}z^4)^{2+\frac{B}{6}} - \omega^2(1-\sqrt{A}z^4)^{2+\frac{B}{6}})}\right)E_1' \\
&+ \left(\frac{\omega^2(1+\sqrt{A}z^4)}{(1-\sqrt{A}z^4)^2} - k_T^2(1-\sqrt{A}z^4)^{-\frac{B}{6}}(1+\sqrt{A}z^4)^{-1-\frac{B}{6}}\right)E_1 = 0.
\end{aligned} \tag{5.44}$$

In both setups the equation for the field component along the momentum is more involved, than the equations for the perpendicular ones, and even at the linearised level they are quite complicated. It can be checked, that in the isotropic limit of $B \to 0$ the resulting equations reduce to the standard massless vector wave equation in the planar AdS-Schwarzschild metric. In this case the field modes along the momentum, respectively E_y and E_1 in the equations above, exhibit a long-lived diffusive behaviour like (5.32) in the hydrodynamical limit $k \to 0$. The field components perpendicular to the momentum in the isotropic limit have non-vanishing damping at any non-zero momentum, which renders them absent in the long wavelength limit. Because of this we will focus in our investigation only on the field components along the momentum in each case.

Let us now proceed to the analysis of equations for E_y and E_1. The derivation is very similar in both longitudinal $p_L \neq= 0$ and transverse $p_T \neq= 0$ channels, with major technical difference laying in the numerical coefficients (the physical properties will however slightly differ between them).

To find the complete solutions one has to integrate the relevant differential equations in (5.43), (5.44), and impose the boundary conditions at the holographic boundary $z = 0$ and singularity. The later one requires imposing ingoing boundary condition akin to the ones described in 5.1.4.

To elucidate the boundary condition at the singularity in the present setting we need to analyse the characteristic behaviour of the differential equations for E_y in (5.43) and E_1 in (5.44). For simplicity let us fix the singularity locus to $z = 1$ by putting $A = 1$ (it can be reinstated by the dimensional analysis afterwards). Then the characteristic behaviour of the solutions consistent with the ingoing wave condition at $z = 1$ is[4]

$$E_y(k; z) \sim (1 - z)^{-i\frac{\omega}{2\sqrt{2}} + \frac{B}{6}}, \qquad E_1(k; z) \sim (1 - z)^{-i\frac{\omega}{2\sqrt{2}} - \frac{B}{12}}. \tag{5.45}$$

With the above asymptotics we can recast the evolution equations in the form explicitly encoding the selected boundary condition. Let us apply this procedure to the field E_y along the momentum k_L. The global solution (in the range $z \in [0, 1]$) with the proper behaviour at the singularity must have the form

$$E_y(k; z) = (1 - z)^{-i\frac{\omega}{2\sqrt{2}} + \frac{B}{6}} g(z^2). \tag{5.46}$$

The variable z^2 in the argument of g mildens the singular behaviour at the boundary $z = 0$, and enforces its positivity, which is justified in view of the complex exponent in the expression above. After fixing asymptotics the equation for the remaining part $g(z^2)$ is still too difficult for a direct analysis, but we should recall, that we are only interested in the hydrodynamic limit of low frequency $\omega \ll 1$ and low momentum $k \ll 1$ (and also small anisotropy $B \ll 1$). We can thus seek a perturbative solution by rescaling the wave vector as $\omega \to \varepsilon\omega$ and $k_L \to \varepsilon k_L$, and subsequently forming an Ansatz

$$g(z^2) = 1 + \varepsilon g_0^a(z^2) + \varepsilon^2 g_0^b(z^2) + B(g_1^a(z^2) + \varepsilon g_1^b(z^2) + \ldots) + \ldots \tag{5.47}$$

The unknown functions $g_n^i(z^2)$ are to be found from the expansion of the original equation (5.43) with the condition, that they all vanish at $z = 1$. This amounts to imposing the strict ingoing wave condition at the singularity, and expresses g_n^i's as functions of the wave vector ω, k_L.

The final step on the way to finding the solution to our eigenproblem is to impose vanishing Dirichlet condition at $z = 0$. Physically it corresponds to the reflection of the

[4] The ingoing wave character is made manifest if we pass to the logarithmic radius, the tortoise coordinate near the singularity: $e^{(-i\frac{\omega}{2\sqrt{2}} + \frac{B}{6})\ln(1-z)}$, with $z \lesssim 1$.

massless field from the boundary. This leads to the following equation[5]

$$g(0) = 1 + \varepsilon g_0^a(0) + \varepsilon^2 g_0^b(0) + B(g_1^a(0) + \varepsilon g_1^b(0) + \ldots) + \ldots = 0. \tag{5.48}$$

This condition binds together frequency and momentum, leading to the desired dispersion relation. Solutions to (5.43) contributing at each order of the perturbation parameter ε yield at the boundary respectively[6]

$$g_0^a(0) = \frac{ik_L^2}{2\sqrt{2}\omega} - \frac{i\ln 2}{2\sqrt{2}}\omega, \tag{5.49}$$

$$g_1^a(0) = -\frac{k_L^2}{6\omega^2} + \frac{\ln 4}{12}. \tag{5.50}$$

and

$$g_0^b(0) = -(\frac{\pi^2}{96} + \frac{\ln^2 2}{16})\omega^2 + \frac{\log 2}{8}k_L^2, \tag{5.51}$$

$$g_1^b(0) = i\frac{\sqrt{2}}{288}(\pi^2 - 12\log^2 2)\omega. \tag{5.52}$$

The problems thus reduces to solving the equation (5.48) with the above contributions. As the initial step of the analysis we find, that in the isotropic limit $B \to 0$ we recover from the first equation[7] in (5.49) the previous result for the isotropic plasma dispersion (5.33):

$$\omega = -i\frac{k_L^2}{2\sqrt{2}}. \tag{5.53}$$

However, if we keep non-zero anisotropy the situation changes. The presence on B introduces a new scale into the system, and its interplay with the momentum k_L leads to a different scheme of evolution.

To visualise this, let us analyse what is the hierarchy of scales in the equations (5.48). We are generally looking for gapless excitations in the low momentum limit $k_L \to 0$, so the general relation between the frequency and momentum must be of the form:

$$\omega \sim k_L^s, \text{ with } s > 0. \tag{5.54}$$

Upon substitution to (5.49) it reveals, that the ratio of g_0^a and g_1^a in the equation (5.48) has the following scaling structure[8]

$$\frac{g_1^a}{g_0^a} \sim \frac{B(k_L^{2-2s} + \text{const.})}{k_L^{2-s} + k^s} \sim Bk_L^{-s} \gg 0 \text{ for } k_L \to 0. \tag{5.55}$$

As a consequence, if momentum is much smaller than the anisotropy B, the term coming from $g_1^b(0)$ dominates. By dropping the subdominant term g_0^a we form an equation

$$1 - B\frac{k_L^2}{6\omega^2} = 0. \tag{5.56}$$

It has two roots,

$$\omega = \sqrt{\frac{B}{6}}k_L + \ldots, \text{ for } B > 0, \tag{5.57}$$

$$\omega = -i\sqrt{\frac{-B}{6}}k_L + \ldots, \text{ for } B < 0. \tag{5.58}$$

[5] Recall, that all the g_n^i's are functions exact in z.
[6] We assume B to also be of the order ε.
[7] We put the auxiliary parameter $\varepsilon = 1$ in what follows.
[8] We drop inessential numerical coefficients.

The dots indicate subleading terms in the momentum, which would be present, if we took into account the full contributions from (5.49). The sign of the second complex root above was identified by using these additional terms, computing the limit $B \to 0$ and ensuring that it reproduces the correct sign of the isotropic case (5.32). We will see the more complete expressions shortly.

The result above demonstrates, that in the regime of $k_L \ll B$, when B is positive perturbations propagate indefinitely (to the leading order in k_L), like free massless modes with linear dispersion relation. If however the anisotropy is negative, $B < 0$, perturbations along the momentum k_L are strongly damped. Since k_L is substantially larger than k_L^2 for $k \sim 0$, the damping is greater than in the isotropic case, (5.53).

Let us now analyse the dynamics at the momentum scale induced by B. If we allow the momentum to be of the order $k_L \sim \sqrt{B}$, the contribution of $g_0^a(0)$ can no longer be neglected. Skipping unimportant coefficients the structure of the equation (5.48) is essentially found to be

$$1 + g_0^a(0) + B g_1^a(0) \sim 1 + \frac{B}{\omega} + \omega + \frac{B^2}{\omega^2} + B = 0. \tag{5.59}$$

For $B \sim 0$ we have $B > B^2$ and since ω is also small we can drop terms of the order of ω^3 and $\omega^2 B$. We are then left with a quadratic equation

$$1 + \frac{i k_L^2}{2\sqrt{2}\omega} - B\frac{k_L^2}{6\omega^2} = 0. \tag{5.60}$$

Now we can see more clearly how the choice of physical roots of this polynomial depends on the sign of B. As was mentioned above, the choice is dictated by compatibility with the isotropic result[9] (5.53). By demanding the regular small B limit we identify the first solution:

$$\omega = -i\frac{k_L^2 + \sqrt{k_L^4 - \frac{16}{3}B k_L^2}}{4\sqrt{2}}, \text{ with } B < 0. \tag{5.61}$$

If on the other hand the anisotropy is positive, $B > 0$, there are two possible solutions, which represent right and left moving waves, and there is a branch point at $B = 0$. The solutions reads

$$\omega = -\frac{i k_L^2 \pm \sqrt{-k_L^4 + \frac{16}{3}B k_L^2}}{4\sqrt{2}}, \text{ with } B > 0. \tag{5.62}$$

The imaginary parts of these expressions for small values of momentum and anisotropy are negative, so all the modes are stable.

This point concludes the analysis of the equation (5.48) to the order ε. The simplifications discussed above can also be directly justified by solving the full equation to the order ε^2 and checking the small momentum and anisotropy expansions. The general solutions to the algebraic equation (5.48) have several roots, but only two of them are physical. The others are found to be non-zero in the limit $k \to 0$, and thus are incompatible with hydrodynamics. The scaling arguments used above reduce the order of the algebraic equations, leading solely to the gapless physical roots with proper asymptotics.

Having completed the discussion of the longitudinal case $p_L \neq 0$, we can now advance to the transverse channel $p_T \neq 0$, and its equation for the field component $E_1(k_T, z)$ along

[9] The solution with the negative sign in front of the square root near $B \sim 0$ behaves as $-i\frac{\sqrt{2}}{3}B$, which vanishes when $B \to 0$, contradicting (5.53).

the momentum in (5.44). It turns out, that the whole analysis proceeds in exactly the same manner as before. There are only subtle differences in numerical coefficients, which lead to almost the same solutions, but with reversed dependence on the anisotropy B. We shall thus limit ourself to just stating the final results.

Because of the similarity to the longitudinal case we skip the linear analysis and focus directly on the higher order equation, the counterpart of (5.60). This time it is found to be

$$1 + \frac{ik_T^2}{2\sqrt{2}\omega} + B\frac{k_T^2}{12\omega^2} = 0. \tag{5.63}$$

The solutions are given by

$$\omega = -i\frac{k_T^2 \pm \sqrt{k_T^4 + \frac{8}{3}Bk_L^2}}{4\sqrt{2}}. \tag{5.64}$$

Here again all the previous restrictions on the isotropic limit (5.53) apply, but with an opposite sign of B. In this case, in the small momentum limit we also find a linear regime

$$\omega = \pm i\frac{\sqrt{B}k_T}{2\sqrt{3}} + \dots, \text{ with } B > 0, \tag{5.65}$$

the analogue of (5.57), and one purely damped mode

$$\omega = -i\frac{\sqrt{-B}k_T}{2\sqrt{3}} + \dots, \text{ with } B < 0. \tag{5.66}$$

This concludes our search for instabilities in the strongly coupled static plasma system. Amid the initial concerns we were able to make use of the singular geometry and answer the question on the fate of instabilities in strongly coupled anisotropic gauge theory, which will be summarised below. The analysis was founded on a very simple vector field and one could think of a more elaborated probes, but one can speculate, that if instability was present, it should manifest itself in any observable due to the mutual couplings in the non-linear strongly coupled theory.

5.3 Closing remarks

In this chapter we have been pursuing the goal of finding a mechanism leading to a swift isotropisation of strongly coupled quark-gluon plasma. The motivation for this investigation emerged from the well understood and experimentally observed instabilities in weakly coupled QED, and also from the instabilities found in perturbative QCD. The instabilities in these systems lead to the development of a small time scale, over which anisotropy is washed away, and the system is stabilised by the ascend into the non-linear regime, resolving the exponential growth of the modes.

The result of the analysis shows no appearance of instabilities, imaginary parts in all the dispersion relations have proper signs leading to damping. However certain traces of its presence in the gauge theory evolution remain. The exponential instability and stability of the weakly coupled Yang-Mills system are transformed to the stable *indefinite* propagation in the previously unstable channel, and *much* stronger damping in the formerly stable channel. The most directly translated trace of the weakly coupled evolution characteristics is the pattern of stability dependence on the sign of anisotropy. In our analysis we find it to agree with the one at weak coupling, with the free propagation-strong damping

pattern being reversed, when we pass from longitudinal to transverse momentum plasma perturbations.

As a last word in this chapter let us remark that the absence of the naively expected instability mechanism shows the lack of a simple equilibration mechanism in QGP. One then is forced to seek more involved explanations, which necessarily must involve full temporal evolution of the plasma and its dual geometry. This will be the goal in the next chapter.

Chapter 6

Time dependent thermalization and isotropization

6.1 Introduction

The goal of the present chapter is to understand selected features of the non-equilibrium $\mathcal{N} = 4$ super-Yang-Mills strongly coupled fluid dynamics by presenting the reasoning of our papers [Heller 2012a, Heller 2012b]. In contrast to the previous chapter dealing with linear response theory, we must now turn to the real time non-linear evolution of the geometry. This amounts to solving time dependent Einstein equations. The interest in dynamical geometries within AdS/CFT correspondence brought several important results in the past, like the described before fluid/gravity duality [Bhattacharyya 2008b, Chesler 2009].

The results of numerical simulations covered below rely on several previous analytical approaches to the real time plasma evolution. The initial AdS/CFT studies of the late time boost-invariant perfect fluid dynamics led to the boosted black brane spacetime solution [Janik 2006a]. Successive refinements of this result to include viscous effects, as well as early time analysis brought further insights, but none allowed to fully follow the evolution from the collision onset to the late equilibrium stage. The natural step then was to try solving Einstein equations numerically.

In this chapter we consider the following questions: how does the transition to thermal equilibrium of the SYM fluid occur and what are its properties? The answers we found and share below appear to be somewhat surprising and have opened further interesting directions of research. Their outcome will be presented in subsequent chapters.

6.2 Analytic results of late time analysis

Historically first analytical results confirming holographic link between dynamical fluids and evolving geometry were obtained in the late time limit of boost-invariant expansion [Janik 2006a]. In this setup we assume the boundary stress energy tensor $\langle T^{\mu\nu}(\tau)\rangle$ to be subject to symmetries discussed in Chapter 2, Section 2.1.5, and the task is to solve effectively $(\tau, z) = 1 + 1$ dimensional Einstein equations for three metric components $a(\tau, z)$, $b(\tau, z)$, $c(\tau, z)$ in large τ limit. The suitable metric Ansatz $G_{\mu\nu}(\tau, z)$ assumes in this case the form

$$ds^2 = \frac{-e^{a(\tau,z)}d\tau^2 + \tau^2 e^{b(\tau,z)}dy^2 + e^{c(\tau,z)}(dx_1^2 + dx_2^2) + dz^2}{z^2}. \tag{6.1}$$

For a generic energy density function at the boundary $\varepsilon(\tau)$ it is not yet a soluble problem, but based on physical grounds one expects to find in this limit $\varepsilon(\tau) \sim \tau^{-s}$ for some positive s, that is expansion with a power-like decreasing energy density. As was thoroughly discussed in Chapter 3, such an assumption leads to the discovery of a simplifying scaling variable $v = z\tau^{-s/4}$, which when introduced into Einstein equations in place of z allows

one to take the scaling limit[1] ($\tau \to \infty,\ v =$ fixed). This step upon Taylor expansion in $\tau^{-2/3}$ recasts the non-linear partial differential equations into a coupled hierarchy of ordinary differential equations in v, the leading of which can be solved exactly in the strict $\tau \to \infty$ limit [Janik 2006a]. Contributions subleading in proper time inverse can also be isolated and are related to viscous corrections, as we know from Chapter 3. We shall see this procedure at work for higher orders in Chapter 7. Here let us briefly emphasize, that the existence of scaling variable expansion is crucial for obtaining the solution, and also that the resulting metric is independent of the initial conditions. The bulk metric is found exactly in variable $v = z\tau^{-1/3}$ as a Dirichlet problem with boundary condition at $v = z = 0$, and perturbatively in τ as $\tau^{-2/3}$ series. A generic structure of the resulting metric functions is then

$$a(\tau, z) = a_0(z\tau^{-1/3}) + \frac{1}{\tau^{2/3}} a_1(z\tau^{-1/3}) + \frac{1}{\tau^{4/3}} a_2(z\tau^{-1/3}) + \dots \tag{6.2}$$

and a typical resulting holographic energy density assumes the form

$$\varepsilon(\tau) = \frac{1}{\tau^{4/3}}(\varepsilon_2 + \frac{\varepsilon_3}{\tau^{2/3}} + \frac{\varepsilon_4}{\tau^{4/3}}) + \dots \tag{6.3}$$

There is an important mechanism at work here however, in place of the missing initial data. At each order of the $\tau^{-2/3}$ expansion in (6.2) an undetermined integration constant remains, which is not fixed by boundary conditions nor constraints. The way to assure regular bulk solution, that is absence of naked singularities one imposes a condition of regularity expressed through the finiteness of the curvature invariant $\mathfrak{R}^2$ (Riemann tensor squared). This choice specifies the power $s = 4/3$ and the transport coefficients of the underlying fluid. On the other hand the independence from initial conditions expresses the physical fact of thermalization, washing away any details on how the system was assembled microscopically.

We will be working a lot in the late time limit scheme described above. First however let us describe certain facts known analytically about the *early* proper time regime, which will be of use later on.

6.3 Analytic results of early time analysis

In contrast to the late time regime, the analysis at early times is significantly different from the late time case. The main difference is the lack of scaling variable whatsoever, and this time the dependence on initial conditions is crucial, for a good physical reason. The point is that for small proper times there should be a strong imprint of the initial data on the subsequent evolution. As we shall see this is indeed the case.

To observe the problem with the lack of scaling variable at small proper times arises let us recall a synthetic description of how scaling variable is found at late times. First we assume the desired boundary condition on the metric fields (in Fefferman-Graham map), that is with $z \to 0$

$$\begin{aligned} z^2 G^{\mu\nu}(\tau, z) &\to \eta^{\mu\nu}, \\ z^6 G^{\mu\nu}(\tau, z) &\to \langle T^{\mu\nu}(\tau) \rangle \text{ with } T^{00}(\tau) \equiv \varepsilon(\tau) = \tau^{-s}. \end{aligned} \tag{6.4}$$

[1] In Chapter 3 we have been using Eddington-Finkelstein coordinates, while the presently discussed observation was made in Fefferman-Graham coordinates, which we use in this subsection. The scaling variable v was *a posteriori* found to originate from the Eddington-Finkelstein static horizon function $f(r) = 1 - 1/(br)^4$, where b denoted the inverse horizon locus and temperature, see (3.75). If following [Janik 2006a] one approximates these with *dynamic* perfect fluid values, $b = b(\tau) \sim T(\tau)^{-1}$ and $T(\tau) \sim \tau^{-1/3}$, then using inverse radial coordinate $z = 1/r$ one finds our scaling variable $v = z\tau^{-1/3}$, with $s = 4/3$ explained further below.

Then one solves perturbatively Einstein equations around the boundary $z = 0$ according to the standards holographic renormalization procedure [de Haro 2001], which produces an infinite series of metric expansion terms $G^n_{\mu\nu}(\tau)$, all of witch with $n > 4$ are specified in terms of the boundary data above with the parameter s. The crucial point is that by inspecting the series for such a perturbative solution, which involves sums of polynomials in τ and z one can notice a particular combination dominating the large time expansion of each terms, $v = z\tau^{-s/4}$. Of course it is our scaling variable. All other terms in each individual $G^n_{\mu\nu}(\tau)$ are subleading with respect to v. Therefore one can use this knowledge and form a non-perturbative Ansatz for the whole metric solution with variables v and τ, insert it to Einstein equations, perform late time expansion and solve it order by order, as we have descried in the previous paragraph and Chapter 3.

The problem at small times is that no such hierarchy of terms arises in each $G^n_{\mu\nu}(\tau)$ if we assume $s < 0$ and $\tau \ll 0$. The existence of the scaling variable is invalidated due to a subtlety, that is the only allowed value of s appears to be $s = 0$ and all the terms, which could potentially lead to an appearance of the scaling variable happen to be multiplied by s, effectively vanishing and leaving no scaling structure in the solution. One thus is left with the necessity to solve equations exactly by other means, or seek ordinary perturbative solutions.

Let us now make a comment on the dependence of small times evolution on the initial data. Suppose we impose boundary condition with energy density of the form[2]

$$\varepsilon(\tau) = \sum_{n=0}^{\infty} \varepsilon_{2n} \tau^{2n}. \tag{6.5}$$

This translates through holographic renormalization [de Haro 2001, Skenderis 2002] to a perturbative solution near the boundary

$$a(\tau = 0, z) = \sum_{n=0}^{\infty} a_{2n} z^{4+2n}, \tag{6.6}$$

with all the coefficients a_{2n} explicitly computable from Einstein equations. Their key property is that they *a priori* depend on all the energy expansion terms ε_{2n}. Therefore there is a one-to-one map between initial data and boundary stress energy tensor form expressed by $\varepsilon(\tau)$. Therefore any individual initial metric function will give raise to a distinct energy density profile, and there is no universality in $\varepsilon(\tau)$ for small τ. Intuitively this reflects the memory of collision data shortly after the plasma formation.

Not every function is however allowed to be used as an initial metric profile, but only solutions to non-linear constraints equations. It turns out, that they play a crucial rôle by enforcing a mandatory coordinates singularity in every member of the space of initial data functions.

Let us briefly see how it happens, [Beuf 2009]. It turns out, that one of the constraint equations for three initial data functions

$$\{a_0(z),\ b_0(z),\ c_0(z)\} = \{a(0, z),\ b(0, z),\ c(0, z)\} \tag{6.7}$$

can be recast with the aid of substitutions

$$\{v(z^2),\ \varsigma(z^2),\ w(z^2)\} \ \equiv\ \{a_0'(z),\ b_0'(z),\ c_0'(z)\}/4z \tag{6.8}$$

[2]Odd powers in the series are ruled out by finiteness of the curvature invariants. Otherwise the resulting solution would exhibit an unphysical singularity, see [Beuf 2009]. It is interesting, that the small proper times solution should be even under time reversal. Note however, that the boost-invariant coordinate system is only well defined in the future light cone, so we cannot evolve backwards across $\tau = 0$.

in the form suitable for integration,

$$\int_0^\infty (v' + \varsigma' + w')\mathrm{d}z^2 + \int_0^\infty (v^2 + \varsigma^2 + w^2)\mathrm{d}z^2 = 0, \tag{6.9}$$

This expression is just the (zz) component of Einstein equations for (6.1) integrated over the whole bulk space slice at initial time $\tau = 0$. The reason to do so is that if we impose physical boundary conditions on the metric fields the first integral on the left will just vanish. These conditions are that derivatives are bounded in the bulk and vanishing at $z \to 0,\ z \to \infty$. Vanishing at $z = 0$ is just the Minkowski boundary condition and vanishing at $z \to \infty$ is an assumption of solely $1/z^2$ essential singularity in the bulk's interior, where the D-branes used to reside. What follows is the observation, that the remaining integral must vanish. This can happen only for all three functions being identically zero, since we integrate a sum of real squared functions. Therefore the only regular solution of constraints is the trivial empty AdS spacetime.

As a consequence we reach a very important conclusion, that initial data on the light cone initial surface $\tau = 0$ must necessarily be singular, because then at least on of the derivatives in (6.9) is unbounded and its integral does not vanish. This implies, that spacetime must be singular already from the onset of evolution, and in fact for all subsequent times $\tau \geq 0$. This however should not be an essential singularity, but only a coordinate one, and we are able assure that this is the case due to the Fefferman-Graham solution based Ansatz. These coordinates as we know are Schwarzschild-like, and can posses harmless coordinate singularities. The benefit of this situation will be discussed later, in the context of initial data generation 6.5.2.

To understand better the issue of singularity we note that the structure of constraints is such, that we have the following simple relation at $\tau = 0$ [Beuf 2009] :

$$a_0(z) = b_0(z). \tag{6.10}$$

Moreover, one can solve constraints equation

$$v' + \varsigma' + 2w' + v^2 + \varsigma^2 + 2w^2 = 0 \tag{6.11}$$

exactly, by putting $\varsigma = v$ in view of (6.10) and introducing linear combinations removing one of the derivatives,

$$v_+ = -w - v,\ v_- = w - v. \tag{6.12}$$

This recasts (6.11) into an algebraic equation for v_- with the physical solution

$$v_- = \sqrt{2v'_+ - v_+^2}. \tag{6.13}$$

Therefore the whole space of initial data is parametrized by just one unknown function $v_+(z^2)$, and we shall use this knowledge during numerical developments further on.

Using v_+ we can address the question of the nature of the singularity. By using curvature invariant one can show, that harmless coordinates singularity occurs only when $v_+(z^2)$ has a simple pole

$$v_+(z^2) \sim \frac{1}{z_0^2 - z^2},\ z \sim z_0, \tag{6.14}$$

for some constant z_0. This ensures we are dealing with just a coordinates singularity. By further analysis it was found, that the general initial data functions can be parametrized as

$$v_+(z^2) = \frac{2}{3}\varepsilon_0 z_0^2 \frac{z^6}{z_0^2 - z^2} f(z^2), \tag{6.15}$$

for some regular function $f(z^2)$ obeying $f(0) = 1,\ f(z_0^2) = 3/(2\varepsilon_0 z_0^8)$, and one has to use (6.13) to find $v_-(z^2)$, ensuring its reality on the way. This completes the analysis of the space of initial data space and gives a prescription on how to generate them, which will be used extensively later on.

6.4 Boost-invariant system in ADM formulation

The ultimate goal of the real time analysis would be to join the two regimes described above. As is often the case, the limiting regimes of small or big parameters (like the proper time above) are significantly simpler, and the intermediate region is where the most exciting phenomena occur. In the present context we would like to observe the process of equilibration and thermalisation, accompanied by the decay of initial non-equilibrium degrees of freedom. This task amounts to solving full nonlinear Einstein equations, and presently can be done only numerically.

As we wrote above, in the context of quark-gluon plasma AdS/CFT research the only previous approach to solving numerically Einstein equations was made by [Chesler 2009]. There, the non-equilibrium state of boundary field theory was artificially created by turning on a so-called non-normalizable mode of the metric. It means that the boundary metric, which for QGP applications is usually kept fixed as Minkowski, was disturbed by compactly supported gravitational wave. In field theory stress-energy tensor couples to the metric, so such an artificial wave might be thought of as a non-zero source. Therefore such a perturbation can be understood as a quench of the system, where energy is swiftly injected causing departure from equilibrium and subsequent evolution of the quantum field towards equilibrium vacuum configuration. In the bulk the presence of boundary wave is felt as a perturbation of the boundary condition, and the bulk metric starts to behave accordingly. In this way one can study equilibration of the strongly coupled gauge system. However there is a drawback: the boundary metric perturbation (which we interpret as our spacetime) is clearly absent in the context of relativistic heavy ion collisions, which are of chief interest to us. Such a quench is well suited for studying strongly coupled equilibration properties *per se*, but is not compatible with the system we are trying to describe. In particular it would be unclear how to match the artificially created boundary state of the gauge field with the configuration originating form a collision. Moreover with this approach one can study plasma evolution starting only from some finite time on, when the boundary metric would have already returned to its flat form. But this prohibits us from studying the very early times dynamics, which is rich and surprisingly contains crucial information on the subsequent evolution, as we shall see.

6.4.1 ADM formulation of Einstein equations

With the goal of observing the whole temporal evolution of $\varepsilon(\tau)$ and difficulties of analytical approach in mind, we attacked the problem of numerical simulation in five dimensional asymptotically AdS spacetime[3] using the machinery of Chapter 4. One of the key assumptions was to leave the boundary flat and keep the physical system close to intuitive understanding by building on the existing Fefferman-Graham analytical results and starting at $\tau = 0$. The perturbative analysis of the early times in 6.3 unravelled the always singular nature of initial data, as well as its close relation to the initial energy density. We will cover issues stemming from this later on and now we focus on the building blocks of

[3]The dimensionality of differential equations though, is of course reduced by all the symmetries to 1+1 problem, which made it tractable.

our solution. The main reason for using ADM approach was that if is perfectly well suited for numerical integration, because as we remarked in 4 it resembles Hamiltonian first order system, as well, as it smoothly connects to the previous Fefferman-Graham formulas. It is crucial, because it will allow us to directly benefit from initial data analysis performed in these coordinates.

The metric Ansatz in ADM form is the following:

$$ds^2 = \frac{-a^2(u)\alpha^2(t,u)dt^2}{u} + \frac{t^2a^2(u)b^2(t,u)dy^2}{u} + \frac{c^2(t,u)dx_\perp^2}{u} + \frac{d^2(t,u)du^2}{4u^2}. \tag{6.16}$$

As the geometry is required to be asymptotically AdS. Therefore the metric coefficients diverge at the conformal boundary and we have explicitly factored the terms $\frac{1}{u}$ out, to ensure the non-singularity of the unknown functions. Further refinement of the Ansatz consists of explicit insertion of an explicit and fixed function $a(u)$, which will play the role of the spatial cut-off (related to the singularity in the initial data). Boost-invariance is imposed by independence of the metric from the rapidity y, and presence of the time factor t^2. The u variable runs from the conformal boundary at $u = 0$ to the interior of the AdS space in the Poincaré patch, $u \to \infty$. It is also motivated by a change from the Fefferman-Graham coordinate z, which near the boundary would approximately be $z \sim \sqrt{u}$ and soften the singular nature of the boundary. Empty AdS space in these coordinates is realized by all the functions being equal to unity and the conformal boundary is the Minkowski flat spacetime in proper time coordinates. Such an Ansatz is capable of describing a wide class of asymptotically-AdS spacetimes, some of which may contain a black brane in the bulk.

The induced metric representing the ADM foliation intrinsic degrees of freedom is

$$\gamma_{ij} = \textsc{Diag}\left[\frac{t^2a^2(u)b^2(t,u)}{u}, \frac{c^2(t,u)}{u}, \frac{c^2(t,u)}{u}, \frac{d^2(t,u)}{4u^2}\right]. \tag{6.17}$$

The extrinsic degrees of freedom coming from the extrinsic curvature are

$$K_{ij} = \textsc{Diag}\left[\frac{ta(u)L(t,u)}{\sqrt{u}}, \frac{M(t,u)}{\sqrt{u}}, \frac{M(t,u)}{\sqrt{u}}, \frac{P(t,u)}{4u\sqrt{u}}\right]. \tag{6.18}$$

Here the unknown functions were defined as $L(t,u)$, $M(t,u)$, $P(t,u)$ and appropriate factors of u were extracted, as above. The object of significant importance to us, lapse function, is chosen as

$$\tilde{\alpha}(t,u) = \frac{a(u)\alpha(t,u)}{\sqrt{u}}. \tag{6.19}$$

The function $a(u)$ is a non-dynamical time independent piece of the lapse, which will play the role of a spatial cut-off. At the boundary it will always be set to unity, $a(0) = 1$. Further motivation for it and the lapse properties will be given below.

Ultimately, the vacuum ADM Einstein equations with a negative cosmological constant $\Lambda = -6$ take the form

$$\partial_t\gamma_{ij}(t,u) = \frac{-2a(u)\alpha(t,u)}{\sqrt{u}}K_{ij}(t,u), \tag{6.20}$$

$$\begin{aligned}\partial_t K_{ij}(t,u) &= -\nabla_i\nabla_j\frac{a(u)\alpha(t,u)}{\sqrt{u}} + 4\frac{a(u)\alpha(t,u)}{\sqrt{u}}\gamma_{ij} \\ &- \frac{2a(u)\alpha(t,u)}{\sqrt{u}}(R_{ij} - 2K^{ij}K_{ij} + KK_{ij}).\end{aligned} \tag{6.21}$$

Explicitly, for the metric functions we have

$$\frac{\partial b(t,u)}{\partial t} = \frac{-b(t,u)^2+\alpha(t,u)L(t,u)}{tb(t,u)}, \tag{6.22}$$

$$\frac{\partial c(t,u)}{\partial t} = \frac{a(u)\alpha(t,u)M(t,u)}{c(t,u)}, \tag{6.23}$$

$$\frac{\partial d(t,u)}{\partial t} = \frac{a(u)\alpha(t,u)P(t,u)}{d(t,u)}. \tag{6.24}$$

The expressions for the extrinsic curvature functions are in turn much longer,

$$\begin{aligned}\frac{\partial L}{\partial t} = & -\frac{4tuaa''\alpha b^2}{d^2}-\frac{4tuaa'\alpha_u b^2}{d^2}-\frac{12tuaa'\alpha bb_u}{d^2}-\frac{8tuaa'\alpha b^2c_u}{cd^2}+\frac{4tuaa'\alpha b^2d_u}{d^3}+\\ & \frac{8taa'\alpha b^2}{d^2}-\frac{4tua'^2\alpha b^2}{d^2}-\frac{4tua^2\alpha_u bb_u}{d^2}+\frac{2ta^2\alpha_u b^2}{d^2}-\frac{8tua^2\alpha bb_uc_u}{cd^2}+\\ & \frac{4tua^2\alpha bb_ud_u}{d^3}+\frac{6ta^2\alpha bb_u}{d^2}-\frac{4tua^2\alpha bb_{uu}}{d^2}+\frac{4ta^2\alpha b^2c_u}{cd^2}-\\ & \frac{2ta^2\alpha b^2d_u}{d^3}-\frac{4ta^2\alpha b^2}{ud^2}+\frac{4ta^2\alpha b^2}{u}-\frac{2a\alpha LM}{c^2}-\frac{a\alpha LP}{d^2}-\frac{\alpha L^2}{tb^2}-\frac{L}{t},\end{aligned} \tag{6.25}$$

$$\begin{aligned}\frac{\partial M}{\partial t} = & \frac{8ua'\alpha c_uc}{d^2}-\frac{4a'\alpha c^2}{d^2}+\frac{4ua\alpha_uc_uc}{d^2}-\frac{2a\alpha_uc^2}{d^2}+\frac{4ua\alpha b_uc_uc}{bd^2}-\frac{2a\alpha b_uc^2}{bd^2}-\\ & \frac{4ua\alpha c_ucd_u}{d^3}-\frac{8a\alpha c_uc}{d^2}+\frac{4ua\alpha c_{uu}c}{d^2}+\frac{4ua\alpha c_u^2}{d^2}+\frac{2a\alpha c^2d_u}{d^3}+\frac{4a\alpha c^2}{ud^2}-\\ & \frac{4a\alpha c^2}{u}-\frac{a\alpha MP}{d^2}+\frac{\alpha LM}{tb^2},\end{aligned} \tag{6.26}$$

$$\begin{aligned}\frac{\partial P}{\partial t} = & 8ua'\alpha_u+\alpha\left(\frac{8ua'b_u}{b}-\frac{8ua'd_u}{d}+\frac{LP}{tb^2}+8ua''\right)+4ua\left(\alpha_{uu}-\frac{\alpha_ud_u}{d}\right)+\\ & a\alpha\left(\frac{4d_u\left(-\frac{ub_u}{b}-\frac{2uc_u}{c}+2\right)}{d}+\frac{4ub_{uu}}{b}+\frac{8uc_{uu}}{c}-\frac{2MP}{c^2}+\frac{P^2}{d^2}-\frac{4d^2}{u}+\frac{4}{u}\right).\end{aligned} \tag{6.27}$$

The shorthand notation in the above equations is that all functions apart from $a(u)$ depend on t and u and the prime and subscript in u denote the u derivative. The Hamiltonian and momentum constraints are given by

$$\begin{aligned}C_0 &= R-K_{ij}K^{ij}+K^2+12,\\ C_i &= \nabla_i(K^{ij}-K\gamma^{ij}).\end{aligned} \tag{6.28}$$

The only non-trivial momentum constraint is the one in the direction of the bulk variable u, C_4.

6.5 Initial and boundary conditions

Evolution equations derived in the above paragraph need to be supplemented with appropriate initial and boundary conditions. The initial data hypersurface $t = 0$ is null, in contrast to subsequent hypersurfaces with $t > 0$, which become spatial as soon as they depart from $t = 0$ plane. We will discuss how to handle this subtlety, as well as the

general constraints on the space of initial data in the ADM setup, and eventually the way to construct initial profiles with non-zero field theory initial energy density.

The spatial boundaries consist of conformal AdS boundary at $u = 0$ and artificial boundary of the simulation domain, in the interior of the AdS space at some specific fixed value of u. We will derive a novel way to implement such a cut-off in AdS-ADM framework, which is different from standard outgoing wave condition at the outer boundary.

6.5.1 Initial conditions analysis

In this paragraph we will first discuss some general properties of initial conditions in ADM formulation and then the structure of equations of motion at infinitesimally small time.

From the point of view of differential equation, we have to solve a system of two-dimensional coupled equations, which are firs order in time. This means, that we will need one initial value profile for each of the seven functions. There are seven and not just six functions to determine, because apart from γ_{ij} and K_{ij} degrees of freedom introduced in (6.17) and (6.18) there is also the lapse function (6.19). The space of allowed initial data is specified by solutions of constraints, which in the ADM formulation are represented by equations (6.28). However, the $t = 0$ hypersurface of the boost-invariant Ansatz (6.16) contains the null cone introduced by the element t^2dy^2 vanishing at $t = 0$. In standard ADM formulation initial value problem is usually not stated on a null hypersurface[4], so this requires careful analysis of the evolution equations and corresponding constraints. In view of the numerical integration we should be careful about potential spurious singularities introduced by metric Ansatz, which although unphysical, can be troublesome.

We can thus assume that the initial evolution will start smoothly from the Cauchy data. To investigate the structure of equations at the first time-step, we expand all the unknown functions in time around $t = 0$:

$$\begin{aligned} b(t,u) &= b_0(u) + b_1(u)t + \dots & M(t,u) &= M_0(u) + M_1(u)t + \dots \\ d(t,u) &= d_0(u) + d_1(u)t + \dots & L(t,u) &= L_0(u) + L_1(u)t + \dots \\ c(t,u) &= c_0(u) + c_1(u)t + \dots & P(t,u) &= P_0(u) + P_1(u)t + \dots \\ \alpha(t,u) &= \alpha_0(u) + \alpha_1(u)t + \dots \end{aligned} \tag{6.29}$$

Next we plug these expressions into the ADM equations (6.22)-(6.28). The presence of potentially singular terms in equations, like $1/t$ in (6.22) implies concrete relations among the initial values of functions, which removes these singularities. In this way we can constrain the space of the initial data by demanding regular initial evolution step.

In this way we obtain the following three relations:

$$b_0(u) = \alpha_0(u),\ L_0(u) = \alpha_0(u),\ M_0(u) = P_0(u). \tag{6.30}$$

Another condition can be imposed by noticing, that the initial data hypersurface has residual diffeomorphism invariance. One can perform transformation of the coordinate u without changing the general form of the initial metric (6.17), $\gamma(0,u)_{ij}$. Using this freedom we can choose $d_0(u)$ to be initially constant: $d_0(u) = 1$. Notice that at the initial time $t = 0$ the dy component of the metric vanishes. Due to this property, only the $c_0(u) \equiv c(0,u)$ function changes to include the gauged-away $d_0(u)$ when we transform u at $t = 0$, and $b_0(u)$ is left untouched. As a consequence, we can think of $c_0(u)$ as of the only undetermined function

[4]For example in Eddington-Finkelstein coordinates one starts at the null hypersurface, but then one uses a completely different evolution scheme based on characteristics analysis (characteristic evolution).

in the initial metric $\gamma_{ij}(0,u)$. Notice also, that the use of this freedom means that $d_0(u)$ was not a degree of freedom at all, since we transferred its contents to $c_0(u)$.

Another ambiguity related to gauge redundancy is the choice of the lapse function $\alpha_0(u)$. We narrow the class of lapse functions to the set reproducing the simplest uniform initial hypersurface, with $\alpha_0(u) = 1$. With this choice, we can see by a comparison between the initial ADM and Fefferman-Graham metrics, that they match at $t = 0$ and $\tau = 0$[5]. For $t \sim 0$ we have

$$\begin{aligned} g_{FG} &= \textsc{Diag}\left[-\frac{A_0(u)}{u}, \frac{\tau^2 A_0(u)}{u}, \frac{C_0(u)}{u}, \frac{1}{4u^2}\right], \\ g_{ADM} &= \textsc{Diag}\left[-\frac{a_0(u)}{u}, \frac{t^2 a_0(u)}{u}, \frac{c_0(u)}{u}, \frac{1}{4u^2}\right]. \end{aligned} \tag{6.31}$$

Above we have taken into account the Fefferman-Graham initial conditions analysis discussed in Section 6.3. It implies, that $A_0(u)$ is completely determined by $C_0(u)$ through (6.11). The $a_0(u)$ is just a fixed function factored out from the lapse for future convenience. At $t = 0$ both line elements reduce to

$$ds^2 = g_{x_\perp x_\perp} dx_\perp^2 + g_{uu} du^2, \tag{6.32}$$

and we can identify the Fefferman-Graham $C_0(u)$ with the ADM function $c_0(u)$. On both sides we have an agreement on the number of independent initial data functions, which is equal to one. It will prove very useful, that such a simple map exists between the two initial data spaces. It also allows us to obtain for every such a constructed initial profile $C_0(u) \equiv c_0(u)$ a power series expansion for the early time energy density $\varepsilon(\tau)$, in accordance with the method outlined in Section 6.3. This was one of the reasons for us to develop such coordinates, with aligned initial hypersurfaces. Owing to this, existing expressions for the energy density series from the Fefferman-Graham patch can be compared for small, but finite values of the time τ with the results of our simulation. This served as one of the crucial tests of the validity of numerical integration, especially in view of the observed exotic initial energy evolution for some initial data profiles (see e.g. Sec. 6.7.3).

An noteworthy feature of our boost-invariant ADM-type evolution is that the initial data are not constrained, owing to the fact that our Cauchy surface is null. In the Fefferman-Graham case (6.1) we had three metric functions, out of which two are initially equal (6.10), and the remaining two are related by (6.11). All this happens in the gauge keeping fixed $g_{zz} = 1/z^2$. When we pass to ADM coordinates, we release this fifth metric component and introduce an arbitrary lapse α in place of g_{tt}. As a consequence the residual diffeomorphism redundancy appears, linking component g_{tt} with g_{uu}. This allows us to fix $d(0,u) = 1$, but only at this initial time instance $t = 0$. For subsequent times $d(t,u)$ evolves in accordance with its equation. If we insisted to keep fixed $d(t,u) = 1$, then following (6.24) it would imply $P(t,u) = 0$, requiring in turn $\partial_t P(0,u) = 0$. It can be show, that this condition is equivalent to the very constraint equation of Fefferman-Graham, (6.11). Therefore by releasing $d(t,u)$ we give up the constraint. There is no initial arbitrariness however, because owing to the null initial data hypersurface the ADM function $b(t,u)$ is absent along with the whole $g_{yy} \sim t^2 dy^2$ component, and we have only $c_0(u)$ and $d_0(u)$ to specify. As we said $d_0(u)$ is removed by the lapse gauge transformation, hence we are left with one unknown function $c_0(u)$. As we shall soon discuss, its properties will be probed with the aid of the Fefferman-Graham constraint equation.

[5]The two initial time hypersurfaces coincide, $\tau_{FG}(t = 0, u) = 0$.

For the purpose of numerical integration and because of the apparent singularity in the evolution equations at $t = 0$, we need to obtain manifestly regular initial integration step, that can be evaluated by the computer. This is done by inserting the expanded initial values of the metric functions (6.29) into the ADM equations, which gives

$$\begin{aligned}
\partial_t b(0,u) &= 0,\ \partial_t c(0,u) = 0,\ \partial_t d(0,u) = 0,\ \partial_t L(0,u) = 0,\\
\partial_t M(0,u) &= \frac{-2\alpha(2u(ca\alpha\partial_u c + \partial_u(a\alpha c\partial_u c)))}{d^2}\\
&+ \frac{a\alpha\partial_u d(c^2+\partial_u c^2)}{d^3} - \frac{2a\alpha c^2}{u} + \frac{2a\alpha c^2}{ud^2}\\
\partial_t P(0,u) &= 4u\partial_u^2(a\alpha) + \frac{4\partial_u d(a\alpha+\partial_u(a\alpha))}{d}\\
&- \frac{2a\alpha(1-d^2)}{u} + \frac{4ua\alpha\partial_u^2 c}{c} - \frac{4ua\alpha\partial_u c\partial_u d}{cd}.
\end{aligned} \tag{6.33}$$

These formulas express just the values of the equations of motion at the initial time $t = 0$. They are clearly non-singular and were used to compute the values of the fields in the very first integration step, which advances time to $t = 0 + \delta t$.

6.5.2 Initial data generation

We will now briefly describe how the actual initial geometry profiles were generated. As we discussed above, locally around $t = 0$ there is the moderately simple relation between our ADM-like and Fefferman-Graham coordinates, (6.31). This enables us to use constraint equations of the latter simpler coordinates (6.11) at $t = 0$ in the process of Cauchy data generation. The major point in this task was to ensure, that all the generated functions had also in ADM a proper singularity structure, according to what we found before in Section 6.3. The mentioned constraints of Fefferman-Graham coordinates assisted us in this process in the following way. First, using the mentioned identification of the initial value functions[6] $c_0(u) = C_0(u)$ we were proposing *ad hoc* various ADM profiles $c_0(u)$. Then we were solving the Fefferman-Graham constraints (6.11) using $C_0(u)$ for the function $A_0(u)$ (see (6.31)), which allowed us to find the initial singularity structure, and its locus for later use. With this information we were able to decide, if the proposed ADM Cauchy data $c_0(u)$ was compatible with physical requirements.

It was also important to assure, that we covered as large class of initial data as we could while preserving the above assumptions. Since no other criteria were available, we were trying to devise functions of qualitatively different behaviour at infinity. We therefore considered profiles, which vanished or diverged in the $u \to \infty$ limit, as well as those assuming some finite values there. To some extent one could hope, that the fine details differentiating functions of the same class had to some degree a subleading impact on their corresponding physical properties. In this sense the profiles used in the simulations were representative for their corresponding families. The summary of the profiles we used can be found in Appendix A, 6.10. The very first data we used in the numerics were found and well understood analytically in [Beuf 2009], which gave us some intuition on what to expect.

In turn, from the boundary direction perspective all the profiles were generates with the condition of corresponding to the same normalized initial energy density, $\varepsilon(\tau = 0) = 1$, which is read-off at $u = 0$. Due to the scale invariance of the $\mathcal{N} = 4$ SYM theory this choice effectively defines a unit of length for us, because we can always rescale coordinates (if $\varepsilon(0)$ has different value), and physical phenomena are insensitive to this.

[6] The spatial coordinate u is the same in both cases at $\tau = t = 0$.

6.5.3 Boundary conditions

Heaving specified the initial data we can now discuss how to impose boundary values on the geometry, which should persist throughout the evolution. The condition at the AdS conformal boundary $u = 0$ is just the standard flat Minkowski metric of the Poincaré patch. Implementing it in ADM is however subtle, due to a possible boundary diffeomorphism ambiguity, and the non-trivial transformation between the Fefferman-Graham and ADM-like Ansatz for a generic t. The way to proceed is to perform a perturbative transformation near $u = 0$ from empty AdS_5 in Fefferman-Graham coordinates to the general ADM Ansatz with arbitrary metric functions. This transformation will carry over general boundary condition constraints on components of the ADM spacetime. The range of allowed ADM metrics will be reduced by this operation to asymptotically Minkowski-ADM AdS spaces, which will differ among each other significantly only in the interior. Boundary conditions in the asymptotic region of the AdS space $u \to \infty$ are more conceptually challenging and will be discussed separately.

6.5.3.1 Boundary conditions at the conformal boundary $u = 0$

In the usual numerical General Relativity one most often deals with asymptotically flat spacetime, corresponding to some physical configuration of matter and gravitational field. In such a situation one can impose the so called outgoing wave boundary condition, which represents flux of radiation leaving the reaction zone and escaping to infinity. The case of compact spacetime is more involved, as one lacks this natural boundary condition at the edge of space, and some well motivated choice has to be taken. To some extent the whole merit of AdS/CFT correspondence lies in the interplay between the boundary and the bulk of the spacetime. We thus have to understand well the issue of the boundary conditions and derive appropriate relations from the general features of the system at hand.

The physical spacetime in which the gauge theory is considered is flat (1+3) dimensional Minkowski. The condition on the asymptotics of the bulk spacetime in Fefferman-Graham coordinates $\{\tau, y, x_\perp, z\}$ is therefore to have the following conformal boundary as $z \to \infty$:

$$ds^2 = \frac{-d\tau^2 + \tau^2 dy^2 + dx_\perp^2 + dz^2}{z^2}. \tag{6.34}$$

Note however, that since we are in a generally covariant theory, within this metric gauge choice we can perform residual coordinate transformation along the field theory directions, $\{\tau,\ y\ x_\perp\}$ at the boundary $u = 0$. In particular we can redefine the ratio of time-flow with $\tau \to f_0(\tilde{\tau})$ substitution, which will not change the form of this Ansatz. This freedom will be important later. As was mentioned above, the strategy to impose condition 6.34 in the ADM metric coordinates $\{t,\ y,\ x_\perp\ , u\}$ is to perform perturbative coordinates transformation near the boundary $z = 0$ from Fefferman-Graham to the new ADM coordinates:

$$\tau = f_0(t) + f_1(t)u + f_2(t)u^2 + \dots \tag{6.35}$$

$$z = g_0(t)u^{1/2} + g_1(t)u^{3/2} + g_2(t)u^{5/2} + \dots \tag{6.36}$$

The specific choice of powers in these expansions is motivated by the knowledge of the general structure of perturbative solution asymptotic to the Minkowski space in Fefferman-Graham coordinates [de Haro 2001, Skenderis 2002]. An additional augmentation is the introduction of squared u coordinate, which softens the singularity of the equations at the boundary. Dependence on the time variable remains to be determined and will encode the details of the boundary conditions.

In order to compute the above expansions only local analysis near the boundary is necessary. In principle the transformation can be carried out to higher orders, although for the present applications only terms up to second order will be of practical use.

The first observation is that the physical time of the gauge theory τ is related to the AdS time t as $\tau = f_0(t)$, which is immediately obtained from setting $u = 0$ in (6.35). Next condition is easily obtained by inserting (6.36) into (6.34) and comparing with (6.16), which yields

$$d(t,0) = 1. \tag{6.37}$$

By inserting this into the equation defining $P(t,u)$, (6.24), we obtain

$$P(t,0) = 0. \tag{6.38}$$

Further, by comparing the components $dx_\perp^2$ and dy^2 of both metrics we have that[7]

$$g_0(t) = \frac{1}{c(t,0)}, \quad \frac{f_0(t)}{g_0(t)} = b(t,0)t. \tag{6.39}$$

By merging the above expressions we reveal how the physical boundary time and the simulation ADM time are related:

$$\tau \equiv f_0(t) = \frac{b(t,0)}{c(t,0)}t. \tag{6.40}$$

That connection reflects the freedom of choosing lapse function through redefinition of the time variable at the boundary. In particular it is possible to find such a gauge (lapse $\alpha(t,0)$ and thus $b(t,0)$), that the boundary and simulations times are equal. Outside of this choice we have to translate the simulation results to the boundary time, to get the physical values of τ.

Combining the above expression for time variable with the dt^2 component of the ADM metric we find a differential condition for $f_0(t)$:

$$\dot{f}_0(t) = \frac{\alpha(t,0)}{c(t,0)}. \tag{6.41}$$

Using the ADM equations (6.22), (6.23) and the latter, we obtain the condition on the boundary value of the functions $L(t,0)$:

$$L(t,0) = b(t,0) + t\frac{b^2(t,0)}{c^2(t,0)}M(t,0). \tag{6.42}$$

For numerical integration it is more favourable to turn this algebraic condition into a differential one:

$$\partial_t L(t,0) = \partial_t\left(b(t,0) + t\frac{b^2(t,0)}{c^2(t,0)}M(t,0)\right) \tag{6.43}$$

[7] We use a(0)=1.

Such an equation is numerically easily integrated at the boundary mesh node and maintains proper value of $L(t,0)$ there.

The last missing condition we need is on the function $M(t,0)$. We can get it by expanding around the boundary the relevant equation of motion, (6.26) and taking into account the conditions obtained so far. Another possibility is to carry further the perturbative transformation (6.35), (6.36) to second order. The main motivation to follow this path is that we will need this result later anyway, in derivation of the formula for holographic energy density $\varepsilon(\tau)$. This result will be derived further below, but here it is natural to complete the construction of the transformation.

As a first step in the second order calculation we demand that the metric maintains diagonal form, e.g. the mixed term $dudt$ is absent. This yields

$$f_1(t) = \frac{g_0(t)\dot{g}_0(t)}{2\dot{f}_0(t)}. \tag{6.44}$$

The derivation of the term $g_1(t)$ uses the first subleading term of the metric component dt^2 to express it as a function of α, $\partial_u\alpha$, $\partial_u a$, f_0, g_0 and their derivatives. Then, by investigating the near boundary Taylor expansion of the function $d(t,u)$ in

$$\frac{d^2du^2}{4u^2} \tag{6.45}$$

and comparing it to the similarly expanded transformed Minkowski part dz^2, one can express $\partial_u d(t,0)$ as

$$\partial_u d(t,0) = -2\partial_u a - \frac{2\partial_u\alpha}{\alpha} + \frac{3M^2}{2c^4} - \frac{\partial_t M}{\alpha c^2}. \tag{6.46}$$

The above equation can be solved for the boundary time derivative $\partial_t M(t,0)$. Just as before in the case of $\partial_t L(t,0)$, it is convenient to have this boundary condition in differential form, for uniform integration along with other equations.

Ultimately we end up with six boundary conditions, which have to be supplemented by the seventh one discussed below, on the lapse function α. The last point which is important here is the manifest regularity of the equations at the boundary $u = 0$. The metric is divergent there, so one may ask if the equations will be tractable numerically. It appears that the equations for the metric coefficients a, b, c are finite, whilst the extrinsic curvature equations behave near the boundary $u = 0$ in the following way:

$$\partial_t L(t,u) \sim \frac{1}{u}(d^2(t,u) - 1) \times \text{finite+regular} \tag{6.47}$$

and similarly for $M(t,u)$ and $P(t,u)$. The potential threat from the pole is however neutralized by the condition $d(t,0) = 1$. Numerically such a cancellation could still lead to influx of error into the integration domain, but the use of spectral methods allows to keep the functions smooth near the edge of the grid. *A posteriori* we observed stable integration near the spacetime boundary.

To summarize the boundary conditions at $u = 0$ we now quote them all in differential form:

$$\begin{aligned}
\partial_t b(t,0) &= \frac{-b^2+\alpha L}{tb},\ \partial_t c(t,0)=\frac{\alpha M}{c},\ \partial_t d(t,0)=0, \\
\partial_t L(t,0) &= \partial_t(b+t\frac{b^2}{c^2}M),\ \partial_t P(t,0)=0, \\
\partial_t M(t,0) &= -2c^2(\partial_u(a\alpha)+\frac{1}{2}\alpha\partial_u d)+\frac{3}{2}\frac{\alpha M^2}{c^2}.
\end{aligned} \tag{6.48}$$

6.5.3.2 Boundary conditions in the interior $u > 0$

For numerical integration we also need appropriate boundary conditions at the other end of the integration domain, $u > 0$. We expect to encounter a curvature singularity somewhere there. It is so, because we aim at reaching late equilibrium evolution stage, which is realised by a dynamical black brane. We do not impose thermalization by hand, and regard its emergence as an open question, but it is the expected outcome of the simulation. Moreover for several initial data profiles we constructed, the geometric curvature grows unbounded with u. We thus anticipate an event horizon to appear, but at *a priori* unknown position. For this reason we had to introduce an appropriate cut-off to expel singularity from the integration grid, which in AdS case appeared to be subtle. This difficulty was a challenge for our ADM-based scheme and the solution is one of the main technical advances of the present work.

The cut-off should allow to capture the relevant physics and keep simulation domain free of numerical artefacts. The first choice for this task would be the event horizon position, as by causality it would suffice to put the cut-off just beyond it. Then no matter what would be happening in the trapped region inside, it would not propagate to the outer physical domain. In the present case this scenario can not be easily realised. The spacetime is dynamical, so there is no direct criterion on the position of the horizon. The point here is that although for simple stationary black branes it suffices to find zeroes or divergences of metric functions, in the dynamical case the actual horizon position usually does not match these positions and one has to use other means to find it.

However there exists also the so-called apparent horizon, which for dynamical spacetimes is different from event horizon and always located behind it, inside the black hole. This type of horizon *can* generically be localized at any instance of time [8]. This is done using expansion scalars, which were introduced in Chapter 4. Unfortunately we need the cut-off to be available from the very first step of the simulation and direct use of apparent horizon is jeopardised by the fact, that the initial time hypersurface $t = 0$ is null. This causes apparent horizon conditions defined with expansion scalars θ_n, θ_l to be inapplicable. We must seek some other way to define cut-off, but in any case it should be closely related to the notion of horizons. It appears it is not trivial to make the proper choice.

If one would set the cut-off blindly too far in the black brane interior, the genuine spacetime singularity would likely approach it and break the simulation. The outgoing boundary conditions can not be imposed, since spacetime in the interior of integration domain can be strongly curved and dynamical, so we cannot formulate outgoing wave condition.

To escape this apparent deadlock we derived an approach utilizing the virtue of ADM formulation being the lapse function, which governs how time flows through the spacetime manifold.

The main idea is that we must introduce cut-off in a way adapted to the dynamical situation at hand. As we have no exact knowledge on the initial horizon locus, we would

[8] It is a spatial hypersurface, as opposed to the null event horizon

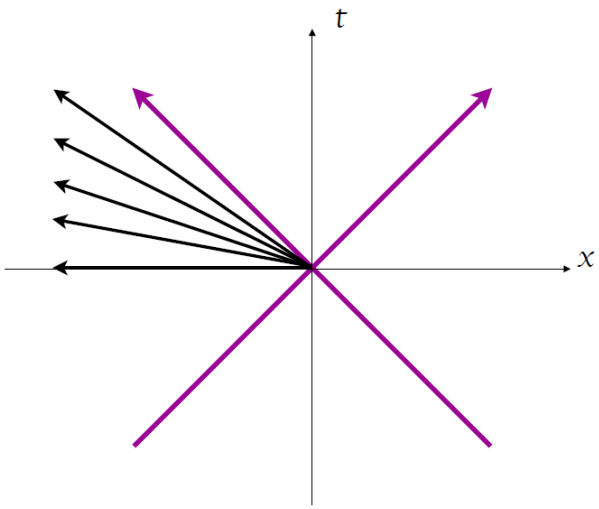

Figure 6.1: A simple figurative analogue of our dynamical spatial foliation based on the light-cone geometry. All the lines to the left of the light-cone are attached to one common space-*time* point in the middle, and represent spatial hypersurfaces foliating the outside region.

wish to estimate somehow its position and freeze its evolution in time. The cut-off then could be set just marginally outside of the event horizon, in the causally disconnected interior of the black brane.

It appears that scenario of this sort can *a priori* be realized with the aid of lapse function in our Ansatz. We can utilize the freedom of choosing arbitrary spatial foliation, represented by lapse, to construct causally disconnected region of spacetime covering selected region of black brane even across the horizon. The condition for such a foliation is to demand all spatial slices of the foliation to pass through a single given common *spacetime* point u_0. Actually, spacetime foliations are usually constructed with explicit condition not to do so, because such a degeneracy leads to singularities (e.g. vanishing of volume element), but in our case this is exactly what we need. By forcing all the constant time hypersurfaces to touch at a single chosen point we effectively freeze the time flow at that point, and divide spacetime into two causally disconnected regions. It then allows to effectively cut out piece of the black brane from integration domain by ending numerical grid at u_0. As an additional benefit we can obtain with this technique a natural boundary conditions for geometry at the freezing point. ADM evolution equations are regular at such a cut-off, so we could take their limit and obtain conditions at $u = u_0$ similar to the ones in differential form at $u = 0$ in 6.48.

The idea at hand can also be visualized on a simple example of the standard light-cone, 6.1. If one considers the region outside of the light-cone, let's say the spatial part of space-time to the left of the cone, one can foliate it with purely spatial semi-lines starting at the origin of the coordinates system. In this case one has spatial foliation with all the hyper-surfaces touching at exactly one point, the apex of the cone. The limiting foliation segment is the light-cone itself, the marginal null hypersurface, which divides causally disconnected regions of the timelike light-cone interior and the spatial exterior. The light-cone effectively acts as a horizon and nothing from the interior can reach the spatial region outside. This is what we have constructed it our ADM case, with the arbitrarily chosen freezing point corresponding in our example to the light-cone origin.

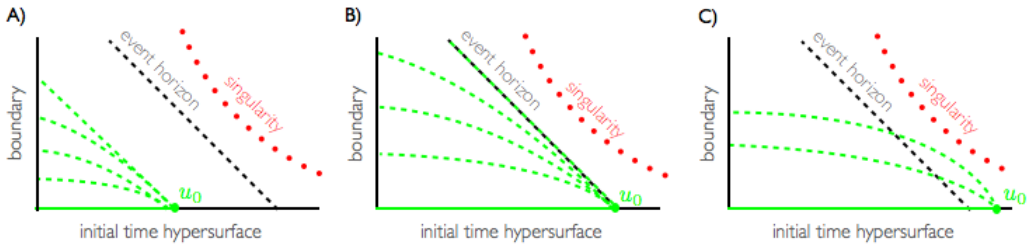

Figure 6.2: Three possible situations when first dealing with the simulation and trial cut-offs u_0. For initial u_0 values most often the geometry patch will cover too little or too much of the spatial domain, leading to the preemptive termination of the simulation discussed in the text. The goal is to tune the precise value of the cut-off, which would permit to follow the null boundary of the black brane *a priori* forever. This would in turn allow to observe the late time stage of the evolution.

The crucial difference from the light-cone case is that due to the black brane spacetime mechanics the null line passing through the freezing point needs not to be a straight, but in general can be curved. The significance of this observation is best explained with the aid of spacetime diagram in Figure 6.2.

If there is a horizon in spacetime located at some initial hypersurface point u_0^{EH}, then there are in principle three possible cut-off scenarios.

If we set the freezing point $u_0 < u_0^{EH}$ too far from the horizon, the constrained foliations will look like in the case of a light-cone, and after some finite boundary proper time the spatial segment will approach the null line asymptotically for infinite bulk time. Even though simulation bulk time would advance towards infinity, it would still correspond to some finite boundary time, and this in turn effectively would stall the simulation. It would therefore disallow us from following the evolution long enough, and moreover it would render the horizon absent from the simulation domain and hence unobservable.

If on the other hand we pushed the cut-off $u_0 > u_0^{EH}$ too far into the black brane interior, after some period of regular evolution the genuine singularity would emerge from the AdS interior and again break the numerics.

We thus need to seek the marginal case, in which we put the freezing point exactly at the horizon, $u_0 = u_0^{EH}$. In this case the numerical evolution could at least in principle be run indefinitely, since the null line of the horizon will end only in the future timelike infinity. Of course in practice we can never do this on a computer, so the simulation will never work infinitely long, but it will last sufficiently long to observe the transition to the potential late time equilibrium hydrodynamical regime. An additional feature of the freezing point technique is that it can be used to observe the early evolution stage of the dynamic apparent horizon. If we put the cut-off u_0 just marginally above the event horizon $u_0 > u_0^{EH}$, we would be able to measure early section of both horizons, as their pieces would lie in the integration domain (see e.g. Figures 6.3, 6.4 later in the text). This is a very useful feature, since the early apparent horizon evolution contains important information about the initial non-equilibrium entropy density of the plasma. We will discuss this point later.

The last issue here is the essential question of how to actually determine the value of freezing point u_0 itself. This can be done with the aid of geodesic equations and will be covered in Section 6.7.2. We shall defer this problem until then and proceed as if we knew the correct value of u_0 in what follows.

As mentioned above, the concrete way to implement the described cut-off idea is to

utilize the lapse function contained in the temporal part of the ADM metric (6.16)

$$\frac{-a^2(u)\alpha^2(t,u)dt^2}{u}. \tag{6.49}$$

The time independent function $a(u)$ was factored out precisely with the present motivation in mind. By letting this function to vanish at some chosen point $u = u_0$ we also cease the time flow there. We can then construct the numerical mesh starting at the boundary $u = 0$ and end it at $u = u_0$. The function $a(u)$ is in principle arbitrary and one simple well behaved example that we used is

$$a(u) = \cos(\frac{\pi}{2}\frac{u}{u_0}). \tag{6.50}$$

By changing u_0 we simply adjust the size of the physical integration domain outside of the black brane, and we numerically integrate in the interval $[0, u_0]$. With $a(u)$ factored out we will now use the term *lapse* for the remaining piece of the temporal metric component, $\alpha(t, u)$. The proper choice of this function is one of the most important steps in numerical integration of ADM Einstein equations. Good choice may allow the simulation to run for a very long time, and wrong choice will swiftly break it. This is of course only a technical point in numerics and physically all the choices are equivalent. On the other hand lapse freedom is very useful as a cross-check, since different choices give different evolution equations. If integration results for physical observables, like energy density $\varepsilon(\tau)$ are independent of the choice, we can assume numerics are reliable.

How to devise a good lapse? The most desired feature is the so called singularity avoidance property, which tries to avoid formation of metric singularities during the integration. Among well known classes of lapses there are the so called harmonic lapses, maximal slicing, and others. The most trivial choice of constant lapse, $\alpha(t, u) = const$ is badly behaved and leads to coordinate singularity (e.g. vanishing of some of the metric warp factors, like $d(t, u)$). Our guiding principle in the search for the best choice was exactly the non-emergence of the metric pathologies. We checked by trial and error several dozens functions with the aim of avoiding zeroing or blow-up of the metric coefficients. The best lapse functions we found are the following:

$$\alpha_1 = \frac{dc^2}{b},\ \alpha_2 = \frac{bd}{1 + \frac{u}{u_0}b^2},\ \alpha_3 = \frac{d}{b},\ \alpha_4 = d. \tag{6.51}$$

Additionally we always normalized the lapse to be initially unit and constant,

$$\alpha(t, u) = \frac{\alpha_i(t, u)}{\alpha_i(0, u)},\ \text{for each } i. \tag{6.52}$$

This choice renders the lapse equal to unity at $t = 0$ for any initial profile or choice (6.51) in the first integration step. Additional feature of lapse function is that for certain choice it may restore the agreement between the simulation time t and the proper time τ at the boundary. It can be done with a lapse that would enforce $b(t, 0) = c(t, 0)$. This is achieved by our lapses α_1 and α_2.

To sum up, the described methods and lapse choices allowed us to perform long and reliable numerical integrations, which in turn allowed to extract meaningful information on the evolution of the dual field theory. To our knowledge the proposed technique of handling the dynamic horizon in the AdS interior is novel and has not been used in the literature before our work.

6.6 Quantum observables from classical geometry

Having completed the discussion of the numerical integration setup, we can describe quantum field theory observables which will be extracted from the resulting simulated spacetime geometry. There are two main quantities which are of interest to us. The first one is thermal expectation value of the gauge theory stress-energy tensor $T_{\mu\nu}$ and an effective temperature defined with its aid. The second observable is the non-equilibrium entropy density of the gauge theory quantum state. We first describe these observables below and then proceed to the actual solution of the gravity equations.

6.6.1 Holographic tress-energy tensor

The practical framework of holographic computations was described in Chapter 3. In particular we discussed how to extract expectation values quantum field theory operators from the bulk fields' near boundary expansion. The procedure described there however was carried out in the simple Fefferman-Graham coordinates, the canonical choice for the Poincaré patch of the AdS spacetime. Presently we need to adapt the holographic procedure to the more involved case of ADM decomposed AdS space. There are two major issues that introduce subtleties into the holographic expansion relative to the standard case described in Chapter 3. Firstly the bulk coordinate variable u metric coefficient is now a dynamical field instead of being fixed, and secondly the time variable at the boundary may not be the same as in the bulk. The way to proceed is to transform the known holographic prescription to the present coordinates using the between the Fefferman-Graham and the ADM charts, similarly to what was done in the discussion of boundary conditions in Section 6.5.3.1. Strictly speaking from the point of view of holographic procedure it is the same step, since the stress-energy tensor and the boundary metric are just the two boundary conditions imposed at the bulk metric:

$$g_{\mu\nu}(t,z) \propto \eta_{\mu\nu} + \langle \hat{T}_{\mu\nu} \rangle z^4. \tag{6.53}$$

Previously we have carried over to ADM the leading part $\eta_{\mu\nu}$ and now we need to repeat it for the subleading part $\hat{T}_{\mu\nu}$. More precisely, we need to transform the metric in Fefferman-Graham coordinates of the following specific form

$$ds^2 = \frac{-(1-\frac{2\pi^2}{N_c^2}\varepsilon(\tau)z^4)d\tau^2 + \tau^2(1+\frac{2\pi^2}{N_c^2}p_L(\tau)z^4)dy^2 + (1+\frac{2\pi^2}{N_c^2}p_T(\tau)z^4)dx_\perp^2 + dz^2}{z^2},$$

to the general metric Ansatz in the ADM coordinates:

$$ds^2 = \frac{-a^2(u)\alpha^2(t,u)dt^2 + t^2a^2(u)b^2(t,u)dy^2 + c^2(t,u)dx_\perp^2}{u} + \frac{d^2(t,u)du^2}{4u^2}.$$

The logic behind this approach is rather intuitive. We know how to obtain the expectation value of the stress-energy tensor from the near boundary expansion in the Fefferman-Graham coordinates, and we want to understand how to repeat this procedure with the expansion in the ADM coordinates. The first metric consists of only the terms up to the z^4 order in the numerator, which correspond exclusively to the boundary data. By confining to this order of the full metric we can be sure that we will transform to the new system only information on the stress tensor, so the ADM functions will depend only on this data. Subsequently by comparing the expansions of the transformed metric and the second generic

ADM Ansatz in the new bulk coordinate u, we can express the energy density $\varepsilon(\tau)$ and pressures $p_L(\tau)$, $p_T(\tau)$ in terms of new ADM boundary fields, $b(t,0)$, $c(t,0)$, $d(t,0)$ and $L(t,0)$, $M(t,0)$, $P(t,0)$. An important point here is that with this approach we are able to extract the pressures directly from the metric. In principle we could have obtained them from the temporal derivative of the energy density $\varepsilon(\tau)$. However the computation of higher derivatives of numerical data is prone to discretisation errors (the energy $\varepsilon(\tau)$ itself is a result of numerical data differentiation, through the holographic procedure). Additionally by this direct computation we can check the energy-momentum conservation throughout the evolution by computing $\nabla_\mu T^{\mu\nu}$ on the data coming from different components of the bulk metric. It thus provides a natural validity check for the numerical integration procedure.

Coming back to the actual computation, we have to perform the near-boundary perturbative transformation:

$$\tau = f_0(t) + f_1(t)u + f_2(t)u^2 + \dots \tag{6.54}$$
$$z = g_0(t)u^{1/2} + g_1(t)u^{3/2} + g_2(t)u^{5/2} + \dots \tag{6.55}$$

This time however we have to compute the second order terms, $f_2(t)$ and $g_2(t)$ along the lines of Section 6.5.3.1.

The concrete way to perform the described computation is first to make the above transformation of the Fefferman-Graham metric, which will turn it into the ADM form. Then we have to expand both of the above metrics in u and applying repeatedly equations of motion and boundary conditions on the ADM fields we have to solve for $\varepsilon(\tau)$ and $p_L(\tau)$, $p_T(\tau)$ in terms of the ADM fields and their spatial derivatives. Any potential temporal derivatives of the ADM fields can be eliminated by utilizing the (first order) equations of motion.

The final expressions for the energy density and pressures obtained in this way are

$$\begin{aligned}\varepsilon(\tau) &= \frac{N_c^2}{2\pi^2}c^4\left(\partial_u^2 a - \partial_u a\partial_u d - \frac{9}{4}(\partial_u d)^2 + \frac{3}{4}\partial_u^2 d + \frac{\partial P}{4tb}\right. \\ &+ \left.\frac{(2\partial_u a - \partial_u d)\partial_u b + \partial_u^2 b}{b} + 2\frac{\partial_u^2 c - \partial_u c\partial_u d}{c} - \frac{3M\partial_u P}{4c^2}\right),\end{aligned} \tag{6.56}$$

$$p_T(\tau) = \frac{N_c^2}{2\pi^2}\frac{1}{4}\left(4c^3\partial_u^2 c - c^4(\partial_u d)^2 + c^4\partial_u^2 d + \partial_u d M^2 - c^2 M\partial_u P\right). \tag{6.57}$$

In the above all the ADM fields are evaluated at the boundary $u = 0$, e.g. $b = b(t,0)$ and the boundary time is a function of the bulk time, i.e. $\tau = \tau(t)$ through (6.35), (6.40). We could have also extracted the longitudinal pressure $p_L(\tau)$, but it can be easily computed from the vanishing trace of the conformal stress tensor as $p_L = \varepsilon(\tau) - 2p_T(\tau)$.

Let us also introduce the notion of dynamical effective temperature $T_{\text{eff}}(\tau)$, which will be of use soon in the simulation data analysis. This quantity extends the equilibrium relation between the energy density and temperature reported first in Chapter 3 through formula (3.69). By using the holographic energy density derived in (6.56) we can introduce the notion of an effective temperature as follows,

$$\varepsilon(\tau) = \frac{3}{8}N_c^2\pi^2 T_{\text{eff}}(\tau)^4. \tag{6.58}$$

The physical interpretation of $T_{\text{eff}}(\tau)$ is that it describes the temperature of a *thermalized* medium with the same energy density as our system, $\varepsilon(\tau)$, hence the name effective.

For small proper times, according to what we said in Section 6.3, the energy density starts as a constant followed by an expansion in even powers of proper time τ. The formula above assumes then the following form

$$\varepsilon(\tau)\Big|_{\tau\sim 0} \sim \frac{3}{8}N_c^2\pi^2\left(T_{\rm eff}(0)+\frac{1}{2}T''_{\rm eff}(0)\tau^2+\dots\right)^4. \tag{6.59}$$

The quantity $T_{\rm eff}(0)\equiv T^{(i)}_{\rm eff}$ will be applied below in formulas expressing various physical observables in units of the initial effective temperature.

6.6.2 Non-equilibrium entropy density from geometry

The second observable that was mentioned above is the local entropy density of the gauge theory nearly thermal state. This quantity is very interesting and important for understanding evolution of systems like heavy ions collisions.

More precisely, the observable we are interested in is the non-equilibrium entropy density per unit spacetime rapidity and unit transverse area, in analogy to the one introduced in Section 3.7. We shall see later, that this quantity surprisingly well characterizes the process of equilibration of the gauge theory plasma. We can also compute the difference of this quantity and final entropy density obtained from hydrodynamics, which forms an interesting observable describing the whole evolution of the system towards equilibrium (see Sec. 6.8.3).

As we said the appearance of entropy in General Relativity was briefly introduced in Chapter 3, where we also gave formulas relevant for planar black brane horizons. The notion of entropy in gravity was initially established for stationary black holes, but later it was generalized to dynamical geometries and horizons [Ashtekar 2004]. This development is important, because it opens the possibility to study entropy dynamics in real-time, in the non-equilibrium regime. In this case however the definition and practical computations of entropy based on a dynamical horizon are much more involved than in the static case, because it is more difficult to localize the event horizon of time-dependent spacetime. In fact as we mentioned in Chapter 4, in such a case one can speak of many different types of horizons, and one has to understand which one of these can be properly associated with the notion of entropy. According to the mentioned development, the apparent horizon, which we described more broadly in Chapter 4, can be used to define a quantity, which can be physically interpreted as the entropy. Let us therefore apply the definitions presented in Sections 4.2, 4.3 to our case, and see how they are used to associate the dynamical entropy density with an apparent horizon.

To demonstrate the defining conditions 4.31 application explicitly, let us assume again following Chapter 4, that the outgoing (with respect to the horizon) null geodesic congruence has l^μ as its tangent vector, and n^μ is tangent to the ingoing one. The generic null characteristic lines obtained from our metric Ansatz (6.16) satisfying conditions (4.21) imply then the following tangent vector fields:

$$l_\mu = h(t,u)\{-\frac{a(u)\alpha(t,u)}{\sqrt{2u}},0,0,0,-\frac{d(t,u)}{2\sqrt{2}u}\}, \tag{6.60}$$

$$n_\mu = \frac{1}{h(t,u)}\{-\frac{a(u)\alpha(t,u)}{\sqrt{2u}},0,0,0,\frac{d(t,u)}{2\sqrt{2}u}\}. \tag{6.61}$$

The function $h(t,u)$ is the irrelevant normalization ambiguity mentioned in 4.2. Vector fields dual to these 1-forms are suitable for describing our null congruences.

Outside of the focusing horizon the outgoing congruence has increasing cross-section. As we know, the apparent horizon is a hypersurface defined by the condition that the outgoing

expansion scalar θ_l based on (6.60) is zero (precisely changes sign at the apparent horizon) and the ingoing expansion scalar θ_n is negative:

$$\theta_l(t, u_{AH}) = 0, \ \theta_n(t, u_{AH}) < 0. \tag{6.62}$$

Both these scalars are functions of the underlying metric components, so having them at disposal (e.g. from numerical integration) makes it in principle easy to test the above conditions and locate the apparent horizon. The important drawback in our case is that our initial hypersurface contains a null segment, which makes it impossible to use the expansions condition from the very onset of the evolution (expansions are both zero at null hypersurfaces, while apparent horizon is a spatial hypersurface admitting non-zero scalars). Due to this we can not check this way, if there is an apparent horizon initially.

Except for that however, with the above definition we have a way to localize it at later instances of time. Let us describe therefore the prescription for associating entropy density with it.

One subtlety we need to mention here, is that in contrast to event horizon, which resembles causal structure of spacetime, the apparent horizon is generically an ambiguous object. To define it one first has to choose a spatial foliation of spacetime, and the apparent horizon depends on this choice. It is thus not a gauge-invariant object in the sense of gravity diffeomorphism redundancy. It is for example known, that in the case of Schwarzshild black hole one can choose coordinates, such that the is no apparent horizon at all [Wald 1991]. Nevertheless the prescription based on the apparent horizon has been used in the literature and it allows to define entropy-like quantity with desired properties, which reduces to the standard entropy in the equilibrium limit. Moreover in the present case of boost-invariant evolution there is a very natural and rigid choice of the preferred spatial foliation, which invalidates the ambiguity altogether. The Bjorken flow in $D = 4$ offers specific timelike four-vector of the fluid velocity, $u^\mu = (1, 0, 0, 0)$, which can define foliation of constant proper-time hypersurfaces.

The crucial property that makes apparent horizon useful is the non-decreasing area law, which holds for consecutive spatial slices associated with it [Booth 2005]. In direct analogy to the standard case, the concrete prescription for apparent horizon entropy density follows the Beckenstein-Hawking entropy formula:

$$s_{AH} = \frac{1}{4G_N}\sqrt{\gamma_{AH}}\Big|_{u=u_{AH}} = \frac{1}{4G_N}\frac{t}{u}a(u)b(t,u)c(t,u)^2\Big|_{u=u_{AH}}. \tag{6.63}$$

The above is basically a proper area element at constant time hypersurface (spatial slice of the horizon), divided by a unit differential hyper-area element $dA_3 = dyd^2x_\perp$. Metric induced at the horizon is denoted as γ_{AH}.

Such a quantity defines entropy density of the black brane in the bulk, but prior to being used as holographic gauge theory observable it must be carried all the way to the spacetime boundary, where we translate all gravity objects to field theory quantities.

To extract entropy from the horizon, one has to apply a consistent method of mapping between the points in the bulk and at the boundary. Such a construction is called bulk-to-boundary map and has been successfully used in the literature before to transport the entropy data to the edge of the spacetime [Bhattacharyya 2008a]. This prescription has been tested within the framework of fluid/gravity duality.

The idea of this construction is to assign in a one-two-one manner the points at the boundary, $(x^\mu, \ u = 0)$ to the points at the horizon, $(\tilde{x}^\mu, \ u = u^{AH})$. Then through this

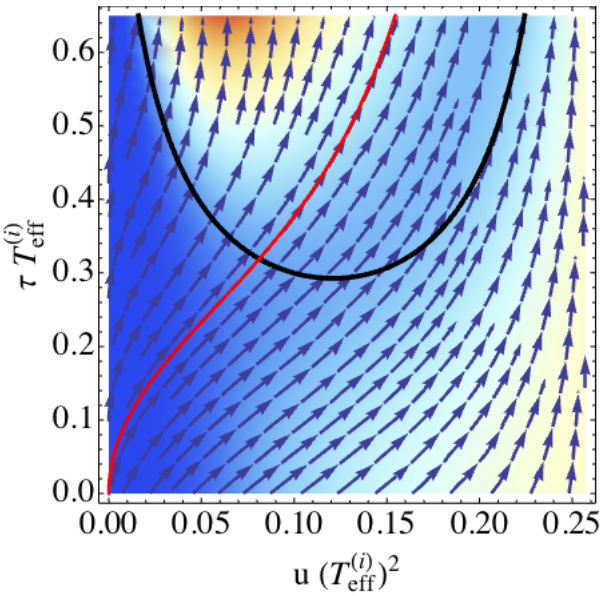

Figure 6.3: Apparent horizon (thick line) determined by the expansion scalars (6.62) is pierced by the ingoing null geodesic (thin red line) to measure the area of the horizon at the intersection point. The geodesic originates at the boundary $u = 0$, and defines the bulk-to-boundary map crucial for extraction of the non-equilibrium entropy density 6.65. The ingoing light ray also corresponds to the ingoing Eddington-Finkelstein coordinates constant time hypersurface, $\tau^{EF} = const.$

relation the value of any quantity computed at spacetime point of the horizon is considered to be the value of this quantity at the corresponding point of the boundary:

$$O(x^\mu,\ u = 0) \ \leftrightarrow\ O(\tilde{x}^\mu,\ u = u^{AH}). \tag{6.64}$$

A concrete implementation of this idea consists of a family of ingoing radial null geodesics originating from points at the boundary and falling to the black brane, crossing the apparent horizon at some corresponding points $u = u^{AH}$. Such a prescription provides us with causal mapping of the observables, because the points are connected along timelike geodesics.

An example of this construction at work is given in the figure 6.3. What is shown there is a typical spacetime with black brane resulting from our numerical simulation. The boundary of spacetime $u = 0$ is on the left and the constant time t hypersurfaces lie horizontally with time flowing upward. The color indicates curvature measured with the Kretschmann scalar, $\mathfrak{R}^2 = R^{\mu\nu\alpha\beta}R_{\mu\nu\alpha\beta}$). The bright spot in the upper middle of the picture is the true geometric singularity, the danger zone. Thick black line depicts the apparent horizon determined with expansions as (6.62). It is bent here due to the choice of our lapse α, vanishing at the cut-off on the right. As a consequence the whole right edge of the picture represent just a single point, stretched here to a line by our visualisation (the true graph should be more like a triangle, much in the spirit of Penrose diagram outside of the horizon, see Fig. 6.2). The vector field represents the flow of ingoing null geodesics originating at the boundary and piercing the horizon. Using the described construction we were able to measure the very initial (strongly non-equilibrium) entropy density of the gauge theory plasma. For all the geometries representing the initial field theory states, we found a non-zero value of the apparent horizon area density. This in fact should imply,

that there also is a genuine event horizon present at the initial data hypersurface, because the apparent horizon must always be hiding behind event horizon. We were however not able to verify this fact directly in any simple way due to the global teleological nature of the event horizon, which we mentioned in Chapter 4. However the pattern of outgoing null geodesics seen in Figure 6.4 supports this claim.

Although the non-equilibrium entropy defined in this way lacks clear microscopic interpretation, its value as we shall later see is a surprisingly good characterisation of the initial state.

The practical formula for the entropy density that we used is obtained upon expressing the value obtained from the apparent horizon in units of the initial effective temperature (6.58) [Balasubramanian 1999]

$$s_{n-eq} = \frac{s_{AH}}{N_c^2 \pi^2 \frac{1}{2} (T_{\text{eff}}^{(i)})^2}, \tag{6.65}$$

with s_{AH} defined in (6.63). By taking into account all the numerical factors we arrive at the following important geometric expression for the non-equilibrium entropy density:

$$s_{n-eq}(t) = \frac{\left[\frac{t}{u} a(u) b(t,u) c(t,u)^2\right]|_{u=u_{AH}}}{\pi^3 (T_{\text{eff}}^{(i)})^2}. \tag{6.66}$$

This formula is free of the factors of N_c^2, which express formally infinite number of the gauge degrees of freedom in large N limit. It represents an intensive measure of the non-equilibrium entropy density in this sense, and is of practical use for the analysis of the simulation results.

6.7 Numerical analysis of the full nonlinear system

We shall now discuss the numerical aspects of the nonlinear system integration. We shall briefly comment on the use of spectral methods and multi-step Runge-Kutta adaptive integrator, technical details of which are deferred to the Appendix B 6.11. An important component of our numerical approach is the discussed above use of spatial integration domain cut-off u_0. After explaining how we define it, we will comment on error control of the integration. The whole numerical integration was performed using code written in C++ with GNU Scientific Library integration routines, running on a GNU/Linux workstation, with equations and auxiliary expressions generated in *Mathematica*.

6.7.1 Statement of the numerical problem

From the point of view of the numerical integration we faced the problem of algebraic-differential system of nonlinear coupled equations in 1+1 dimensions, which defines certain Cauchy initial value problem. The domain of integration is compact and not periodic, thus at each edge one has to impose appropriate boundary conditions, as discussed in Section 6.5.3. The nature of the system revealed upon initial evaluation, that it requires high accuracy in both spatial discretisation and temporal integration. The amplitudes of the numerical fields involved orders of magnitude between e.g. $O(10^{-9})$ to $O(1)$. The total number of independent equations is seven: six ADM functions b, c, d, L, M, P, and the lapse α. On the top of that are the ADM Hamiltonian and momentum constraints. In our ADM approach equations are first order in time t, which is the integration variable, and

second order in the spatial direction u. The evolution was unconstrained in the sense that the ADM constraints were used solely to probe the quality of the numerical solution.

These characteristics of the problem motivated an appropriate choice of methods. Due to the doubly bounded spatial domain we chose the so-called fixed spectral spatial mesh, based on Chebyshev polynomials [Trefethen 2000]. This was particularly successful solution to our initial problem with one-sided finite difference derivatives. It is a common difficulty present in numerical problems, as one-sided derivatives tend to inject numerical inaccuracies into the integration domain, which subsequently propagate and amplify in the nonlinear system. Moreover we needed very accurate treatment of second order boundary derivatives as our key observable, $\varepsilon(\tau)$ was expressed in terms of these quantities, see (6.56). The use of Chebyshev-based derivatives effectively eliminated this problem and multiple numerical differentials gave satisfactory results. A complication of this approach is that the information on the numerical function is much more non-local, than in the finite difference method, thus any problem with e.g. boundary condition would propagate almost instantly to the whole integration mesh. These were however not real obstacles to our numerical procedure. The differential based on the Chebyshev grid is essentially realized by a big matrix, and differentiation amounts to just consecutive multiplication of the vector representing the function[9]. The details of this construction can be found in the Appendix B sec6:AppB.

The temporal integrator used to obtain the values of the fields in the subsequent time steps was also subject to stringent accuracy requirements. The integrator of choice was the standard RK89 adaptive algorithm. It evaluates the new function proposal several times, and if subject to accuracy check gives too big error with respect to the requested level, it decreases the time-step length. Similarly if errors are small it increases the time stepping. The actual points with values of the function thus tended to be non-uniformly distributed and for practical reasons we extracted them at a given constant rate. Then the results were exported to *Mathematica* for a subsequent analysis. An additional measure taken was the modification of data structures used by the GSL library to use `long double` C++ variables. This allowed for more accurate computations and reduced errors.

6.7.2 Construction of the spatial domain

We come back now to the issue of determining cut-off value u_0. Many details concerning this point were given in Section 6.5.3.2 and relied on the expansion scalars covered in sections 4.2 and 6.6.2. The procedure of fixing u_0 consists of one or more initial trial integration evaluations and subsequent proper integration. The reason is that in the first stage we were determining the optimal value of u_0 as described below, and applied it in stage two.

The spatial piece of the mesh that we used as the physical space outside the expected black hole for all integrations ranged in variable u from zero to some u_H. Recall now from the remarks around (6.50), that using our metric Ansatz function $a(u) = cos(\frac{\pi}{2}\frac{u}{u_H})$ we were mapping this bounding point to $u = \pi/2$, so effectively the spatial domain was always $[0, \pi/2]$, albeit we numerically integrated up to $u = u_H$.

The practical rule for choosing initial cut-off u_H was based on the value of the Fefferman-Graham coordinates singularity always present in the initial data as we described in Section 6.3. This value was equal to some $u_\star$ and served as a hint, that the genuine event horizon was somewhere around this point, because it is was the only readily available scale in the initial profile. Then the numerical cut-off was set to e.g. $u_H = 1.1 - 1.2 \times u_\star$. After setting this limit the simulation was performed and the results analysed. Usually the integration broke abruptly, because the singularity was promptly hit due to overshoot of the cut-off. Then by inspecting the expansion scalar θ_l the apparent horizon was localized.

[9] For numerical efficiency we also used an alternative implementation based on discrete cosine transform.

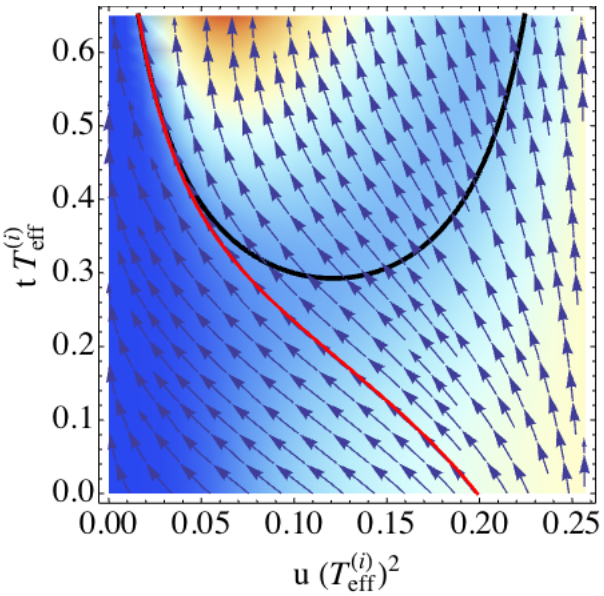

Figure 6.4: The apparent horizon (thick line) again determined by the expansion scalars (6.62) is a marginal null line between two families of outgoing light rays, trying to escape to the boundary at $u = 0$. By fine tuning the marginal null geodesic origin to be *at its endpoint* asymptotically touching the horizon at $u^{EH}(t_\star)$, and propagating it backward in time, one localises the initial event horizon at $t = 0$. This defines the cut-off for the numerical mesh u_0^{EH} (at the Figure around $u(T_{\rm eff}^{(i)})^2 \propto 0.2$).

Subsequent step was the most important and interesting. The nature of the event horizon and its relation to the apparent horizon is such, that the apparent horizon approaches the event horizon asymptotically when the spacetime reaches stationary stage. Thus at late times in the simulation one can hope (and hence assume) that the two are almost the same. On the other hand the event horizon consists of the so-called null generators, which are the marginal null geodesics, such that they are bound to the horizon forever, neither leaving nor entering the black brane. The main way to reconstruct the evolution of the true *event* horizon at earlier times, prior to the equilibration, is to follow such a null geodesic backward in time. If one was able to pick the exactly last null line joining event horizon, and follow its evolution to the earlier values of the affine parameter, then one would reconstruct the whole past evolution of the event horizon. This is the basis of our approach.

An example of this procedure can be seen in Figure 6.4. The dark semicircle indicates an apparent horizon at $u_H(t)$. The flow of arrows indicates the outgoing radial null geodesics. All of them start at the initial time hypersurface $t = 0$ and travel towards the boundary at $u = 0$. One can see that some of them cross the apparent horizon, terminating at the singularity, and some reach the boundary. Between the two families there is a marginal null geodesic, which at the end of simulation only touches the apparent horizon. The simulation terminates at certain time $t_\star$, due to the presence of geometry singularity. At this stage the marginally trapped geodesic is our best approximation to the dynamical event horizon. The actual way to obtain it is to read off the leftmost position of the apparent horizon at the given time, $u^{EH}(t_\star)$ and solve the geodesic equation backward in time, starting from $u^{EH}(t_\star)$. The crossing of the marginal null line with the initial hypersurface $t = 0$ gives the desired approximated initial event horizon locus, u_0^{EH}. This point is then set as the ultimate boundary of the simulation. In the optimal case it should allow for a much

longer numerical integration, because now we enter much less into the interior of the black brane[10] and defer meeting the singularity. The approximation of the actual event horizon in not perfect, as we are never able to reach the final equilibrium horizon. However such a procedure can be iterated, leading to finer and finer approximations, sufficient for clear and unambiguous observation of the late time stage of the black brane evolution. This is in turn is crucial for the detection of the transition to hydrodynamics and extraction of clean numerical values of late time observables. Also, by modifying the cut-off u_0^{EH} we are able to measure both early and late time evolution of the apparent horizon. For larger cut-off the initial part of its evolution is visible better. For finer selection of u_0^{EH} later segment of the horizon is well visible, and the initial one is highly compressed. This allows to measure early and late temperatures and entropy densities. In the ideal case of perfectly determined u_0^{EH} matching the exact initial position of the event horizon, the evolution could be run indefinitely, up to the systematic hardware numerical errors accumulation.

6.7.3 The numerical integration and error control

As was mentioned in Section 6.7.1, we have used the Chebyshev grid for the spatial domain representation. Such a grid has a feature, that it covers the line segment non-uniformly, with data points covering more densely the edges of the domain, as described in the Appendix B sec6:AppB. This allows one to achieve very high precision at relatively modest grid size, which has a crucial impact on the simulation time. The actual grid sizes we used were $N = 201$, 257, 513 or 1025, depending on the initial data[11]. Sometimes different mesh densities N were used for the the same profile to assess the accuracy. The most important factor for the success of the numerical integration was the choice of the proper lapse. If made correctly, the simulation would work for a long time without any problems. On the other hand, for poor choice of the lapse (or the cut-off u_0^{EH}), even huge mesh density would not be a remedy to the problems.

The main accuracy monitor relied on the ADM Hamiltonian and momentum constraints, C_0 and C_i. From these normalized functions were constructed, like

$$test_{C0} = \frac{R - K_{ij}K^{ij} + K^2 + 12}{|R| + |K_{ij}K^{ij}| + K^2 + 12}, \tag{6.67}$$

with similar expression for the momentum constraint C_i, see 6.28. By checking at each step that these quantities do not exceed e.g. 10^{-7}(a value dictated by typical initial field amplitude for some functions), we estimated the quality of the integration, as well as when to stop. Interestingly, even for some numerically difficult profiles we observed that when constraints reached levels at which they were not well conserved (like to the order 10^{-3}), the obtained results for the energy density were still of good quality.

Further measures taken to ensure high accuracy relied on repeating the simulation with a different lapse choice, for the same initial data. This resulted in significantly different expressions for the evolution equations, but gave the same results for the observables, like the energy density $\varepsilon(\tau)$. Moreover, we checked the apparent horizon area evolution for some range of the boundary time τ, and non-trivial curvature invariant $\mathfrak{R}^2 = R^{\mu\nu\alpha\beta}R_{\mu\nu\alpha\beta}$ at the intersection points of the null ingoing geodesics and the apparent horizon. In both cases the observables matched for different lapse choices. The ultimate test of the integration quality relied on the comparison between the numerically computed early time energy density (6.56), and the analytical power series expression, obtained from the initial data as was mentioned in Section 6.3. Later in Section 6.8.2 we will see a good agreement, depicted

[10] In practice for most initial data the single initial trial value u_0^{EH} was enough.

[11] The peculiar size of $2^n + 1$ was motivated by optimisation of the numerical operations on data vectors.

in Figure 6.8 (up to the initial energy power series convergence radius) and reflecting high quality of the numerical integration, which after the non-trivial holographic operations on the numerical data matches closely the analytical prediction.

6.8 Analysis of the simulation results

We will now proceed to the discussion of the simulation results. We shall describe the discovered properties of strongly coupled non-Abelian gauge theory under consideration at finite temperature in Minkowski spacetime. It will be shown that with the aid of gauge/string duality several unexpected phenomena were observed, access to which would be unavailable on the grounds of standard perturbative field theory. The results may prove to be useful for the heavy ion community working on understanding quark-gluon plasma.

6.8.1 Initial geometric properties of the evolved spacetimes

In this paragraph we focus on certain features of initial and evolved geometries, which turned out to be crucial for all the subsequent analysis of observables. The quantities of interest are Fefferman-Graham singularity position of the initial spacetime profiles, initial apparent horizon position and event horizon position, which as we described could have been determined only *a posteriori* from the evolved spacetime.

The first point to mention is that due to our specific construction of coordinates the initial data hypersurface of ADM Ansatz coincides at $t = 0$ with the initial data hypersurface of the Fefferman-Graham coordinates $\tau_{FG} = 0$. This allows us to determine the potential initial data coordinate singularity in the Fefferman-Graham coordinates, as we already mentioned in Section 6.5.2, by using the corresponding Fefferman-Graham constraint equation,

$$\frac{A_0''(u)}{A_0(u)} + \frac{C_0''(u)}{C_0(u)} = 0. \tag{6.68}$$

From that, given the initial profile $C_0(u)$ we can solve (numerically) for $A_0(u)$ and locate the initial coordinates singularity[12]:

$$A_0(u^{FG}) = 0. \tag{6.69}$$

As was discussed in Section 6.6.2 above, in the case of dynamical spacetimes the vanishing of a metric coefficient is not sufficient to determine the position of the apparent or event horizon, which can be located at a completely different point. However it is intuitive to expect, that the horizons are somehow related to the value of u^{FG}. For example in the static limit the event horizon would be located at the coordinate singularity, like in the standard AdS-Schwarzschild case. So one can expect, that the eventual event horizon will be located somewhere in the vicinity of u^{FG}.

It turns out, that indeed this is the case and there is a relation between them. By using the procedure described in the Section 6.7.2 we have extracted the positions of the event horizon at the initial time $t = 0$ (up to numerical precision) for spacetimes evolved from each initial profile. Relation between the initial data singularity parameter u^{FG} and the genuine initial event horizon position u^{EH} exists and is seen in the Figure 6.5. The correlation between their inverses seems to be simple and roughly linear.

[12] We call it u^{FG} for brevity, and simple interpretation through its initial derivation in these coordinates.

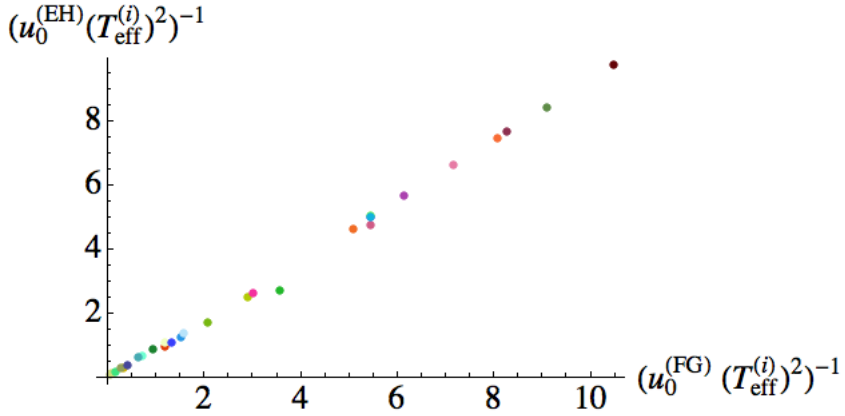

Figure 6.5: Close correlation between the initial event horizon of the dynamic spacetime and the coordinates singularity u^{FG} determined by the equation (6.69).

This is also interesting for another more fundamental reason. The fact, that there is a non-zero *event* horizon present from the very beginning means, that we are dealing with at most extremely deformed black brane, and not a collapse forming the black brane. This in turn means that we are working with some very far from equilibrium system, but nevertheless not completely disconnected from thermalized state, represented by the presence of event horizon. One should distinguish this situation from e.g. AdS dual of a shock-wave collision, where the horizon forms only during the evolution process and is initially absent.

We thus learn, that the initial position of the event horizon, which is a physical entity, is approximately parametrized by u^{FG}.

The second important observation is that the apparent horizon surface area also turns out to be proportional to the initial Fefferman-Graham singularity u^{FG}. A geometric remark, that can be made here is that there is such a relation between these objects at all. The point is that the two quantities are related to completely different hypersurfaces. As was mentioned above the entropy is not just the position of apparent horizon, but is extracted from it through the bulk-to-boundary map, using the ingoing null geodesics. The initial entropy thus lies on the ingoing Eddington-Finkelstein constant time hypersurface[13], $\tau_{EF} = 0$, which is different from the initial Fefferman-Graham (and our ADM) hypersurface $t = 0$, which is not geodesic and where in turn u^{FG} is defined. The relation between the two is thus non-local and it would be very interesting to understand why they are so closely correlated. This is therefore an independent observation from the former one on the correlation between u_0^{FH} and u_0^{EH}.

The significance of the above statement stems from the fact, that the apparent horizon is associated with the non-equilibrium entropy density. As can be inferred from Figure 6.6 at the initial time slice $t = 0$ the entropy density s^0_{n-eq} read-off from the apparent horizon turns out to be closely correlated with the initial singularity position u^{FG}. This is very useful observation, because now we can interpret the initial non-equilibrium entropy density as the *physical* parameter of initial data, instead of u^{FG}. This is a much more natural and physically intuitive in the context of e.g. fluid or collision dynamics, than the geometrical parameter u^{FG}. Moreover it is obvious from the above, that the initial event horizon is also parametrized by this non-equilibrium entropy.

[13]Given simulation initialization time $t = 0$ this is the first and earliest null line one can emit from the boundary.

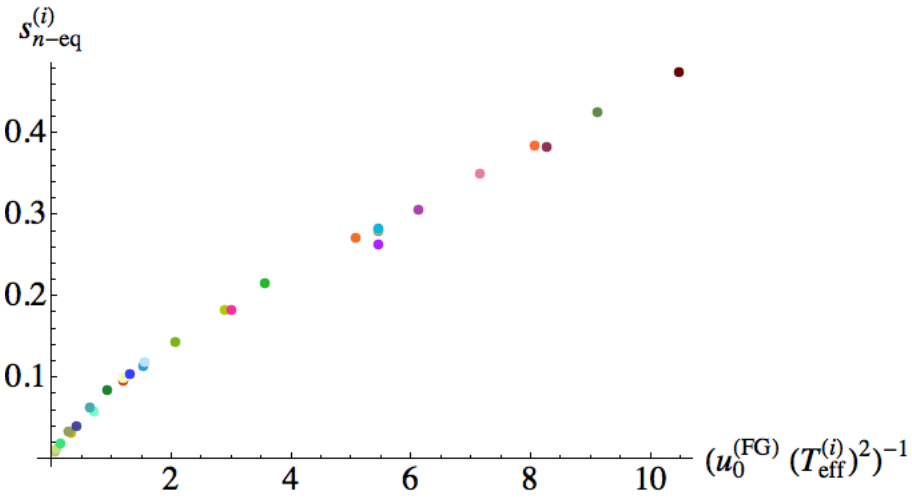

Figure 6.6: Initial non-equilibrium entropy density $s^{(i)}_{n-eq}$ extracted from the apparent horizon at the initial hypersurface $t = 0$ is clearly correlated with the coordinates singularity at u_0^{FH}.

However the most intriguing fact about s^0_{n-eq} becomes apparent after further analysis of the simulation results. It turns out, that *most* of the investigated features of the plasma evolution were relatively simply characterized by this single quantity. That interesting observation will be covered shortly, but in the present paragraph concerning geometric properties of initial data we can give some motivation for this.

In general one can expect that in the case of non-linear partial differential equation there are infinitely many scales hidden in the initial data. However by inspecting the initial positions of the event horizons, Fig. 6.5, one can see how little of the actual spacetime lies outside of the black brane, as seen in the Figure 6.7. Since event horizon is a causal boundary, it cuts-off large portion of the geometry from the outside world, and in particular from the boundary where the field theory resides. It is thus natural to speculate that initial data are characterized by fewer scales than they could have, and that s^0_{n-eq} via u^{FG} is the most important one among them, along with the initial effective temperature. Then many of the observable quantities would be to the leading order characterized by just s^0_{n-eq}. We will return to this point below.

6.8.2 Towards the transition to hydrodynamics

We have came to the point where we can start asking physical questions about the dynamics. In contrast to the discussion of Chapter 5, where only a static configuration was considered, we can now observe in the nonlinear case how the observables of the plasma system evolve.

Among the main questions of interest is the mechanism of transition to hydrodynamics during the heavy ion collision. From the partially experimentally motivated point of view, the observables we have considered are: the form of energy-momentum and its anisotropy at the transition to hydrodynamics, entropy production during the evolution, temperature at the thermalization time and the thermalization time itself.

In view of the application to the near-equilibrium physics, instead of the energy-momentum tensor *per se* we will use the effective temperature $T_{\text{eff}}(\tau)$ introduced in (6.58).

This quantity can be used at early times, in the far-from-equilibrium period of the evo-

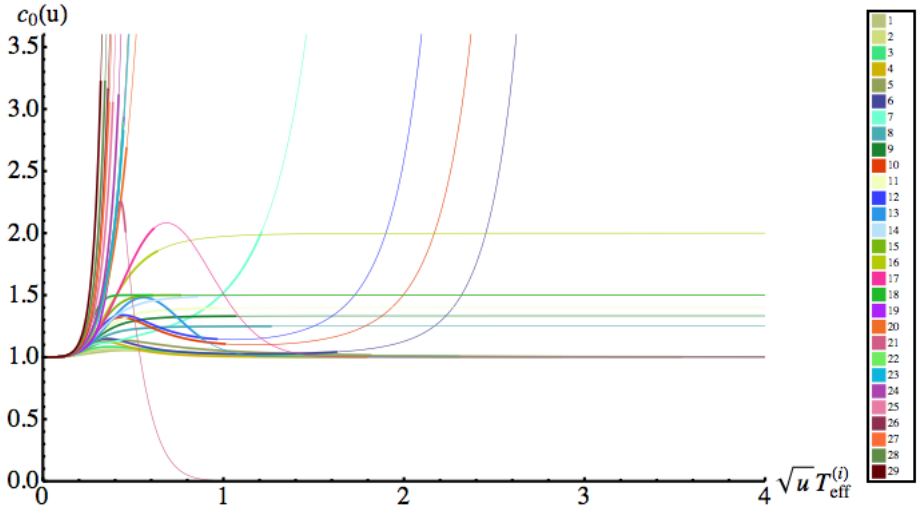

Figure 6.7: Metric components $c_0(u)$ of all the analysed initial profiles. The thicker part of the lines indicates the portion of spacetime lying outside of the initial event horizon. The Figure qualitatively explains conjectured origin of simplified parametrization of the initial data. The more diverse part of the geometries is chopped-off by the horizon, and thus leaves no mark on the outside world.

lution, as well as at later near-equilibrium times. By using $T_{\rm eff}$ we factor out the numerical constant N_c^2 as the specific number of degrees of freedom in the $\mathcal{N}=4$ super-Yang-Mills. This function also becomes the real temperature at late times, near the equilibrium.

Let us now demonstrate the evolution of $T_{\rm eff}(\tau)$ in three representative examples. In Figure 6.8 we can see qualitatively distinct possibilities, with rapid fall-off, intermediate plateau and even an initial rise of temperature. All three plots end up in a long power-like tail expected from hydrodynamics. The correctness of numerically computed initial stage dynamics is confirmed by agreement with power series expression for energy density. Both these regions were indicated with appropriate dashed lines. The intermediate regime is the land of transition to hydrodynamics. Note that the evolution clearly shows a possibility of a surge in temperature, which we call reheating. It contradicts the energy positivity conditions discussed in Section 2.1.5, but nevertheless is legitimate, as seen from the initial series agreement. It has been observed in the literature, that such a behaviour is indeed

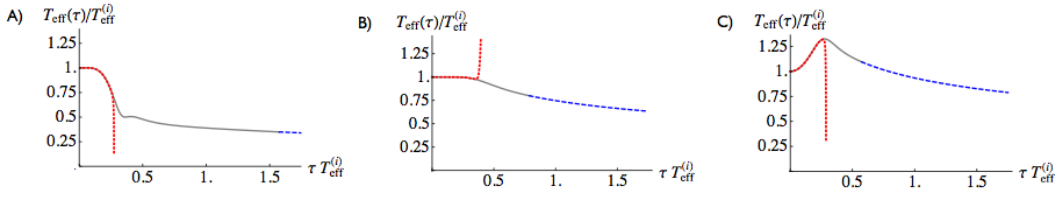

Figure 6.8: Three examples of qualitatively different (effective) temperature behaviours during the whole plasma evolution. The temperature is directly related to the energy density, and as can be seen on the last picture (C), it may initially violate the energetic condition (2.48). This however occurs only during the early non-equilibrium stage of the evolution.

encountered, [Epstein 1965] and can be attributed to highly quantum initial stages of evolution. Quite interestingly this phenomenon has been recently addressed in [Arnold 2014]. It appears that it follow from the lack of a temporal eigenvector of the quantum stress-energy tensor $\langle T^{\mu\nu}\rangle$ in highly non-equilibrium initial states[14]. The initial violation of the energy positivity condition reflects thus the lack of a local rest frame of the fluid in a highly quantum state. From what follows we will see, that this phenomenon occurs only in the early non-equilibrium stage and shall not interfere with the hydrodynamics. Moreover it occurs only for a subset of initial conditions with large initial entropy.

If we want to discuss hydrodynamic features of evolution we should first develop a criterion indicating, that we have indeed entered its domain. We will now construct a criterion based not on a thermal equilibrium, but on the applicability of hydrodynamics equations of motion[15]. To this end let us clarify what we mean by hydrodynamics. We say the system is in hydrodynamic stage if the stress-energy tensor expressed in terms of the effective temperature $T_{\text{eff}}(\tau)$ indeed behaves in accordance with some fixed order hydrodynamics. This does not e.g. require the system to be isotropic, but only that the effective temperature depends on time in a specific way. The criterion seems to be as accurate as the order of hydrodynamics used to formulate it. In the presently analysed context of boost-invariant conformal system in four dimensions, possessing holographic AdS dual, the highest order analytically known hydrodynamics is of third degree in viscosities [Booth 2009, Baier 2008]. The temperature changes according to it in the following way:

$$T(\tau) = \frac{\Lambda}{(\Lambda\tau)^{1/3}}\left[1 - \frac{1}{6\pi(\Lambda\tau)^{2/3}} + \frac{-1-\log 2}{36\pi^2(\Lambda\tau)^{4/3}} + \frac{-21+2\pi^2+51\log 2-24\log 2^2}{1944\pi^3(\Lambda\tau)^2}\right]. \tag{6.70}$$

This series contains several numerical factors representing transport coefficients like shear viscosity, as we described in Chapter 2. They are specific numbers intrinsic to the particular fluid of $\mathcal{N}=4$ SYM. Notice also, that this formula for temperature diverges near $\tau = 0$, which can be understood as the limit of hydrodynamics applicability at early times.

The parameter Λ has dimension of energy, governs the leading late time scaling of the effective temperature with time and is of different nature than transport coefficients. It appears as the only integration constant of the first order (in time) hydrodynamics equation $\nabla_\mu T^{\mu\nu} = 0$. The measurement of this important number is performed by fitting the analytic expression for the third order hydrodynamics (6.70) to numerical data from simulation.

The physical interpretation of Λ relates it to the final entropy density. This assertion can be validated through the thermodynamic relations found to hold [Janik 2006a] for perfect fluid dominating at $\tau \to \infty$, and are generalizing the laws reported for the static plasma in Section 3.7. Let us demonstrate this statement by constructing an explicit expression for the final entropy, which we shall need in our analysis. The formula for an infinitesimal entropy increase reads

$$dS = s(\tau)\tau dy d^2x_\perp, \tag{6.71}$$

where $s(\tau)$ is the familiar entropy density read-off from the horizon area, $s(\tau) = \text{Area}/4G_N$ and the volume element is that of the boost-invariant metric, $dV = \sqrt{-\gamma}dyd^2x_\perp$. The thermodynamic relation we mentioned reads

$$s(\tau) = \frac{N_c^2\pi^2}{2}T_{\text{eff}}(\tau)^3. \tag{6.72}$$

[14] We remind here that the local velocity field u^α is a timelike eigenvector of the stress-energy tensor, $T^\alpha{}_\beta u^\beta = -T_{00}u^\alpha$

[15] Very loosely one could compare it to a sort of on-shell condition.

This formula holds for all proper times, but contains the large N parameter. We would like therefore to remove it by considering instead a dimensionless entropy (without time dependence in the large τ limit) defined per unit rapidity and transverse area element, and measured in units of the initial effective temperature. In short,

$$s = \frac{dS}{dyd^2x_\perp}\frac{1}{\frac{1}{2}N_c^2\pi^2(T_{\rm eff}^{(i)})^2}. \tag{6.73}$$

In the asymptotic limit $\tau \to \infty$, using (6.72) and regarding $T_{\rm eff}(\tau)$ equal to the leading piece of (6.70) we arrive at the following relation for the final entropy,

$$s^{(f)} = \frac{\Lambda^2}{(T_{\rm eff}^{(i)})^2}, \tag{6.74}$$

which completes our argument above on the nature of Λ. This formula will be useful in Section 6.8.3 for discussing physical content of numerical solutions.

To proceed we now make the following observation. Purely on the dimensionality grounds, by putting together proper time and effective temperature we can introduce a dynamical dimensionless parameter:

$$w(\tau) = T_{\rm eff}(\tau)\tau. \tag{6.75}$$

This entity is independent of any assumptions on the thermodynamic equilibrium and $T_{\rm eff}$ is just the fourth root of energy density, (6.58). Such an object was previously discussed in the context of QGP in e.g. [Lublinsky 2007]. The crucial step now is to observe, that the general stress-energy conservation in the boost-invariant case,

$$\nabla_\mu T^{\mu\nu} = 0, \tag{6.76}$$

is one dimensional differential equation of first order in time. It may then be rewritten with the aid of the new parameter $w(\tau)$ in the following dimensionless form:

$$\frac{\tau}{w}\frac{d}{d\tau}w = \frac{F(w)}{w}. \tag{6.77}$$

We can be sure, that $F(w)$ depends solely on w because it is the only dimensionless combination we have at our disposal, and the left side of (6.77) is dimensionless.

This observation has certain deep consequences for our task of finding criterion of transition to hydrodynamic regime, and for hydrodynamics *per se*. In general this is just another form of microscopic energy-momentum conservation, but *if* the stress-energy tensor assumes the form provided by hydrodynamics (of arbitrary order, not just e.g. perfect fluid), then the function $F(w) = F_{hydro}(w)$ is uniquely specified by the *hydrodynamic* equation of motion[16],

$$\nabla_\mu T^{\mu\nu}_{hydro}(\tau) = 0, \tag{6.78}$$

and depends only on w and numerical transport coefficients. No other ambiguity nor any initial condition or integration constant is present in its definition. It then means, that for every solution $w_{hydro}(\tau)$ of the hydrodynamic equation of motion (6.78), function

[16] Take note of the subscript *hydro*. It means that $T_{\mu\nu}$ assumed a special form and is expressed through constitutive relations by the 'true' near-equilibrium temperature $T(\tau)$.

$F = F_{hydro}(w)$ understood as the *left* hand side of (6.77) evaluated on the solution assumes the very same values, irrespective of e.g. initial condition. It is so, because this function defines the equation, which $w_{hydro}(\tau)$ obeys, and so it must assume the same value on its every given solution[17].

This is very subtle but also crucial point, so let us be very explicit about this argument. The way to verify if a given $w(\tau)$ is a solution to the hydrodynamics equation, we need to test the left hand side of (6.77) by independently providing $w(\tau)$ and $\partial_\tau w(\tau)$. Then one has to evaluate their combination and parametrically check the values of the $(w,\ \frac{\tau}{w}\frac{d}{d\tau}w)$ pair. If the values would be the same for every given considered function $w(\tau)$, and would match similarly evaluated $(w(\tau),\ F_{hydro}(w(\tau))$, then we would conclude that $w(\tau)$ indeed follows evolution of the assumed hydrodynamic equation. We shall soon see, that this is precisely what happens for our numerical profiles of $w \equiv w(T(\tau), \tau)$.

Let us now proceed to the formulation of the transition criterion. First let us give the expression for $F_{hydro}(w)$ for the quoted above third order boost-invariant hydrodynamics:

$$\frac{F_{hydro}^{(3rd\ order)}(w)}{w} = \frac{2}{3} + \frac{1}{9\pi w} + \frac{1-\log 2}{27\pi^2 w^2} + \frac{15 - 2\pi^2 - 45\log 2 + 24\log 2^2}{972\pi^3 w^3}. \tag{6.79}$$

We are now ready to verbalize our claim: if the deviation of the ratio of the numerically provided function $F(w)$ and analytically known third-order function $F_{hydro}(w)$ does not exceed 0.005:

$$\left| \frac{\tau\frac{d}{d\tau}w}{F_{hydro}^{(3rd\ order)}(w)} - 1 \right| < 0.005, \tag{6.80}$$

then we shall say, that the field theory state evolves in a hydrodynamical way. Of course the level 0.005 is somewhat arbitrary, but we expect (and observe) only a relatively sharp crossing to hydrodynamics and not a unique transition point.

We are now ready to demonstrate, that the described mechanism is indeed functioning. In Figure 6.9 one can see analysis based on twenty nine profiles of energy density holographically derived from the evolved geometries and processed with the aid of (6.77). The plot shows parametric curves $(w(\tau),\ F(w(\tau))/w(\tau))$. As is manifest, for all the initial data we first observe rich and diverse evolution of the profiles[18]. Then abruptly in the neighbourhood of $w \propto 0.7$ all curves collapse to just a single line, asymptotic to roughly 2/3, which is the leading term of (6.79).

What we observe here is the long sought transition to hydrodynamics in action. The numerical curves merge when gauge theory plasma system starts following the equations of hydrodynamics. To be able to decide which order of viscous hydrodynamics we follow, we need to apply the relation (6.80). On the plot there are visible three curves F_{hydro} of ascending hydrodynamics order, the first, the second, and the third. All of them diverge near $w = 0$, but in the region of interest $w \propto 0.7$ all follow closely the exact numerical $F(w)$. This also indicates the fact (seen before in [Chesler 2009]), that the deviations from hydrodynamics do not occur due to the large gradient corrections, but rather through dissipation of non-hydrodynamical degrees of freedom.

[17] For example, in the simple case of harmonic oscillator, $\ddot{x}(t)/x(t) = -1$ the right hand side assumes value -1 on every solution. This point is trivial, but now if someone would hand us *independently* values of $x(t)$ and $\ddot{x}(t)$, we could test it they correspond to a solution, if their ratio would be -1.

[18] The curves initially forming spiral-like shapes come from the non-monotonic behaviour of energy density defining $w(\tau)$.

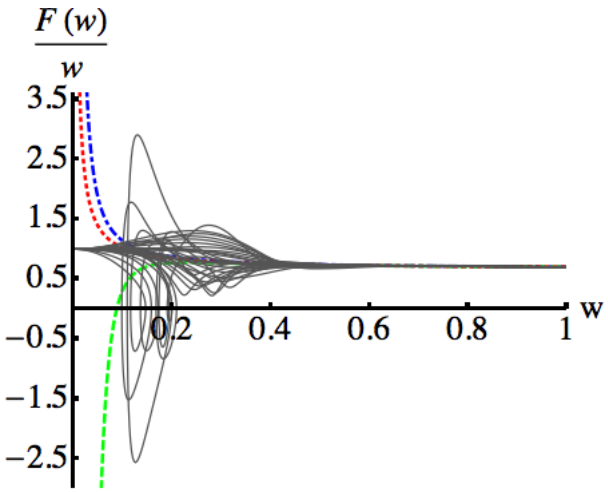

Figure 6.9: Expression (6.77) evaluated for all analysed initial profiles and displayed together. It is readily visible, that albeit initially diverse evolution, all the profiles collapse quite abruptly to just one common line. This indicates the moment of *hydrodynamisation*.

An application example of this condition is given in Figure 6.10a. The horizontal bar represents the threshold set at 0.005, which indicates 0.5% deviation from third order boost-invariant hydrodynamics. The plot represents the ratio of exact numerical value of $F(w)/w$ divided by the corresponding analytic expression (6.79) for $F_{hydro}^{(3rd\ order)}(w)/w$, with good match at zero towards increasing $w = \tau T_{\rm eff}(\tau)$. The value of $w(\tau)$ for which the two lines cross defines the moment of transition to hydrodynamics. One clearly visible effect is that the approach towards hydrodynamics is not monotonic, with two bumps present below the threshold band. This indicates, that since the confidence level 0.005 is arbitrarily chosen and the analytic expression for hydrodynamics is of only third order, the transition is not absolutely determined moment, but is subject to refinements (and rather never a sharp event).

To address concerns on the stability of our criterion we first give an example of a potential problem for profile with very small initial entropy (compared to average among others). In Figure 6.10b one can see how the ratio drops below the band, only to jump up above it and decrease again. This indicates a possible trouble, to which sensitive are especially profiles with small initial entropy. We however define our criterion by demanding to take the *last* crossing with the band. We have tested stability of this rule by changing the band to 0.01 and 0.02 (respectively two- and four-fold values of the threshold) and we observed little difference among the determined transition times. We thus conclude that even though not perfect, the criterion is fairly robust.

Let us now describe one of the most important findings of the present work, also related to the main quest for explaining thermalization mechanism. Prior to our investigation [Beuf 2009, Chesler 2009], the condition of transition to thermodynamics relied on the pressure anisotropy parameter $\xi = 1 - \frac{p_L}{p_T}$. The equilibration was declared when this ratio dropped below e.g. 10%. A more convenient combination to use is

$$\Delta p(\tau) = 1 - \frac{3p_L(\tau)}{\varepsilon(\tau)}. \tag{6.81}$$

This takes into account the fact that in thermal equilibrium $p_L = p_T$ and for conformal

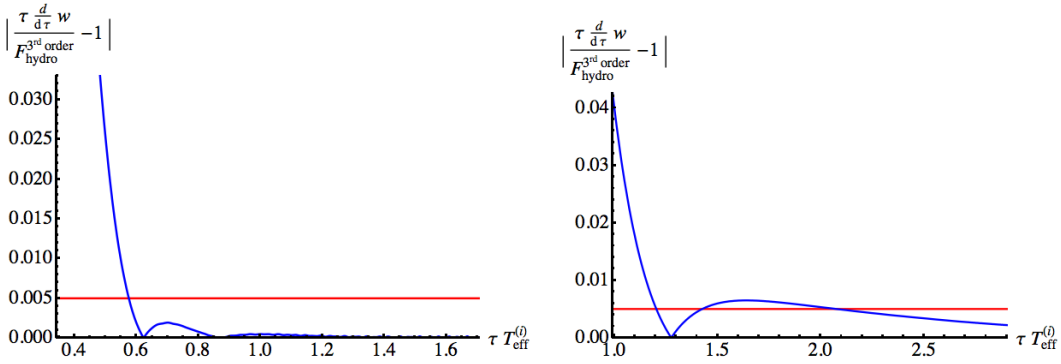

(a) Hydrodynamisation criterion (6.80)

(b) Criterion (6.80) exceeded by the small initial entropy profile 'c1'.

Figure 6.10: Hydrodynamisation criterion for two qualitatively different initial profiles, with respectively from the left: normal and small initial entropy density.

system $\varepsilon = p_L + 2p_T = 3p_L$.

Now let us plot this parameter for a typical sample profile, Fig. 6.11. Along the exact numerical line there are also three curves for respectively 2nd, 1st and 3rd order hydrodynamics (counting from above). What can be readily observed, is that in the region of $w \propto 0.7$ quite uniformly determined by the criterion (6.80) and seen in Fig. 6.9, the pressure anisotropy if of order 0.6, which is still significant. This value is however fully described by viscous hydrodynamics.

Let us rephrase this to clarify the statement. The value of $w \propto 0.7$ means according to (6.80) that the stress-energy tensor assumed special hydrodynamic form (6.70) and is governed by hydrodynamic equation of motion. Nevertheless as seen in Figure 6.9, the pressures are highly anisotropic, contradictory to the usual assumption of thermalization. The fact, that the stress tensor follows law of hydrodynamic clearly indicates presence of collective phenomena. It seems however that it may not be the standard thermalisation. Such a possibility was signalled in the first numerical work on holographic dual to expanding SYM plasma, [Chesler 2009]. Subsequently to our work a new term was coined to describe this phenomenon: 'hydrodynamisation'. However awkward it may sound, it aptly reflects the process under consideration and avoids the subtlety of speaking of equilibrium with significant anisotropy.

The discussed observation suggests that a new mechanism may be at work in heavy ion collision, one that differentiates isotropisation and thermalisation from *hydrodynamisation*. It also points at the significance of viscous and anisotropic hydrodynamics applications to RHIC data analysis [Florkowski 2011], as the 3rd order viscous line readily follows closely the exact numerical profile of the pressure anisotropy.

6.8.3 Features of hydrodynamisation

With the tool for detecting transition to hydrodynamics in simulation results (6.80), we can proceed to qualitatively characterise the details of this process.

We have signalled in Section 6.8.1 particularly simplified description of the hydrodynamisation in terms of initial non-equilibrium entropy density, $s^{(i)}_{n-eq}$. Its notion was linked to the concept of apparent horizon. For the purpose of the present analysis we have employed this connection to measured the initial entropy, as outlined in Section 6.6.2. The concrete formula we used to extract the entropies from geometry was (6.66).

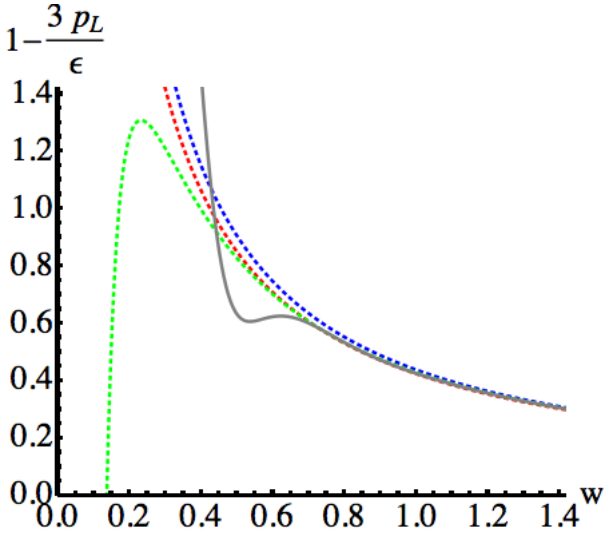

Figure 6.11: Evolution of the anisotropy parameter Δp, (6.81) during the plasma evolution.

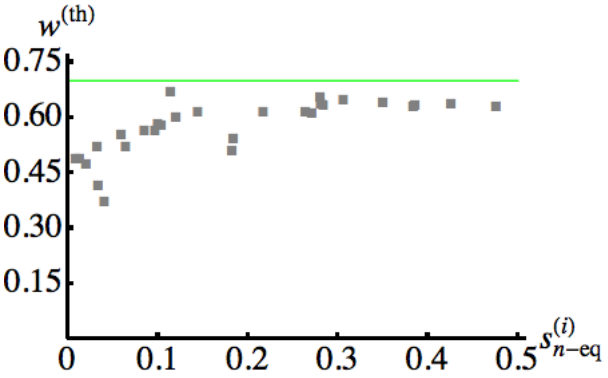

Figure 6.12: Effective dimensionless thermalisation time in units of temperature $w(\tau)$, at the hydrodynamisation point.

As a first step we determine the moment of hydrodynamisation by measuring with (6.80) the values of $w = w^{(th)}$ for all the analysed profiles, and express[19] them as functions of $s^{(i)}_{n-eq}$ extracted from the corresponding profiles. The result is depicted in Figure 6.12. This plot justifies the recent remark, that this value is more or less uniform among all the profiles. The significant deviation from 0.7 occurs only for states with particularly small initial non-equilibrium entropy density, $s^{(i)}_{n-eq} < 0.1$. These states seem to be slightly different in nature from the rest, as for instance for such states we experienced the increased sensitivity to thermalisation criterion exemplified in Fig. 6.10b. Figure 6.12 also justifies the additional conjecture, that to some extent the parameter $w(\tau)$ may be well suited to universally describe thermalisation, because it assumes similar values for all the profiles. Curiously, sample initial conditions for hydrodynamisation at RHIC ($T_0 = 500$ MeV, $\tau_0 = 0.25$fm for central collisions, [Broniowski 2008]) correspond after all units are taken into account to $w = 0.63$, which is quite close to the value 0.7. Our results are therefore of similar

[19] Both $w^{(th)}$ and $s^{(i)}_{n-eq}$ are labelled by their corresponding initial profile number n, so this is just a simple parametric plot in n. This method is also used in other cases.

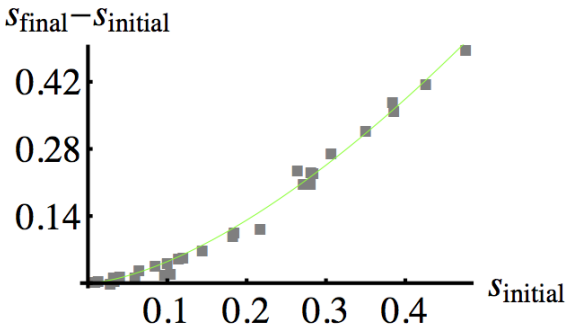

Figure 6.13: Total entropy production Δs during the plasma evolution.

order of magnitude to those of the physical QCD, which is encouraging in the context of qualitatively approximating it with super-Yang-Mills theory.

Proceeding further, we note one of the more intriguing observations we made, which concerns the total entropy production during the whole process of plasma evolution. The production is defined as the difference between the recently introduced final entropy $s^{(f)}$ and the initial non-equilibrium entropy $s^{(i)}_{n-eq}$ defined through (6.66),

$$\Delta s = s^{(f)} - s^{(i)}_{n-eq}. \tag{6.82}$$

The value of $s^{(f)} = \Lambda^2/(T^{(i)}_{\text{eff}})^2$ is obtained by fitting Λ from the late time power tail of the third order hydrodynamic temperature (6.70), after the observed transition to hydrodynamics. The obtained with its aid dependence of the entropy production on the initial entropy is reported in Figure 6.13.

This simply looking curve suggests, that during the *a priori* strongly diverse initial evolution and subsequent thermalisation, the entropy produced is well parametrized by just the value of $s^{(i)}_{n-eq}$. Simple two parameter fit of exponential-like behaviour gives dependence of a sort

$$\Delta s = 1.64(s^{(i)}_{n-eq})^{1.58}. \tag{6.83}$$

The apparent simplicity of the relation between the two entropies is interesting, since one would expect no memory to persist of the initial state during the process of thermalisation. Recall that the final entropy $s^{(f)}$ is obtained as a fit of the leading late time fluid tail (6.70), when only leading viscous corrections are present, and (hydrodynamic) equilibrium is assumed. However one can also make a remark, that according to the comment made earlier there is a non-zero event horizon from the onset of spacetime evolution. This suggests some remote contact with equilibrium, and hence the possible origin of this interesting regularity. It would be interesting to understand this phenomenon in more detail in the future.

Two further observables characterising the moment of hydrodynamisation are the temperature $T(\tau^{(th)})$ and proper time $\tau^{(th)}$ of thermalisation, both expressed in units of the initial effective temperature $T^{(i)}_{\text{eff}}$[20], and parametrically plotted as functions of the initial entropy $s^{(i)}_{n-eq}$ in Figure 6.14. Again we can see that the dimensionless ratios ordered along the ascending initial entropy reflect simple dependence on the initial condition.

[20]Recall from Section 6.5.2, that the initial energies were all normalized to the same value, so the temperatures are also all the same.

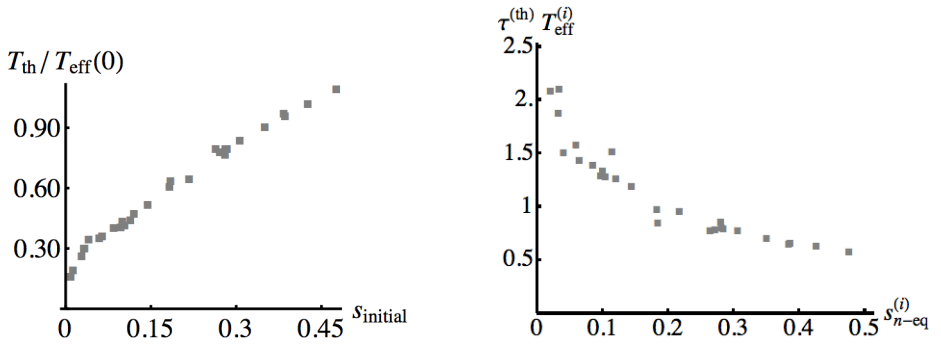

(a) Thermalisation temperature (b) Thermalisation time

Figure 6.14: Temperature and proper time at hydrodynamisation, in units of the initial temperature $T^{(i)}_{\rm eff}$. Quite clear correlation with the initial entropy density is visible.

The plot showing the temperature at thermalisation point is important for understanding how much cooling may be attributed to the far-from-equilibrium stage, and how much to the (viscous) hydrodynamic phase of the evolution. From the plot it can be seen, that the ratio steadily grows with the increasing initial entropy, to even *exceed* its initial value. This effect can be linked to the phenomenon of reheating, encountered before in Figure 6.8. This means that during the non-equilibrium stage some significant amount of temperature can be generated for states with high initial entropy, after which system arrives at equilibrium, and not that thermalisation is instantaneous when temperature is still high. For states with small initial entropy the temperature at thermalisation is much smaller than the initial one, and thus for such states cooling occurs largely in the non-equilibrium stage. For these states we also observe slight departure from the generally linear dependence of the thermalisation temperature on initial entropy, again pointing at slightly different nature of such states. On the overall these remarks imply, that cooling may be both equilibrium and non-equilibrium process, and based solely on the value of temperature one can not judge in which state the fluid is.

On the plot of thermalisation time we can see that the dependence is to some extent reciprocal to the similar one for temperatures (so that the product of the two observables will give approximately constant values of $w^{(th)}$). The states of very small initial entropy need excessively large amount of time to equilibrate, as compared to the large initial entropy configurations. The whole dependence is again strongly correlated with values of $s^{(0)}_{n-eq}$. Maybe one way of thinking of this is that small initial entropy reflects high purity of the corresponding quantum field state. Such system may then need more time to become mixed and develop thermal equilibrium.

The above statement concludes our description of simulation results. We shall now move to the final section of this chapter, containing overview of the findings and brief discussion of their meaning.

6.9 Closing remarks

In the present chapter we have reached the point, in which we could have qualitatively described in a simple manner several characteristics of the non-equilibrium evolution of a strongly coupled gauge theory fluid. The observables that we presented are the following:

- The function $F(w)/w$ encapsulating hydrodynamic expansion, (6.77) (see also per-

turbative part, (6.79)) and Fig. 6.9

- Hydrodynamisation criterion based on $F(w)$, Fig.6.10
- Pressure anisotropy, (6.81) and Fig. 6.11
- Effective thermalisation time in units of effective temperature, $w^{(th)}$, Fig. 6.12
- Entropy production during the whole plasma evolution Δs, Fig. 6.13
- Temperature at the thermalisation time in units of initial effective temperature, $T_{\text{eff}}^{(th)}/T_{\text{eff}}^{(i)}$, Fig. 6.14a
- Thermalisation proper time in units of the initial effective temperature, $\tau^{(th)}T_{\text{eff}}^{(i)}$, Fig. 6.14b

Access to these variables has been made available by application of numerical relativity methods to the AdS/CFT or gauge/string duality. We have discovered interesting mechanisms that may be of interest to the community investigating real-world strongly coupled fluids, like the one observed at RHIC or LHC. The interesting point is that probably from the viewpoint of numerical relativists the methods applied may not seem very sophisticated compared to state of the art cosmic black holes simulations (however their development was by far not a trivial task). The amount of (physically well justified) symmetries assumed and the effective two-dimensional nature of the problem significantly contributed to this relative simplicity. Nevertheless it is apparent how much physical understanding have been gained. One may make an observation, that in this part of the AdS/CFT correspondence, related to gravity duals of fluid evolution, the whole field matured to the stage similar to the General Relativity: many of the results possible to obtain analytically have been obtained. Now great amount of interesting hard to get otherwise information has to be accessed with numerical methods. Another point of view is that to some extent AdS/CFT may play a role similar to powerful lattice methods, used to obtain non-perturbative insight into strongly coupled properties of e.g. QCD. The advantage of AdS/CFT relies on the fact, that it is naturally a dynamical construction embedded in well understood theory of General Relativity, which allows for real-time Minkowski space measurements of observables.

The novel aspects of fluid dynamics that we have observed are:

- A strong indication, that one should recognize different types of equilibration. In addition to conventional thermalisation there can also be *hydrodynamisation*, which occurs at highly anisotropic stage of the flow, where Δp may very well be of the order 50%. It may be an intermediate step before the isotropic thermal equilibrium takes over.
- Significance of viscous corrections to the leading perfect fluid dynamics. The 'empirical' AdS/CFT exact numerical solution for the temperature is best reproduced by third order boost-invariant hydrodynamics. This is important for the real-world systems analysis (e.g. RHIC, LHC), in case of which one does not have full control of the difficult microscopic theory at the disposal to derive effective low energy description. Our analysis may help to argue for the use of viscous hydrodynamics.
- A possible good effective parameter to indicate hydrodynamisation, $w(\tau) = T_{\text{eff}}\tau$, which acquires similar value of $\propto 0.7$ at this moment for all initial data.
- Very clear correlation between several observables and the initial non-equilibrium entropy density $s_{n-eq}^{(i)}$. This points at an important role played by this quantity, in particular when plugged into the hydrodynamic codes aimed at collision data analysis.

Apart from these physical conclusions, some interesting techniques have been develop during this research:

- ADM-inspired formulation of asymptotically-AdS spacetime was derived with specific coordinate system suitable for numerical simulation, tangent at the initial time hypersurface to the standard Fefferman-Graham hypersurface.
- To our knowledge, for the first time in the ADM-based approach a technique was proposed to handle boundary conditions in the highly curved region of spacetime close to the horizon, based on the vanishing lapse. In the non-asymptotically flat case of AdS space, with the need to observe patches of apparent and event horizon, this method proved to be valuable.
- For some purposes other coordinates systems generally better suited for black hole numerics are not feasible. For example Eddington-Finkelstein coordinates are aligned along null geodesics and thus make it difficult or impossible to describe constant time hypersurface. Hence for the purely spatial observables our coordinates (or similar related) may be the only choice to describe the observable at its whole length, starting at $t = 0$. An example of such observable is the two point correlation function of a scalar operator, which is well described by a spatial geodesic.
- An important advantage of our setup is also the fact, that we are able to start the evolution at the initial time $t = 0$ and keep the boundary metric fixed as physical Minkowski space. The previous work on the numerical equilibration [Chesler 2009] necessary had to start from some initial time $\tau_\star > 0$. We are free to follow the evolution from its onset, because the creation of the non-equilibrium state and its subsequent evolution towards the equilibrium are vividly separated.

Among the points worth clarifying, one can mention the observed simplification in the initial data parametrization through initial entropy density (or equivalently, by the coordinates singularity u^{FG}). It would be interesting to investigate this effect in more detail in the Eddington-Finkelstein coordinates, which allow for explicit observation of event or apparent horizons from the very beginning.

6.10 Appendix A: The summary of initial conditions

TABLE I: Below following [Heller 2012a] we collect information about the initial profiles we considered: $C_0(u)$ is the initial condition as discussed in Section 6.5.1 with $\gamma = \frac{1}{2}\sqrt{3}\pi^2\left(T^{(i)}_{\text{eff}}\right)^2$; $u_0^{(FG)}$ is a position of corresponding coordinate singularity in the Fefferman-Graham chart; $u_0^{(EH)}$ is the approximate position of the event horizon on the initial time slice; $w^{(th)}$ is thermalization time measured in terms of an effective temperature at thermalization as defined by equation (6.75); $\tau^{(th)}T^{(i)}_{\text{eff}}$ is the thermalization time in units of the initial effective temperature; $T^{(th)}_{\text{eff}}/T^{(i)}_{\text{eff}}$ is the ratio of the effective temperature at thermalization to the initial effective temperature; $s^{(i)}_{n-eq}$ is dimensionless initial entropy density (6.66) defined by apparent horizon, as described in Section 6.6.2; $s^{(f)}_{n-eq}$ is the final entropy density obtained from perfect fluid hydrodynamics.

No.	$C_0(u)$	$u_0^{(FG)}\left(T_{\rm eff}^{(i)}\right)^2$	$u_0^{(\rm EH)}\left(T_{\rm eff}^{(i)}\right)^2$	$w^{(th)}$	$\tau^{(th)}T_{\rm eff}^{(i)}$	$T_{\rm eff}^{(th)}/T_{\rm eff}^{(i)}$	$s_{n-eq}^{(i)}$	$s_{n-eq}^{(i)}$
1	$\frac{\left(1-\frac{1}{\gamma u+1}\right)\tanh\left(\frac{\gamma u}{2}\right)}{4\gamma u+1}+1$	23.9980	12.5030	0.4853	3.2287	0.1503	0.0086	0.0120
2	$\frac{1-\frac{1}{\gamma^2u^2+1}}{2(3\gamma u+1)}+1$	12.8410	8.2419	0.4868	2.6686	0.1824	0.0127	0.0178
3	$\frac{\gamma u\left(1-\frac{1}{\gamma u+1}\right)}{2(2\gamma^2u^2+1)}+1$	7.0707	5.3189	0.4722	2.0759	0.2275	0.0200	0.0270
4	$\frac{\gamma^2u^2}{2(\gamma^2u^2+1)^2}+1$	3.0462	3.2053	0.5209	1.8717	0.2783	0.0322	0.0435
5	$\frac{\gamma u\left(1-\frac{1}{\gamma u+1}\right)}{2(\gamma^2u^2+1)}+1$	3.6404	3.2898	0.4153	2.0940	0.2963	0.0333	0.0420
6	$\frac{\gamma^2u^2e^{\frac{\gamma u}{6}}\left(1-\gamma^4u^4e^{-6\gamma^2u^2}\right)}{2(\gamma^2u^2+1)^2}+1$	2.4453	2.6413	0.3713	1.4999	0.3433	0.0402	0.0522
7	$\frac{\gamma^2u^2e^{\frac{\gamma u}{6}}\left(\frac{\gamma^6u^6}{8}+\frac{\gamma^4u^4}{4}+\frac{1}{2}\right)}{(\gamma^4u^4+\gamma^2u^2+1)^2}+1$	1.4390	1.4639	0.5507	1.5759	0.3494	0.0592	0.0713
8	$\frac{\gamma^2u^2}{2(2\gamma^2u^2+1)}+1$	1.6148	1.5908	0.5200	1.4265	0.3646	0.0641	0.0923
9	$\frac{\gamma^2u^2}{2\left(\frac{3\gamma^2u^2}{2}+1\right)}+1$	1.0747	1.1372	0.5625	1.3841	0.4064	0.0847	0.1217
10	$\frac{\gamma^2u^2e^{\frac{\gamma u}{6}}}{2\left(\frac{\gamma^2u^2}{2}+1\right)^2}+1$	0.8425	1.0125	0.5634	1.2806	0.4400	0.0968	0.1152
11	$\frac{\gamma^2u^2}{2\left(\frac{5\gamma^2u^2}{4}+1\right)}+1$	0.8437	0.9252	0.5809	1.3300	0.4368	0.0998	0.1438
12	$\frac{\gamma^2u^2e^{\frac{\gamma u}{5}}}{2\left(\frac{\gamma^2u^2}{2}+1\right)^2}+1$	0.7676	0.9264	0.5768	1.2787	0.4511	0.1039	0.1231
13	$\frac{1}{2}\gamma^2u^2e^{-\frac{3\gamma u}{4}}+1$	0.6609	0.7884	0.6691	1.5080	0.4437	0.1139	0.1658
14	$\frac{\gamma^2u^2}{2(\gamma^2u^2+1)}+1$	0.6430	0.7269	0.5978	1.2556	0.4761	0.1199	0.1748
15	$\frac{1}{2}\tanh^2\left(\frac{\gamma^2u^2}{25}+\gamma u\right)+1$	0.4884	0.5788	0.6154	1.1825	0.5204	0.1441	0.2131
16	$\frac{\gamma^2u^2}{2\left(\frac{\gamma^2u^2}{2}+1\right)}+1$	0.3475	0.4006	0.5098	0.7948	0.6414	0.1826	0.2825
17	$\frac{1}{2}\gamma^2u^2e^{-\frac{\gamma u}{2}}+1$	0.3336	0.3764	0.5396	0.8448	0.6388	0.1841	0.2919
18	$\frac{1}{2}\tanh^2\left(\gamma^2u^2+\gamma u\right)+1$	0.2807	0.3652	0.6139	0.9465	0.6486	0.2168	0.3307
19	$\exp\left(\frac{1}{2}\int_0^{\gamma u}\left\{\sqrt{2v_+'(x)-v_+(x)^2}-v_+(x)\right\}dx\right)$ with $v_+(x)=\tan x-\tanh\left(x+x^4\right)$	0.1838	0.1996	0.6150	0.7719	0.7968	0.2642	0.5009

20	$\frac{\gamma^2 u^2}{2}+1$	0.1971	0.2147	0.6111	0.7817	0.7817	0.2711	0.4797
21	$\exp\left(\frac{1}{2}\int_0^{\gamma u}\left\{\sqrt{2v'_+(x)-v_+(x)^2}-v_+(x)\right\}dx\right)$ with $v_+(x)=\tan x-\tanh\left(x-\frac{1}{4}x^4\right)$	0.1838	0.2097	0.6548	0.8525	0.7681	0.2803	0.4891
22	$\exp\left(\frac{1}{2}\int_0^{\gamma u}\left\{\sqrt{2v'_+(x)-v_+(x)^2}-v_+(x)\right\}dx\right)$ with $v_+(x)=\tan x-\tanh\left(x+\frac{1}{6}x^4\right)$	0.1838	0.1979	0.6346	0.7952	0.7980	0.2810	0.5146
23	$\cosh(\gamma u)$	0.1838	0.1987	0.6306	0.7886	0.7997	0.2839	0.5142
24	$e^{\frac{\gamma^2 u^2}{2}}$	0.1634	0.1762	0.6453	0.7682	0.8401	0.3062	0.5778
25	$\cosh\left(\frac{3\gamma^2 u^2}{10}+\gamma u\right)$	0.1398	0.1503	0.6380	0.7029	0.9077	0.3501	0.6687
26	$\gamma^4 u^4+\frac{\gamma^2 u^2}{2}+1$	0.1210	0.1303	0.6293	0.6460	0.9742	0.3838	0.7624
27	$\frac{1}{2}\gamma^2 u^2 e^{\gamma u}+1$	0.1243	0.1338	0.6324	0.6571	0.9624	0.3859	0.7465
28	$\cosh\left(\frac{4\gamma^2 u^2}{5}+\gamma u\right)$	0.1099	0.1187	0.6356	0.6227	1.0207	0.4259	0.8433
29	$\frac{1}{2}\gamma^2 u^2 e^{2\gamma u}+1$	0.0955	0.1026	0.6298	0.5754	1.0947	0.4761	0.9634

6.11 Appendix B: Numerical methods and spectral differentiation

The key concept in the development of a numerical method designed to solve partial differential equations is the proper discretisation of the integration domain. The most direct consequence of the chosen mesh pattern is the way spatial differentiation will be represented on the grid. The choice must reflect the geometry of the problem at hand. Different techniques apply to periodic or unbounded domains, and different for finite domains with non-periodic boundary conditions. Suboptimal discretisation scheme may lead to loss of numerical accuracy or even complete failure of the numerical method after few initial integration steps.

The numerical problems we consider in the Thesis belong to the latter category of non-periodic finite domain systems. The problems we initially faced with finite discretisation, or finite difference schemes, motivated us to implement our numerical codes using spectral methods. The main technical problem, that forced us to seek more advanced methods was the necessity to compute one sided derivatives at the edges of the integration domain. Finite elements methods rapidly developed errors, while spectral methods based on algebraic Chebyshev polynomials demonstrated rather spectacular accuracy, even for long lasting simulations.

We will now briefly describe how they work following an excellent introductory book by Trefethen [Trefethen 2000].

First let us describe the general philosophy used to integrate our system of non-linear partial differential equations. By design, as we explained in the main body of Chapter 6, our system of seven equations based on ADM formulation is of first order in time. This means, that in general they assume the form

$$\partial_t \mathbf{f}(t,z) = \mathbf{F}(f_1(t,z),\ldots,f_7(t,z),\partial_z^a f_1(t,z),\ldots,\partial_z^a f_7(t,z),t,z),\ a=1,2. \tag{6.84}$$

The vector $\mathbf{F}$ defining the equations depends on the unknown functions and their spatial derivatives. Such a system is already in the form suitable for temporal integration with Runge-Kutta method, provided all expressions on the right hand side are known at the given instance of time t. The above equation is represented on a numerical grid defined as a two-dimensional mesh of nodes:

$$\{t,z\} \to \{m,n\},\ m=0,1,2,\ldots,M,\ n=0,1,2,\ldots,N. \tag{6.85}$$

The indices m and n label the spacetime points of the domain, and their physical values are computed with the aid of discretisation parameters. For time it is simply $t_n = m\Delta t$, but in the case of spectral methods spatial positions are less directly related to n and are encoded in the discretisation scheme, which we will describe in a moment. The number N corresponds to the density of spatial discretisation (which however will not be uniform in our case) and M defines the timespan of the simulation.

The temporal integration is performed for each spatial grid point independently (which allows for parallel optimisation). The algorithm of numerical integration is the following:

- Start from the initial condition and integrate one step in time.
- Compute all the necessary derivatives using spectral differentiation.
- Check constraints and boundary conditions.
- Enter the main integration loop by repeating the steps.

We see, that once differentials are known we can perform one integration step. In our case the temporal integrator was adaptive Runge-Kutta RK89 algorithm, which is a refined version of RK4 integrator. In this sense our problem is in fact a collection of N ordinary differential equations, each one for the independent mesh point. The only way they communicate is through the derivatives. Runge-Kutta is a standard algorithm in the field of numerical methods and we shall not discuss it here. Instead we finally focus on the spectral discretisation.

The way spectral differentiation based on Chebyshev polynomials works is the following [Trefethen 2000]. For a smooth function $f(x)$ and sample finite interval $x \in [-1, 1]$:

- Define natural number $N > 0$.
- Define spatial Chebyshev grid represented by point

$$x_j = \cos(j\pi/N), \ j = 0, \ldots, N. \tag{6.86}$$

- Find polynomial of degree N, $p_N(x)$, interpolating the function $f(x)$ on the grid $\{x_j\}$

$$p_N(x_j) = f(x_j) \equiv f_j, \ j = 0, \ldots, N. \tag{6.87}$$

- Define spectral derivative of the function on the grid:

$$f'(x_j) = p'_N(x_j) \tag{6.88}$$

The above procedure is carried out for the specified function $f(x)$. Derivative is however a linear operator. This great virtue allows us to realise it on the grid as a matrix operator D_N acting on vectors representing *arbitrary* functions, e.g. w,

$$w' = D_N w, \tag{6.89}$$

because the differential matrix D_N extracted from the above procedure happens to be the same for all functions. This crucial feature follows from the fact, that the differentiation performed in the last step above acts on the interpolating polynomial $p_N(x)$. This function has a specific fixed structure based on the grid nodes, in which the values f_j of the interpolated function $f(x)$ play the role of linear external parameters.

To illustrate this consider the simple case of $N = 3$, in which we find [Trefethen 2000]:

$$p_3(x) = \frac{1}{2}x(x+1)f_0 + (1+x)(1-x)f_1 + \frac{1}{2}x(x-1)f_2. \tag{6.90}$$

The derivative is equal to

$$p'_3(x) = (x + \frac{1}{2})f_0 - 2xf_1 + (x - \frac{1}{2})f_2. \tag{6.91}$$

From this analytical expression we now need to compute values of the derivatives $p'_3(x_j)$ in three grid points, $x_j = 1, 0, -1$. The resulting expressions allow us to extract the following differentiation matrix

$$D_3 = \begin{bmatrix} \frac{3}{2} & -2 & \frac{1}{2} \\ \frac{1}{2} & 0 & -\frac{1}{2} \\ -\frac{1}{2} & 2 & -\frac{3}{2} \end{bmatrix}. \tag{6.92}$$

Expressions for general N and demonstrations of the so called spectral accuracy of such a matrix derivative can be found in [Trefethen 2000]. The great feature of this method is

that equally high accuracy is maintained if we interpose differentiation matrices to computer higher order derivatives, e.g. $D_N^2 = D_N D_N$.

This concludes our inception of spectral methods. As a last comment we emphasise again, that apart from the overall performance in numerical integration, spectral derivatives were instrumental in the holographic procedure of extracting observables from near boundary region of the numerical solution. This required computing fourth order one-sided derivatives and would be much more difficult without spectral methods.

Chapter 7

Non-equilibrium modes in hydrodynamics

7.1 Introduction

This chapter describes fascinating results published in our paper [Heller 2013a], unravelling intricate link between hydrodynamical degrees of freedom and non-hydrodynamical ones. As we shall see the boundary between them is more blurred that one might initially expect.

We have seen how full evolution of a quantum system passes from highly non-equilibrium regime to local equilibrium without any dramatic events, but in a rather smooth way. The distinction between them was made by us with the aid of an analytic expression for the third order boost-invariant hydrodynamics solution. Therefore the criterion of passing to local equilibrium seems to rely on the gradient expansion order used for this, which only due to the technical complexity was limited to in our case to three. For instance in cases with small initial entropy our criterion (6.80) was prone to offering less accurate predictibility, as we have seen in Figure 6.10b. It therefore asks for refinement, and the most straightforward way to achieve this could be *a priori* based on a higher order expression for the function $F(w)/w$. We are thus motivated to investigate the nature of hydrodynamic gradient expansion at possibly high order. Such a question is also justified on its own. Since we are defining hydrodynamics as truncated power series expansion one should analyse the properties of this series before embracing it and applying to arbitrary systems.

7.2 Very high order hydrodynamics

Determining high order hydrodynamics is difficult. We have seen in Chapter 2 how complex the tensorial structures of hydrodynamics become when the expansion order grows. We have also seen in Chapter 3 how cumbersome the calculations are when one tries to derive the exact numerical values of transport coefficients present in the expansion. Boost-invariance may however improve the situation to some degree. Its main virtue in this context is the restriction of energy density to be a function of only proper time τ, which renders gradient expansion to be effectively one dimensional and leading to significant simplifications. We will use this fact access higher order hydrodynamics.

We know from the fluid/gravity duality that large proper time energy density expansion in boost-invariant model is

$$\varepsilon(\tau) = \frac{3}{8} N_c^2 \pi^2 \frac{1}{\tau^{4/3}} (\varepsilon_2 + \varepsilon_3 \frac{1}{\tau^{2/3}} + \varepsilon_4 \frac{1}{\tau^{4/3}} + \ldots), \tag{7.1}$$

where numerical the coefficients ε_n are related to transport coefficients. This function is an expansion in inverse powers of proper time, $\tau^{-2/3n}$, and in this form is valid only for large τ. Such a parameter is remnant of the gradient expansion, which is implicitly parametrized by the number of applied derivatives. Indeed at each order, new transport coefficients from

n-th order start contributing to ε_{2+n}. Qualitatively the structure of the series at each order is given by the product[1]

$$\frac{\nabla_\mu u_\nu}{T(\tau)} \sim \frac{1}{\tau} \times \frac{1}{\tau^{-1/3}} = \frac{1}{\tau^{2/3}}, \tag{7.2}$$

which is our expansion parameter. The question whether the above series is convergent even for large τ is open in hydrodynamics. In general the energy density is related to the local temperature as

$$\varepsilon(\tau) = \frac{3}{8} N_c^2 \pi^2 T(\tau)^4, \tag{7.3}$$

which should be a solution to

$$\nabla_\mu T^{\mu\nu}(T(\tau)) = 0. \tag{7.4}$$

The question is what are the properties of the above equation based on an *a priori* infinite expansion? To understand its structure better we recall how we have seen around (6.70) the way combined conformal and boosts symmetry allows us to recast hydrodynamics equation and solution in a very convenient way using the dimensionless variable

$$w(\tau) = T(\tau)\tau. \tag{7.5}$$

With its aid the first order in proper time hydrodynamic equation (7.4) of arbitrary gradient order can be rewritten as

$$\frac{\tau}{w}\frac{dw(\tau)}{d\tau} = \frac{F_{\text{hydro}}(w)}{w}. \tag{7.6}$$

The function $F_{\text{hydro}}(w)$ on the right encompasses any terms apart from temperature derivatives which might appear in the equation. This expression makes a good starting point for analysis of gradient expansion convergence, because in boost-invariant model gradient expansion is represented by just a polynomial in inverse powers of w. For example third order hydrodynamics used in the preceding chapter reads:

$$\frac{F_{\text{hydro}}^{(\text{3rd order})}(w)}{w} = \frac{2}{3} + \frac{1}{9\pi w} + \frac{1-\log 2}{27\pi^2 w^2} + \frac{15 - 2\pi^2 - 45\log 2 + 24\log 2^2}{972\pi^3 w^3}. \tag{7.7}$$

This expression is obtained directly from the energy density (7.1).

Our goal is to obtain further terms in the above series for $F(w)$ and inspect what are its analytic properties. If this series is convergent, so is the hydrodynamic gradient expansion procedure[2].

This is however not a simple task. Yet we should recall that equation (7.4) is also a specific component of Einstein equations, which dictates all the exact tensorial structures one can think of in hydrodynamics. Therefore we can try generating the equation implicitly by considering high-order expansion of Einstein equations. If we would be able to solve them, we could holographically extract the corresponding energy density $\varepsilon(\tau)$, form $F(w)$ and understand its nature at high order in w.

We are thus going to follow the same steps as before and form holographic dual of Bjorken flow. This time however we are going to obtain a semi-analytic expression for the

[1] Recall, that since we are working in the proper time curvilinear coordinates we are using a covariant derivative. Even though the velocity field u^α is locked to be unit vector, the affine connection gives a term $1/\tau$.

[2] At least in our conformal boost-invariant system.

geometry in the large τ expansion, in contrast to the full numeric solution of the previous chapter.

This time the basis of analysis will be Eddington-Finkelstein metric in the form adapted to boost-invariance:

$$ds^2 = 2d\tau dr - Ad\tau^2 + \Sigma^2 e^{-2B} dy^2 + \Sigma^2 e^B (dx_1^2 + dx_2^2). \tag{7.8}$$

The metric fields are functions of proper time and bulk radius, $\{\tau \in [0,\infty), r \in [0,\infty)\}$, and boundary is located at $r = \infty$. We are not using our newly developed ADM scheme of the preceding chapter, because we are after the late time expansion and not initial value problem crucial for non-hydrodynamical physics.

The main goal is to derive energy density in the form of late time expansion in powers of $\tau^{-2/3}$. Using [Kinoshita 2009] we are led to the following Ansatz:

$$\begin{aligned} A(\tau, r) &= r^2 \sum_{n=0} \frac{1}{\tau^{2/3n}} A_n(r\,\tau^{1/3}), \\ B(\tau, r) &= \frac{2}{3} \log \frac{r}{1+rt} + \sum_{n=0} \frac{1}{\tau^{2/3n}} B_n(r\,\tau^{1/3}), \\ \Sigma(\tau, r) &= r^{2/3}(1+rt)^{1/3} \sum_{n=0} \frac{1}{\tau^{2/3n}} \Sigma_n(r\,\tau^{1/3}). \end{aligned} \tag{7.9}$$

This structure is based on the scaling variable[3] enforcing gradient corrections:

$$v = r\tau^{1/3}. \tag{7.10}$$

Each metric series component is therefore a function of v.

The first term of the expansion is known from the leading perfect fluid dynamical black brane. A useful feature of the Eddington-Finkelstein metric Ansatz is that the dynamic horizon locus (or a similar quantity – see below) can be held fixed at $v = 1$ for any value of τ. We can observe this by inspecting the leading metric components:

$$A_0(v) = 1 - \frac{1}{v^4},\ B_0(v) = 0,\ \Sigma_0(v) = 1. \tag{7.11}$$

The key point is that the naive horizon position of this geometry defined by $A_0(v) = 0$ can be held fixed in each order at $v = 1$ due to a residual diffeomorphisms symmetry [Kinoshita 2009],

$$r \to r + f_n(\tau), \tag{7.12}$$

which leaves the functional form of (7.8) unchanged. Adapting appropriate $f_n(\tau)$ at each order we can modify $A_n(\tau)$ to keep the superficial horizon locked. We will appreciate this fact soon, when discussing the numerical implementation.

The solution to the corresponding gravity equations is found iteratively. We insert the Ansatz (7.9) into Einstein tensor $R_{AB} + 4g_{AB} = 0$ and expand the nonlinear coupled system of partial differential equations in powers of inverse proper time, $\tau^{-2/3n}$. Subsequently we take the late time limit, $\tau \gg 0$ and separate equivalent contributions according to the given order for each Einstein tensor component. The outcome is that in place of the non-linear system we obtain an *infinite* set of coupled *linear ordinary inhomogeneous* differential equations in variable v:

$$\hat{H}^a \left[g^{(0)}(v) \right] g^{a\ (n)}_{\mu\nu}(v) = s^{a\ (n)}_{\mu\nu}(v),\ n = 0, 1, ...,\ a = A,\ B,\ \Sigma. \tag{7.13}$$

[3]Coordinates v and r are linearly proportional to each other, with rescaling through always positive term $\tau^{1/3}$. This implies, that for a fixed time in both variables the boundary and AdS interior correspond to ∞ and 0.

The general structure of the above chain of equations is such, that for each of the metric partial components, $A_n(v)$, $B_n(v)$, $\Sigma_n(v)$, the expansion produces an equation with a unique ordinary differential operator $\hat{H}^a[g^{(0)}(v)]$, with a denoting the appropriate component. Each linear operator depends only on the initial unperturbed metric (7.11) and is the same at all orders n of the new equations hierarchy for each warp-factor (7.9). The distinct equations for A_n, B_n, Σ_n are in turn coupled through the sources $s^{a\ (n)}_{\mu\nu}(v)$, which accumulate progressively the contributions from all the orders $k < n$ subordinate to the given computation order n. This coupling through the increasingly convoluted source terms gradually builds up the effect of non-linearity, which was expelled during the expansion (7.9), and thus become very complicated. Yet crucially, this is still a linear system and can by integrated without any fundamental obstacles, provided the sources are regular. They are indeed regular, since we are working in a well-behaved coordinate system. The described procedure is in fact a numerical implementation of the scheme described in Chapter 3, which has never been done before.

7.2.1 Numerical procedures

The setup for numerical integration is such that we use a compact domain defined by a variable $z = 1/v$ ranging from the boundary $z = 0$ to the fixed naive horizon locus $z = 1$. This is the technical application of the horizon fixing discussed above feature. It is crucial for the numerics to have a well established integration domain, and we are provided with one by the variable v.

From the differential equations point of view we are solving an infinite chain of three ordinary equations system[4] at each order on a compact domain and hence we are only going to need boundary conditions. No initial data are present in the late time approach. The boundary conditions are imposed at the boundary and at the horizon.

The boundary conditions at $z = 0$ are given by the dual field theory background, which is the planar Minkowski geometry:

$$ds^2 = r^2\left[-Ad\tau^2 + \Sigma^2 e^{-2B}dy^2 + \Sigma^2 e^{B}(dx_1^2 + dx_2^2)\right] \to r \to \infty - d\tau^2 + \tau^2 dy^2 + dx_1^2 + dx_2^2 \quad (7.14)$$

Corresponding conditions on the *total* warp factors (7.9) are then[5]

$$A(\tau, z) = \frac{1}{z^2} + o(z^{-2}),\ \Sigma(\tau, z) = \frac{\tau^{1/3}}{z} + o(z^{-1}),\ B(\tau, z) = -\frac{2}{3}\ln(t) + o(z). \quad (7.15)$$

These conditions are compatible with the founding metric (7.11). For higher warp factor expansion coefficients the above relations imply vanishing conditions at the boundary $z = 0$:

$$A_n(0) = 0,\ \Sigma_n(0) = 0,\ B_n(0) = 0,\ \text{for } n > 0. \quad (7.16)$$

The second set of boundary conditions is imposed inside the spacetime at the horizon $z = 1$. We are able to work directly with the metric there owing to the chosen regular coordinates. As we mentioned above we have five equations at our disposal, but there are only three unknown functions. The two extra equations serve as constrains and can provide us with two boundary conditions for functions $B_n(z)$ and $\Sigma_n(z)$ at the horizon. The last remaining condition is set by utilizing the discussed above residual gauge freedom in the system, corresponding to the radial variable redefinition $r \to r + f(\tau)$. We fix it by imposing

$$A_n(1) = 0 \text{ for all } n. \quad (7.17)$$

[4] Formed out of five dependent Einstein equations.

[5] Recall that we are matching to the AdS conformal boundary and not just Minkowski space. This implies the asymptotic $1/z$ terms.

This concludes the boundary conditions derivation.

Having collected all the necessary elements the numerical integration can be carried out. This time the procedure was implemented as a matrix inversion integration with spectral representation of derivatives. As before the use of spectral methods greatly enhances accuracy in the case of non-periodic bounded domain integration. The spatial discretisation turns all the functions of z to M-dimensional vectors with M representing the number of spectral grid points:

$$z \to i \in [1, M],\ A_n(z) \to X_n^A(i),\ B_n(z) \to X_n^B(i),\ \Sigma_n(z) \to X_n^\Sigma(i), \tag{7.18}$$

where $n \in [0, N]$ is the current perturbation order. Then, in a schematic way the integration amounts to solving a set of M linear algebraic equations for each unknown partial warp factor a:

$$\hat{D}^a X_n^a = J_n^a,\ \text{with } a = A,\ B,\ \Sigma. \tag{7.19}$$

Technically this step has been carried out with the aid of LinearSolve[ ] in *Wolfram Mathematica*. Generally such an approach to ODE solving is a direct generalization of the finite differences scheme for the boundary problem in a (spectral) matrix notation. The differential operators H^a of (7.13) are represented by the matrices[6] $\hat{D}^a$, the unknown functions at the given order n are the vectors X_n^a and the corresponding sources are J_n^a. The boundary conditions are embedded in the differential matrices $\hat{D}^a$ and the solutions are found through matrix inversion. This is in direct analogy to the Green's function method of solving boundary problems, where the Greens function being the inverse of the differential operator contains the boundary conditions. The solution is given by its convolution with the source.

The outcome of integration is the set of vectors, each one representing the n-th order contribution to the full solution (7.9), e.g.

$$A(i, \tau) \sim \sum_n X_n^A(i) \tau^{-2/3n},\ \text{and similarly for } B \text{ and } \Sigma. \tag{7.20}$$

From now on the analysis can proceed as if we had an actual analytic solution. In particular the perturbative series for the main observable $\varepsilon(\tau)$ can be holographically extracted by taking the fourth derivative of $X_n^A \equiv A_n$ at $z = 0$. We invoke here the significance of the employed spectral differentiation. We are taking fourth-order discrete derivative at the domain *boundary*, i.e. side derivative. This is reliable owing to spectral precision.

The overall accuracy of the numerical integration has been monitored by comparing at the given order in $\tau^{-2/3n}$ the normalized values the evaluated Riemann tensor (defining the equations of motion) and the normalized ratio of gradient expanded warp-factors (the $X_n^A(i)$) to the energy density coefficients (the ε_n). The norm was defined by the maximum of the absolute value of the given argument. Thus the order of the equations of motion violation was compared to the energy density contributions at the scale of the warp factors contributions, from which the energy density is obtained through high order derivative. In this way we tested the numerical quality of the energy density series. As an additional check we compared the numerical values found for $\varepsilon(\tau)$ to the known analytical solution at the third order, with satisfying agreement.

In the end the holographic procedure gives us the desired perturbative solution to the hydrodynamic equation of motion (7.4) at the given computation order N. We were able to reach $N = 240$, which on a decent desktop computer consumed roughly four weeks. On

[6] There is no n dependence here as we discussed above, just the same differential operator at each order.

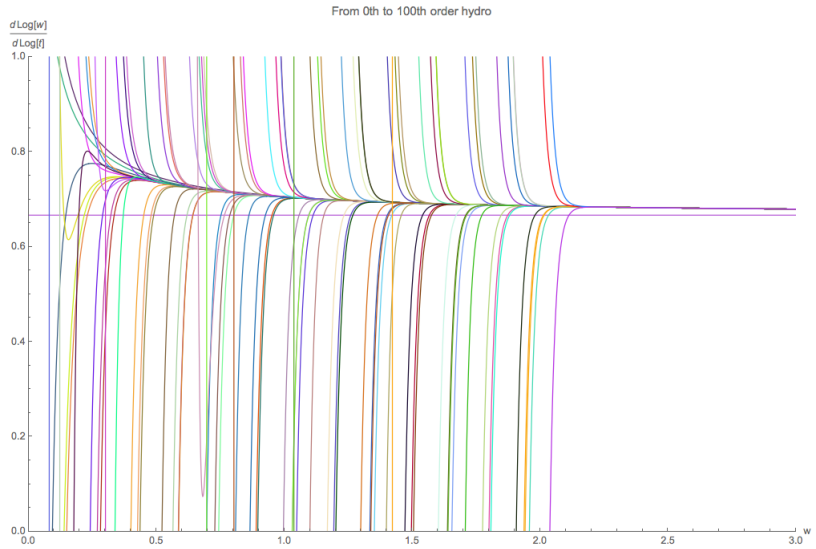

Figure 7.1: The function $\frac{\tau}{w}\frac{dw}{d\tau} \equiv F(w)/w$ (with $w(\tau) \sim \tau\varepsilon(\tau)^{1/4}$) evaluated on the first one hundred orders of the perturbative numerical series for $\varepsilon(\tau)$. The plot is a direct perturbative counterpart in $1/\tau$ of the plot 6.9 obtained from the full all-proper-time solution. Clearly the perturbative solution does not follow the well behaved exact answer. The hydrodynamics order grows from zero (perfect fluid) on the left to one hundred on the right, steadily loosing the approximation quality.

the other hand, if we would be interested in few first coefficients the calculation would be very quick and efficient. An additional factor making the computation so time consuming was the necessity to use and maintain very high order numerical `WorkingPrecision[]` in Mathematica, which we had to set at ∼1000, based on the observed loss of integration quality with lower level choices. The numerical accuracy of the result was monitored by comparing the normalized values of Einstein equations evaluated at each order of the $\tau^{-2/3}$ expansion to the ratio of gradient-expanded energy density coefficients and the gradient-expanded metric warp-factors, from which these coefficients were extracted. Additionally we checked, that numerical integration reproduces the known analytic expression for the third order energy density.

7.2.2 Energy density series analysis

With the numerical integration completed we can now analyse the physics it unlocked. The first test is to inspect the function $F(w)/w$, which we know from the previous chapter that is regular for all w (and hence all τ). With some surprise comes then what may be seen in Figure 7.1. We plot there $F(w)/w$ evaluated on first one hundred orders of hydrodynamic expansion, starting from the leftmost perfect fluid and going to the right with increasing order. Perturbative solutions tend to cover less and less of the exact numerical solution fount in Chapter 6. This is clearly a hallmark of asymptotic series and indicates, that if we had infinite order expansion it would be of no use as it would formally be infinite for all w.

We must therefore analyse properties of the resulting series by understanding how its coefficients ε_n behave. The prime question to ask is what is the convergence radius of this series? Of course we have at our disposal only a finite order polynomial in $\tau^{-2/3}$, but using Cauchy root convergence criterion [Whittaker 1996] we can elucidate an approximation to

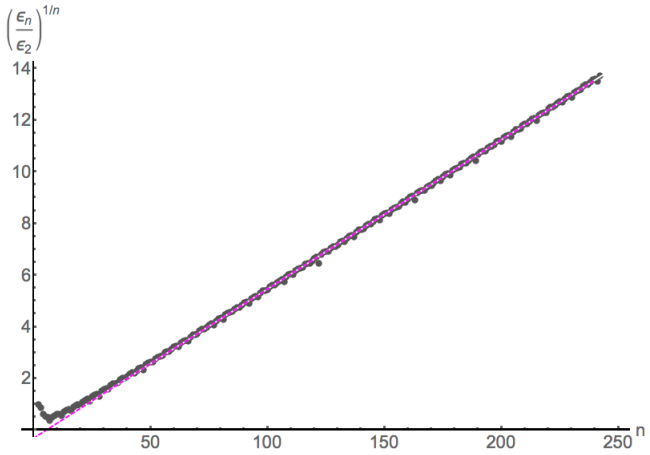

Figure 7.2: The scaling of the Cauchy criterion r_n with the series order n seems to be linear. This type of the coefficients behaviour is typical of asymptotic series.

it. If the series is to be absolutely convergent the quantity

$$C = \lim_{n\to\infty} |\varepsilon_n|^{1/n} \tag{7.21}$$

related to the convergence radius as $R = 1/C$ should be less than one. If on the other hand $C > 1$, the series in divergent (the marginal case $C = 1$ is inconclusive). In our case we will investigate the quantity normalized by the first term $r_n = (\varepsilon_n/\varepsilon_2)^{1/n}$ to see how this ratio behaves with n. By looking at Figure 7.2 we convince ourselves, that indeed we encounter an approximately linear (but not stronger) growth of the ratio r_n with n, which wouldn't be the case if the series was convergent.

A well known physical example of perturbative series with such a behaviour is the factorially divergent expansion, often encountered in perturbation theory. Indeed, suppose a series has the generic structure

$$f(z) := \sum_{n=0}^{\infty} f_n z^n, \text{ with } f_n \sim \alpha A^n n!, \tag{7.22}$$

with α being a constant and A being a subleading power-like growth. The relation of this series to our's is seen by applying Stirling's formula:

$$n! = \Gamma(n+1) \sim (2\pi n)^{1/2}(n/e)^n, \; n \gg 0. \tag{7.23}$$

Because $(|\alpha|2\pi n)^{1/n} \underset{n\to\infty}{\longrightarrow} 1$ we can observe asymptotically a linear growth of the Cauchy ratio for such a series coefficients:

$$r_n \sim \frac{A}{e} n, \tag{7.24}$$

much like the one depicted in the Fig. (7.2). Actually if we fit a line $an + b$ to the series[7] depicted in the Fig. (7.2) we can estimate the subleading growth strength $A = ea$. With a roughly equal to 0.057 we obtain $A \sim 0.155$. We shall understand significance of its inverse $1/A \sim 6.37$ further below.

[7] We skip first few terms (~ 10) in this fit, the so-called non-universal behaviour and take only leading part into account, with $n \geq 10$.

7.2.3 The notion of asymptotic series

The situation might not be so bad if the series at hand happens to be asymptotic, so let us introduce and review its basic notion to see, if we are in fact dealing with one. Asymptotic series are members of a special class of divergent series, which after Poincaré is characterized by the feature, that for a given analytic function $f(z)$ and all fixed $N \in \mathbb{N}$ we have:

$$\lim_{z\to 0}\left| z^{-N}\left(f(z) - \sum_{n=0}^{N} f_n z^n = 0 \right)\right| = 0. \tag{7.25}$$

In other words, the series approximates the function the better the smaller its argument is (being closer to the zero radius of convergence region). Such a series is unique for a given function $f(z)$, which has only one asymptotic expansion of the sort given above, but there is no equivalence, because unfortunately many different functions may have the same asymptotic expansion. This can be seen by noticing, that we can always add e.g. $exp(-1/z)g(z)$ to the original function and this still will have the same asymptotic $z \to 0^+$ expansion as $f(z)$, provided that $g(z)$ is regular.

As is well known such series are often encountered in physics[8] . Indeed in the case of quantum mechanics or quantum field theory we have this type of a problem and we should not trust expansions beyond certain accuracy bounds. The situation could be better if the series at hand happens to possess the feature that for all z in a cone $|z| < R,\ \arg(z) \leq \pi/2 + \delta,\ \delta > 0$ a constants σ, C exist such, that the inequality holds:

$$|f(z) - \sum_{k=0}^{N} f_n z^n| \leq C\sigma^{N+1}(N+1)!|z|^{N+1}. \tag{7.26}$$

It is difficult in general to check, if we are dealing with such an expansion. Nevertheless for this class of asymptotic series there follows a condition bounding the growth of the individual series terms[9]

$$f_k \leq CB^k k!. \tag{7.27}$$

This can be at least in principle compared to the large order behaviour of the series under consideration and give a premise, that the series is indeed unique approximation of the full answer. We have seen at the end of the previous paragraph, that exactly this type of a growth is numerically seen in our case. It is therefore reasonable to work with the series for $\varepsilon(\tau)$, which we now consider to be asymptotic.

A contemporary approach towards this kind of series is to employ resummation theory (in physics see e.g. [Zinn-Justin 2002]) to capture the information we know was last in the perturbation calculation (when we e.g. interchange integration and summation while violating convergence requirements), and whose remnants are encoded in the divergent series. Usually by doing so one discovers the physical reasons for the failure of the expansion and unravels new degrees of freedom secretly present in the system. This will also be the case for us, when we will find the cause of the hydrodynamics divergence.

The resummation theory is a vast and beautiful branch of mathematics touching upon the core of complex analysis. The approach that is already established in physics relies on the use of Borel resummation with Padé approximation [Zinn-Justin 2002, Whittaker 1996].

[8] After Dyson we know, that 'all important series in physics are asymptotic'...

[9] This condition in short implies, that we are able to pinpoint precisely the difference caused by an addition of exponentially small contribution.

These techniques combined allow one to perform an approximate resummation based on *part* of the full asymptotic series, which is just a finite order polynomial. It is the situation one usually encounters in physics, where only few first terms of the perturbative series are known (e.g. from some hard multi-loop calculations, or from numerics), hence the success of this approach in physics. In our case we have roughly 240 terms of the series, making use of the approximate resummation quite accurate and justified. We will now introduce and review the notion of Borel-Padé resummation.

7.2.4 Borel transform and Padé extrapolation

Suppose, that we are given a factorially divergent series,

$$f(z) := \sum_{n=0}^{\infty} f_n n! z^n. \tag{7.28}$$

We wish to uncover the true analytic function it encodes. Following Borel, let us define another series associated with $f(z)$

$$\varphi(w) := \sum_{n=0}^{\infty} f_n w^n, \tag{7.29}$$

and using the integral representation of Gamma function $\Gamma(n+1) = n!$ recast the original divergent series in a form containing $\varphi(w)$:

$$f(z) = \sum_{n=0}^{\infty} f_n z^n \int_0^{\infty} d\zeta \zeta^n e^{-\zeta} = \int_0^{\infty} d\zeta e^{-\zeta} \sum_{n=0}^{\infty} f_n (z\zeta)^n \equiv \int_0^{\infty} e^{-\zeta} \varphi(z\zeta) d\zeta. \tag{7.30}$$

In the second step we have interchanged the order of summation and integration. This in principle would be allowed if the original series for $f(z)$ was uniformly convergent. Since we know it was not, we should examine the analytic properties of the resulting expression. Now under the integral, which is in fact a Laplace transform, we have the function $\varphi(z\zeta)$ (with $\zeta \in \mathbb{R}_+$) defined above. It is clear, that it has a non-zero radius of convergence by removing the $n!$ growth from $f(z)$. The convergence of the Laplace integral requires the integrand to be analytic along the real axis $\mathbb{R}_+$. This crucial condition is provided by the Whittaker's theorem, stating, that the Borel function $\varphi(w)$ can be analytically continued from its finite radius of convergence to include a cone $|arg(w)| < \delta$, with $\delta > 0$ ([Flory 2012]). Based on that we obtain, that the integral in (7.30) defines an analytic function, and therefore may be regarded as the definition of the *resummed* function $f(z)$. The interchange of the integral and sum in (7.30) is the exact moment of undoing the unjustified interchange of these in the past, during the perturbative calculation of $f(z)$.

In principle this would conclude the resummation procedure if we had a full perturbative series for $f(z)$ at our disposal. However even then it is very nontrivial to deduce the global analytical structure of the Borel transform $\varphi(w)$ based on the power series definition (7.29). Obviously in most cases of perturbative calculations we have a limited number of terms in a polynomial form coming from the Borel transformed asymptotic series:

$$\varphi_N(w) = \sum_{n=0}^{N} f_n w^n. \tag{7.31}$$

If such a series would be inserted to the Borel transform (7.30) all that would happen would result in reappearance of the $n!$ terms back in $\phi_N(w)$, since we would simply evaluate the

Gamma function $\Gamma(n+1)$ in the finite sum. We therefore need an approximation of the full Borel function $\varphi(w)$, that has infinite Laurent expansion and is integrable along the Laplace contour in (7.30). Such an approximation of provided by the Padé analytic continuation [Zinn-Justin 2002] of the polynomial $\varphi_N(w)$.

The method of Padé approximation relies on the rational extrapolation of the data contained in a finite polynomial of degree N [Yamada 2013]. One considers a generic ratio of polynomials

$$\tilde{f}(w) = \frac{\sum_{n=1}^{K} a_n w^n}{\sum_{n=1}^{L} b_n w^n}, \tag{7.32}$$

with the condition $K + L = N$. The coefficients a_n b_n are specified by expanding $\tilde{f}(w)$ around $w = 0$ to the order N and imposing $\tilde{f}_N(w) = f_N(w)$. By comparing the coefficients one solves for a_n b_n as a functions of f_n. This ensures equality of the two functions up to the given order N, but $\tilde{f}(w)$ is now a function containing poles and possessing potentially finite asymptotics as $w \to \infty$ as opposed to polynomials, which is controlled by the ratio of K to L. If $K = L$ we speak of symmetric Padé approximation.

The essential feature of the function $\tilde{f}(w)$ is that contrary to the approximated polynomial it contains poles in the denominator. Therefore it is capable of crossing beyond the potential singularities limiting the radius of convergence of the original series, from which the polynomial $\varphi_N(w)$ originates[10]. In this way the analytical Padé continuation is even capable of completely resumming simple expansions to reproduce the original expanded function, e.g. it works well for $w/(1-w)$ [Marino 2014].

The above feature allows one to check, if the Borel function $\varphi_N(w)$ is uniquely resummable by inspecting the poles of its Padé approximation. If there are no poles on $\mathbb{R}_+$ the Laplace integral can be carried out[11] and one can define approximate Borel-Padé resummation:

$$f_R(z) = \int_0^\infty d\zeta e^{-\zeta} \tilde{f}(\zeta z). \tag{7.33}$$

We shall apply this scheme in our case for the polynomial $\varepsilon(\tau)$ containing 240 terms.

7.2.5 Borel-Padé analysis of the energy density series

Let us recast the semi-numerical series for $\varepsilon(\tau)$ in a form suitable for its resummation analysis. First we form its Borel transform with a substitution of new expansion variable $u = \tau^{-2/3}$. This inverts the temporal infinity and transforms the series into expansion in integer powers of u around the origin:

$$\varepsilon_B(\zeta) = \sum_{n=2}^{240} \frac{\varepsilon_n}{n!} \zeta^n. \tag{7.34}$$

[10] Of course the Borel function may exhibit more complex analytic structure than just poles, e.g. may contain cuts, and we will soon discuss this point

[11] We would like to point out here, that if there are poles on $\mathbb{R}_+$ the case has been historically called non-Borel summable. The contemporary view is that it is resummable, but in the framework of the so-called resurgence theory, which makes sense of all the ambiguities that arise from the need to avoid singularities on the resumation path.

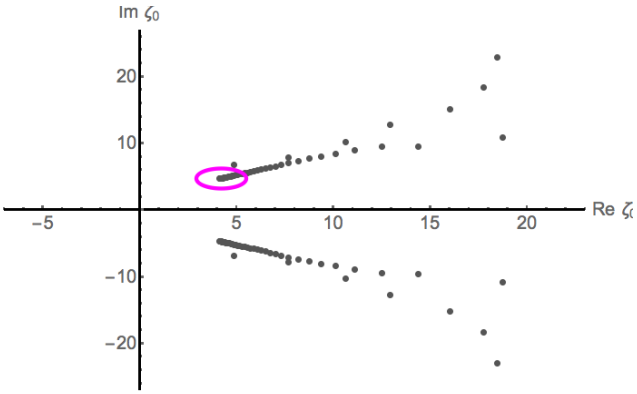

Figure 7.3: The array of poles defined by the zeros of the Borel-Padé energy density transform $\tilde{\varepsilon}_B(\zeta)$. The ellipse encircles the tip of the structure resembling condensation of poles, which might indicate the presence of a cut in the full (unknown) Borel transform.

This expression is now a convergent power series, so we should first estimate its radius of convergence. If we assume its large order structure to be of the sort descried in 7.2.2, αA^n (we have removed the factorial, so there is no e factor here), then by the Cauchy criterion again we find the convergence radius as the inverse of A: $r \sim 6.37$. This is the value we found before from the fit in 7.2.2 using the original series before the Borel transform. This should be the distance to the nearest singularity along any ray emanating from the origin $\zeta = 0$. To locate this singularity we need to furnish Padé approximation to the polynomial (7.34),

$$\tilde{\varepsilon}_B(\zeta) = \text{Padé}\{\varepsilon_B(\zeta); \frac{240}{2}|\frac{240}{2}\}. \tag{7.35}$$

We are using a symmetric Padé here, which is compatible with finite non-zero value of energy density $\varepsilon(\tau)$ at $\tau = 0$ (which is now at $\zeta \to \infty$).

With the newly constructed rational function $\tilde{\varepsilon}_B(\zeta)$ we can localize its poles on the Borel-Padé plane of complex ζ. By computing zeros of the denominator in (7.35) we can plot their location as depicted in the Fig. 7.3. The pattern of poles assembles into two strings with accumulation points. They also seem to be symmetric with respect to complex conjugation and initially align in a way departing from the real axis $\mathbb{R}_+$. This structure in complex analysis points at the possibility, that there actually should be a cut on the Riemann surface of the full $\varepsilon_B(\zeta)$ analytic function if it was known explicitly instead of the finite polynomial (7.34). Nevertheless the Padé approximation allows us to probe its properties through the many poles condensing at the apexes. Given the fact that poles are obtained numerically and that the Padé approximation is reliable mostly up to the first singularity of the mimicked function we regard trustworthy only the poles near the edges along the initial straight line. It is likely that points further away are embarked with more significant numerical errors, as well as it might be that the structure bends away from its linear nature, but we do not know this at this stage of the computation. We assume therefore that to the leading order we have two cuts on the complex Borel plane, and that the resummation should at least in principle be possible as there are no obstructions on the real line.

The plot 7.3 teaches us again about the radius of convergence of the hydrodynamic series Borel transform (7.34), but this time in a more direct and informative manner. The

first singularities defining the radius are located at

$$\zeta_B^{\pm} = 4.120 \pm 4.678i, \ |\zeta_B^{\pm}| = 6.234. \tag{7.36}$$

The absolute value of this pole is in numerical agreement with the value found previously for the convergence radius from the Cauchy criterion. This reaffirms us in the use of the Padé approximation as the correct analytic continuation of the Borel transform $\varepsilon_B(\zeta)$.

The key question that arises now is: what is the physics of the discovered poles $\zeta_B^{\pm}$? Are these just some incidental complex numbers, or do they emerge for some deeper reasons? The way to answering these questions leads through analysis of the uniqueness of the resummation process.

In principle it seems, that in the absence of any singularities *on* $\mathbb{R}_+$ one should be able to carry out the Laplace transform and obtain a convergent expression for $\varepsilon_R(u)$:

$$\varepsilon_R(u) = \int_0^{\infty} d\zeta e^{-\zeta/u} \tilde{\varepsilon}_B(u) \text{ with } u \equiv \tau^{-2/3}. \tag{7.37}$$

This conclusion is validated by the standard theorems quoted above and the resurgence theory [Dorigoni 2014]. However because the Borel(-Padé) transform $\tilde{\varepsilon}_R(u)$ has singularities on the complex plane we can deform the contour and reach $|u| \to \infty$ in more that one way. Should the Borel transform be an entire function the Laplace transform would be independent of this choice and it would not matter, if we integrated along $\mathbb{R}_+$ or along some $e^{i\vartheta}\mathbb{R}_+$. We should therefore analyse the ambiguity induced by singularities. This step will bring us closer to understanding the physics of it, which we will decipher in the next paragraph.

To clarify the issue of ambiguity we should realize, that from the complex analysis point of view we are presently reconstructing the energy density $\varepsilon_R(u)$ as an analytic function in the narrow region $u \in |\arg \varepsilon_R(u)| < \delta$, but in general it should exist on its whole Riemann surface universally covering $\mathbb{C}^*$. In particular it means that we can carry out the integral (7.37) along direction *above* the cut and reach $|u| \to \infty$ at a certain angle if only the integral will converge. This in would define function analytic in a different region than the one determined by integration along $\mathbb{R}_+$.

We should therefore analyse what would be the difference between integrals along the two contours. It is defined as

$$\delta\varepsilon_R(u) = (\int_K - \int_L) d\zeta e^{-\zeta/u} \tilde{\varepsilon}_B(\zeta) \equiv \int_\Gamma d\zeta e^{-\zeta/u} \tilde{\varepsilon}_B(u), \tag{7.38}$$

and has been indicated in Figure 7.4. We see, that due to the difference in orientation the common contour will localize on the cut and resulting integral will reduce to the discontinuity of the Borel transform across the cut.

Unfortunately we have only a limited knowledge of the Borel plane analytic structure, so the complete information about the cut properties is unavailable to us. The best we can do is to approximate the neighbourhood of its origin[12] with the string of poles confined to those numerically stable. In this case the semi-infinite contour Γ defining $\delta\varepsilon_B(u)$ will collapse to encapsulate just the first several poles closest to the leading singularity at ζ_B^+, and it will contain only the structure shown in the Fig. 7.5.

What kind of expression for the resummation difference $\delta\varepsilon_R(u)$ should we expect from the outlined procedure? The discontinuity of the integrand in (7.38) will result in an

[12] Note that the ambiguity at large proper times is exactly governed by the poles closest to the origin in the Borel plane, and thus the poles which are most reliable in our construction.

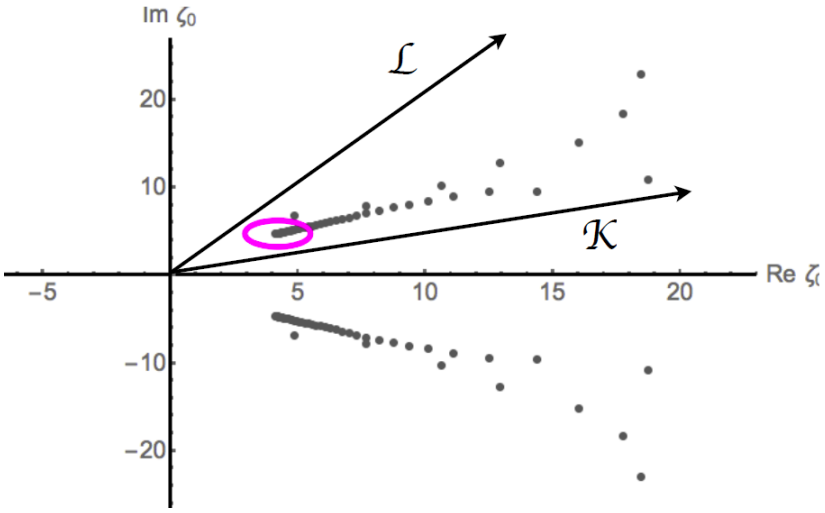

Figure 7.4: Two possible integration contours circumventing the cut and inducing a difference in resummation schemes (7.38).

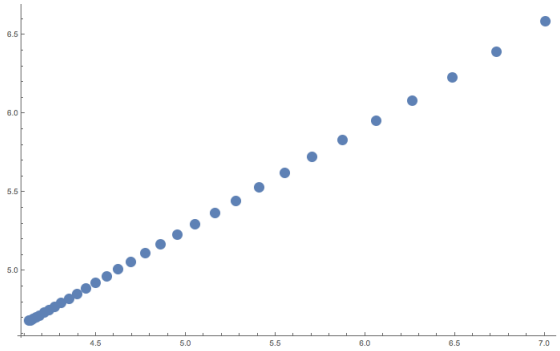

Figure 7.5: The close-up of the selected edge structure at ζ_B^+ contributing quantity $\delta\varepsilon_R(u)$ to the energy density in (7.38).

exponent localized at the edge of the cut ζ_B multiplied by power-like contribution from the cut itself and some piece regular at the origin[13]

$$\delta\varepsilon_R(u) \sim Ce^{-i\zeta_B/u}u^\alpha w(u), \text{ with } \alpha,\ C \in \mathbb{C}. \tag{7.39}$$

The justification to this assertion was found to some extent *a posteriori*, as it is not at all obvious what is the actual structure of the cut. Nevertheless if one assumes as a first guess the cuts to be power-like branch points located at $\zeta_B^\pm$, then indeed one finds a similar asymptotics as above. It should be stressed however, that in general the Borel transform may be any singular function, and that simple trials with power-like cuts $(\zeta_B^\pm - \zeta)^\gamma$ did not reproduce the observed pattern of poles in a satisfactory way. Let us now determine complex number α in the Ansatz above. The power of u can be isolated by suitably differentiating logarithm of $\delta\varepsilon_B(1/u)$:

$$\log(\delta\varepsilon_B(1/u)) = \tilde{C} - i\zeta/u - \alpha\log(u) + \log(w(1/u)), \tag{7.40}$$

[13]The function $w(u)$ must start as $1 + Au + \ldots$, because we have extracted the leading common power u^α of the whole contribution.

so that

$$\frac{d^2}{dv^2}\log(\delta\varepsilon_B(1/v)) \sim \alpha u^2 + \beta u^3 + o(u^{-3}), \text{ with some } \beta \in \mathbb{C}. \tag{7.41}$$

The double derivative in the inverse of u liquidated the normalization and the exponent containing $1/u$, leaving just the pieces including α and derivative of the regular function $w(u)$. Ultimately we are only interested in small u, so we have expanded the latter term, which gave the part containing u^3. Finally to determine α the obtained expression should be compared to the integral carried out over the selected poles in the Fig. 7.5, which essentially reduces to the sum over the corresponding residues. We therefore have to compute[14]

$$\delta\varepsilon_R(u) = \int_\Gamma d\zeta e^{-\zeta/u}\tilde{\varepsilon}_B(\zeta) \sim 2\pi i \sum_{\zeta_i\in\Gamma} \text{Res} e^{-\zeta/u}\tilde{\varepsilon}_B(\zeta) \tag{7.42}$$

The sum over the residues can be performed swiftly with the aid of the de l'Hospital rule, which allows one to compute the whole required expression at once. We can therefore recast the result in a form suitable for comparison with our Ansatz (7.39) by explicitly factoring out the leading exponent. We then get

$$\delta\varepsilon_R(u) \sim Ce^{-\zeta_B^+/u} \sum_{\zeta_i\in\Gamma} e^{-(\zeta_B^+-\zeta_i)/u}\frac{n(\zeta_i)}{d'(\zeta_i)}, \tag{7.43}$$

where $n(\zeta)$ and $d(\zeta)$ are the numerator and denominator of the Borel-Padé energy density (7.35).

By applying derivatives as in (7.41) we should expect the above expression to yield for small u a polynomial starting as u^2 with subleading term of u^3. The desired power α can be then obtained by fitting (7.41) to the similar expansion of (7.43). The result is

$$\tilde{\alpha} = 1.0284 - 0.3461i. \tag{7.44}$$

To present the complete leading order contribution of the cut we need to reinstate the original variable $\tau = u^{-3/2}$, after which we arrive at

$$\delta\varepsilon_R(\tau) \sim \tau^{\alpha_B} e^{-\zeta_B^+\tau^{\frac{2}{3}}}, \tag{7.45}$$

with

$$\zeta_B^+ = 4.120 + 4.678i \text{ and } \alpha_B = -1.5426 + 0.5192i. \tag{7.46}$$

This is the major result of this paragraph, let us thus recapitulate the facts and findings. We have found, that the energy density series $\varepsilon(\tau)$ is an asymptotic expansion approximately valid only for a very large proper time $\tau \to \infty$. Nevertheless it seems to admit a unique resummation, at least as far as we could have investigated its Borel plane analytic structure. It revealed an existence of singularities, which explains asymptotic nature of the hydrodynamic gradient expansion. Its resummation however is not entirely unique, due to the many inequivalent ways in which we can carry out the Laplace transform in (7.37). We should therefore understand, what is the physical reason behind this phenomenon. We have found, that the difference between two resummation trajectories is proportional to exponentially suppressed term multiplied by power tail. This type of contribution is notorious in the realm of perturbative calculus and resembles the instanton effects. Instantons are manifestation of additional hidden degrees of freedom in the system, which were excised

[14] We use the proportionality sign $\sim$ to indicate the approximation of the cut through the poles.

by the perturbative analysis. We should thus expect some deeper explanation of all of the described effects, and indeed it is found in the following paragraphs by considering general possible contributions to the overall energy density $\varepsilon(\tau)$.

As the last remark in this section we should explain why we do not carry out the explicit resummation, but instead stop short of displaying the contribution $\delta\varepsilon_R(u)$. The point is that the major drawback of directly taking the integral leading to $\varepsilon_R(u)$ is that the result we found did not satisfy the proper asymptotics at $\tau = 0$. We have argued in Chapter 6 following [Beuf 2009], that at small proper times the energy density should be a function of only even powers of the proper time:

$$\varepsilon(\tau) \sim \sum_{n=0}^{M} \varepsilon_{2n}\tau^{2n} \text{ for } \tau \sim 0. \tag{7.47}$$

It was not possible to implement the above correct asymptotics with the Borel-Padé analytic continuation used in the Laplace transform (7.37). Moreover a deeper problem, which will be unravelled in the next section, is that in fact we have only accessed a fraction of the whole analytic structure of the Borel transform $\varepsilon_B(\zeta)$. First of all its knowledge was limited by the numerical accuracy (as can witnessed by looking at the Padé poles graph 7.3), but more importantly there are actually infinitely many more singularities (leading to cuts), which are difficult to reach in the present approach, and whose existence will be revealed in the next paragraph. Taking these facts into account we shall not make an attempt at presenting the resummed energy density, which might be more feasible in the future with more information about $\varepsilon_B(\zeta)$ available.

7.3 Quasi-normal modes on dynamic background

We would like now to give physical interpretation of the Borel plane poles and the associated complex numbers $\zeta_B^{\pm}$ and α, as well to the whole exponentially suppressed contribution $\delta\varepsilon_R(\tau)$.

The interpretation of these effects is primarily provided by the study of quasi-normal modes, which we encountered before in Chapter 5. We recall, that these are small but arbitrarily rapid perturbations of static black brane geometry, as opposed to the long wavelength non-linear solutions giving raise to hydrodynamics, as was discussed before. In the presence of a horizon such a linearised field equations induce exponentially decaying solutions, reflecting the dissipative nature of the horizon and dual holographic viscous fluid. Thus one can inject such a contribution to energy density by perturbing static black brane and observing its return to local equilibrium. This mechanism is well known and has been analysed mostly for static geometries with temporal Killing vectors.

The solution we study is however dynamical, i.e. time dependent. Fortunately also in this case there is already certain insight [Janik 2006b] developed in the boost-invariant perfect fluid system, which can be extended to include viscosity. We shall exploit this approach in what follows.

To see how exponentially decaying energy density contribution can emerge in the fully *dynamical* spacetime of the paragraph above we should derive equations of motion in this background being already compatible with hydrodynamics to the given viscosity order. On general grounds we expect that a static black brane background[15] $G_{AB}^{(\text{stat})}$ with perturbation of the form

$$G_{AB}(t,r) = G_{AB}^{(\text{stat})}(r) + h_{AB}(t,r) \sim G_{AB}^{(\text{stat})}(r) + f_{AB}(r;\omega)e^{-it\omega}, \tag{7.48}$$

[15] Which is dual to a thermal fluid at rest, i.e. (3.51).

with purely dumped quasi-normal spectrum

$$\omega_n \in \mathbb{C} \text{ and } \mathfrak{Im}(\omega_n) < 0,\ n \in \mathbb{N} \tag{7.49}$$

would holographically yield constant underlying energy density ε_0 with decaying contribution on the top of it,

$$\varepsilon(t) \sim \varepsilon_0 + \delta\varepsilon(t) \sim \varepsilon_0 + \varepsilon_1 e^{-it\omega_n}. \tag{7.50}$$

To understand quick perturbations of dynamic backgrounds we need to adapt the above static method to the analytically known spacetimes dual to viscous fluids. The way to proceed will be thus to consider a linearisation on the top of zero-th and first order dynamic geometries. This task however is not straightforward, because partial differential equation for the perturbation is no longer guaranteed to separate in time-dependent setting. Moreover, as is well known there are several possible perturbation channels corresponding to which metric tensor components get excited. Obtaining a closed decoupled equation for the given sector might therefore be a challenging task, but it will turn out to be possible.

We are therefore motivated to analyse the following Ansatz for perturbation of dynamic fluid background (7.8) based on expansions (7.9)

$$\begin{aligned} A(\tau,r) &= A^{\text{Hydro}} + \varepsilon\delta A(t,r), \\ B(\tau,r) &= B^{\text{Hydro}} + \varepsilon\delta B(t,r), \\ \Sigma(\tau,r) &= \Sigma^{\text{Hydro}} + \varepsilon\delta\Sigma(t,r), \end{aligned} \tag{7.51}$$

where the label *Hydro* indicates part of the series (7.9) defining hydrodynamic background of the chosen order.

Given such a rather complicated expression for metric fields one may wonder weather the resulting equations, even linearised, will be tractable. It is known, that general perturbations of the tensor field give raise to different coupled dynamical channels, which reflect these encountered in hydrodynamics (see Chapter 2). To understand better what happens let us consider the following class of perturbations, the rationale for which will be given in a moment. We form products of exponential term similar to the static case with another gradient expansion independent from the basic one in (7.51):

$$\begin{aligned} \delta A(\tau,r) &= e^{-i\int \omega_0\tau^{-1/3}+\omega_1\tau^{-1}+\dots} \times \left[\delta A_0(v) + \frac{1}{\tau^{2/3}}\delta A_1(v) + \dots\right], \\ \delta B(\tau,r) &= e^{-i\int \omega_0\tau^{-1/3}+\omega_1\tau^{-1}+\dots} \times \left[\delta B_0(v) + \frac{1}{\tau^{2/3}}\delta B_1(v) + \dots\right], \\ \delta \Sigma(\tau,r) &= e^{-i\int \omega_0\tau^{-1/3}+\omega_1\tau^{-1}+\dots} \times \left[\delta \Sigma_0(v) + \frac{1}{\tau^{2/3}}\delta \Sigma_1(v) + \dots\right]. \end{aligned} \tag{7.52}$$

The above combinations contain an essentially non-perturbative component, the exponential which vanishes at large time and does not posses gradient expansion. It is the quasi-normal part of the Ansatz, and it is followed by a standard fluid-gravity expansion. The numbers ω_i are to be determined and their origin will be explained shortly. It is clear, that any such component of a full non-linear metric would disappear during late time gradient expansion. Considering such fluctuations we aim at understanding physics of the sector excised by hydrodynamic approximation. The structure of equations allows us to isolate this part, because upon linearisation it is proportional to the exponential factor.

The above scheme of perturbations was motivated by the work of [Janik 2006b], where it was found that wave equation for a scalar $\phi(\tau,z)$ in perfect fluid background separates $\phi(\tau,z) = \varphi(\tau)f(v)$ and has solutions, which at large proper time behave as

$$\varphi(\tau) \sim e^{-i\int d\tau\omega\pi T(\tau)}. \tag{7.53}$$

The integrand $T(\tau)$ is the local temperature of the evolving perfect fluid, $T(\tau) \sim \Lambda_0/\tau^{1/3}$ and ω indicates the lowest non-hydrodynamic scalar quasi-normal mode of a *static* black brane.

The first connection to our computation is that perturbations (7.51), (7.52) also happen to reduce in the late time regime to a massless scalar wave equation for $\delta B(\tau, r)$, similar to the case found in [Janik 2006b], where this occurred for a metric component $h^{h_1}_{x_2}$. This is highly non-trivial, since it requires decoupling of the various elements in (7.52), which is made possible due to the linearisation and late time expansion.

The second connection is based on the fact, that the exponent in (7.53) contains an integral of the local temperature of the fluid. Since *a priori* we are interested in higher orders than just perfect fluid, we should generalize $T(\tau)$ to include also viscous contributions (see (6.70)):

$$T(\tau) \sim \varepsilon(\tau)^{\frac{1}{4}} \sim \frac{\Lambda_0}{\tau^{1/3}} + \frac{\Lambda_1}{\tau} + \frac{\Lambda_2}{\tau^{5/3}} + \dots \tag{7.54}$$

At this point it becomes apparent, that the structure emerging from the Ansatz (7.52) closely resembles the contribution to energy density, that we found during resummation. First two terms of the exponent give an expression

$$\tau^{-i\omega_1} e^{-i\frac{2}{3}\omega_0 \tau^{2/3}}, \tag{7.55}$$

which has exactly the functional form of (7.45). It is therefore a strong indication, that we are on the right track to identify the origins of the resummation ambiguity directly with the quasinormal modes over the expansing boost-invariant background. Viscous background may alter the values present in the original temperature expansion and in a sense dress them through the non-equilibrium evolution. We therefore replace the constants Λ_i in favour of the unknown ω_i, which should be determined by solving the equations for the fields $\delta A_i(v)$, $\delta B_i(v)$ and $\delta\Sigma_i(v)$.

Let us have a closer look at how the reduction to scalar equation occurs in our case. First we refine an Ansatz. For the hydrodynamic part we substitute the known solution (here for brevity up to the first viscous order),

$$\begin{aligned}
A^{\text{Hydro}}(\tau, r) &= r^2(A_0(r\tau^{1/3}) + \frac{1}{\tau^{2/3}} A_1(r\tau^{1/3}) + \dots), \\
B^{\text{Hydro}}(\tau, r) &= \frac{2}{3}\ln(\frac{r}{1+rt}) + \frac{1}{3} d_{\text{Hydro}}(\tau, t) - \frac{1}{2} b_{\text{Hydro}}(\tau, t) \\
\Sigma^{\text{Hydro}}(\tau, r) &= r^{2/3}(1+rt)^{1/3} e^{1/3 d_{\text{Hydro}}(\tau, r)}, \\
b_{\text{Hydro}}(\tau, r) &= \frac{1}{\tau^{2/3}} b_1(r\tau^{1/3}) + \dots, \\
d_{\text{Hydro}}(\tau, r) &= \frac{1}{\tau^{2/3}} d_1(r\tau^{1/3}) + \dots,
\end{aligned} \tag{7.56}$$

All the fields above come from the analytic solution of [Heller 2009]. For the non-equilibrium part we take

$$\begin{aligned}
\delta A(\tau, r) &= r^2 g(\tau)(\delta A_0(r\tau^{1/3}) + \frac{1}{\tau^{2/3}} \delta A_1(r\tau^{1/3}) + \dots), \\
\delta B(\tau, r) &= g(\tau)(\delta B_0(r\tau^{1/3}) + \frac{1}{\tau^{2/3}} \delta B_1(r\tau^{1/3}) + \dots), \\
\delta\Sigma(\tau, r) &= r^{2/3}(1+r\tau)^{1/3} g(\tau)(\delta\Sigma_0(r\tau^{1/3}) + \frac{1}{\tau^{2/3}} \delta\Sigma_1(r\tau^{1/3}) + \dots).
\end{aligned} \tag{7.57}$$

with the non-analytic exponent

$$g(\tau) = \tau^{\alpha} e^{-i\int d\tau \omega_0 \tau^{-1/3} + \omega_2 \tau^{-5/3} + \dots}. \tag{7.58}$$

As was discussed above the prefactor τ^{α} comes from integrating the term $-i\omega_1/\tau$ in the exponent, which results in a logarithm. Note, that for the second expansion in (7.57) we take just another general fluid-gravity expansion series, to be determined by the numerics, and not the knowns solution of 7.56.

The next step is to evaluate Einstein equations on the metric (7.8) with the substitution (7.51) and subsequently linearise the small δ-terms.

At first we confirmed, that the hydrodynamic part satisfies the equations up to first order in gradients. Further, the equations for the leading perturbations $\delta A_0(v)$, $\delta B_0(v)$ and $\delta\Sigma_0(v)$ are obtained by excluding the overall exponential part $g(\tau)$ from the linearised Einstein tensor, and by taking the large proper time scaling limit keeping $v = r\tau^{1/3}$ fixed. The outcome is a set of three ordinary differential equations, which admits solutions

$$\delta A_0(v) = 0,\ \delta\Sigma_0(v) = 0. \tag{7.59}$$

The third remaining equation for $\delta B_0(v)$ turns out to be parametrized by the number ω_0 from the non-analytic exponent $g(\tau)$ (7.58)

$$v^2 A_0(v)\delta B_0''(v) + \delta B_0'(v)\left(v^2 A_0'(v) + 5vA_0(v) - 2i\omega_0\right) - \frac{3i\omega_0}{v}\delta B_0(v) = 0. \tag{7.60}$$

This equation turns out to coincide with the equation for a scalar field quasi-normal mode in a *static* black brane background. This surprising occurrence is however reminiscent of a familiar phenomenon reported first in [Janik 2006b]. We shall soon see how our current investigation extends this finding, which will turn out to be very useful, and contribute to our physical understanding of resummation ambiguity.

Let us now investigate what happens at first viscous order by obtaining equations for $\delta A_1(v)$, $\delta B_1(v)$ and $\delta\Sigma_1(v)$.

First we observe, that the equation for $\Sigma_1(v)$ decouples and is determined solely in terms of the presumably known at this stage lower order and background fields:

$$\delta\Sigma_1''(v) + \frac{2\delta\Sigma_1'(v)}{v} = \frac{1}{2}b_1'(v)\delta B_0'(v) - \frac{1}{3}d_1'(v)\delta B_0'(v) - \frac{2\delta B_0'(v)}{3v^2}. \tag{7.61}$$

Therefore we can focus just on $\delta A_1(v)$ and $\delta B_1(v)$. It follows that remaining equations can be solved for $\delta A_1(v)$, $\delta A_1'(v)$ and $\delta A_1''(v)$ in a way, which upon compilation allows us to eliminate them completely (keeping $\delta\Sigma_1(v)$ away), and form one last equation for the function $\delta B_1(v)$ alone. This leads to

$$\begin{aligned}
&3v^2(v^2 A_0(v)\delta B_1''(v) + \delta B_1'(v)\left(v^2 A_0'(v) + 5vA_0(v) - 2i\omega_0\right) - \frac{3i\omega_0}{v}\delta B_1(v)) = \\
&3i\delta B_0(v)(v^2\omega_0 d_1'(v) + v\omega_0 d_1(v) + 3i\alpha v - \omega_0) - v^2(v\delta B_0''(v)(vA_0(v)d_1(v) + 3vA_1(v) + 2) \\
&+ \delta B_0'(v)(6\alpha + v^2 d_1(v)A_0'(v) + A_0(v)(3v^2 d_1'(v) + 5vd_1(v) - 3))) \\
&- v^2\delta B_0'(v)(3v^2 A_1'(v) + 15vA_1(v) - 2i\omega_0 d_1(v) + 8)
\end{aligned} \tag{7.62}$$

The above points allow us to argue, that we can from this moment on focus just on computing the function $B(\tau, r)$, and ignore $A(\tau, r)$, $\Sigma(\tau, r)$ completely in our considerations. The reasons are that we are interested in computing the contribution to energy density from the leading exponentially suppressed corrections in (7.56) and (7.57). In view of (7.59) we see, that there will be no input from δA and $\delta\Sigma$ at the leading order. Moreover, due to the

linearisation and decoupling discussed above, the impact of the first order terms δA_1, $\delta\Sigma_1$ on δB_1 will be also absent. Therefore we can confine out attention to δB alone.

The long expression (7.62) has been put forth to show explicitly the structure of the equation, including a source, which depends only on the lower order fields, hydrodynamic background components, ω_0 and additionally α. The kinematic part has exactly the same structure as the lower order counterpart (7.60). In the above, ω_0 is understood as being already determined by the preceding equation, and this time we should be looking for the value of α.

Coming back to the remark made below (7.60), an important observation, that we can now make having the above equations for δB_0 and δB_1 is that they can be identified with large time gradient expansion of a free massless scalar field carrying no transverse momentum, propagating over first order *hydrodynamic* background. It is derived by considering an Ansatz

$$\phi(\tau,r)=g(\tau)(\phi_0(r\tau^{1/3})+\frac{1}{\tau^{2/3}}\phi_1(r\tau^{1/3})+\frac{1}{\tau^{4/3}}\phi_2(r\tau^{1/3})+\ldots), \tag{7.63}$$

and substituting it to

$$\frac{1}{\sqrt{-G^{\rm Hydro}}}\partial^A(\sqrt{-G^{\rm Hydro}}G^{\rm Hydro}_{AB}\partial^B\phi(\tau,z))=0. \tag{7.64}$$

Both our equations can be identified by expanding the above in large τ while keeping $v=r\tau^{1/3}$ fixed. With $u=\tau^{-2/3}$ the term of the order u^0 gives equation identical to (7.60) and subsequently at the order u^1 we recover (7.62), provided we change all the labels B to ϕ. We have therefore reached a result similar to the one in [Janik 2006b], where analogous reduction emerges for the off-diagonal metric component $h^{x_1}_{x_2}$.

Why do we emphasize formal similarity of the tensorial perturbation to the scalar one? It is due to the fact, that under equivalent boundary conditions these equations will determine exactly the same spectrum for ω_0 and α (at zero transverse momentum). We expect therefore for ω_0 the well known value from the static black brane analysis.

7.3.1 Scalar wave equation boundary conditions

Having found the connection to scalar field on a dynamic background we can start searching for appropriate boundary conditions for the numerics, which due to this finding is a simpler task, than for a tensor field. This computation is canonical in AdS/CFT correspondence, and resembles the similar analysis of Chapter 5, but it is nevertheless not identical to the standard static case and we will report it here for the sake of explaining how boundary conditions are arrived at.

The derived equations are eigenvalue problems, which must be solved numerically on a compact domain

$$\frac{1}{v}=z\in[0,1], \tag{7.65}$$

where the AdS_5 conformal boundary is located at $z=0$, while the superficial dynamic black brane horizon has been localised at $z=1$. This property has been already emphasised below equation (7.11). In order to obtain spectrum and stable solutions decaying with time we must enforce appropriate boundary conditions both at the horizon and at the boundary. To derive them for $\delta B_0(z)$ and $\delta B_1(z)$ we should analyse behaviour of the corresponding differential equations (7.60) and (7.62) near $z=0$ and $z=1$. We must do this order by order, i.e. first derive the conditions on $\delta B_0(z)$, because these need to be inserted to the equation for $\delta B_1(z)$.

Let us concentrate on the boundary $z = 0$. This is a singular point of the evolution equation, and as such determines characteristic exponents for the associated boundary solutions. To find them we substitute

$$\delta B_0(z) \sim z^{\Delta_B} \tag{7.66}$$

to (7.60), and expand around $z = 0$ to the leading order. This yields solutions

$$\Delta_B = 0, \ \Delta_B = 4. \tag{7.67}$$

The above result is independent of any details inside the spacetime and is as we said canonical in the correspondence: we are dealing with a massless real scalar field in dimension $d + 1 = 5$, therefore we should get one scaling dimension Δ_B equal to zero, and one to the boundary theory dimension $d = 4$. The physical requirement we impose on fields in AdS_5 is that the solutions are normalizable, hence we must select $\Delta_B = 4$, which guarantees rapid vanishing of the solution at the boundary (see [Kovtun 2005] for applications to quasi-normal modes problems).

Proceeding to the horizon analysis we are focusing on the region $z \sim 1$, which is also the locus of the equation singularity. We expect therefore again a characteristic scaling at the horizon:

$$\delta B_0(z) \sim (1 - z)^{\Delta_H}. \tag{7.68}$$

The result is

$$\Delta_H = 0, \ \Delta_H = \frac{i\omega_0}{2}. \tag{7.69}$$

Owing to the regularity of the Eddington-Finkelstein coordinates at the horizon one of the solutions converges simply to a constant, while the other one has a non-analytic structure[16] near $z \sim 1$. The regular solution corresponds to the ingoing waves entering the horizon. We therefore choose $\Delta_H = 0$, which combined with the mentioned earlier linearity of the equations allows us to fix $\delta B_0(1) = 1$. These condition imposed at the differential equation (7.60) will lead to a normalizable (in AdS_5) solution with a discrete complex spectrum (since of course we are dealing with a non-self-adjoint operator).

We can now proceed to the subleading order equation, which should determine the values of α. The analysis parallels exactly the one above, with the physical restriction, that we need to use the appropriate exponents for $\delta B_0(z)$ in the corresponding equation expansions (this represents the chosen boundary conditions for the lower order field). With this condition we reach exactly the same scaling dimensions as before, $\Delta_B = 4$ at the boundary (the source vanishes there) and $\Delta_H = 0$ at the horizon. We thus again have a constant solution at $z = 1$. There is however a subtlety related to this concerning numerical integration. It turns out, that the particular value of $\delta B_1(1)$ does not affect the determination of the power α. As long as we use proper expression for $\delta B_0(z)$ the resulting solution vanishing at the boundary leads always to the same value of α regardless of the choice of $\delta B_1(1)$. We therefore set it to zero.

7.3.2 Numerical integration of the eigenvalue problems

With boundary conditions determined we can integrate the corresponding equations numerically, which should lead to an infinite set of complex eigenvalues. We shall be

[16] It should be emphasized that we use Eddington-Finkelstein coordinates associated with ingoing null geodesics choice (this is determined by the sign of the $d\tau dz$ term in the metric). There is a dual map based on the outgoing rays, which would render the physical solution non-analytic.

interested only in the first smallest values of ω_0 and α, since these should correspond to the least damped and therefore longest lived contributions to the hydrodynamical energy density read-off holographically from (7.51).

Numerical integration for the eigenvalue problem is performed in both cases using shooting method based on the horizon $z = 1$ and aiming at reaching a vanishing Dirichlet condition at $z = 0$. The boundary conditions are also of Neumann type and are imposed for both function and its first derivative at the horizon. These in turn are parametrized by the complex numbers ω_0, α determined whenever the resulting solutions obey the Dirichlet condition at the boundary. The parametrization of the Neumann condition by the yet-unknown eigenvalues is derived by finding power series local solutions to both equations near the horizon and isolating first order term for each function. More precisely we consider expansions

$$\delta B_0(z) = 1 + \delta B_0'(1)(1-z) + \dots, \ \delta B_1(z) = C_B + \delta B_1'(1)(1-z) + \dots. \tag{7.70}$$

Substitution to (7.60) and (7.62) leads to solutions for the coefficients defining Neumann boundary conditions

$$\delta B_0'(1) = \frac{3\omega_0}{2(\omega_0+2i)}, \ \delta B_1'(1) = \frac{-12\alpha + \omega_0(6C_B(\omega_0+2i)+\omega_0+4i)}{4(\omega_0+2i)^2}. \tag{7.71}$$

As was discussed above we put the horizon value for $\delta B_1(1)$ to zero in the actual computation, so we set $C_B = 0$.

At this point we can start searching for eigenvalues. First one has to find ω_0, and then with its aid α. The algorithm starts by choosing an initial guess for ω_0 and inserting it to (7.71). Then the equation is numerically integrated by the same spectral methods, that were used for solving (7.19). Upon integration we check if the solution vanishes at the boundary. If not we iteratively scan the neighbourhood of the initial guess by altering it by a small amount (in two dimensions, for real an imaginary parts of the complex eigenvalues) until the value of the integrated function reaches zero at the boundary $z = 0$ with sufficient accuracy. At this point we declare the proposed eigenvalue to be the correct one. Having obtained ω_0 we repeat the procedure for α in the very same way.

The indication for the value with which to start the search for ω_0 is provided by the similarity of our equation to the free scalar evolution, which was emphasised before. We simply start from the value for the static black brane, $\tilde{\omega}_0 = 3.119451 - 2.746675i$. This guess immediately leads to a stable solution, confirming that this is indeed the correct value for ω_0.

Let us see what it means from the perspective of the general form of our solution. By referring to (7.57), (7.58) we expect to have the following structure in the leading exponent:

$$\delta B(\tau, r) \sim e^{-i\frac{3}{2}\omega_0 \tau^{2/3}}. \tag{7.72}$$

The value we found numerically leads then (up to the computational accuracy) to the overall exponent factor

$$-i\frac{3}{2}\omega_0 = -4.12001 - 4.67918i \equiv \zeta_B^+. \tag{7.73}$$

Apparently we have obtained precisely the value found previously from energy density resummation. This is rather intriguing result. However in our case to establish a definite link of the bulk geometry linear fluctuation to the energy density perturbation we need to translate the impact of $\delta B(\tau, r)$ on the holographic value of $\varepsilon(\tau)$. We shall focus on this task below upon finding the remaining variable α.

In view of the above result we are motivated to use α_B of (7.46) as a guide on where to start the numerical search for α itself. Beginning with $\tilde{\alpha} \sim 0.5 + 0.5i$ we indeed reach a stable solution of $\alpha = 0.4577792 + 0.519908i$. This time however the result seems to be in discrepancy with the value encountered during resummation.

The resolution of this superficial clash comes from two sources and is bound to the proper use of holographic renormalisation, which is necessary to translate the contribution of $\delta B(\tau, r)$ to the energy density, as we have signalled above.

Let us first derive the general structure of the holographic expansion relating metric component $B(\tau, r)$ with the boundary stress-energy tensor. Recall from (7.8) that in the initial coordinates $\{\tau, r\}$ the component $B(\tau, r)$ can be phrased as a combination of the general metric tensor components as

$$B(\tau, r) = \frac{1}{3} \ln \frac{g_{xx}(\tau, r)}{g_{yy}(\tau, r)}. \tag{7.74}$$

Following [Kinoshita 2009] we know, that the generic near-boundary expansion of the metric components is given by

$$\begin{aligned} g_{yy}(\tau, r) &= r^2((\tau + \frac{1}{r})^2 + \frac{\tau^2(\varepsilon(\tau) + \frac{3}{4}\tau\partial_\tau\varepsilon(\tau))}{r^4} + o(\frac{1}{r^4})) \\ g_{xx}(\tau, r) &= r^2(1 - \frac{\varepsilon(\tau) + \frac{3}{4}\tau\partial_\tau\varepsilon(\tau)}{2r^4} + o(\frac{1}{r^4})) \end{aligned} \tag{7.75}$$

This is yet another incarnation of the holographic expansion (3.50) encoding relation between the metric tensor and the boundary energy-momentum operator expectation value $\varepsilon(\tau) = \langle \hat{T}_{00}(\tau) \rangle$. To extract energy density contribution of the perturbation $\delta B(\tau, r)$ alone we need to take a closer look at the structure of the $B(\tau, r)$ series Ansatz (7.9) and (7.51)

$$B(\tau, r) = \frac{2}{3} \ln \frac{r}{1 + rt} + B_{\text{Hydro}}(\tau, r) + \delta B(\tau, r). \tag{7.76}$$

It is apparent, that to use the above in (7.74) with (7.75) we we should remove the leading non-dynamical logarithm, which is just a part of the underlying empty AdS construction basis. We then arrive in the near-boundary limit $r \sim \infty$ at

$$B_{\text{Hydro}}(\tau, r) + \delta B(\tau, r) = \frac{1}{3} \ln \frac{g_{xx}(\tau, r)}{g_{yy}(\tau, r)} - \frac{2}{3} \ln \frac{r}{1 + rt} \sim -\frac{1}{2} \frac{\varepsilon(\tau) + \frac{3}{4}\tau\partial_\tau\varepsilon(\tau)}{r^4}. \tag{7.77}$$

The above result is linear in energy density, which now can be split into the background hydrodynamical and non-equilibrium parts, $\varepsilon(\tau) = \varepsilon_{\text{Hydro}}(\tau) + \delta\varepsilon_{\delta B}(\tau)$. This shows, that for the sake of isolating the contribution of the non-analytic perturbation $\delta B(\tau, r)$ we can ignore the hydrodynamic contribution of $B_{\text{Hydro}}(\tau, r)$ altogether and focus just on $\delta\varepsilon_{\delta B}(\tau)$ in what follows:

$$\frac{1}{2} \frac{\delta\varepsilon_{\delta B}(\tau) + \frac{3}{4}\tau\partial_\tau\delta\varepsilon_{\delta B}(\tau)}{r^4} \sim -\frac{1}{r^4} \frac{\partial^4}{\partial_{(1/r)^4}} \delta B(\tau, r), \ r \sim \infty. \tag{7.78}$$

This formula tells us, that to find energy density perturbation induced by the corresponding geometry perturbation in the bulk one has to expand the relevant metric component near $r \to \infty$ and retain only the r^{-4} term. Subsequently one has to solve the above first order differential equation for $\delta\varepsilon_{\delta B}(\tau)$, which can be done in the late time approximation $\tau \to \infty$ relevant for hydrodynamics. The outcome is the ultimate result we are looking for.

Therefore to make use of (7.78) we need to compute the necessary near-boundary expansion of the solution for $\delta B(\tau, r)$, which we have obtained through numerical integration. Recall that our solution to the leading order in proper time τ has the form[17]

$$\delta B(\tau, r) = \tau^{\alpha} e^{-\frac{3}{2} i \omega_0 \tau^{2/3}} \delta B_0(\frac{1}{v}), \;\; v = r\tau^{1/3}. \tag{7.79}$$

It is important to realise, that above the subleading hydrodynamic series staring with $\delta B_0(\frac{1}{v})$ is obtained from numerics as a function in $z = 1/v$, not r. Therefore before using it in (7.78) we need to translate the solution and its spatial derivatives from the hydrodynamic scaling variable v to the standard AdS radius r. This amounts to saying

$$\frac{\partial^4}{\partial(1/r)^4} \delta B_0(\frac{1}{r\tau^{1/3}}) = \tau^{-4/3} \frac{\partial^4}{\partial(1/v)^4} \delta B_0(\frac{1}{v}), \tag{7.80}$$

and the equation we need to solve becomes

$$\delta\varepsilon_{\delta B}(\tau) + \frac{3}{4}\tau\partial_\tau \delta\varepsilon_{\delta B}(\tau) = -2C\tau^{\alpha - 4/3} e^{-\frac{3}{2} i \omega_0 \tau^{2/3}}, \tag{7.81}$$

with $C = \delta B_0^{(4)}(\infty)$. The large time asymptotics of the solution reads

$$\delta\varepsilon_{\delta B}(\tau) \sim \tau^{\alpha - 2} e^{-\frac{3}{2} i \omega_0 \tau^{2/3}}. \tag{7.82}$$

Inserting the previously found power α we arrive at the second number familiar from the resummation ambiguity computation (7.46):

$$\begin{aligned} \alpha - 2 &= 0.4577792 + 0.519908i - 2 \\ &= -1.54222 + 0.519908i, \\ \alpha_B &= -1.5426 + 0.5192i. \end{aligned} \tag{7.83}$$

With this result we conclude, that both complex numbers found as the resummation ambiguity parameters can be given particularly elegant physical interpretation. The same numbers are recovered during the well defined and known procedure of perturbing system undergoing slow hydrodynamic evolution with a small yet rapid fluctuation. The perturbation spreads quickly in the viscous expanding boost-invariant medium, decaying with the characteristic time scale set by the quasi-normal mode complex frequency ω_0, which in the dynamic fluid background obtains an additional multiplicative factor $3/2$ found in (7.73). The contribution to energy density $\varepsilon(\tau)$ induced by this perturbation exhibits the corresponding exponential decay $\delta\varepsilon_{\delta B}(\tau)$ towards hydrodynamic local equilibrium, and we observe that both its parameters, which we have computed in this paragraphs coincide with the resummation findings of $\delta\varepsilon_R(\tau)$ in (7.45).

This ultimately allows us to claim, that the origin of the Borel plane poles leading to the resummation riddles is physical and represents the emergence of degrees of freedom excised from hydrodynamical evolution in the course of gradient expansion. This is because any exponentially decaying component of the full energy density $\varepsilon(\tau)$ vanishes at late time $\tau \gg 0$. However remnants of such missing contributions emerge as the divergent nature of hydrodynamic expansion, and can be systematically recovered through the resummation procedure. Physically it is so, because very high orders in gradient expansion correspond to very high momenta, which seem to be asymptotically connected to fast perturbations of

[17] We will ignore the correction $\frac{1}{\tau^{2/3}} \delta B_1(\frac{1}{v})$, which was instrumental in finding α, but is subleading in proper time.

thermal medium. This beautiful picture shows, that the missing fast degrees of freedom are in fact not alien to hydrodynamics, but instead linger in the high orders of the expansion. This could intuitively be similar to the situation in effective pion model for QCD, where at sufficiently high energies we could expect to witness the emergence of quarks and gluons.

We can make now a comment on feasibility of a complete energy density resummation. From the above considerations it seems clear, that performing it in the most general form is out of reach using just perturbative hydrodynamics series. It is because black branes have not one or two, but infinitely many quasi-normal modes. One would need to know them in the first place and determining them from numerical Borel poles seems very challenging. Even worse, we expect these modes to interact at the non-linear level, so obtaining the energy density series must be fact more difficult, than for the one quasi-normal case. These are some of the technical reasons for which one can not for now think of reconstructing $\varepsilon(\tau)$.

Moreover the appearance of these additional quasi-normal modes would introduce further resummation ambiguities. Therefore to fully recover the actual non-equilibrium energy density which would be valid beyond hydrodynamic expansion and obey physical requirements (e.g. be real and positive) we would have to pour in additional information on how to deal with these ambiguities during resummation. The field of mathematics allowing to do this in a rigorous manner emerged only recently and is known as the resurgence theory [Marino 2014]. An elegant example of its application in hydrodynamic setting can be seen in [Heller 2015]. Even with this theory however we would need an infinite amount of information extracted from exact numerical solution in order to systematically resolve all the ambiguities.

What one therefore may hope for in practise is only a resummation of some finite number of quasi-normal modes up to certain accuracy, which would still be a significant improvement over standard hydrodynamics. We shall see this sort of improvement (although not by resummation) in the next chapter, where we manifestly include non-equilibrium mode in hydrodynamical description.

7.4 Closing remarks

Let us note however, that all these problems appear only when we try to resum all orders hydrodynamics from the four-dimensional point of view. In the five-dimensional picture, it is enough to solve the full Einstein equations numerically, as we did in the previous chapter, which encodes for us the dynamics of all those higher quasi-normal modes, hydrodynamic excitations, and their nonlinear interactions. This is however technically quite involved, so it is of interest to find an approximate four-dimensional formulation including both hydrodynamics as well as the least nonhydrodynamical degrees of freedom. We will discuss this in the following chapter.

Chapter 8

Generalized non-equilibrium hydrodynamics

8.1 Introduction

One of the major results presented in Chapter 6 concerned the discovery, that relativistic fluid may obey laws of hydrodynamics amid strong pressure anisotropy of the evolving medium. This development led to inception of a new term in heavy-ions realm known as the hydrodynamization and is related to the fact, that one may use hydrodynamics also in anisotropic stages of evolution canonically regarded as not yet thermalized. From the hydrodynamic gradient expansion perspective, e.g. (2.17), (2.19), it means that this approximation can be used even if the correction terms supposedly subleading to lower orders are in fact of sizeable comparable magnitude. Physically it means, that albeit facing strong gradients in the medium hydrodynamic evolution already holds. However it has its limitations. These become visible when we enter the earlier, genuinely non-equilibrium regime of plasma evolution. At this point global conservation laws leading to the hydrodynamic equations of motion cease to suffice and one requires actual short-lived dynamical degrees of freedom.

The goal of the present chapter is to introduce a scheme of generalizing hydrodynamics to incorporate precisely these new ingredients. We shall achieve this by coupling the conventional gradient expansion equations to new fluid field variables, representing non-equilibrium degrees of freedom found in the previous chapter, namely the quasi-normal modes. We will do so along the lines of our last paper [Heller 2014] considered in this Thesis, and concluding to some extent the research programme initiated in Chapter 5.

Parallel to the phenomenological motivation outlined above the driving idea behind derivations given below is to construct a holographically justified theory containing purely four-dimensional objects. That is, with applications completely outside string theory in mind it is desirable to have a model expressed in terms of standard field theory variables. Gravity would then serve as a source of limited number of phenomenological parameters inaccessible within the field theory itself due to e.g. strongly coupled dynamics. As we shall see it is possible to give such a formulation.

8.2 Excitation decay in thermal medium

To begin with, we should recall how near equilibrium dynamics is probed in thermal field theory [Kapusta 2006] and holography [Son 2002, Son 2007]. In the context of fluid dynamics the criterion for departure from local equilibrium is subtle as we have seen in Chapter 6, if we focus on the overall stress-energy tensor average. However a way to more directly discriminate between near and far from equilibrium phenomena is to employ linear response theory, which examines how locally equilibrated medium responds to small per-

turbations. Such fluctuations are represented by exponentially decaying oscillatory modes[1], like the ones found in resummation and originating from quasi-normal spectrum of the dual black brane. These modes directly correspond in AdS/CFT to singularities of retarded Green's function of the given operator excitation.

More precisely, the quasi-normal spectrum comprises of two sets of associated complex numbers $\omega(k)^{\pm} = \pm\omega_{\mathrm{R}}(k) - i\omega_{\mathrm{I}}(k)$, each of which defining momentum dependent excitation mode dispersion relation. For scalar operator $\hat{O}$ in field theory embodiment of this is the analytic structure of its thermal retarded real-time Green's function assuming the form

$$G_R^O(\omega, k) \sim \frac{Z(\omega, k)}{\Pi_{n=0}^{\infty}(\omega - \omega_n^+(k))(\omega - \omega_n^-(k))}, \tag{8.1}$$

where $Z(\omega, k)$ is a function containing residues[2], and we have an infinite set of isolated pairs of poles defining spectrum of thermal excitations given by the quasi-normal modes. Such a function encapsulates the linear response of the system to perturbations, which can result in gapped non-equilibrium modes (i.e. with $\omega(k = 0) \neq 0$) or hydrodynamical poles (with $\omega(k = 0) = 0$). Linear response theory makes use of such a Green's function in general formula of the form

$$\delta O(t, x) \sim \int \mathrm{d}\omega \mathrm{d}^3 k G_R^O(\omega, k) J_O(\omega, k), \tag{8.2}$$

with $J_O(\omega, k)$ being the small arbitrarily fast source inducing the perturbation in $\hat{O}$. If we focus on the gapped non-equilibrium mode, upon suitable contour integration the resulting behaviour of the excited observable is that oscillatory fluctuations decay towards local equilibrium, with time-scale of $1/\mathfrak{Im}(\omega(k))$, and oscillation wavelength is $\mathfrak{Re}(\omega(k))$. In our conformal $\mathcal{N} = 4$ super-Yang-Mills plasma the quasi-normal spectrum is proportional to the only scale available, the local fluid temperature T. Therefore typical re-equilibration time-frame is $O(1/T)$, which is compatible with customary values in hydrodynamic simulation codes, where initialization is performed with $T_0 = 500$ MeV and hydrodynamics onset proper time is $\tau_{\mathrm{H}} = 0.25$ fm, as we mentioned in Section 6.8.3, [Broniowski 2008]. This means we have $\tau_{\mathrm{H}} \sim 1/T$, which is on the par with our holographic model.

The leading idea of the work we are about to explain, is to explicitly capture the least damped non-equilibrium mode and couple it to the underlying hydrodynamical background. This phenomenologically means, that we focus on the smallest gapped pole of the thermal Green's function, which is the lowest gapped quasi-normal mode, and forge its impact into a new independent fluid field. This procedure can be carried out for the intermediate-to-late stage of the fluid evolution, where almost all the non-equilibrium oscillations have already died, except the least damped one with the smallest imaginary part. For the stress-energy tensor this is exactly the leading mode we have found in resummation. The corresponding operator excitation assumes then the following form

$$\langle \hat{O} \rangle \sim \int \mathrm{d}^3 k A(k) e^{-\omega_{\mathrm{I}}(k) T t} \cos(\omega_{\mathrm{R}}(k) T t + \vec{k} \cdot \vec{x} + \phi(k)). \tag{8.3}$$

The above structure can be understood as originating from momentum integration of (8.1) in (8.2) over the stable[3] lowest pair of the spectrum, containing the associated frequencies $\omega^{\pm}$, so imaginary part remains the same and leads to the suppressing exponential, while

[1] Of e.g. local temperature, or velocity fields.

[2] These impact e.g. lifetime of thermal quasi-particles.

[3] Stable in the sense of Chapter 5, where all imaginary parts had signs leading to decay, not exponential growth of the excitation.

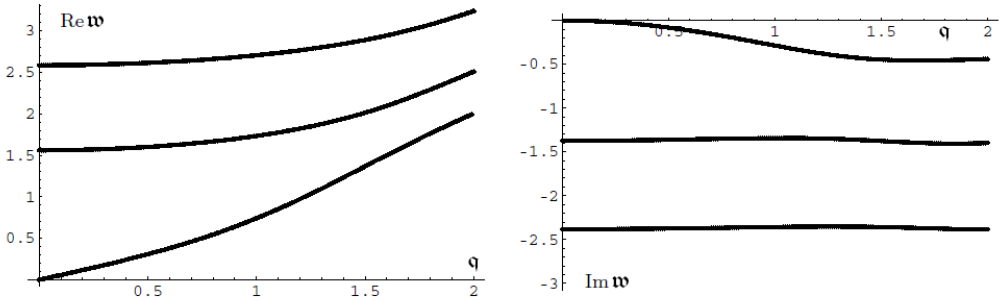

Figure 8.1: The first three sound channel quasi-normal modes $\omega(q)$, with real and imaginary parts displayed separately. The lowest mode represents the hydrodynamical excitation, which vanishes for $q \to 0$. We can readily see the difference in this regard exhibited by the weak dependence on the momentum of the non-hydrodynamical modes, especially for the imaginary part. This supports our assumption of ultralocality.

real parts get combined to form the cosine function upon integration over the poles in (8.2). The functions $A(k)$ and $\phi(k)$ encompass the perturbation initial data and characterise the shape of the decaying excitation. In the above we have also defined

$$\omega/T = \pm\omega_{\mathrm{R}}(k/T) + i\omega_{\mathrm{I}}(k/T). \tag{8.4}$$

8.3 Evolution equations for non-equilibrium modes

The formula (8.3) can be though of a solution to some linear partial differential equation, defining the dispersion relation (8.4). Generically the numerical value and momentum dependence of the Green's function pole like this one is encoded in the given theory's microscopic dynamics. In the case of our strongly coupled theory with gravity dual it is provided to us by the black brane fluctuations, which exhibit intriguing dependence on the momentum, $\omega = \omega(k)$, such that the non-equilibrium quasi-normal mode is almost independent of it up to the scale $k \sim 2\pi T$. This behaviour can be observed in Figure 8.1, reproduced from [Kovtun 2005]. Therefore in the near-equilibrium regime, where typical fluctuation momenta involved are small by assumption, one can regard frequency to be momentum independent. Apparently this important feature has not been widely appreciated before our work, and we shall refer to it as ultralocality.

Based on this crucial fact we can observe, that the function $\langle\hat{O}(t,\vec{x})\rangle$ of (8.3) obeys a specific damped oscillator equation, for every spatial position[4] $\vec{x}$:

$$\left(\frac{1}{T}\frac{\partial}{\partial t}\right)^2\langle\hat{O}\rangle + 2\omega_{\mathrm{I}}\frac{1}{T}\frac{\partial}{\partial t}\langle\hat{O}\rangle + |\omega|^2\langle\hat{O}\rangle = 0, \text{ with } |\omega|^2 = \omega_{\mathrm{R}}^2 + \omega_{\mathrm{I}}^2. \tag{8.5}$$

For a scalar operator $\hat{O} = \mathrm{Tr}F^2$ in $\mathcal{N} = 4$ SYM zero momentum value of the complex frequency is

$$\omega \sim 9.800 + i8.629 \tag{8.6}$$

The above equation is of second order in time, therefore as opposed to the conservation laws it is truly dynamical and may contains wave-like behaviour.

[4] Being manifestation of the said ultralocality. Otherwise it would be the PDE mentioned a moment ago.

The key point of interest in our endeavour to generalize hydrodynamics is an analogue of equation (8.5) for the stress-energy tensor. We recall from Chapter 2, that once fast phenomena pass away in the medium, the structure of the prevailing thermal stress average can be parametrized by the reduced thermodynamic limit fluid variables. This imposes on the late time expectation value the following constitutive relation decomposition:

$$\langle T^{\mu\nu}\rangle = \mathcal{E}u^\mu u^\nu + \mathcal{P}(\mathcal{E})(\eta^{\mu\nu} + u^\mu u^\nu) + \Pi^{\mu\nu}. \tag{8.7}$$

The velocity field is temporal, $u_\mu u^\mu = -1$ and the symmetric tensor $\Pi^{\mu\nu}$ is subject to Landau frame condition, as we discussed in Chapter 2: $u_\mu \Pi^{\mu\nu} = 0$. Moreover conformality imposes equation of state, $\mathcal{E} = 3\mathcal{P}$, which in turn implies $\Pi^\mu{}_\mu = 0$. The role of this 'viscous' tensor is to represent departures from local equilibrium.

Global rest frame description of equilibrated fluid is given by constant fields

$$u^\mu = (1,0,0,0),\ T,\ \text{while } \Pi^{\mu\nu} = 0. \tag{8.8}$$

Its small perturbations subject to overall constraints introduced a moment ago are given by the remaining degrees of freedom,

$$\delta T,\ \delta u^\mu \text{ with } \delta u^t = 0 \text{ and } \delta\Pi^{\mu\nu} \text{ with } \delta\Pi^{t\nu} = 0. \tag{8.9}$$

These are subject to the usual energy-momentum conservation

$$\nabla_\mu \langle T^{\mu\nu}\rangle = 0, \tag{8.10}$$

which allows one to solve for δu^μ and δT, while of course for $\delta\Pi^{\mu\nu}$ we need additional equations. Let us focus now on their derivation.

As we know from ordinary hydrodynamics considerations summarized in Chapter 2, for general momentum different tensorial components of $T^{\mu\nu}$ form distinct dynamical channels, divided into $O(2) \subset O(3)$ rotation subgroup representations. This decomposition is relevant when there is an explicit momentum dependence in the system[5]. In the lack thereof all the channels reduce to a simple scalar evolution equation. Owing to our novel observation of ultralocality at the scale $k \lesssim 2\pi T$ we are authorized to assume precisely this behaviour for the whole tensor $\Pi^{\mu\nu}$. As a consequence the quasi-normal frequency, which should be used to construct tensor version of (8.5) is in fact the scalar value (8.6), and the corresponding equation follows immediately,

$$\left(\frac{1}{T}\frac{\partial}{\partial t}\right)^2 \delta\Pi^{\mu\nu} + 2\omega_{\mathrm{I}}\frac{1}{T}\frac{\partial}{\partial t}\delta\Pi^{\mu\nu} + |\omega|^2\delta\Pi^{\mu\nu} = 0. \tag{8.11}$$

The resulting system (8.10), (8.11) with (8.7) and (8.9) describes evolution of the lowest quasi-normal mode propagating atop near-equilibrium linearised fluid, with no backreaction to its presence.

8.4 Towards generalized theories of hydrodynamics

So far the new system of equations enriched with (8.11) is by design bound to the fixed coordinates frame, in which new non-equilibrium degrees of freedom do not propagate. Moreover it implements only a minimal coupling to the near-equilibrium stress-energy tensor (8.7). As we said above such a system describes temporal evolution of the

[5] Precisely this vector breaks the $O(3)$ symmetry and defines distinct channels.

non-hydrodynamical perturbation in thermal medium, which is otherwise unaffected by its presence. It is therefore a minimal generalization of pure hydrodynamic, but based on a clear physical reasoning.

However it would be desirable to generalize our new theory to include actual quasi-normal mode propagation over evolving *viscous* hydrodynamical background, and even further to include backreaction of the fluid background to the far from equilibrium perturbation.

The result of the first task would be interesting, because it is a hydrodynamical counterpart of the problem in General Relativity concerning quasi-normal modes propagation over a dynamical horizon spacetime. Not much is known about such systems, and what we are trying to develop here could be of use in the analytical studies of these related problems.

The second task, apart from the above motivation, is interesting from the phenomenological perspective. The standard gradient based hydrodynamics suffers from certain pathologies related to causality, which reduce their usefulness in practical applications, and which were addressed with heuristic constructions, like the familiar Israel-Stewart hydrodynamics. We would wish to formulate a non-linear coupling to non-equilibrium perturbations, which could be of use in e.g. heavy-ion physics, and which would go beyond such Israel-Stewart based constructions.

There are *a priori* no firm guiding criteria for how to perform the described generalizations and we will have to make some well educated guesses on how to proceed. Since we are now working exclusively in the four dimensional theory we have to find a way to proceed without directly using holographical correspondence (although we shall very soon see, that it indeed validates our reasoning).

We will approach the propagation problem first, as it will turn out to be more transparent and then we will describe our attempt at the second more speculative problem.

8.4.1 Inducing propagation over viscous fluid background

To introduce spatial dynamics of the new mode we should recall, that a standard way of moving away from a fixed coordinate frame it to *covariantize* the equation. This will turn out to be quite involved and based on properly employing symmetries of the underlying physical system.

On the other hand viscous corrections to (8.7) can be incorporated in a fairly straightforward manner. It relies on the usual inclusion of gradient terms, allowing for local variations in T and u^μ, in the full viscous tensor,

$$\Pi^{\mu\nu}_{\text{Hydro}} = -\eta(T)\sigma^{\mu\nu} + \dots, \tag{8.12}$$

with $\eta(t)$ being the shear transport function, $\sigma^{\mu\nu}$ the shear tensor, and we have omitted higher gradient structures, which however could *a priori* be included.

Coming back to the covariantization problem, we must realize, that we are dealing with a conformal system, in which Weyl symmetry plays a prominent role. Interestingly, it has recently been shown by an explicit construction in holography [Loganayagam 2008], that manifestly Weyl-covariant formulation for relativistic conformal hydrodynamics exists and allows for a very compact expression of its evolution laws.

We will make use of this formalism and demand, that our new system of equations is manifestly Weyl covariant. This will require certain technical tools of the mentioned construction, so let us first explain what Weyl symmetry is. In brief, it is an invariance under local metric rescalings:

$$\eta_{\mu\nu} \to e^{-2\omega(x)}\eta_{\mu\nu}. \tag{8.13}$$

We call field a Weyl covariant tensor, if it transforms homogeneously under such rescalings, with a parameter called Weyl weight w:

$$\phi(x) \to e^{w\omega(x)}\phi(x). \tag{8.14}$$

The precise tensor weight is determined with the aid of appropriate invariants, e.g. action, or some other fields combinations, with already known Weyl weights. For instance, a covariant metric tensor has $w = -2$, and for $T^{\mu\nu}$ we have $w = 6$. Basic fluid variables transform as

$$\begin{aligned} T &\to e^{-\omega(x)}\tilde{T} \;\Rightarrow\; w = -1, \\ u^\mu &\to e^{-\omega(x)}\tilde{u}^\mu \;\Rightarrow\; w = -1. \end{aligned} \tag{8.15}$$

The central object in Weyl covariant formulation is the Weyl connection, and the associated with it covariant derivative. Their existence is helpful, because ordinary covariant derivative does not transform homogeneously with Weyl rescaling, and the non-dynamical Weyl connection is designed precisely to account for this failure. This object is build out of fluid velocity field and is defined as

$$\mathcal{A}_\mu = u^\lambda \nabla_\lambda u_\mu - \frac{1}{3}\nabla_\mu u^\lambda u_\mu. \tag{8.16}$$

For a rank-two tensor of weigh w we have then

$$\begin{aligned} \mathcal{D}_\lambda T^{\mu\nu} &= \nabla_\lambda T^{\mu\nu} + w\mathcal{A}_\lambda T^{\mu\nu} \\ &+ [g_{\lambda\alpha}\mathcal{A}^\mu - \delta^\mu_\lambda \mathcal{A}_\alpha - \delta^\mu_\alpha \mathcal{A}_\lambda]T^{\alpha\nu} \\ &+ [g_{\lambda\alpha}\mathcal{A}^\nu - \delta^\nu_\lambda \mathcal{A}_\alpha - \delta^\nu_\alpha \mathcal{A}_\lambda]T^{\mu\alpha}. \end{aligned} \tag{8.17}$$

Returning to the main problem we note, that a naive covariantization of (8.5) would amount to locally boosting it to an arbitrary fluid reference frame by substituting $\partial_t \to u^\mu\nabla_\mu$. But such an operation would render resulting equation inconsistent with the manifest Weyl covariance. Moreover an important problem would then arise, because alongside defining the non-equilibrium constitutive relations (8.7) we have imposed Landau transversality condition $u^\mu \Pi_{\mu\nu} = 0$. This property should hold throughout the evolution, and this can not be guaranteed by such a simple covariantisation. These facts were gathered during our first attempt at covariantizing the equations, and this led us to considering the Weyl based generalization. This became one of our heuristic assumptions mentioned above.

We were therefore motivated to introduce a directed Weyl derivative of the form $\mathcal{D} \equiv u^\mu \mathcal{D}_\mu$, which is Poincaré scalar, and following (8.17) acts on a rank two Landau-transverse tensor as

$$\mathcal{D}\Pi^{\mu\nu} = u^\lambda(\nabla_\lambda + (6-2)\mathcal{A}_\lambda)\Pi^{\mu\nu} - 2\mathcal{A}_\lambda u^{(\mu}\Pi^{\nu)\lambda}, \tag{8.18}$$

where $(6-2)$ comes from the weight $w = 6$ reduced by 2 from velocity contraction. Moreover, by a coincidence the above definition combined into the term $1/T\mathcal{D}$ has the same Weyl weight, as the object being differentiated, and therefore a second directed Weyl derivative is obtained by just plain iteration of the above.

Having realised that, we can approach the problem of properly covariantizing equation (8.5), including viscous fluid corrections. To To do this let us divide the whole viscous transverse tensor Π^μ into the near-equilibrium gradients part and the genuinely non-equilibrium component,

$$\Pi^{\mu\nu} = \Pi^{\mu\nu}_{\text{Hydro}} + \tilde{\Pi}^{\mu\nu}. \tag{8.19}$$

With this partition let us now introduce the following equation for the non-equilibrium tensor

$$\left(\frac{1}{T}\mathcal{D}\right)^2 \tilde{\Pi}^{\mu\nu} + 2\omega_{\rm I}\frac{1}{T}\mathcal{D}\tilde{\Pi}^{\mu\nu} + |\omega|^2\tilde{\Pi}^{\mu\nu} = 0. \tag{8.20}$$

The above formula transforms homogeneously under Weyl rescalings and employs spatial derivatives, which means, that the perturbation will now propagate over the viscous fluid. The equation (8.20) is therefore our candidate for the local non-equilibrium generalization of viscous hydrodynamics.

The natural next step is to perform necessary tests of our proposed generalization. At this point we can again make use of the dual holographic theory and gravitational computations.

As a first check we have investigated that the lowest quasi-normal mode evolution equation in a viscous gravity background indeed leads to the same result as the covariantization of the equation (8.20). In more detail notice, that Weyl connection contains fluid velocity derivatives, and hence to visualise its impact one must consider at least first order (viscous) gravity backgrounds. Taking this into account, by manipulating Einstein equations linearised on the top of evolving viscous geometry it can be shown, that the quasi-normal modes wave equation defined in this way can be rewritten in a manifestly Weyl invariant fashion. This reveals the source and confirm the validity of the equation (8.20), which is holographically dual to the described quasi-normal mode equation.

Furthermore, we have checked, that the dynamical quasi-normal mode, which we computed in [Heller 2013a] and studied extensively in the previous chapter solves the new equation (8.20). This confirms, that purely field-theoretical equation is capable of describing plasma perturbations originally found and studied on the gravity side. This is also a non-trivial test, because due to the boost-invariant dynamical background various components of the equation assume more complicated form.

8.4.2 Back-reaction beyond hydrodynamic approximation

We should now approach the second task defined above and try to incorporate interactions between the quasi-normal mode perturbation and the underlying evolving fluid in a casual generalization of hydrodynamics. As we warned this step is more speculative, because as always there are many ways, in which one can introduce covariant couplings. We shall try doing this in a way possibly minimally deviating from the established hydrodynamics properties.

First we note, that the cornerstone of conventional hydrodynamics, the systematic gradient expansion leading to the definition of viscous tensor, is at the same time a source of certain physical pathology in this effective theory. Due to arbitrarily high order differential terms in the expansion, resulting equations of motion are not hyperbolic and lead to superluminal signal propagation. Severity of this problem is amplified in phenomenological applications, in which numerical codes are used to solve non-linear equations. Absence of causality leads then to instabilities and renders initial value problems ill defined [Kostädt 2000, Hiscock 1985].

Phenomenologically attractive workaround has been introduced by the mentioned in Chapter 2 Müller, Israel, Stewart theory, which makes an attempt at defining UV-completion of a finite order viscous hydrodynamics. This theory is very similar in spirit to our approach (yet still in the realm of hydrodynamics) and as we know relies on replacing gradient expanded viscous tensor by an object independent of T and u^μ, the MIS

tensor $\Pi^{\mu\nu} = \Pi^{\mu\nu}_{\text{MIS}}$. The new set of degrees of freedom is then supplemented by necessary evolution equations, the simplest example of which is

$$\left(\hat{\tau}_\Pi \frac{1}{T}\mathcal{D} + 1\right) \Pi^{\mu\nu}_{\text{MIS}} = -\eta\sigma^{\mu\nu}. \tag{8.21}$$

Notice the presence of Weyl covariant derivative, which implies, that this expression is already Weyl covariant. Alongside the additional equation a phenomenological parameter $\hat{\tau}_\Pi/T$ is introduced, which is often called relaxation time. Its relation to standard hydrodynamics is established, if we proceed and include quadratic terms in $\Pi^{\mu\nu}$, in a way similar to the procedure described in Chapter 2 (and explained in [Baier 2008]). By solving the resulting hydrodynamics equations iteratively in gradients, which would produce series in powers of inverse time, we would identify the relaxation time with one of the conventional second order transport coefficients.

Upon such a modification the benefit of causality is achieved, if assuming $\eta/s = 1/(4\pi)$ we impose $\hat{\tau}_\Pi \geq 1/(2\pi)$. But the price for this is that a spurious purely decaying mode appears in linear perturbations spectrum, with exponential decay governed by imaginary 'frequency' $\omega = iT/\hat{\tau}_\Pi$. It is clearly related to the newly introduced relaxation time parameter and follows from the first order differential equation in (8.21). We have commented on the unphysical nature of this mode before in Section 2.1.4.3. In particular it is clear, that this decaying mode is not related to the quasi-normal modes originating from gravity.

We can however enrich such a theory with similarly behaving *physical* degrees of freedom through the procedure elucidated in the preceding sections. In this way we would arrive at a theory having virtues of both causal and non-hydrodynamical behaviour.

The first step towards constructing such a theory is again to define the viscous tensor partition into hydrodynamical and non-hydrodynamical parts, but this time replace the hydrodynamical gradient part by the just described MIS tensor:

$$\Pi^{\mu\nu} = \Pi^{\mu\nu}_{\text{MIS}} + \tilde{\Pi}^{\mu\nu}. \tag{8.22}$$

This corresponds to including non-equilibrium, and both viscous and causal hydrodynamics in the constitutive relations.

The complete set of equations for all our independent variables is then assembled from equations (8.10), (8.20) and (8.21):

$$\begin{gathered} \nabla_\mu \langle T^{\mu\nu} \rangle = 0, \\ \left(\frac{1}{T}\mathcal{D}\right)^2 \tilde{\Pi}^{\mu\nu} + 2\omega_{\text{I}} \frac{1}{T}\mathcal{D}\tilde{\Pi}^{\mu\nu} + |\omega|^2 \tilde{\Pi}^{\mu\nu} = 0, \\ \left(\hat{\tau}_\Pi \frac{1}{T}\mathcal{D} + 1\right) \Pi^{\mu\nu}_{\text{MIS}} = -\eta\sigma^{\mu\nu}. \end{gathered} \tag{8.23}$$

Notice, that the role of the conservation law (8.10) is to couple the perfect fluid part to the non-equilibrium components (8.22), each of which obeys its own Weyl covariant equation of motion. The set of equations 8.23 is our candidate for completing the second task defined in Section 8.4.

The theory defined above has linear spectrum similar to standard hydrodynamics, as we required, but enhanced with inclusion of the quasi-normal modes and the spurious MIS damped mode.

From the practical perspective, a phenomenological way to reduce the impact of the unphysical mode is to set initial data for $\Pi^{\mu\nu}_{\text{MIS}}$ to $-\eta(T)\sigma^{\mu\nu}$, which by inspecting (8.21) sets $\Pi^{\mu\nu}_{\text{MIS}}$ as close to conventional Landau $\Pi^{\mu\nu}_{\text{Hydro}}$ tensor as possible. Moreover, the smallest

value of $\hat{\tau}_\Pi = 1/2\pi$ allowed by causality makes dumping of the spurious mode maximal, reducing influence on the physical answer.

From the initial value problem point of view our generalization introduces an equation involving second temporal derivatives of a tensor field $\tilde{\Pi}^{\mu\nu}$ (although subject to constraints discussed above). Therefore the set of initial data for our new system must include also the corresponding initial values and temporal derivatives for these variables.

In the case of boost-invariant system, which we were mostly interested in, the symmetries reduce the number of the new tensor components, and therefore also the space of initial data. In Bjorken flow approximation one would then need to specify initial energy density $\varepsilon(0)$, pressure anisotropy $\xi(0)$ and its first derivative $\xi'(0)$. These two last functions correspond to the new non-equilibrium degree of freedom, which in the highly symmetric case of boost-invariant flow is represented by just one scalar component of $\tilde{\Pi}^{\mu\nu}$, precisely the anisotropy $\xi(\tau)$.

What is the phenomenological attractiveness of our newly introduced equations? Their prime applicability should be sought in describing fluid dynamics in the regime, when mostly one last non-equilibrium excitation is dominating the final approach to local hydrodynamic equilibrium. Perhaps one such a scenario could be realised in the stage between a regular hydrodynamics and the Colour Glass Condensate, or a similar model providing initial form of $T^{\mu\nu}$ in the far from equilibrium regime. We shall also see soon, that the applicability scope of our equations covers situation lacking Landau gradient based hydrodynamic description at all, like the homogeneous isotropisation [Chesler 2009]. Equations have also 'classical' limit reached by imposing vanishing initial conditions for $\tilde{\Pi}^{\mu\nu}$, which reduces the dynamics to the pure MIS theory.

Before describing the necessary confrontation with holographic computations we will briefly discuss alternative definition of the generalized hydrodynamics aiming at alleviating the main MIS theory drawback of the spurious mode, while keeping causality intact.

The starting point is to merge gradient expansion philosophy with the non-equilibrium equation (8.20). By inserting conventional Landau viscous tensor with non-equilibrium part (8.19) to (8.20) and regarding $\Pi^{\mu\nu}$ as an independent set of variables, while acting with Weyl derivatives $\mathcal{D}$ on the gradient expansion $\Pi^{\mu\nu}_{\text{Hydro}}$, we obtain a hybrid equation fusing (8.20) and (8.21) together:

$$\left(\left(\frac{1}{T}\mathcal{D}\right)^2 + 2\omega_{\text{I}}\frac{1}{T}\mathcal{D} + |\omega|^2\right)\Pi^{\mu\nu} = -\eta|\omega|^2\sigma^{\mu\nu} - c_\sigma\frac{1}{T}\mathcal{D}(\eta\sigma^{\mu\nu}) + \dots \tag{8.24}$$

Terms on the right hand side form gradient expansion modified by the differential operator in (8.20) and have been limited to second order in gradients, with just one term of this sort retained. The reason to keep it is that together with the arbitrary parameter c_σ it ensures linear stability of the equation. Higher order terms can be included through $\Pi^{\mu\nu}_{\text{Hydro}}$ as well, and we represent them collectively by ellipses.

Linear perturbation analysis of (8.24) around equilibrium fluid configuration (8.8) reveals, that the above equation (together with stress conservation $\nabla_\mu T^{\mu\nu} = 0$) defines hyperbolic system of partial differential equations, provided $c_\sigma \geq 0$. The characteristic velocity in the sound channel is

$$v = \frac{1}{\sqrt{3}}(1 + \frac{c_\sigma}{\pi})^{1/2}. \tag{8.25}$$

The above quantity extracted from characteristics equation should not be confused with the speed of sound, which in our conformal theory is locked at $c_s = 1/\sqrt{3}$. Using v we obtain second bound ensuring causality, $c_\sigma \leq 2\pi$.

Equation (8.24) is our alternative candidate for the solution to the second task from Section 8.4. However despite appealing properties (8.24) contains pathology of its own. Linear stability analysis unravels problematic feature, that small perturbations Fourier modes start growing exponentially once momentum reaches high values of $k \gtrsim 18.5T$ for $c_\sigma = 2\pi$. Such an instability renders this system unsuitable for numerical treatment, since it is difficult to confine momentum from spreading towards higher values. This problem appears however far away from the hydrodynamics region of validity (which is far away even for our ultralocal non-equilibrium quasi-normal mode modification, assumed to hold roughly for $k \lesssim 2\pi T$). One may hope, that more educated refinement of the prescription (8.24) could remove this obstruction, or maybe proper account of the momentum dependence instead of ultralocality would amend the issue. For now will focus on the stable MIS based theory (8.23).

8.5 Comparison to holographic experiment

We should now put to test the newly proposed equations. We will treat gravitational dual of the thermal $\mathcal{N} = 4$ $d = 4$ SYM plasma system as a numerical experiment (akin to the *in silico* lattice QCD experiments) and try reproducing so defined exact data with our phenomenological hydrodynamical model (8.20). The method is to focus on two relevant, yet particularly simple scenarios, and use them as a source of initial data for our numerical hydrodynamic solutions. As in phenomenology our new equations are expected to be general and relation to a particular system is established by a suitable choice of parameters. In our case this translates to selecting $\eta/s = 1/(4\pi)$ and $\omega_{\mathrm{R,I}}$ as in (8.6). For the sake of hampering the impact of the MIS spurious mode we set $\hat{\tau}_\Pi = 1/(2\pi)$.

The system we are going to study represent two particular configurations of $\mathcal{N} = 4$ $d = 4$ SYM plasma, boost-invariant Bjorken flow and homogeneous isotropisation [Chesler 2009]. The former one is already well known to us and is defined by symmetries reducing overall form of the stress tensor expectation value to

$$\langle T^{\mu\nu}(\tau)\rangle = \mathrm{Diag}[\mathcal{E}(\tau), \tau^2\mathcal{P}_{\mathrm{L}}(\tau), \mathcal{P}_{\mathrm{T}}(\tau), \mathcal{P}_{\mathrm{T}}(\tau)]^{\mu\nu} \tag{8.26}$$

The second system is on the other hand interesting, because by construction it has constant energy density and no spatial dependence in the stress tensor, which is assumed to have anisotropic pressures:

$$\langle T^{\mu\nu}(t)\rangle = \mathrm{Diag}[\mathcal{E}, \frac{1}{3}\mathcal{E} - \frac{2}{3}\Delta\mathcal{P}(t), \frac{1}{3}\mathcal{E} + \frac{1}{3}\Delta\mathcal{P}(t), \frac{1}{3}\mathcal{E} + \frac{1}{3}\Delta\mathcal{P}(t)]^{\mu\nu} \tag{8.27}$$

Notice, that this time the standard flat Minkowski coordinate system is used, as opposed to the proper time variables of (8.26). Therefore one can not form gradient expansion of (8.27), and the holographic dual will contain only non-equilibrium excitations, like quasi-normal modes.

We shall not describe here methods used to integrate relevant Einstein equations system, as these are isomorphic to those used in Chapters 6-7, and can be found in [Chesler 2009, Heller 2012c, Heller 2012a, Heller 2013b, Heller 2012b]. Instead in what follows we demonstrate plots of our main observable evolution. We choose for this a quantity bound to non-equilibrium behaviour, the pressure anisotropy:

$$\Delta\mathcal{P} \equiv \mathcal{P}_{\mathrm{T}} - \mathcal{P}_{\mathrm{L}}. \tag{8.28}$$

Initial data are derived from the holographically determined stress tensor, based on a particular example of gravity solution, which for the sake of providing initial conditions is

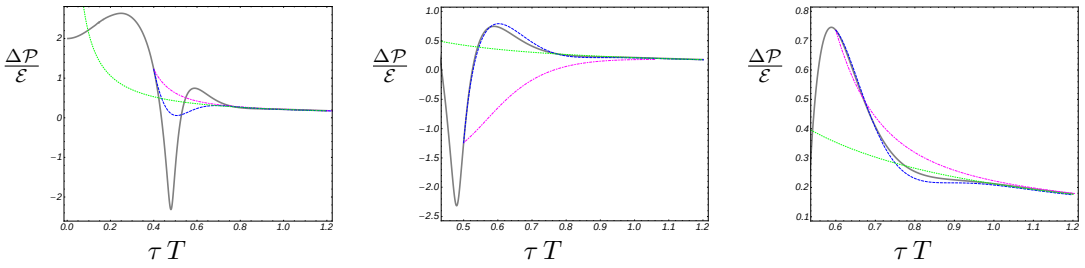

Figure 8.2: Boost-invariant flow. Gray curves denote the numerical solution based on AdS/CFT, magenta dash-dotted curves are solutions of MIS theory and the blue dashed curves are solutions of the new theory defined via eq. (8.20). The dotted green curve represents the most basic first order viscous hydrodynamics. Initial conditions were set at $\tau T = 0.4$ (left), 0.5 (centre) and 0.6 (right).

as good as any other solution. The data read-off from it are as we listed before the energy density, pressure anisotropy and its first temporal derivative at a given positive value of time, which on the phenomenological side corresponds to the hydrodynamic code initialization time (in applications is can be equal to e.g. 0.25 fm/c). By varying this value (in units of the effective temperature at this moment, $tT(t)$) we kick-off hydrodynamic simulations from different stages of exact holographic evolution, and observe how phenomenological equations follow the exact solution. Such a procedure in standard heavy-ion numerical hydrodynamic studies is in fact used to determine, when data from real experiment start exhibiting collective flow.

Let us therefore look at the first set of plots, Fig. 8.2, depicting boost-invariant expansion. What we can see here is the evolution of the normalized pressure anisotropy $\Delta\mathcal{P}/\mathcal{E}$ as a function of time rescaled by the momentary temperature[6], tT. Colours used are explained in the caption and different lines correspond to exact numerical AdS/CFT solution, MIS theory, our new equation and classical first order hydrodynamics. The three pictures correspond to initialization times $tT = 0.4,\ 0.5$ and 0.6. The exact numerical solution exhibits initially violent non-equilibrium behaviour (with reheating, surge of temperature not depicted here but known from Chapter 6) and transition to near equilibrium regime followed by uniformly decaying hydrodynamic power tail. We can see how first order hydrodynamics fails to capture any of the pre-hydro features, and how its prediction is corrected by the MIS theory. However due to its lack of oscillatory modes, MIS hydrodynamics is unable to capture any of the non-monotonic behaviours and even fails to depart smoothly from the exact graph, as starkly visible on the middle plot of Figure 8.2. In contrast out new equation based on the generalisation (8.22) is doing a better job at capturing non-equilibrium behaviour of the fluid. It is not perfect, but starting from $tT = 0.5$ we see, that it closely mimics the exact evolution, while even before it tries reproducing correct dip in the observable plot.

The discrepancy between our new equations predictions and 'experimental' data can be made more manifest, and elegantly explained by focusing on our second example, the homogeneous isotropisation. Figure 8.3 depicts again three consecutive initialization times interposed with the result based on an exact solution to Einstein equations. The lines represent the exact solution, solution based on linearised Einstein equations, which takes into account all the quasi-normal modes, MIS hydrodynamics and our new equations (colors map is given in the caption). This example is very interesting for its lack of gradient-based

[6]This is our familiar variable $w = T(\tau)\tau$ of Chapter 6. Relation between them can be locally numerically inverted, provided independent values of τ and $T(\tau)$ are known.

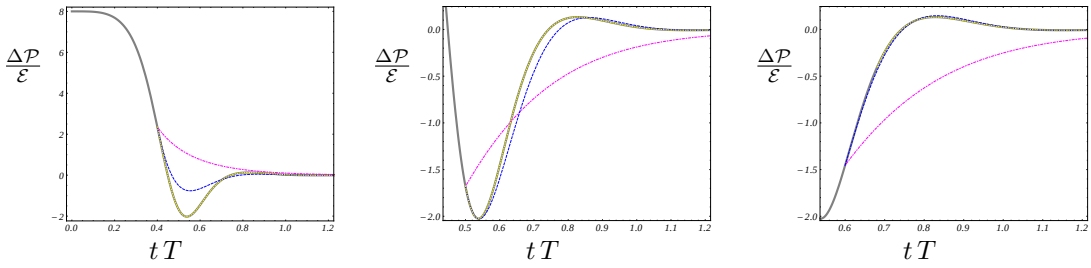

Figure 8.3: Homogeneous isotropisation.The gray curve denotes the numerical solution of Einstein's equations. The dotted yellow curves denote solutions of linearized Einstein's equations (including all the QNM's), dot-dashed magenta curves are solutions of MIS theory and the dashed blue curves represent solutions of the new theory given by (8.20). The initialization times are $tT = 0.4$ (left), 0.5 (centre) and 0.6 (right). The approximation by a sum of quasi-normal modes describes the evolution of the system very well already at $tT = 0.3$.

hydrodynamic description, as we have explained above.

To underscore the meaning of this feature we have combined the plot with another striking phenomenon discovered in fluid/gravity duality, that from some moment on the solution to full non-linear Einstein equations can be very accurately approximated by just linear evolution [Heller 2013b]. It means, that if at some finite time one decomposes even highly disturbed evolving solution into a large but finite set of quasi-normal modes (in a way similar to Fourier transform) and use this decomposition as initial data to linearised Einstein equations, the resulting solution will very closely resemble the exact non-linear evolution. This means, that some intrinsic linearisation must be taking place leading to a drastic simplification of the non-equilibrium dynamics at this stage. Such a procedure works only from some moment on, but it is long before the transition to hydrodynamics and in our case it holds already at $tT = 0.3$, when exact non-linear and QNM-based gravity solutions are indistinguishable. We have described this phenomenon to underline, that for the most part of the plots in Figure 8.3 the evolution is linear and based on numerous quasi-normal modes only, which allows us to test limitations of our new equations.

Lessons one can draw from it are the following. MIS theory fails significantly at describing the evolution, leading up to 100% underestimation of the hydrodynamisation time, as seen on the third plot of Figure 8.3. It seems to be capturing well the data only given enough time to decay from the initial stage, which however seems trivially expected. On the other hand the new equations behave qualitatively and later quantitatively well, by capturing initial tendencies of the solution and completely reproducing it for the later initialization time $tT = 0.6$. This clearly shows, that in the lack of standard hydrodynamic degrees of freedom limitation of our new system stems from the presence of higher quasi-normal modes. Once these are mostly gone and evolution seems to be governed by the longest lived lowest non-hydrodynamical mode our new equations lead to an almost exact match to the data, in contract to the MIS theory.

8.6 Closing remarks

In this chapter we have explained how one can generalize near-equilibrium hydrodynamics, in particular in its causal modified version to include genuinely non-equilibrium degrees of freedom bound to no gradient expansion whatsoever. It appeared, that due to

the holography enabled observation of ultralocality a general-purpose equations for holographic gauge fluids stress tensor can be constructed and seamlessly coupled to the standard near-equilibrium theories. The main results can by summarised as follows

- It is possible to formulate a purely four-dimensional (i.e. AdS boundary) based fluid equations capturing ingredients of the dynamics discovered in gravity.
- Quasi-normal mode plays a role of new phenomenological parameter, which should be specified for a given theory based on the microscopic evolution. In the case of holographic field theories it is provided by the dual black hole calculation.
- New set of equations is capable of describing systems with real part of the exponentially suppressed mode, enabling it to capture non-monotonic behaviours in the non-equilibrium flow stage. This is beyond the MIS theory capabilities.
- Weyl symmetry plays a prominent role in dictating a proper generalization and coupling among near- and non-equilibrium fluid fields.
- New theory can be applied to systems lacking conventional hydrodynamic gradient expansion construction.

Naturally there are several challenges, overcoming which would significantly improve phenomenological value of the newly proposed theory. One could focus on the following issues first:

- The theory (8.20) still possesses the spurious MIS damped mode. An attempt to alleviate this drawback led to another pathology of high momentum instability in (8.24). One could hope to hinder this problem by providing more gradient terms, which would alter the dispersion relation at high momenta. Another possibility is to decode the correct momentum dependence in tensorial channels, i.e. lift the ultralocality constraint.
- As seen in Figure 8.3 the applicability of the new theory is primarily limited by the presence of higher quasi-normal modes in the system. Giving proper account to these is both promising and challenging task. On the one hand one could easily add another damped oscillator equation with second quasi-normal mode parameter. But then a non-trivial question arises how to properly couple it to the remaining equations. Apart from the simple linear extension of the decomposition (8.22) one could e.g. consider non-linear coupling among the quasi-normal modes. There is also an issue of relative coefficient between their viscous tensors. On the overall however this does not seem to be intractable challenge, but testing it would be very subtle as would amount to fitting exponentially small terms to the gravity based solutions.
- New theory introduces structures requiring specific initial conditions and phenomenological parameters, whose microscopic interpretation is not entirely understood. In particular one needs to tune parameters to achieve maximal damping of the spurious modes.

On the overall we conclude, that the introduced equations constitute an attractive viable alternative to the established near-equilibrium theories and offer a prototypical model of plasma evolution in the regime, where no other hydrodynamics based theory was able to reach yet. Perhaps one could use generalized and pure hydrodynamic theories combined to determine more exact hydrodynamization time by comparing predicted transition times according to both models and 'averaging' them.

Chapter 9

Summary and Outlook

9.1 Summary of the Thesis results

Time has come to summarize all the things said above and, from the completed research programme perspective, try to look critically at the findings. We have began this treatise with the introductory chapter, where we briefly laid down the experimental heavy ion background and motivated the whole research. Accordingly we have outlined several questions inspired by the quark-gluon plasma experiments, which remained too challenging to be treated purely within the realm of QCD. Subsequently a model theory of $\mathcal{N} = 4$ super-Yang-Mills was proposed as a simple yet related theoretical laboratory to study these difficult questions. This theory was approached with the aid of AdS/CFT correspondence, which allowed for its rigorous study (assuming the duality to be exact). This led to a series of results, obtaining which is still beyond the reach of analytical methods in the real-world theory of strongly coupled QCD or Yang-Mills.

The main research questions we have aimed at were:

- To understand the very rapid equilibration mechanism in strongly coupled non-abelian fluid.
- To see, if there is some instability mechanism at work in anisotropic plasma.
- To characterize the process of transition to late local equilibrium.
- To characterize the early post collision non-equilibrium stage.

As often in the course of research, addition questions emerged based on the findings of our investigation:

- What to actually declare as the thermalized state of the fluid?
- How much can one refine the criterion of transition to hydrodynamics?
- What is the analytic structure of hydrodynamic gradient expansion?
- What are the degrees of freedom secretly present in hydrodynamics?
- Can we merge standard hydrodynamics with genuinely non-equilibrium excitations and form a purely boundary (non-gravitational) phenomenological theory?

As we have witnessed through the pages above, we managed to give answers to these (any several other) questions. Each chapter contains its own closing discussion section, so here we can give an overall synthetic summary of the major results, being resolutions to the questions just outlined above. We should bear in mind, that most of what we declare was found in the boost-invariant case.

- The holographic model of non-equilibrium gauge fluid indeed reproduces the very small equilibration time, defined roughly at the timescale of an effective inverse local temperature $1/T(\tau)$. The AdS/CFT dual theory is based on a black brane gravitational system, which is essentially the source of the very rapid equilibration. It is known [Susskind 2008], that black hole and black brane horizons (representing in holography the nearly thermal state) are most likely the fastest perturbation scramblers, swiftly dissipating any distortions. Therefore through the duality we find how one can expect the experimentally observed fast thermalization. This is an example of intuition one can draw from string theory model for real strongly coupled field theories.

- According to Chapter 5 there are no instabilities in strongly coupled anisotropic gauge fluids. The source of rapid equilibration is much more fundamental and as mentioned above resides in the properties of the spacetime horizons. Of course real-world theories have no known holographic duals, but such is the nature of a new intuition, we may still need to uncover some secret properties of QCD, which would be analogous in this regard to the holographic super-Yang-Mills theory.

- Isotropisation can not be used as the sole criterion of transition to equilibrium. It was found (in Chapter 6), that strongly anisotropic system can be already following hydrodynamical evolution. As a result of our research a new term was coined by the community for this, *hydrodynamisation*, to distinguish such a state from the standard isotropic equilibrium.

- There is a surprising simplicity in qualitative properties of the final local equilibrium fluid state, which can be dominantly characterised by its corresponding initial state features. Various properties, like equilibration temperature and time seem to be determined mostly by the initial entropy density. This is surprising, because between the initial and final stages a complicated evolution occurs, and one could expect the thermalization to wash away the initial state data. As it appears in Chapter 6 it is not entirely the case.

- By trying to refine the hydrodynamisation criterion defined in Chapter 6 with higher order expansion, we found that strictly speaking hydrodynamics (as an expansion) does not exist at all. More terms used for e.g. temperature expansion in Chapter 7 led to worse approximation of the exact numerical holographic solution. In this way asymptotic nature of the gradient expansion revealed itself along with genuinely non-equilibrium excitations, lurking in the very high order hydrodynamics. By considering its 240 orders we discovered, that exponentially decaying modes (as opposed to power law tails of hydrodynamics) also exist in the expansion, and in holography they correspond to the dual black brane quasi-normal modes. These beautiful findings imply, that one should be careful when using higher order hydrodynamics, because in this case more is less (accuracy).

- The above discovered non-equilibrium modes were cast into the form of differential equations in Chapter 8, where we performed a fusion of these with hydrodynamics. This step generalized the established in heavy ion physics Israel-Steward theory to include *oscillatory* exponentially suppressed modes, which renders such a system capable of describing fast equilibration of a strongly perturbed fluid. The resulting phenomenological theory contains holographically computed quasi-normal modes as fluid parameters, akin to the usual transport coefficients, but describing the non-equilibrium stage of the expansion. In this manner we use holography in a way similar

to the lattice methods, as a source of non-perturbative information on the strongly coupled field theory system.

- The new set of equations recalled above was found in Chapter 8 to improve results of hydrodynamic approximation to the exact gravity computations, also in the case lacking hydrodynamical gradient expansion. It proved thus itself to be applicable in the case dominated by the quasi-normal modes evolution.

These highlights complete our list of major results of the Thesis, which however include many more elements scattered throughout the text. Having said that, we can put them into certain perspective and ask, what are the shortcomings and limitations of the described findings, what interesting developments followed since then in the field and, in the next section what are the potential future open research directions. The limitations and assumptions mentioned below naturally suggest subsequent avenues further research.

- On the downside, one can clearly point at the major role played by boost-invariance assumption in most of the developments. The validity of this physically well justified approximation, performing good in experiments analysis, has been frequently addressed during conferences, where the present work was presented. One may wonder, if this somewhat artificial assumption of formally infinite collision energy does not pour in secretly pathologies, and in particular if it is not the culprit responsible for the asymptotic nature of hydrodynamic gradient expansion. It seems morally justified to expect, that this last result should not depend on the Bjorken flow assumption, because we do not hope hydrodynamics to hold at arbitrarily high energy scale. Moreover, boost-invariance significantly reduces possible tensorial structures in the expansion, and hence it should rather be the lower bound on the hydrodynamic series terms growth rate.

- Another point related to the high symmetry employed is that hydrodynamical properties depend strongly on the dimensionality. Although we keep spacetime dimension fixed as $d = 4$, we effectively constrain the dynamics to be one dimensional. Accordingly, the dual Einstein equations are two dimensional. This removes certain physical phenomena from our system, like for example turbulence, the elliptic flow, and dynamics related to the vorticity tensor described in Chapter 2.

- Further, conformality of the system is a severely constraining assumption, which implies the idealised plasma equation of state and absence of bulk viscosity ζ. Furthermore, as we mentioned in Chapter 3 there is no phase transition in our model theory.

- In the context of hydrodynamics resummation one can point out, that we have not carried out this procedure. The reasons for this were signalled in Chapter 7. Most significantly it proved to be difficult to assure a proper value of the resummed temperature at the initial proper time, where we have small time perturbative solution at our disposal to compare. Moreover, the numerical Laplace transform was prone to errors and resummation quality was unsatisfactory. There is clearly room for improvement, by understanding better the Borel-Padé asymptotics and Borel plane poles structure.

- Naked singularity found in Chapter 5 is also a sort of unorthodox case to study and one could wonder if there is a more reassuring way to assess conclusions derived from it. However based on a subsequent related study one can speculate, that such a spacetime can be embedded in a larger dynamical spacetime picture and understood as a piece of the answer, [Rebhan 2012, Ren 2016].

- Lastly, one could argue, that all the results were based on an essentially local observable, constituted by the one point correlation function of $\langle T^{\mu\nu}(\tau)\rangle$. It would be interesting to investigate also non-local observables, like Wilson lines or two-point correlators. The one-point function probes thermal fluid only locally at certain scales, but non-local probes could provide us with an interesting insight into the plasma evolution.

Some of the above issues were addressed by the advances of the subsequent research conducted by the holographic community. Let us briefly list selected interesting developments, which extend understanding beyond our results.

- There was a significant progress towards building higher dimensional gravity duals of fluids and ion collisions, like shock-waves scatterings and more general configurations [Chesler 2015, van der Schee 2015]. Currently the field is progressing towards numerically simulating full fledged actual *ion* collisions, that is localised lumps of energy and charge densities. This amounts to solving five dimensional Einstein equations in the anti-de Sitter backgrounds, and requires advanced numerical tools developed for General Relativity. Progress like that will allow for a detailed study of the super-Yang-Mills finite energy density, strongly coupled states evolution, turbulence, and more, nearing us to imagining what *may* happen in QCD. Such a simulation lifts also the boost-invariance constraint.

- There was a considerable development of non-conformal holographic models, in which e.g. scalar field potential in the bulk geometry (on the gravity side) is used to introduce scale dependence. Such an approach allows to study e.g. RG flows and phase transitions, both static and dynamic [Janik 2016, Janik 2015, Gursoy 2016]. One subtlety in this approach is tied to the somewhat arbitrary form of the scalar field potential, for the form of which one must find suitable constraints. One of these comes from the asymptotically AdS spacetime boundary condition, and another comes from the desire to model a specific equation of state on the dual field theory side [Gubser 2008, Gursoy 2008].

- In the context of resummation, a whole powerful field of mathematics called the resurgence theory enjoyed significant growth in physics, in recent years. This theory, mentioned before in Chapter 7 allows one to fully decipher and reconstruct an analytic function, a glimpse of which is visible through the initial asymptotic series. This approach however requires a set of additional data necessary to link the resummed resurgent function to the original problem. This must be provided by some "experiment", that is some exact solution found from e.g. numerics, or localisation (in field theory). A recent beautiful example of this theory application is an extension of our resummation in the well controlled case of Israel-Stewart hydrodynamics and our generalization of it [Heller 2015, Aniceto 2016]. There, arbitrarily many terms of gradient expansion can be generated and one can rigorously apply the principles of resurgence to reconstruct temperature evolution up to the initial time. This led to the discovery of the so-called hydrodynamical attractor in Israel-Stewart theory, which in some sense generalizes hydrodynamics, see [Heller 2015] for the detailed explanation for this.

- Another important point is the issue of the dual field theory coupling strength. As was introduced in Chapter 3, we were working in the leading $\lambda \to \infty$ approximation. There were however attempts to alleviate this assumption. In the context of fluid/gravity a new direction of research has been opened by considering the stringy

α' corrections [Myers 2009, Grozdanov 2016b], which as was mentioned in Chapter 3 lead to supergravity higher curvature terms. These translate to $1/\lambda$ corrections, which allow to investigate how hydrodynamic approximation behaves as we change the field theory coupling.

The examples given above were only the most relevant ones in our context. The whole field of gauge/string research is among the most active and diverse branches of theoretical physics. This point ties the remark made in the first Chapter, that holography transforms the way we perceive gravity and field theory. Namely, among recent advances there is the the programme to properly recognize the role of entanglement entropy in quantum gravity and field theory. A potential deep (although still not rigorous) connections are made between hyperbolic spaces and quantum systems, in particular related to the MERA constructions of quantum systems and computers [Pastawski 2015], as well as a completely new perspective on quantum computation complexity has been proposed in the context of black holes quantum evolution. Clearly we are at the verge of a possible revolution in quantum physics. It is yet to be seen, if it will devour its children, or bring true solid breakthrough in physics.

9.2 Outlook and closing remarks

After enumerating derived results, their limitations, and selected examples of progress in the field, let us now point out some directions, in which one could extend the results presented in the Thesis.

First of all, building on the high order expansion techniques one can consider generalization to charged geometries. By introducing vector potential in the bulk, as we did in Chapter 5, we could investigate the influence of charge density on hydrodynamics convergence and its related analytic structure. Similarly one can try extending this approach to non-conformal and finite coupling cases. For the $1/\lambda$ corrections one can build on the recent study of the so-called Gauss-Bonnet gravity [Grozdanov 2016b], which contains in the Lagrangian higher curvature terms, but whose equations of motion remain to be second order, and hence avoiding the causality riddles. The ultimate challenge would be to combine all these regimes into one picture.

Secondly, by incorporating properly the mechanisms of resurgence one could reapproach the problem of $\mathcal{N} = 4$ super-Yang-Mills hydrodynamics resummation. By building on the intuition gathered in [Aniceto 2016, Heller 2015] one could try proving, that holographic fluid description indeed exhibits resurgent features. This task is challenging, because in contrast to Israel-Stewart hydrodynamics in the full holographic theory there are infinitely many resummation ambiguities induced by the infinite tower of quasi-normal modes (playing the role of infinitely many complex instanton actions), and rendering resummation unique in such a case is considerably more difficult. It is however tractable with the tools of [Aniceto 2015], and undoubtedly interesting.

Other more distant derivations could aim at analysing non-local observables, like Wilson lines and correlation functions in dynamical backgrounds. Here part of the challenge resides in the task of solving numerically the variational problem for the extreme surfaces in the bulk spacetime. Such a computation however would be interesting, because it would allow to probe the evolving geometry, and hence field theory state, at various length scales by submerging the corresponding string arc more or less into the bulk.

With the above time has come to make the final comment of the Thesis. One may ask, how lasting these results will turn out to be, and what is their actual utility for the heavy ion programme. It is difficult to judge how long will they be actively discussed by the

community, because of the very rapid progress. However two observations should endure the test of time: the observation, that one may and should apply viscous hydrodynamics to describe still anisotropic fluid evolution, and the observation of the zero radius of hydrodynamics convergence. We hope these will become canonical elements of the field, on the par with the famous result on the $\eta/s = 1/4\pi$ bound, which is more or less regarded as universal for strongly coupled gauge field theories.

Bibliography

[Alcubierre 2003] Miguel Alcubierre. *Hyperbolic slicings of space-time: Singularity avoidance and gauge shocks.* Class.Quant.Grav., vol. 20, pages 607–624, 2003. (Cited on page 61.)

[Aniceto 2015] Ines Aniceto and Ricardo Schiappa. *Nonperturbative Ambiguities and the Reality of Resurgent Transseries.* Commun. Math. Phys., vol. 335, no. 1, pages 183–245, 2015. (Cited on page 169.)

[Aniceto 2016] Ines Aniceto and Michal Spalinski. *Resurgence in Extended Hydrodynamics.* Phys. Rev., vol. D93, no. 8, page 085008, 2016. (Cited on pages 168 and 169.)

[Arnold 2014] Peter Arnold, Paul Romatschke and Wilke van der Schee. *Absence of a local rest frame in far from equilibrium quantum matter.* JHEP, vol. 10, page 110, 2014. (Cited on page 111.)

[Arnowitt 1959] Richard L. Arnowitt, Stanley Deser and Charles W. Misner. *Dynamical Structure and Definition of Energy in General Relativity.* Phys.Rev., vol. 116, pages 1322–1330, 1959. (Cited on page 57.)

[Ashtekar 2004] Abhay Ashtekar and Badri Krishnan. *Isolated and dynamical horizons and their applications.* Living Rev. Rel., vol. 7, page 10, 2004. (Cited on page 100.)

[Baier 2008] Rudolf Baier, Paul Romatschke, Dam Thanh Son, Andrei O. Starinets and Mikhail A. Stephanov. *Relativistic viscous hydrodynamics, conformal invariance, and holography.* JHEP, vol. 04, page 100, 2008. (Cited on pages 15, 16, 17, 18, 24, 111 and 158.)

[Balasubramanian 1999] Vijay Balasubramanian and Per Kraus. *A Stress tensor for Anti-de Sitter gravity.* Commun. Math. Phys., vol. 208, pages 413–428, 1999. (Cited on page 103.)

[Baumgarte 2003] Thomas W. Baumgarte and Stuart L. Shapiro. *Numerical relativity and compact binaries.* Phys.Rept., vol. 376, pages 41–131, 2003. (Cited on pages 57 and 60.)

[Baym 1983] Gordon Baym, Bengt L. Friman, J.-P. Blaizot, M. Soyeur and W. Czyz. *Hydrodynamics of ultra-relativistic heavy ion collisions.* Nuclear Physics A, vol. 407, no. 3, pages 541 – 570, 1983. (Cited on page 20.)

[Becker 2006] K. Becker, M. Becker and J.H. Schwarz. String theory and m-theory: A modern introduction. Cambridge University Press, 2006. (Cited on page 30.)

[Bekenstein 1973] Jacob D. Bekenstein. *Black Holes and Entropy.* Phys. Rev. D, vol. 7, pages 2333–2346, Apr 1973. (Cited on page 44.)

[Beuf 2009] Guillaume Beuf, Michal P. Heller, Romuald A. Janik and Robi Peschanski. *Boost-invariant early time dynamics from AdS/CFT.* JHEP, vol. 10, page 043, 2009. (Cited on pages 4, 83, 84, 90, 114 and 141.)

[Bhattacharyya 2008a] Sayantani Bhattacharyya, Veronika E. Hubeny, R. Loganayagam, Gautam Mandal, Shiraz Minwalla*et al. Local Fluid Dynamical Entropy from Gravity.* JHEP, vol. 0806, page 055, 2008. (Cited on page 101.)

[Bhattacharyya 2008b] Sayantani Bhattacharyya, Veronika E Hubeny, Shiraz Minwalla and Mukund Rangamani. *Nonlinear Fluid Dynamics from Gravity.* JHEP, vol. 02, page 045, 2008. (Cited on pages 41, 55 and 81.)

[Bjorken 1983] James D. Bjorken. *Highly Relativistic Nucleus-Nucleus Collisions: The Central Rapidity Region.* Phys.Rev., vol. D27, pages 140–151, 1983. (Cited on page 20.)

[Blumenhagen 2012] R. Blumenhagen, D. Lüst and S. Theisen. Basic concepts of string theory. Theoretical and Mathematical Physics. Springer Berlin Heidelberg, 2012. (Cited on page 31.)

[Booth 2005] Ivan Booth. *Black hole boundaries.* Can.J.Phys., vol. 83, pages 1073–1099, 2005. (Cited on pages 63 and 101.)

[Booth 2009] Ivan Booth, Michal P. Heller and Michal Spalinski. *Black brane entropy and hydrodynamics: The Boost-invariant case.* Phys. Rev., vol. D80, page 126013, 2009. (Cited on pages 20, 23, 63 and 111.)

[Brandt 1995] Fernando T. Brandt, J. Frenkel and J. C. Taylor. *High temperature QCD and the classical Boltzmann equation in curved space-time.* Nucl. Phys., vol. B437, pages 433–446, 1995. (Cited on page 23.)

[Broniowski 2008] Wojciech Broniowski, Mikolaj Chojnacki, Wojciech Florkowski and Adam Kisiel. *Uniform Description of Soft Observables in Heavy-Ion Collisions at s(NN)**(1/2) = 200 GeV**2.* Phys. Rev. Lett., vol. 101, page 022301, 2008. (Cited on pages 116 and 152.)

[Caron-Huot 2008] Simon Caron-Huot and Guy D. Moore. *Heavy quark diffusion in QCD and N=4 SYM at next-to-leading order.* JHEP, vol. 02, page 081, 2008. (Cited on page 30.)

[Casalderrey-Solana 2006] J. Casalderrey-Solana, E. V. Shuryak and D. Teaney. *Hydrodynamic flow from fast particles.* 2006. (Cited on page 16.)

[Chesler 2009] Paul M. Chesler and Laurence G. Yaffe. *Horizon formation and far-from-equilibrium isotropization in supersymmetric Yang-Mills plasma.* Phys.Rev.Lett., vol. 102, page 211601, 2009. (Cited on pages 57, 81, 85, 113, 114, 115, 120, 159 and 160.)

[Chesler 2015] Paul M. Chesler and Laurence G. Yaffe. *Holography and off-center collisions of localized shock waves.* JHEP, vol. 10, page 070, 2015. (Cited on page 168.)

[de Haro 2001] Sebastian de Haro, Sergey N. Solodukhin and Kostas Skenderis. *Holographic reconstruction of space-time and renormalization in the AdS / CFT correspondence.* Commun.Math.Phys., vol. 217, pages 595–622, 2001. (Cited on pages 39, 83 and 91.)

[D'Hoker 2002] Eric D'Hoker and Daniel Z. Freedman. *Supersymmetric gauge theories and the AdS / CFT correspondence.* In Strings, Branes and Extra Dimensions: TASI 2001: Proceedings, pages 3–158, 2002. (Cited on pages 32 and 33.)

[Di Vecchia 2000] Paolo Di Vecchia and Antonella Liccardo. *D Branes in String Theory, I.* NATO Sci. Ser. C, vol. 556, pages 1–60, 2000. (Cited on pages 32 and 34.)

[Di Vecchia 2003] Paolo Di Vecchia and Antonella Liccardo. *Gauge theories from D-branes.* In Frontiers in Number theory, Physics and Geometry II. Edited by P Cartier, B. Julia, P. Moussa and P. Vanhove, 2006. pp. 161-222, pages 161–222, 2003. (Cited on page 32.)

[Dorigoni 2014] Daniele Dorigoni. *An Introduction to Resurgence, Trans-Series and Alien Calculus.* 2014. (Cited on page 138.)

[Eling 2010] Christopher Eling, Itzhak Fouxon and Yaron Oz. *Gravity and a Geometrization of Turbulence: An Intriguing Correspondence.* 2010. (Cited on page 52.)

[Epstein 1965] H. Epstein, V. Glaser and A. Jaffe. *Nonpositivity of the energy density in quantized field theories.* Il Nuovo Cimento (1955-1965), vol. 36, no. 3, pages 1016–1022, 1965. (Cited on page 111.)

[Florkowski 2011] Wojciech Florkowski and Radoslaw Ryblewski. *Highly-anisotropic and strongly-dissipative hydrodynamics for early stages of relativistic heavy-ion collisions.* Phys. Rev., vol. C83, page 034907, 2011. (Cited on pages 25 and 115.)

[Florkowski 2013] Wojciech Florkowski, Radoslaw Ryblewski and Michael Strickland. *Testing viscous and anisotropic hydrodynamics in an exactly solvable case.* Phys. Rev., vol. C88, page 024903, 2013. (Cited on page 25.)

[Flory 2012] Mario Flory, Robert C. Helling and Constantin Sluka. *How I Learned to Stop Worrying and Love QFT.* 2012. (Cited on page 135.)

[Grozdanov 2016a] Saso Grozdanov and Nikolaos Kaplis. *Constructing higher-order hydrodynamics: The third order.* Phys. Rev., vol. D93, no. 6, page 066012, 2016. (Cited on page 20.)

[Grozdanov 2016b] Saso Grozdanov, Nikolaos Kaplis and Andrei O. Starinets. *From strong to weak coupling in holographic models of thermalization.* JHEP, vol. 07, page 151, 2016. (Cited on page 169.)

[Gubser 1998] S. S. Gubser, Igor R. Klebanov and Alexander M. Polyakov. *Gauge theory correlators from noncritical string theory.* Phys. Lett., vol. B428, pages 105–114, 1998. (Cited on page 35.)

[Gubser 2008] Steven S. Gubser and Abhinav Nellore. *Mimicking the QCD equation of state with a dual black hole.* Phys. Rev., vol. D78, page 086007, 2008. (Cited on page 168.)

[Gursoy 2008] Umut Gursoy, Elias Kiritsis, Liuba Mazzanti and Francesco Nitti. *Deconfinement and Gluon Plasma Dynamics in Improved Holographic QCD.* Phys. Rev. Lett., vol. 101, page 181601, 2008. (Cited on page 168.)

[Gursoy 2016] Umut Gursoy, Aron Jansen and Wilke van der Schee. *A new dynamical instability in Anti-de-Sitter spacetime.* 2016. (Cited on page 168.)

[Hawking 1975] S. W. Hawking. *Particle creation by black holes.* Communications in Mathematical Physics, vol. 43, no. 3, pages 199–220, 1975. (Cited on page 44.)

[Heinz 2005] Ulrich W. Heinz. *Thermalization at RHIC.* AIP Conf. Proc., vol. 739, pages 163–180, 2005. [,163(2004)]. (Cited on page 5.)

[Heinz 2013] Ulrich Heinz and Raimond Snellings. *Collective flow and viscosity in relativistic heavy-ion collisions*. Ann. Rev. Nucl. Part. Sci., vol. 63, pages 123–151, 2013. (Cited on pages 4 and 5.)

[Heller 2009] Michal P. Heller, Piotr Surowka, R. Loganayagam, Michal Spalinski and Samuel E. Vazquez. *Consistent Holographic Description of Boost-Invariant Plasma*. Phys. Rev. Lett., vol. 102, page 041601, 2009. (Cited on pages 20, 23, 46 and 143.)

[Heller 2012a] Michal P. Heller, Romuald A. Janik and Przemyslaw Witaszczyk. *A numerical relativity approach to the initial value problem in asymptotically Anti-de Sitter spacetime for plasma thermalization - an ADM formulation*. Phys. Rev., vol. D85, page 126002, 2012. (Cited on pages 6, 81, 120 and 160.)

[Heller 2012b] Michal P. Heller, Romuald A. Janik and Przemyslaw Witaszczyk. *The characteristics of thermalization of boost-invariant plasma from holography*. Phys. Rev. Lett., vol. 108, page 201602, 2012. (Cited on pages 6, 81 and 160.)

[Heller 2012c] Michal P. Heller, David Mateos, Wilke van der Schee and Diego Trancanelli. *Strong Coupling Isotropization of Non-Abelian Plasmas Simplified*. Phys. Rev. Lett., vol. 108, page 191601, 2012. (Cited on page 160.)

[Heller 2013a] Michal P. Heller, Romuald A. Janik and Przemyslaw Witaszczyk. *Hydrodynamic Gradient Expansion in Gauge Theory Plasmas*. Phys. Rev. Lett., vol. 110, no. 21, page 211602, 2013. (Cited on pages 6, 127 and 157.)

[Heller 2013b] Michal P. Heller, David Mateos, Wilke van der Schee and Miquel Triana. *Holographic isotropization linearized*. JHEP, vol. 09, page 026, 2013. (Cited on pages 160 and 162.)

[Heller 2014] Michal P. Heller, Romuald A. Janik, Michal Spalilski and Przemyslaw Witaszczyk. *Coupling hydrodynamics to nonequilibrium degrees of freedom in strongly interacting quark-gluon plasma*. Phys. Rev. Lett., vol. 113, no. 26, page 261601, 2014. (Cited on pages 6, 25 and 151.)

[Heller 2015] Michal P. Heller and Michal Spalinski. *Hydrodynamics Beyond the Gradient Expansion: Resurgence and Resummation*. Phys. Rev. Lett., vol. 115, no. 7, page 072501, 2015. (Cited on pages 150, 168 and 169.)

[Hiscock 1985] William A. Hiscock and Lee Lindblom. *Generic instabilities in first-order dissipative relativistic fluid theories*. Phys. Rev. D, vol. 31, pages 725–733, Feb 1985. (Cited on page 157.)

[Huang 1987] K. Huang. Statistical mechanics. Wiley, 1987. (Cited on page 46.)

[Hubeny 2012] Veronika E. Hubeny, Shiraz Minwalla and Mukund Rangamani. *The fluid/gravity correspondence*. In Black holes in higher dimensions, pages 348–383, 2012. [,817(2011)]. (Cited on page 55.)

[Huot 2007] Simon C. Huot, Sangyong Jeon and Guy D. Moore. *Shear viscosity in weakly coupled $N = 4$ super Yang-Mills theory compared to QCD*. Phys. Rev. Lett., vol. 98, page 172303, 2007. (Cited on page 30.)

[Janik 2006a] Romuald A. Janik and Robert B. Peschanski. *Asymptotic perfect fluid dynamics as a consequence of Ads/CFT*. Phys.Rev., vol. D73, page 045013, 2006. (Cited on pages 47, 81, 82 and 111.)

[Janik 2006b] Romuald A. Janik and Robert B. Peschanski. *Gauge/gravity duality and thermalization of a boost-invariant perfect fluid.* Phys. Rev., vol. D74, page 046007, 2006. (Cited on pages 141, 142, 143, 144 and 145.)

[Janik 2008] Romuald A. Janik and Przemyslaw Witaszczyk. *Towards the description of anisotropic plasma at strong coupling.* JHEP, vol. 09, page 026, 2008. (Cited on pages 6 and 65.)

[Janik 2011] Romuald A. Janik. *The Dynamics of Quark-Gluon Plasma and AdS/CFT.* Lect. Notes Phys., vol. 828, pages 147–181, 2011. (Cited on pages 41 and 56.)

[Janik 2015] Romuald A. Janik, Grzegorz Plewa, Hesam Soltanpanahi and Michal Spalinski. *Linearized nonequilibrium dynamics in nonconformal plasma.* Phys. Rev., vol. D91, no. 12, page 126013, 2015. (Cited on page 168.)

[Janik 2016] Romuald A. Janik, Jakub Jankowski and Hesam Soltanpanahi. *Nonequilibrium dynamics and phase transitions.* Phys. Rev. Lett., vol. 117, no. 9, page 091603, 2016. (Cited on page 168.)

[Kapusta 2006] Joseph I. Kapusta and Charles Gale. Finite-temperature field theory. Cambridge University Press, second édition, 2006. Cambridge Books Online. (Cited on pages 16, 17 and 151.)

[Karsch 1990] Frithjof Karsch. *SIMULATING THE QUARK - GLUON PLASMA ON THE LATTICE.* Adv.Ser.Direct.High Energy Phys., vol. 6, pages 61–115, 1990. (Cited on page 45.)

[Kinoshita 2009] Shunichiro Kinoshita, Shinji Mukohyama, Shin Nakamura and Kin-ya Oda. *A Holographic Dual of Bjorken Flow.* Prog. Theor. Phys., vol. 121, pages 121–164, 2009. (Cited on pages 23, 45, 129 and 148.)

[Kolb 2003] Peter F. Kolb and Ralf Rapp. *Transverse flow and hadrochemistry in* $\mathrm{Au}+\mathrm{Au}$ *collisions at* $\sqrt{s_{\mathrm{NN}}} = 200\mathrm{GeV}$. Phys. Rev. C, vol. 67, page 044903, Apr 2003. (Cited on page 5.)

[Kostädt 2000] P. Kostädt and M. Liu. *Causality and stability of the relativistic diffusion equation.* PRD, vol. 62, no. 2, page 023003, jul 2000. (Cited on page 157.)

[Kovtun 2003] Pavel Kovtun and Laurence G. Yaffe. *Hydrodynamic fluctuations, long time tails, and supersymmetry.* Phys. Rev., vol. D68, page 025007, 2003. (Cited on page 9.)

[Kovtun 2005] Pavel K. Kovtun and Andrei O. Starinets. *Quasinormal modes and holography.* Phys. Rev., vol. D72, page 086009, 2005. (Cited on pages 17, 53, 71, 146 and 153.)

[Landau 1953] Lev Davidovich. Landau. *On the multiparticle production in high-energy collisions.* Izv.Akad.Nauk Ser.Fiz., vol. 17, pages 51–64, 1953. (Cited on page 20.)

[Landau 1987] L. D. Landau and E. M. Lifshitz. Fluid Mechanics, Second Edition: Volume 6 (Course of Theoretical Physics). Course of theoretical physics / by L. D. Landau and E. M. Lifshitz, Vol. 6. Butterworth-Heinemann, 2 édition, 1987. (Cited on page 14.)

[Loganayagam 2008] R. Loganayagam. *Entropy Current in Conformal Hydrodynamics.* JHEP, vol. 05, page 087, 2008. (Cited on page 155.)

[Lublinsky 2007] Michael Lublinsky and Edward Shuryak. *How much entropy is produced in strongly coupled Quark-Gluon Plasma (sQGP) by dissipative effects?* Phys. Rev., vol. C76, page 021901, 2007. (Cited on page 112.)

[Maldacena 1999] Juan Martin Maldacena. *The Large N limit of superconformal field theories and supergravity.* Int. J. Theor. Phys., vol. 38, pages 1113–1133, 1999. [Adv. Theor. Math. Phys.2,231(1998)]. (Cited on page 35.)

[Marino 2014] Marcos Marino. *Lectures on non-perturbative effects in large N gauge theories, matrix models and strings.* Fortsch. Phys., vol. 62, pages 455–540, 2014. (Cited on pages 136 and 150.)

[Meyer 2007] Harvey B. Meyer. *A Calculation of the shear viscosity in SU(3) gluodynamics.* Phys. Rev., vol. D76, page 101701, 2007. (Cited on page 16.)

[Mrowczynski 1993] Stanislaw Mrowczynski. *Plasma instability at the initial stage of ultrarelativistic heavy-ion collisions.* Physics Letters B, vol. 314, no. 1, pages 118 – 121, 1993. (Cited on pages 17, 65 and 72.)

[Myers 2009] Robert C. Myers, Miguel F. Paulos and Aninda Sinha. *Quantum corrections to eta/s.* Phys. Rev., vol. D79, page 041901, 2009. (Cited on page 169.)

[Pastawski 2015] Fernando Pastawski, Beni Yoshida, Daniel Harlow and John Preskill. *Holographic quantum error-correcting codes: Toy models for the bulk/boundary correspondence.* JHEP, vol. 06, page 149, 2015. (Cited on page 169.)

[Philipsen 2014] Owe Philipsen and Christian Schafer. *The second order hydrodynamic transport coefficient κ for the gluon plasma from the lattice.* JHEP, vol. 02, page 003, 2014. (Cited on page 16.)

[Poisson 2004] Eric Poisson. A relativist's toolkit: The mathematics of black-hole mechanics. Cambridge University Press, 2004. (Cited on pages 57, 61 and 62.)

[Polchinski 1998] J. Polchinski. String theory: Volume 1, an introduction to the bosonic string. Cambridge Monographs on Mathematical Physics. Cambridge University Press, 1998. (Cited on page 31.)

[Policastro 2001] G. Policastro, Dan T. Son and Andrei O. Starinets. *The Shear viscosity of strongly coupled N=4 supersymmetric Yang-Mills plasma.* Phys. Rev. Lett., vol. 87, page 081601, 2001. (Cited on pages 46 and 51.)

[Rebhan 2012] Anton Rebhan and Dominik Steineder. *Probing Two Holographic Models of Strongly Coupled Anisotropic Plasma.* JHEP, vol. 08, page 020, 2012. (Cited on page 167.)

[Ren 2016] Jie Ren. *Asymptotically AdS spacetimes with a timelike Kasner singularity.* JHEP, vol. 07, page 112, 2016. (Cited on page 167.)

[Skenderis 2002] Kostas Skenderis. *Lecture notes on holographic renormalization.* Class.Quant.Grav., vol. 19, pages 5849–5876, 2002. (Cited on pages 39, 83 and 91.)

[Sohnius 1978] Martin F. Sohnius. *Supersymmetry and central charges.* Nuclear Physics B, vol. 138, no. 1, pages 109 – 121, 1978. (Cited on page 28.)

[Son 2002] Dam T. Son and Andrei O. Starinets. *Minkowski space correlators in AdS / CFT correspondence: Recipe and applications.* JHEP, vol. 09, page 042, 2002. (Cited on page 151.)

[Son 2007] Dam T. Son and Andrei O. Starinets. *Viscosity, Black Holes, and Quantum Field Theory.* Ann. Rev. Nucl. Part. Sci., vol. 57, pages 95–118, 2007. (Cited on pages 71 and 151.)

[Stewart 1971] John M. Stewart. Non-equilibrium relativistic kinetic theory, pages 1–113. Springer Berlin Heidelberg, Berlin, Heidelberg, 1971. (Cited on page 23.)

[Susskind 2008] Leonard Susskind and Yasuhiro Sekino. *Fast Scramblers.* JHEP, vol. 10, page 065, 2008. (Cited on page 166.)

[Trefethen 2000] Lloyd N. Trefethen. Spectral methods in matlab. Society for Industrial and Applied Mathematics, Philadelphia, PA, USA, 2000. (Cited on pages 104, 123 and 124.)

[Tseytlin 1997] Arkady A. Tseytlin. *On nonAbelian generalization of Born-Infeld action in string theory.* Nucl. Phys., vol. B501, pages 41–52, 1997. (Cited on page 34.)

[van der Schee 2015] Wilke van der Schee and Bjoern Schenke. *Rapidity dependence in holographic heavy ion collisions.* Phys. Rev., vol. C92, no. 6, page 064907, 2015. (Cited on page 168.)

[Wald 1991] Robert M. Wald and Vivek Iyer. *Trapped surfaces in the Schwarzschild geometry and cosmic censorship.* Phys.Rev., vol. D44, pages 3719–3722, 1991. (Cited on page 101.)

[Whittaker 1996] E.T. Whittaker and G.N. Watson. A course of modern analysis. Cambridge University Press, 1996. (Cited on pages 132 and 134.)

[Wiedemann 2013] Urs Achim Wiedemann. *Introductory Overview of Quark Matter 2012.* Nucl. Phys., vol. A904-905, pages 3c–10c, 2013. (Cited on page 2.)

[Witten 1998] Edward Witten. *Anti-de Sitter space and holography.* Adv. Theor. Math. Phys., vol. 2, pages 253–291, 1998. (Cited on page 35.)

[Witten 2012] E. Witten, M.B. Green and J.H. Schwarz. Superstring theory 25th anniversary edition: Volume 1, introduction. Cambridge Monographs on Mathematical Physics. Cambridge University Press, 2012. (Cited on pages 27, 31 and 34.)

[Yamada 2013] H. S. Yamada and K. S. Ikeda. *A Numerical Test of Pade Approximation for Some Functions with singularity.* ArXiv e-prints, August 2013. (Cited on page 136.)

[Zinn-Justin 2002] J. Zinn-Justin. Quantum field theory and critical phenomena. International series of monographs on physics. Clarendon Press, 2002. (Cited on pages 134 and 136.)